PHYSICAL METALLURGY OF TUNGSTEN

AND TUNGSTEN BASE ALLOYS, Part III.

TECHNICAL REPORT NO. WADD-TR-60-37, Part III

November 1962

JUL 26 1968

Directorate of Materials and Processes

USAF. Aeronautical Systems Division

Air Force Systems Command

Wright-Patterson Air Force Base, Ohio

Project No. 7351, Task No. 735101

NOTICES

When Government drawings, specifications, or other data are used for any purpose other than in connection with a definitely related Government procurement operation, the United States Government thereby incurs no responsibility nor any obligation whatsoever; and the fact that the Government may have formulated, furnished, or in any way supplied the said drawings, specifications, or other data, is not to be regarded by implication or otherwise as in any manner licensing the holder or any other person or corporation, or conveying any rights or permission to manufacture, use, or sell any patented invention that may in any way be related thereto.

Qualified requesters may obtain copies of this report from the Armed Services Technical Information Agency, (ASTIA), Arlington Hall Station, Arlington 12, Virginia.

This report has been released to the Office of Technical Services, U.S. Department of Commerce, Washington 25, D.C., in stock quantities for sale to the general public.

Copies of this report should not be returned to the Aeronautical Systems Division unless return is required by security considerations, contractual obligations, or notice on a specific document.

FOREWORD

This report was prepared by the Metals Research Section of the Lamp Division of Westinghouse Electric Corporation under USAF Contract No. 33 (616)-6933. The contract was initiated under Project No. 7351, "Metallic Materials," Task No. 735101, "Refractory Metals." The work was administered under the direction of the Directorate of Materials and Processes, Deputy for Technology, Aeronautical Systems Division, Wright-Patterson Air Force Base, Ohio. Lt. W. E. Smith was the project engineer.

This report covers work done from 1 April 1961 to 31 March 1962.

The authors of this report have shared in the execution of the various programs of the contract as follows:

Project Manager (Single Crystal Growth, Electron Theory)	H. G. Sell
High Temperature Base Line Data on Pure Tungsten, Dispersed Second Phase Alloy Development	G. H. Keith
Deformation of Tungsten Single Crystals Below R.T. D.-B. Transition of Pure Polycrystalline Tungsten	R. C. Koo
Deformation of Tungsten Single Crystals Above R.T., Twinning and Fracture, Fabrication and Recrystallization Behavior of Tungsten and Tungsten-Tantalum Alloy Single Crystals, Internal Friction	
Interstitial Dosing of Tungsten and Alloys, Activation Analysis	R. Corth

The authors wish to acknowledge the valuable contribution of Lt. W. E. Smith of Materials Central (extrusion of W-TaC billets), Messrs. M. Spewock, F. Bender, and E. F. Vandergrift of the Materials Manufacturing (compacting and presintering), and Dr. G. Comenetz and Mr. L. E. Hays of Central Research Laboratories (vacuum sintering, compression tests). The authors are also grateful for the assistance of many members of the laboratory staff. Particular mention is made of Messrs. E. Gritz, M. F. Quaely and T. Ellis (wet chemical, vacuum fusion and spectrographic impurity analyses); Dr. C. K. Lui Wei (X-ray analyses); Messrs. R. Courtney, T. McFall, R. L. Fitzmaurice, J. J. Britton, J. J. Corcoran and C. D. Johnson for material preparation, mechanical testing and specimen preparation for metallography. The authors also note with regret the death of one of their fellow scientists, Mr. W. C. Lilliendahl, who developed the process for the preparation of high purity tungsten powders.

ABSTRACT

The tensile properties of polycrystalline tungsten were investigated. Ductility decreased between 2000°F and 4000°F, and it was found that annealing temperature has a greater effect on the D.-B. transition temperature than does grain size.

Single crystals with a [100] orientation were grown by electron beam floating zone melting. The tensile deformation behavior of these crystals was studied from -196°C to 800°C. Internal friction measurements were made on single crystals between 20°C and 600°C and it was attempted to correlate damping peaks found at about 300°C and 475°C with interstitial effects, carbon dosing experiments, and yield point phenomena. Single crystals were worked by rolling and their recrystallization response was investigated as a function of cold work and working temperature. Twin morphology was thoroughly studied.

Binary solid solution alloy single crystals of W-Ta were produced by electron beam floating zone melting from compacted ingots. Alloy single crystals containing .25% and 4% tantalum were worked and the recrystallization response was determined to be 400°C to 600°C higher than that of worked pure tungsten single crystals.

The tensile strength of sintered and swaged W-TaC alloys was determined at 3000°F and 3500°F as a function of alloy composition (0.1-1%). Also measured at 3000°F and 3500°F were the tensile strengths of the systems $W-2\%ThO_2$ and $W-.5\%HfO_2$.

This technical documentary report has been reviewed and is approved.

I. Perlmutter
Chief, Physical Metallurgy Branch
Materials Laboratory

iii

TABLE OF CONTENTS

iv

TABLE OF CONTENTS (cont'd)

LIST OF FIGURES

vi

•

LIST OF TABLES

PHYSICAL METALLURGY OF TUNGSTEN
AND TUNGSTEN BASE ALLOYS

I. INTRODUCTION

The research and development work presented and discussed in
this report has been carried out as a continuation of two previous
programs undertaken under contracts AF33(616)-5632 and AF33(616)-
6933. The results of the latter two contracts were documented in
WADD Technical reports 60-37, Part I and II (1,2). Broadly stated,
the objective of the two previous contract programs, as well as
that of the programs discussed here, is the development of high
temperature dispersion strengthened alloys of tungsten, supplemented
by a variety of fundamental studies of the mechanical properties of
high purity polycrystalline and single crystal tungsten.·

In the course of the two previous contract programs the main
investigation concerned the following three alloy systems (not
exceeding 2% of alloy concentration): $W-ThO_2$, $W-TaC$, $W-HfO_2$. The
high temperature tensile strength of these alloy systems was
measured concurrently with that of the high purity tungsten up to
3000°F and it was thus possible to establish the strengthening
imparted by a dispersed second phase. The greatest problem of this
portion of the program was the poor reproducibility of test results,
even though the alloys were produced and fabricated under seemingly
identical conditions. This led to a more fundamental approach which
would allow for a mechanistic interpretation of the test results.

During the first and second contract periods, substantial effort
was expended to produce high purity single crystal tungsten by elec-
tron beam floating zone melting in order to study the mechanical
properties of tungsten in its purest and most perfect form. Single
crystals 9-11 inches long x 0.200 inch diameter were produced and
preliminary mechanical properties of these crystals were investigated
prior to the initiation of the present contract. Dilute binary solid
solution alloy single crystals of tungsten with tantalum and columbium
were grown and the mechanical properties of the alloys were evaluated.
By comparing the properties of alloy single crystals with those of
pure tungsten single crystals first, and by then extending this study
to fabricated pure tungsten and tungsten alloy single crystals
it should in principal be possible to interpret test results

mechanistically and design dispersion strengthened alloys. This is assuming, of course, that it would also be possible to dose these alloy single crystals with a third constituent and precipitate a second phase by appropriate diffusion anneals.

After a thorough consideration of all the areas requiring investigation, effort was focused during the third contract period on (a) enlarging the scope of base line information on high purity polycrystalline tungsten produced by powder metallurgy techniques, (b) thoroughly investigating the deformation behavior of single crystalline tungsten, including a study of twinning, (c) studying the fabricability and the recrystallization behavior of single crystalline tungsten, (d) dosing with carbon and oxygen and studying internal friction of single crystalline tungsten, (e) developing methods of producing binary solid solution tungsten base single crystal alloys, (f) evaluating the properties of W-Ta alloy single crystals, (g) investigating the effects of fabrication variables on the alloy W-.38%TaC, and (h) two supplemental programs concerned with Ta activation analysis and the electronic structure of tungsten. A large volume of data was obtained and is presented and discussed in this report.

By improving the grip design it was possible to extend tensile tests on pure tungsten to 4000°F, and the base line data on high purity tungsten were thus essentially completed. A loss of ductility previously noted at 2500°F was magnified by higher test temperatures. This loss in ductility as measured by %R.A. was found to amount to a difference of almost 80% between 2000 and 4000°F.

The importance of impurities, in particular their state in the matrix, was also apparent in the investigation of grain size on the ductile-brittle transition temperature of pure tungsten. A rather unexpected result was obtained here in that the ductile-brittle transition was found to depend to a much greater extent on annealing temperature than it does on grain size.

Single crystal tensiles machined from single crystal rods having one and five melting passes were tested in the temperature range from -196°C to room temperature. A yield stress of from 37 to 50% lower was measured in tensiles having 5 melting passes. The deformation of single crystals below and at room temperature is caused to a substantial degree by twinning and this is increasingly evident in crystals of higher purity. It was observed that twinning occurs only in a limited temperature range. The exceptional high purity of tungsten single crystals (liquid helium residual resistance ratios greater than 16000 have been measured) is considered to be the reason for this observation.

The deformation behavior of single crystals having a [100] orientation was further studied in the temperature range from room temperature to 800°C. The results were analyzed in terms of current theories in conjunction with internal friction measurements. A ductile-brittle transition was found to occur at 150°C.

2

Single crystal specimens were fabricated by rod rolling at temperatures from 400 to 1100°C, and per cent cold work was found to affect the recrystallization temperature in the classic manner. The recrystallization temperature decreased from 1800 to 1200°C with increasing degree of cold working from 20-90%.

Deformation twinning was studied and it was found that preheat temperature has a strong effect on the profusion of twinning, and that twinning occurred at substantially higher temperatures than previously thought. There is also some evidence that twinning inhibits recrystallization. The relationship between twinning and fracture is not yet fully understood, although certain mechanisms are indicated from a study of twin morphology.

A series of dosing experiments was conducted using poly-crystalline tungsten in low vapor pressures of hydrocarbons like napthalene and hexadecane. The efficacy of this method for controlled dosing was demonstrated.

Internal friction measurements on tungsten single crystals over the range from room temperature to 600°C yielded well-resolved peaks at approximately 300°C and 475°C. These show interstitial origin and in some instances appear to be caused by a single relaxation mechanism. Attempts to identify the peaks as to their origin revealed that the peak at 475°C is probably due to carbon, while the interstitial origin of the peak at 300°C is still unknown.

Binary solid solution alloy single crystals of W-.35% Ta, W-5% Ta and W-5% Nb were grown from compacted and vacuum pre-sintered ingot electrodes by electron beam floating zone melting. The W-Ta alloys had uniform composition over an 8 inch length.

Binary solid solution alloy single crystals of W-.35% Ta and W-5% Ta were successfully fabricated by rod rolling at 1100°C. Alloying increased the recrystallization temperature as much as 600°C. Alloy concentration plays an important role, for, at equivalent reductions in area the alloy with the higher concentration recrystallized at a higher temperature.

The alloy development phase of the contract was primarily concerned with controlled fabrication as exemplified by the extrusion and swaging of a hydrogen-sintered 3 x 6 inch W-.38%TaC billet. A slightly undersized billet of 89% of theoretical density was successfully extruded and swaged to approximately 0.432 inch diameter. A second billet which was entirely vacuum sintered to 92% of theoretical density was successfully extruded. Additional tests were carried out on W-HfO2 and W-ThO2 alloy tensiles and also on W-TaC alloys previously prepared by sintering and swaging. The concentration of TaC, which imparts greatest strengthening in H_2 sintered ingots, was determined to be approximately 0.4% by weight.

. Finally, mention must be made of two supporting programs: the determination of tantalum by activation analysis and a study of the electronic structure properties of tungsten. Tantalum activation analysis was developed to cover the concentration range from 0.1% to 10% tantalum and this method was used to determine tantalum concentrations in the various tantalum alloys investigated. The electronic structure study was restricted to a theoretical evaluation of the temperature dependence of the spectral emissivity of tungsten and other refractory metals. This temperature dependence provides an insight into the electronic band configuration.

Since the contract work program was built on several specific study areas, it was considered desirable to present the details of each in separate sections. Each section virtually stands on its own as a separate report. In order to clearly establish the inter-relationships between the various areas, and to present the implications of all results, the individual programs are critically analyzed in the general discussion at the end of the report.

II. FUNDAMENTAL MECHANICAL PROPERTIES OF PURE TUNGSTEN

A. Polycrystalline Tungsten Produced by Powder Metallurgy Techniques

1. High Temperature Strength between 2000 and 4000°F

The importance of base line data in an alloy development program lies in the reference levels which these data provide when improvements or deficiencies in properties occur upon alloying. Also, clues are obtained as to the fundamental mechanisms involved in imparting the observed base line behavior.

Although commercial tungsten is one of the purer metals by normal standards, its properties are significantly affected by the presence of trace levels of both substitutional and interstitial impurities. It was therefore deemed absolutely necessary that all base line data be obtained on material made under carefully controlled conditions in small research size (10 Kg) batches.

With this philosophy in mind, the base line data on high purity powder metallurgy tungsten have been extended to 4000°F, and this phase of the program is essentially completed with the data now on hand. There are, however, certain areas which require further work using a somewhat different approach.

Experimental

The test equipment has been described previously (1) for test temperatures below 3000°F, and a description of the modifications made as well as the equipment used at the higher temperatures has been published (3).

The test procedures used have been kept constant throughout the course of the contract period, and were as follows:

a. Tests were conducted in vacuum.
b. Temperature was uniform over the gage length within $\pm$ 15°F at and below 3000°F.
c. Temperature fluctuation at and above 3500°F was less than 3/4%.
d. Gage length/diameter ratio was 8:1 with a gage length of 1.5 inches.
e. Specimens were stabilized at temperature for a minimum of 12 minutes prior to test.
f. Strain rate was constant at 30% per hr.

The test materials used were processed from high purity tungsten powders ($\sim$ 99.98%W) produced in the Research Laboratory in small (10 Kg) pilot batch quantities. Compacted 2 Kg ingots were hydrogen sintered to $\sim$90% density and swaged $\sim$60% R.A. The tensile specimens were fully recrystallized after grinding and prior to testing. In addition, the recrystallization anneal was conducted at a temperature which was at least equal to the test temperature.

An additional pilot batch of high purity tungsten (PB-19) was processed in order to complete the high temperature experiments with equivalent materials. The reduced powder had a particle size of 1.8 μ (FSSS) and was acid washed in HF in an attempt to purify it still further since HF washing is effective in reducing Al and Si. Chemical and vacuum fusion analyses of this material during the various processing stages are given in Table 1 along with data from PB-14 (the previous batch) for comparison.

Table 1
Spectrographic and Vacuum Fusion Analyses of High Purity Tungsten
Used for Base Line Data*

Material	Al	Fe	Si	Mg	Cu	Ni	Ca	C	O	N	H
PB-19 (reduced)	31	64	64	9	3	2	2	ND	ND	ND	ND
PB-19 (acid washed)	2	60	10	10	3	7	2	ND	ND	ND	ND
PB-19 (tensile)	3-55	77	19	19-28	7	2	2	37	ND	ND	ND
PB-14 (tensile)	3-10	30-55	0-25	10	ND	5	10	30	4	23	1
PB-6 (rod)	8	<5	3	<3	ND	<3	31	50	3	24	1

* = ppm by weight
ND = not determined

Short Time Tensile Tests

The test results at 3500 and 4000°F have been compiled in Table 2 . Included in Table 2 are the data for two specimens tested at 2500°F after annealing at 4000°F. All high temperature data obtained during the course of the past three contract periods over the temperature interval 2000-4000°F are summarized in Figs. 1 and 2 .

Table 2
High Temperature Strength of High
Purity Powder Metallurgy Tungsten

Test Temp.	.2% Yield Strength (psi)	Ult. Tensile Strength (psi)	Uniform Strain (%)	Elong. (%)	Red. in Area (%)
3500°F	4900	6300	3.5	18	18
3500	4000	6600	5.1	19	18
3500	4100	6300	5.8	18	18
4000	2900	4000	2.7	13	13
4000	3200	4200	3.2	13	13
4000	3300	4200	2.9	12	13
2500 (a)	14000	20500	11.0	37	93
2500 (b)	12000	19000	13.6	79	93

(a) PB-14
(b) PB-19

Discussion

In analyzing the results it can be seen from Fig. 1 that the yield strength decreases nearly linearly over the test interval at a rate of approximately 450 psi per 100°F. The ultimate strength decreases more rapidly and is approaching the yield strength at 4000°F. The ductility data presented in Fig. 2 are of considerable interest. The drastic reduction in ductility, as measured by the parameters of uniform strain, total elongation, and reduction in area, found above 2500°F continues to increase at all test temperatures up to 4000°F.

While the general trends of the data presented here are similar to those reported by Hall and Sikora (4,5), several important differences are to be noted. Perhaps the most important is that the absolute strength values reported here are significantly lower than those given by Hall and Sikora for commercial purity tungsten. It is thought that this difference can be accounted for by the following two important facts: First, the high purity of the base material used, and secondly, the fact that the tensile
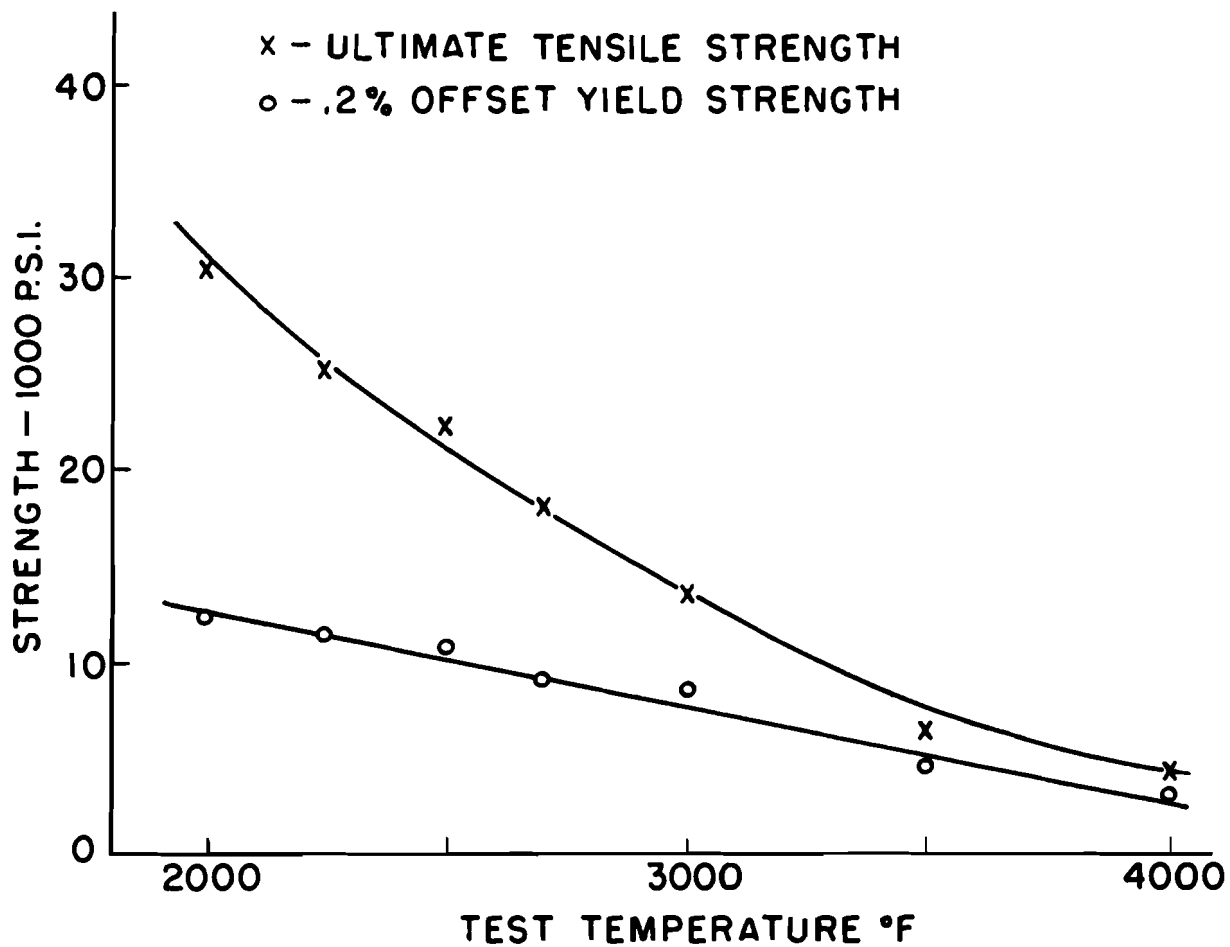
FIG. I STRENGTH VS TEST TEMPERATURE OF HIGH PURITY
POWDER METALLURGY TUNGSTEN.
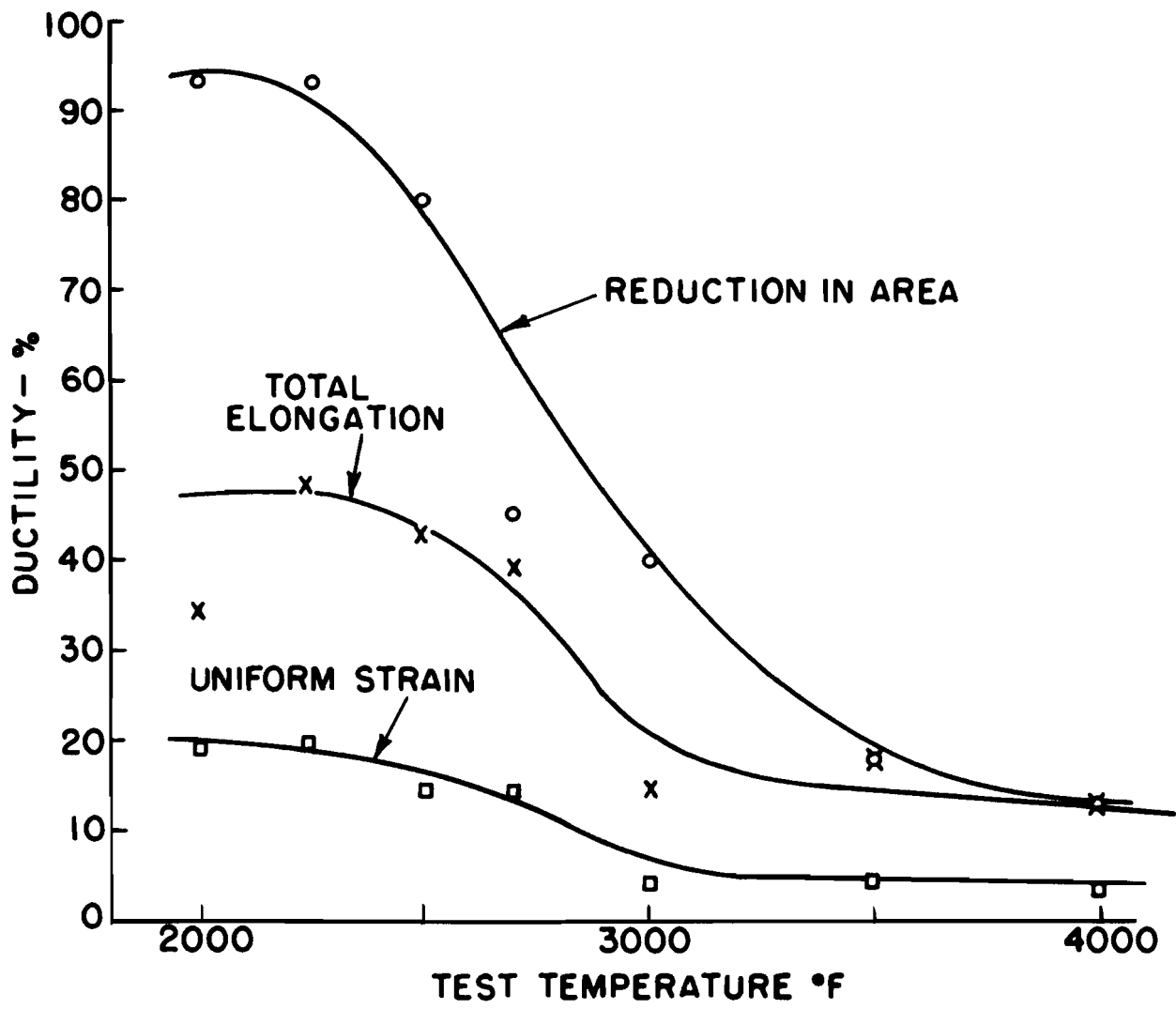
FIG. 2 DUCTILITY VS TEST TEMPERATURE OF HIGH PURITY
POWDER METALLURGY TUNGSTEN.

8

specimens were fully recrystallized and had been stabilized by
annealing at temperatures at least equal to the test temperature
prior to actual testing. In fact, the strength values at 3500
and 4000°F reported here are even somewhat lower than the values
given by Witzke (6) for pure single crystals of tungsten tested
at the same temperatures. It will be shown in the section on
deformation behavior of single crystals that the strength values
of these high purity powder metallurgical materials at lower
temperatures (~600°F) are equal to those of single crystals
which were produced by electron beam floating zone melting.
Aside from possible orientation effects, either of the following
conclusions may be drawn from these data.

     a. The presence of the boundaries weakens polycrystalline
tungsten to the same extent that purification weakens tungsten
single crystals,

     b. Boundaries play a relatively minor role in the strength
properties of high purity polycrystalline tungsten and there is
no significant difference in the purity of the powder metallurgy
product and the single crystals.

     Since current analytical techniques have been unable to
reveal any significant difference in purity between single crystals
and the polycrystalline starting material (2,6), (if the starting
material is itself of high purity), no choice can be made between
the two hypotheses. An experiment which suggests itself and must
be performed is the measurement of the high temperature strength
of polycrystalline tungsten processed from a very pure single
crystal rod.

     The measured ductility values are somewhat disturbing when
considering tungsten for use at temperatures above 3000°F. The
decrease in ductility at and above 2500°F reported in the early
work of this contract (1) continues to 4000°F. It is believed
that the loss in ductility at a lower temperature than that found
by Hall (4,5) can be attributed to the high purity tungsten used
here. Although surprising, an indication that this is true was
reported earlier (1) when it was shown that a material of
commercial purity was not as severely affected at 2500°F as was
a high purity tungsten. Confirmation is also seen in Hall's
work using commercial purity tungsten which did not show the
decrease in ductility except at temperatures in excess of 3000°F.

     An explanation for this phenomenon is not readily apparent.
A study of the broken tensiles confirms the measured ductility
data. At test temperatures up to about 2500°F, the fracture area
shows a worked structure with transgranular failure. At test
temperatures above about 2700°F the fracture area shows void
formation and intergranular cracking (Figs.3 and 4). These photo-
micrographs also reveal a tendency for an increase in void
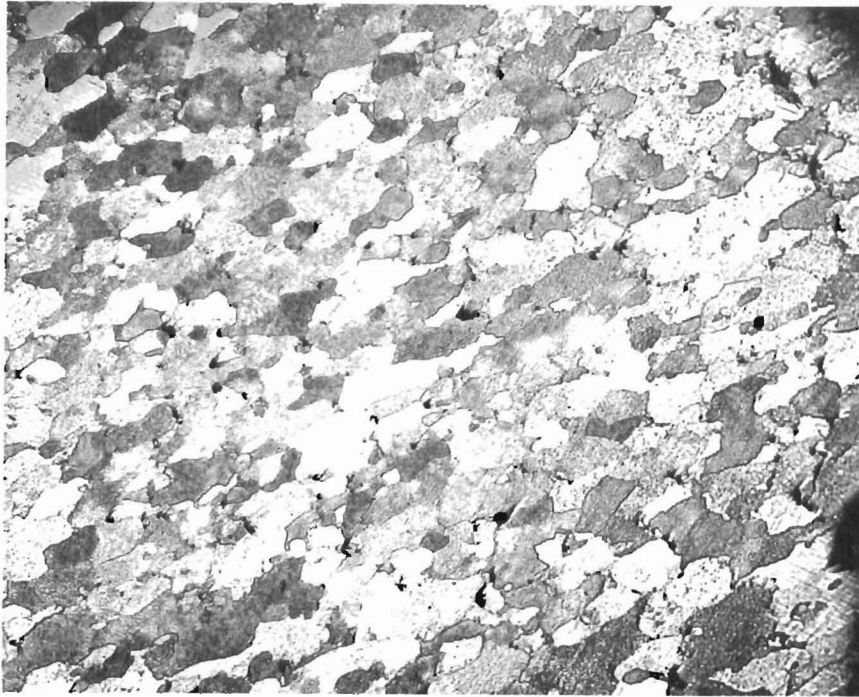
Fig. 3   Microstructure near Fracture of
          Tensile Specimen After Testing
          at 3000°F - 100X
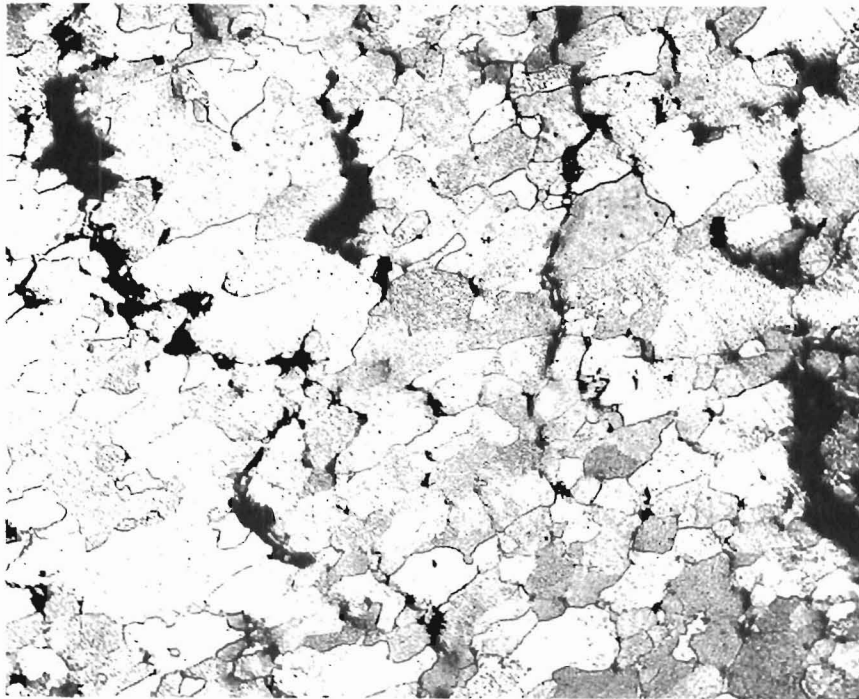
Fig. 4   Microstructure near Fracture of
          Tensile Specimen after Testing
          at 3500°F - 100X

10

formation and cracking with increase in test temperature. This decrease in ductility with increase in test temperature has been seen in other metals and alloys and was thoroughly discussed by Grant (7) and Gifkins (8). Generally it occurs in conjunction with void formation and intercrystalline cracking. Strain rate is also important, with decreasing rate favoring void formation and intergranular cracking. It has also been shown (7) that minor elements and impurities can have large effects on the fracture characteristics of materials under high test temperature and low strain rate conditions.

One can therefore speculate that one or more of the impurities in the commercial tungsten has effectively tied up a deleterious impurity present in both materials tested here. The identity of such impurities is not yet known. The tests at 2500°F after annealing at 4000°F lead to the following conclusions:

a. The ductility loss is probably not a strong function of the state of the impurities or the grain size alone since the values at 2500°F do not appear dependent on prior annealing conditions.

b. Iron may be one of the active impurities since both the materials used (PB-19 and PB-14) exhibited higher ductility (at 2500°F) than that found in the original data which was obtained on a somewhat higher purity material (PB-6). Note that the major difference is the iron content. See Table 1 .

However, it must be emphasized that the above is pure speculation. Considerable additional effort using both high purity single crystals and polycrystalline material, as well as extensive chemical controls is required to resolve this question. It is also appropriate to state that at none of the test temperatures used can tungsten be considered to be particularly ductile since it is difficult to consider 50% elongation or 20% uniform strain as representative of a truly ductile material. Of course, the base material tested is still not the purest tungsten one would like to have available for testing, and the properties of a purer tungsten may be radically different from those reported here.

Stress-Rupture Tests

Stress-rupture data at 3000°F were obtained on tensiles manu-factured from the high purity tungsten batch PB-14. These tests were carried over from the previous contract period, because the furnace had to be improved first in order to make long creep measurements at 3000°F possible. The results are reported in Table 3 together with previous measurements at 2700°F.

11

Table 3
High Temperature Creep of Pure Tungsten

Test Temperature	Stress (PSI)	Life (hrs.)	M.R.C. (%/hr.)	Rupture Strain %
2700°F	12500	3.3	3.7	18
2700	12500	3.0	1.75	11
2700	10000	16.0	0.320	11
2700	10000	25.0	0.085	5
2700	7500	30.0	0.075	5
2700	7500	97.0	0.029	6
3000°F	7500	2.5	0.632	8
3000	5000	21.0	0.037	2
3000	6000	16.0	0.069	3.2
3000	5000*	>34.0	<0.034	>2.1

* Test interrupted by furnace failure.

The repeat test at 5000 psi was interrupted by furnace failure. A third test was also run but the results were inconclusive due to several interruptions of the test.

The stress vs rupture time for this high purity material appears to be normal at 3000°F. The rupture time at 5000 psi is estimated to be 40-50 hours using minimum creep rates as a basis for extrapolation. This estimate falls in line with the data for the higher stresses. Since the emphasis was shifted to short time tensile testing only, no further work was done on stress-rupture properties.

2. Ductile-Brittle Transition as Affected by Impurities.

The effect of grain size on the mechanical properties of the b.c.c. metals has been a subject of intensive theoretical and experimental study in the past decade (9-21). The quantitative relationship between yield stress and grain size in iron (14,15), molybdenum (16), columbium (17,18), tantalum (19), and chromium (20), and the quantitative relationship between the ductile-brittle transition temperature and grain size in mild steel (21) were established experimentally by mechanical tests on specimens having widely different grain sizes. When the lower yield stress is plotted as a function of the inverse square-root of the average grain diameter (known as the Petch analysis) the data can generally be fitted to a straight line, and the slope of this line (known as the Petch slope) is usually greater the higher the ductile-brittle transition temperature of the metal (11,19). (Tantalum is an exception (19).) Because of this correlation and the quantitative dependence of the ductile-brittle transition temperature on grain size (10,21), much theoretical significance

has been attached to the dependence of the mechanical properties on grain size (9-13).

Quantitative information on the relationship between grain size and the mechanical properties of tungsten, however, was not available. It was found that for tungsten the Petch slope for a plot of yield stress versus the inverse square-root of the average subgrain diameter at 600°C was only $3.3 \times 10^7 /cm^{3/2}$ (22). Since the Petch slope may be related to the average strength of boundaries in resisting the passage of dislocations (12,13), and since the strength of average high-angle grain boundaries is expected to be higher than that of subgrain boundaries, it is conceivable that in the case of tungsten the Petch slope for a grain-size plot might be appreciably higher than that for a subgrain size plot. Furthermore, recent experimental results on tantalum suggest that the effective surface energy for cleavage crack propagation is the dominating factor in the ductile-brittle behavior of b.c.c. metals (19) rather than the Petch slope as had been thought earlier (11,17).

Experiments were therefore undertaken on tungsten in order to establish the quantitative relationship between grain size and the ductile-brittle transition temperature, as well as to determine the effective surface energy for crack propagation. As will be discussed in the following paragraphs, the results revealed an unexpectedly strong dependence of mechanical properties on the state of the impurities present. Apparently the condition of the impurities was altered considerably when the specimens were annealed at various temperatures in the attempt to produce a wide range of grain sizes. Since this impurity effect outweighed any existing grain-size effect, the experimental results obtained could not be interpreted in the manner originally planned.

Experimental Technique

Prior to the initiation of the experimental work, consideration was given to the choice of a group of tungsten specimens having the proper concentration of impurities. Although very high purity would be desirable from the standpoint of mechanical properties, past experience has shown that very high purity tungsten presents a problem in that fine grain sizes by annealing cannot be achieved. This is primarily due to the occurrence of pronounced grain growth before the completion of primary recrystallization even at a minimum recrystallization temperature. For this reason, a somewhat less pure tungsten was chosen. Results of the impurity analyses of the material used are given in Table 4.

13

Table 4

Impurity Analyses of Tungsten Specimens Used for Study of Impurity Effects on
D.-B. Transition.*

Specimen No.	Annealing Temperature	Grain Size	Mg	Fe	Si	Cu	Ni	Al	C	O_2	N_2	H_2
1		-	5	45	25	1	10	4	62	8	5	0.9
A-7	2000°C	Fine	6	22	40	-	6	7	77	6	5	2
F-6	2550°C	Coarse	7	85	43	-	6	6	85	7	3	0.9
C-5	2800°C	Coarse	2	33	110	-	7	40	37	8	2	3

* Precision of analyses is approximately ± 2 ppm for non-metallic elements and
± 5 ppm for metallic elements.

14

Ductile-brittle transition temperatures in tension were determined on specimens recrystallized at various temperatures. The tensile specimens had a gage length of 1.50 inches and a gage diameter of 0.18 inch. They were recrystallized at 1450, 2000, 2550, 2750 and 2800°C for thirty minutes in a vacuum furnace at a pressure of 1×10^{-5} mm of Hg and then tested at a constant extension rate of 1/2 % per minute in an argon atmosphere in the temperature range from 100 to 800°C. Typical quantitative impurity analyses as given in Table 4, show that within the precision of the analyses annealing did not result in any detectable change in the impurity contents of the specimens, nor was there any detectable difference in purity between specimens having large differences in grain size annealed at the same temperature.

Experimental Results and Discussion

The tensile tests resulted in three distinct ductile-brittle transition curves, approximately 225°C apart. The yield stress data, however, have too much scatter for a meaningful Petch plot. As shown in Fig. 5, data of specimens annealed at 1450°C (full circles) and those specimens annealed at 2000°C (open circles) fall on Curve A. Data of specimens annealed at 2350°C and 2550°C (open and full triangles, respectively) fall on Curve B, and those of specimens annealed at 2750°C and 2800°C (open and full squares, respectively) fall on Curve C. The decrease in ductility with an increase in annealing temperature was so pronounced that one third of the specimens annealed at 2750°C and two-thirds of the specimens annealed at 2800°C fractured while they were being set into the tensile grips. Although the increase in the ductile-brittle transition temperature with an increase in annealing temperature suggests the existence of a grain-size effect, metallographic examination on all specimens tested proved unambiguously that the observed differences in the ductile-brittle transition temperature were not caused by differences in grain size.

Quantitative measurements of grain size in all specimens tested revealed no correlation between grain size and the transition temperature.

While all the specimens annealed at 1450°C and 2000°C had uniform grains of 0.0032 cm to 0.0047 cm in diameter, a very large range of grain sizes was found in specimens annealed at all other temperatures. The open triangles and the open squares in Fig. 5 represent specimens which had grains approaching the gage diameter (0.18 inch) and extending along the specimen axis as much as four times the gage diameter. The solid triangles and the solid squares represent specimens having uniform grains approximately 0.0046 cm to 0.0087 cm in diameter. Thus the results show that the data which fall on each of the curves B and C represent specimens having grain sizes differing by a factor of nearly 100. Furthermore, for specimens having the same grain size (e.g. 0.0046 cm) whether the
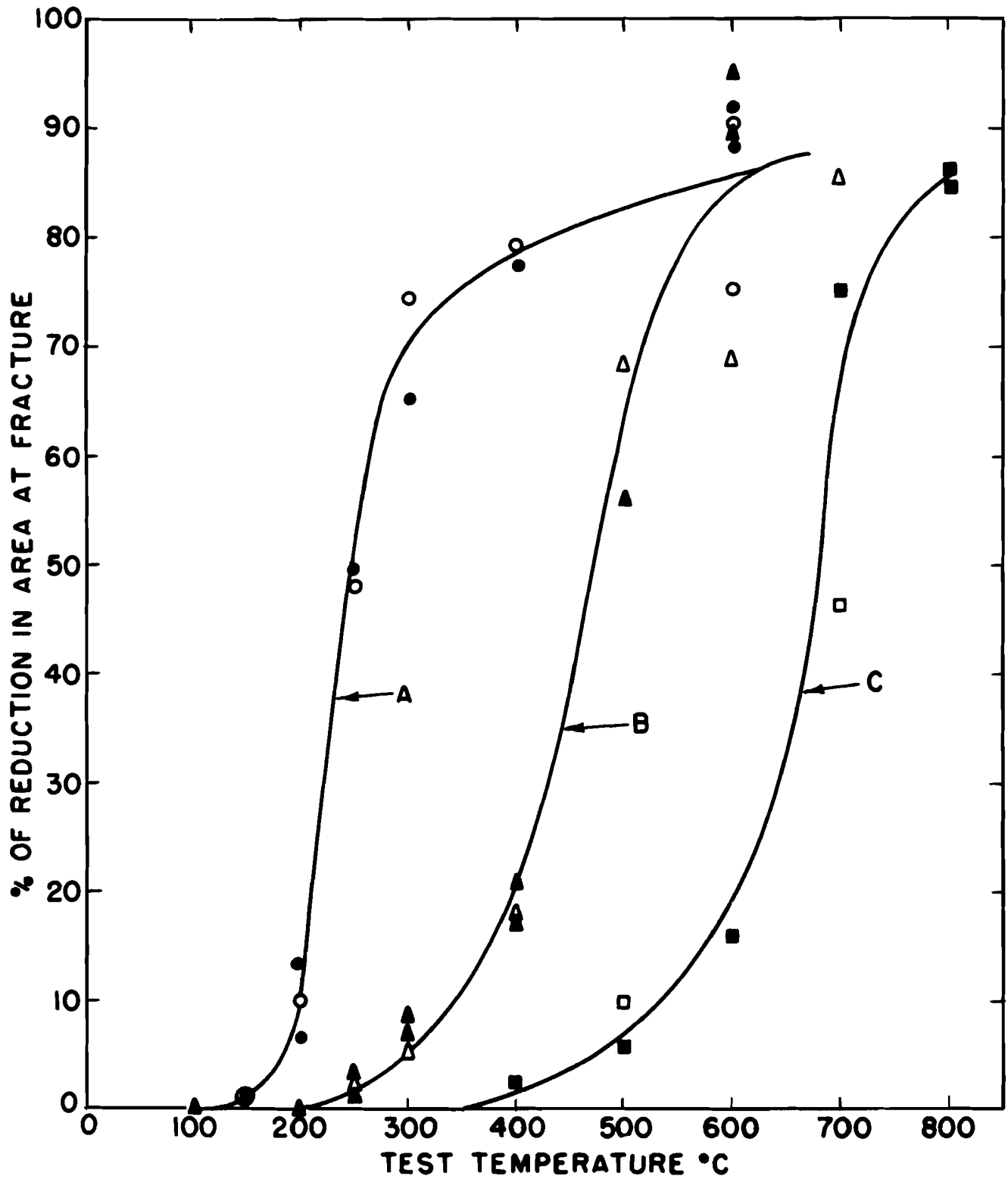
FIG. 5 DUCTILE-BRITTLE TRANSITION IN TENSION OF TUNGSTEN
RECRYSTALLIZED AT VARIOUS TEMPERATURES AND TESTED
AT A RATE OF 8×10^{-5}/SEC.

16

ductile-brittle transition falls on Curve A, B or C depends upon the annealing temperature. It is therefore concluded that the observed ductile-brittle transition temperatures are relatively independent of grain size and depend primarily on the temperature at which the specimens were annealed.

Metallographic examination of the fractured specimens suggests that this loss of ductility with increasing annealing temperature is primarily due to precipitation (or melting) of impurities along grain boundaries. Fracture in specimens annealed at temperatures of 2350°C and higher was completely intergranular. Numerous intergranular cracks extending inward from the surface of the specimen were present, as shown by the arrow in Fig. 6. Further evidence that cleavage in a coarse-grain specimen originated at a grain boundary is shown by the "river markings" on the cleavage surface of Fig. 7. The arrow in Fig. 7 indicates where the cleavage crack started to propagate into the large grain, and the dark area where the arrow is marked consists of a few small grains not resolved on the photomicrograph.

The impurities responsible for the observed loss of ductility are not known. Recent experiments on the tungsten-carbon constitution diagram show that a eutectic reaction occurs at 2475°C and the maximum solubility of carbon in tungsten is about 130 ppm by weight (23). For the average concentration of carbon found in these specimens (see Table 4), annealing at temperatures of 2750°C and 2800°C is therefore not expected to produce partial melting. It is conceivable that the impurity phenomenon associated with annealing is multi-component in nature. Unfortunately, other phase diagrams with interstitial impurities are not available for tungsten so that a more detailed evaluation is not possible.

The change of the state of impurities along grain boundaries with annealing, as deduced from the present experiments, not only reveals the uncertainty associated with experimental studies of the real grain-size effects on mechanical properties, but it also may have other ramifications. For example, recent transmission electron microscopy studies have shown that high-angle grain boundaries can act as sources and sinks for dislocations (24). This suggests that the frequent observation of discontinuous yielding in fine-grain specimens, but not in coarse-grain specimens of molybdenum (16), silicon iron (25), and tungsten (22) may be associated with precipitation of impurities along grain boundaries.

17
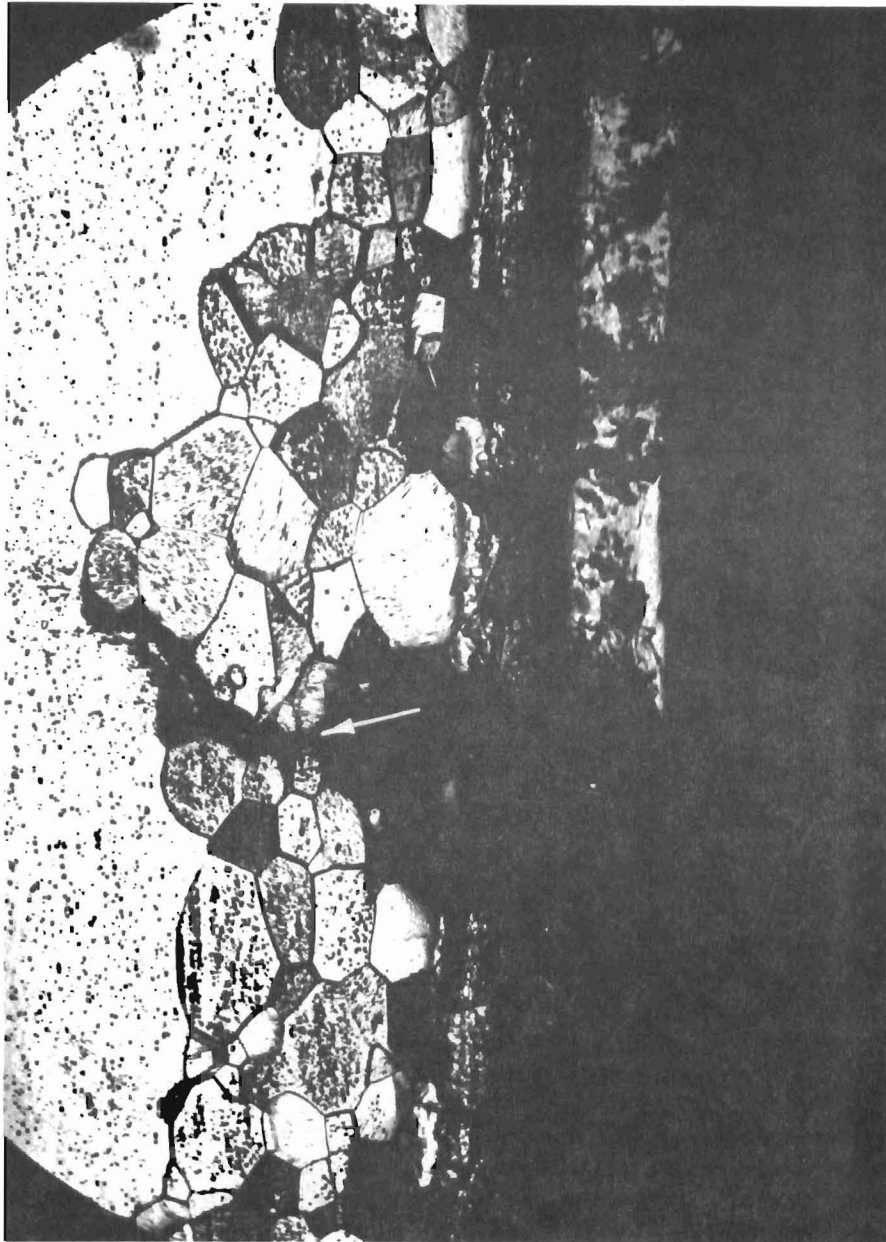
Fig. 6   Longitudinal Cross Section of a Tungsten
          Specimen Recrystallized at 2550°C and
          Pulled in Tension at 500°C - 150X
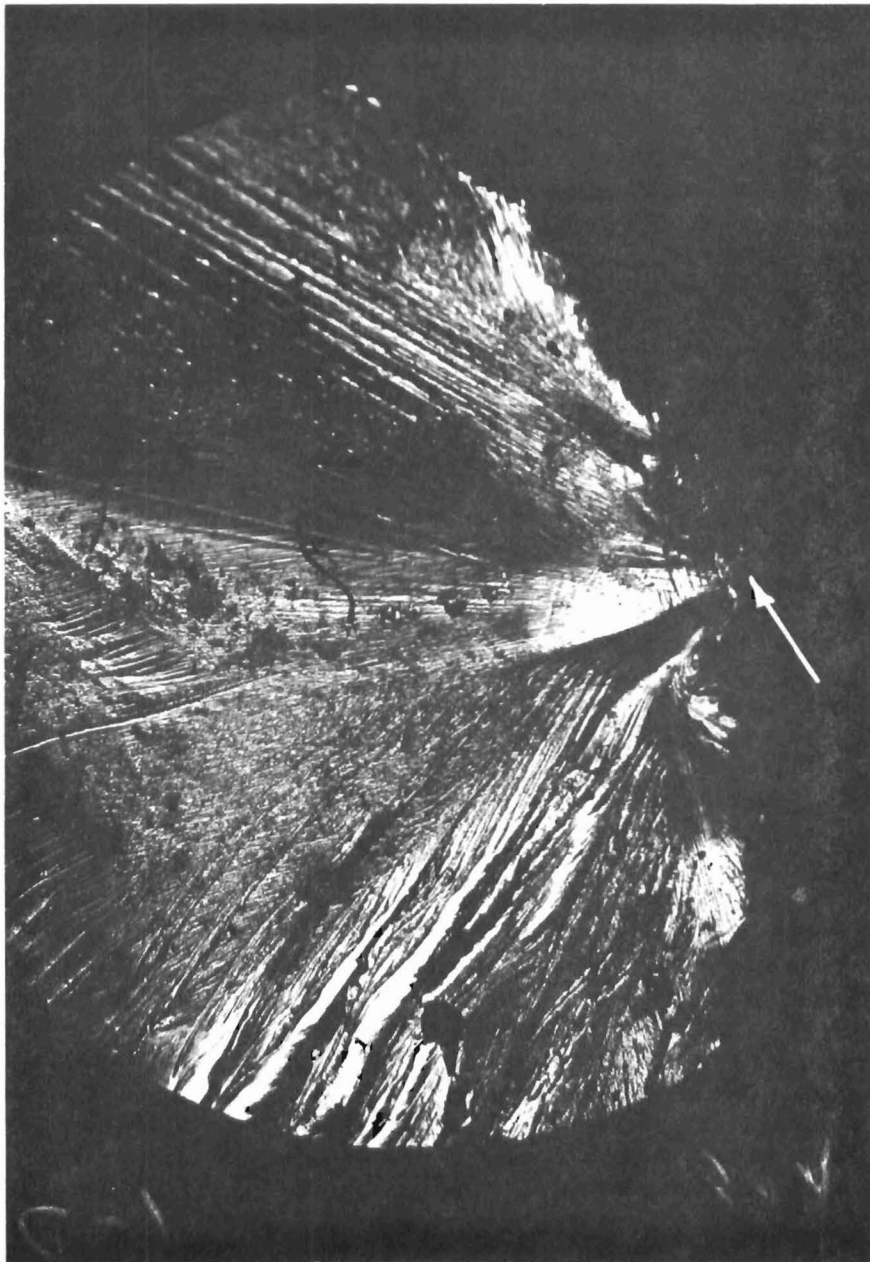
Fig. 7   Fracture Surface of a Tungsten Specimen
         Recrystallized at 2550°C and Pulled in
         Tension at 500°C - 50X

19

B. Single Crystal Tungsten Produced by Electron Beam Floating
   Zone Melting.

1. Growth and Impurity Analyses

A large number of tungsten single crystals, each about nine to
ten inches long and approximately 0.2 inch in diameter, were grown
by electron beam floating zone melting for the various investiga-
tions discussed in this report. Special attention was paid at all
times to the purification aspects of the single crystal growth
technique by means of spectrographic, vacuum fusion and carbon
analyses.

Since the ratio of the resistance measured at 298°K to that
at 4.2°K (referred to as the residual resistance ratio) of a metal
is known to be a sensitive measure of its overall purity, an attempt
was also made to correlate the resistance ratio determined along
various sections of a crystal with quantitative impurity analyses
on corresponding sections of the same crystal. The crystal (No.79)
used for this experiment had the standard five zone-melting passes
in one direction at an approximate speed of 5 mm per minute. The
measurements were carried out at the Osram Research Laboratories
(26) and are presented in Table 5.

Table 5
Residual Resistance Ratios Determined on
Tungsten Single Crystal No. 79

Position	$R(273°K)/R(4.2°K)$
Average (4" length)	11400
Starting end section	14300
Middle section	11100
Finishing end section	9500

The resistivity measurements show that the ratio decreases
continuously toward the finishing end of the crystal, indicating
the presence of a zone-refining effect.

Although resistivity measurements by Schadler also indicated
the presence of a zone-refining effect (27), the ratios obtained
in the present experiment (14,300 for the starting end) are sub-
stantially higher than his (5600 for the starting end). Inciden-
tally, an even higher ratio of 16700 was measured on a middle
section of crystal No.36. Quantitative spectrographic analyses of
metallic impurities, vacuum fusion analyses of gaseous impurities,
and carbon analyses were obtained along crystal No.79. The data
have been plotted in Figs. 8 and 9 together with the corresponding
resistivity ratios.
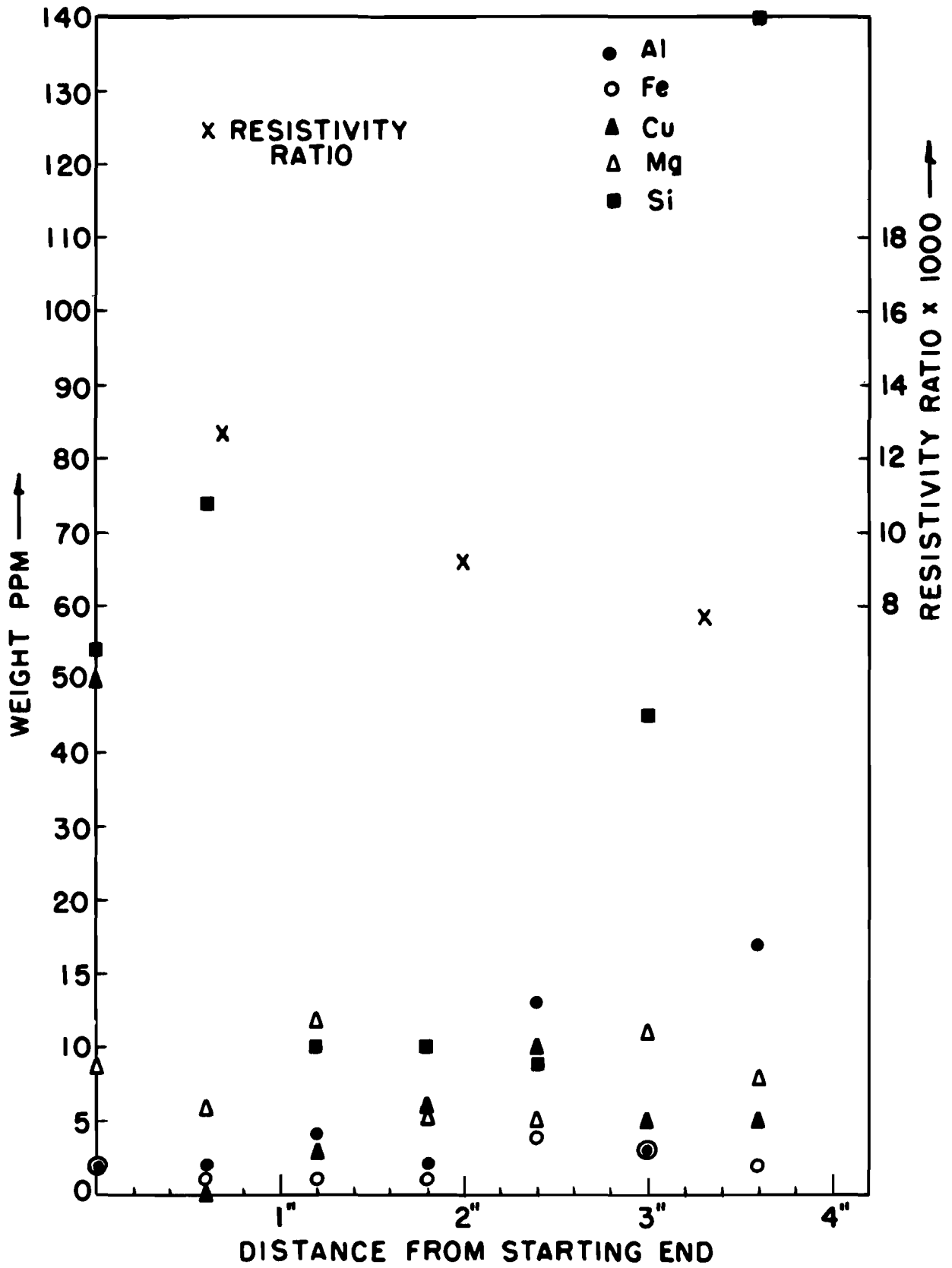
FIG. 8 SPECTROGRAPHIC ANALYSES OF METALLIC
IMPURITIES IN CRYSTAL 79.

21
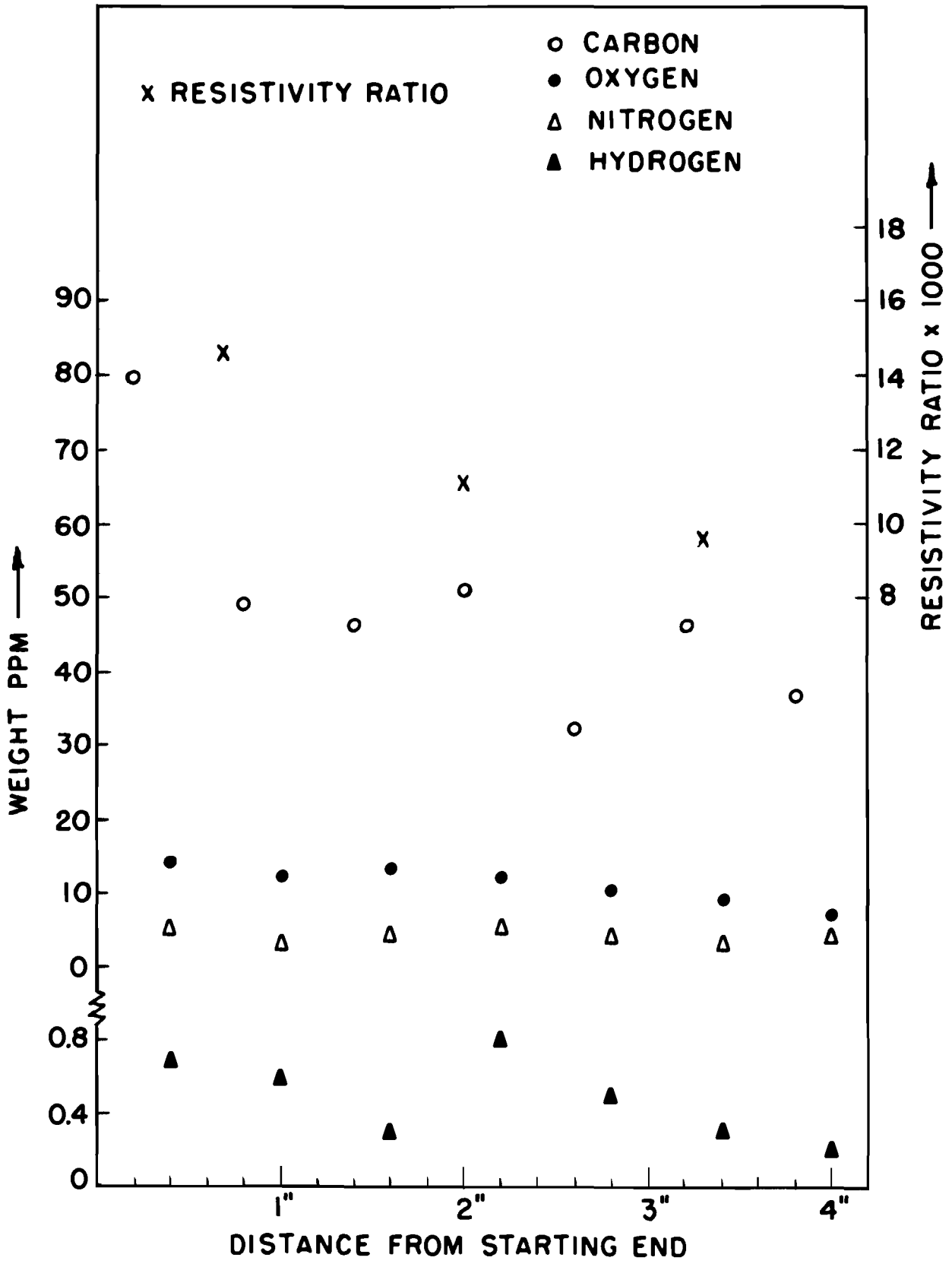
FIG. 9 VACUUM FUSION ANALYSES OF NON-METALLIC
IMPURITIES IN CRYSTAL 79.

A definite trend is apparent in that the metallic impurity content increases toward the finishing end, i.e. a zone refining mechanism is operative and the analyses correlate with the residual resistance ratios. As had been noted often before, silicon is present in a rather high concentration. This may, however, be the result of some backstreaming from the diffusion pump oil. In regard to carbon and oxygen, the opposite trend was noted. Both these elements, with the effect being more pronounced for carbon, increase in concentration toward the starting end. The measured high residual resistance ratios are therefore interpreted to mean that the interstitial impurities are mostly precipitated and do not contribute to the measurement. This conclusion has far-reaching implications. First, since there are only very small traces of interstitial impurities in solution these must have a tremendous effect on mechanical properties. Secondly, it will be very difficult to decrease the interstitial impurity content to a level at which their influence on properties will become negligible. Experimentation now in progress will place heavy emphasis on these two points.

2. Deformation of Tungsten Single Crystals Below Room Temperature.

The mechanical properties of the b.c.c. metals are known to depend strongly on the purity of the material. In general, the yield stress decreases and the ductility increases with increase in purity. Experimental observations reported in the literature on the role of purity governing deformation twinning, however, are rather conflicting. Decreasing the purity of iron by adding nitrogen, silicon, or carbon appears to facilitate twinning (28, 29, 30). On the other hand, there has been overwhelming evidence in recent years for the opposite effect of purity: increase in the overall purity facilitates twinning. For example, deformation twinning at low temperatures was found to be most extensive in the purest iron specimens prepared by zone-refining (31). In electron-beam melted iron (32) and tantalum (33) deformation twins were observed even in specimens deformed at room temperature. Similarly, electron-beam melted vanadium twinned more readily than powder-metallurgy vanadium (34). Furthermore, twinning in coarse-grain tantalum (19) and electron-beam melted columbium (35) at -196°C could be suppressed entirely by the addition of approximately 0.01 wt. % of oxygen. Since most of the observations which showed that increasing the overall purity facilitates twinning were made on materials prepared by electron-beam zone-melting, the apparent contradiction may be related to those impurities which are removed most readily by electron-beam melting.

Although an increase in the overall purity appears to facilitate deformation twinning in all the Group Va metals, no observations have yet been reported on the effect of purity on twinning in any of the Group VIa metals. Experiments were therefore under-

taken to investigate the effect of purity on the mechanical behavior of tungsten single crystals at low temperatures prepared by electron-beam zone-melting. Results have shown that an increase in the over-all purity by making additional zone-melting passes decreases the yield stress, increases the ductility, and facilitates deformation twinning.

Specimen Preparation

Seven single crystals, each about ten inches long and 0.20 inch in diameter, were grown by the electron-beam floating zone-melting technique (36) at a speed of 5 mm per minute.* In order to obtain crystals of two different purity levels with the same orientation, one melting pass was first made on the entire length of two crystals (Nos. 54 and 67), and then four additional melting passes were made in the same direction on half of each of these two crystals. The other five crystals were grown with five melting passes in the entire length.

As revealed by a dislocation etch-pitting technique (22), no significant difference was found in the substructure between the one-pass and the five-pass sections of each crystal. Both sections had about four to eight subgrains per cross section elongated in the growth direction, and a total dislocation density of $\sim 10^6/cm^2$. The axial orientations of these crystals determined by Laue back reflection are given in Fig. 10.

Tensile specimens having a gage diameter of 0.90 inch, a gage length of 0.500 inch, and a 0.625 inch radius of curvature of the shoulders, were made from these crystals by centerless grinding. Since the grinding operations introduced cold-work into the surface, the worked surface was removed by electropolishing each specimen in a 5% KOH solution until its diameter was reduced to 0.080 inch. X-Ray evidence that this procedure was sufficient to remove the entire cold-worked surface has already been given (1).

Mechanical Testing

Tensile tests were made at various temperatures ranging from 29°C to -196°C on an Instron machine operated at a constant exten-sion rate of $3.3 \times 10^{-3}/sec$. Prior to testing, the electropolished specimens were annealed at 600°C for one hour in vacuo. In order to maximize uniaxial tension each specimen was loaded through ball joints. Tests at -196°C were made with the specimens immersed in a bath of fresh liquid nitrogen, and tests between 29°C and -70°C were made with the specimen immersed in a mixture of cellusolve and liquid nitrogen. Test temperatures between -70°C and -196°C

*Two additional crystals were grown at a higher speed of ~ 9 mm per minute. These crystals were porous and since the test results were erratic, they were not included in this report.

24
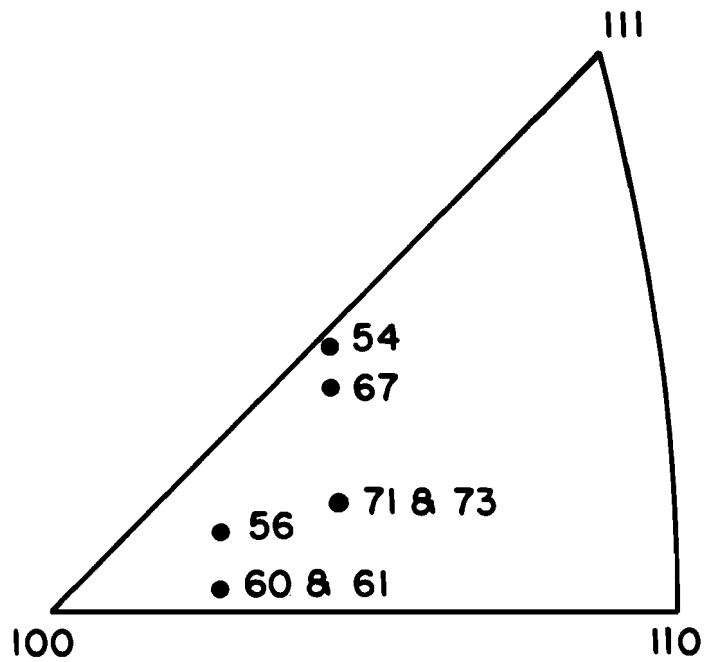
FIG. 10 ORIENTATION OF SINGLE CRYSTALS USED FOR
DEFORMATION STUDY AT SUBZERO TEMPERATURES.

were achieved as follows: A large volume of 1/32 inch diameter lead balls was placed around the specimen on which a thermocouple was taped for temperature measurements. (Lead was chosen because of its high heat capacity at low temperatures.) The whole apparatus containing the specimen and the lead balls was immersed in a liquid nitrogen bath. When equilibrium temperature was reached, the liquid nitrogen bath was removed and the specimen was allowed to warm up slowly. The specimen was then stretched when the desired test temperature was reached. Since the warm-up rate was only 2° per minute, under these conditions a test could be completed within 1°C rise in temperature for the strain rate used.

Effect of Impurity Distribution on Mechanical Properties

Since all the crystals used in the present experiments were grown with the zone passed in one direction, it was conceivable that a sufficiently steep impurity gradient due to zone-refining might exist in the crystal and thus might cause a substantial variation in the mechanical behavior of specimens cut from different sections of the same crystal. This possibility was investigated by testing nine specimens at -196°C, which were cut from one five-pass crystal (No.56). The load-elongation curves of these specimens are shown in Fig. 11. The middle number of each specimen refers to the number of zone-melting passes given to the crystal, and the last number indicates the section of the crystal from which the specimen was cut, with numbers starting from the starting end of zone-melting of the crystal.

As shown in Fig. 11, no yield point was observed in any of the tests, so that the proportional limit, (which could be estimated with an accuracy of approximately $\pm$ 5%), was taken as a measure of the yield stress. Since elongation was uniform in each specimen and since no necking occurred prior to fracture, the amount of plastic elongation was taken as a measure of ductility. These data are tabulated in Table 6. Note that except for specimen 56-5-1, which was cut from the end of the crystal where melting started, the mechanical properties of the specimens do not reveal any consistent variation which might suggest the existence of a steep impurity gradient. Although resistivity measurements along different positions of a crystal showed the presence of an impurity gradient (see Section IIB-1), the gradient evidently was not sufficiently steep to cause a substantial variation in mechanical properties.
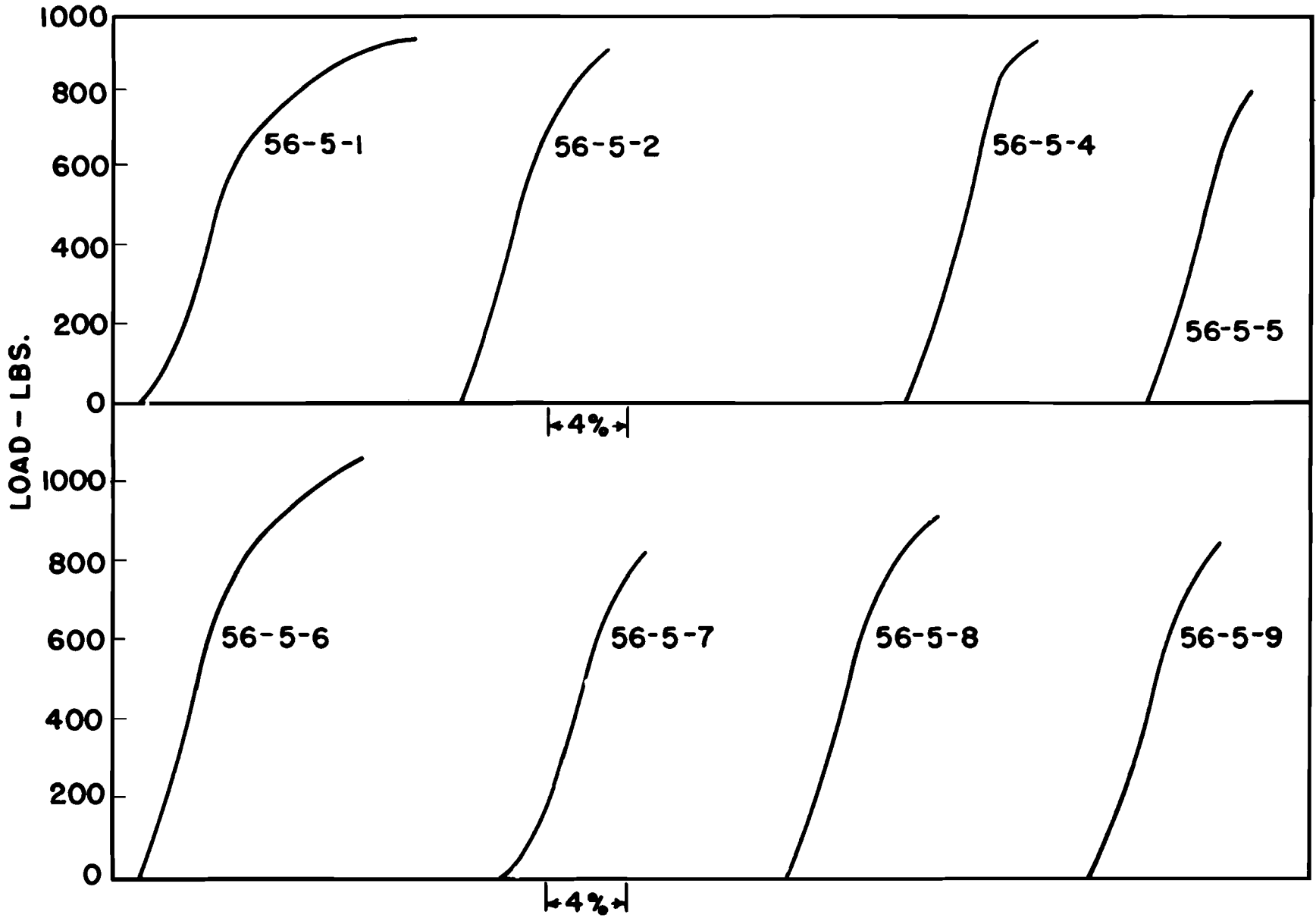
FIG. 11   LOAD VS ELONGATION OF W SINGLE CRYSTALS AT −196° C;
STRAIN RATE = 3.3 x 10⁻³/SEC.

Table 6
Yield Stress and Elongation of Tensile Specimens
Cut from Crystal No. 56

Specimen No.	Test Temp.°C	Proportional Limit	Total Plastic Elongation to Fracture
56-5-1	-196°C	111,000 psi	9.2%
56-5-2	-196°C	117,000 psi	4.0%
56-5-4	-196°C	137,000 psi	2.5%
56-5-5	-196°C	130,000 psi	1.2%
56-5-6	-196°C	122,000 psi	7.6%
56-5-7	-196°C	124,000 psi	2.2%
56-5-8	-196°C	122,000 psi	3.6%
56-5-9	-196°C	122,000 psi	2.8%

Effect of Temperature on the Yield Stress and Ductility

The effect of temperature on the mechanical behavior of tungsten crystals which had five zone-melting passes was investigated by making tensile tests at temperatures from 29°C to -196°C. Since the mechanical behavior of a single crystal depends on its orientation, crystals 60 and 61, 71 and 73 were grown by seeding, so that a sufficient number of specimens having the same orientation could be tested at various temperatures.

Results showed that no yield point was observed at any of the temperatures investigated. The yield stress as a function of test temperature is plotted in Fig. 12. It must be emphasized that the yield stress varied linearly with test temperature and could not be fitted to the Fisher relationship (37) where the yield stress is inversely proportional to the test temperature. Nevertheless, the linear relationship between yield stress and test temperature found in the present experiments is in agreement with the behavior of high-purity iron single crystals (38). However, recent experiments by Lawley et al (39) on molybdenum single crystals also prepared by electron-beam zone-melting showed that although the yield stress varied almost linearly with test temperature in the range from room temperature to -196°C, the yield stress below -196°C increased very steeply with decrease in test temperature. In view of the results on molybdenum, it is conceivable that the yield stress for tungsten may also increase rapidly with a decrease in test temperature below -196°C.

Although the yield stress in the present experiments was found to vary linearly with test temperature, the ductility underwent a non-linear, rapid decrease with decreasing test temperature. Deformation was found to be uniform along the gage length without any detectable necking prior to fracture in specimens tested at any of these temperatures. The percentage of plastic elongation prior to fracture as a function of test temperature is shown in Fig. 13. It exhibits a typical ductile-brittle transition similar to that in
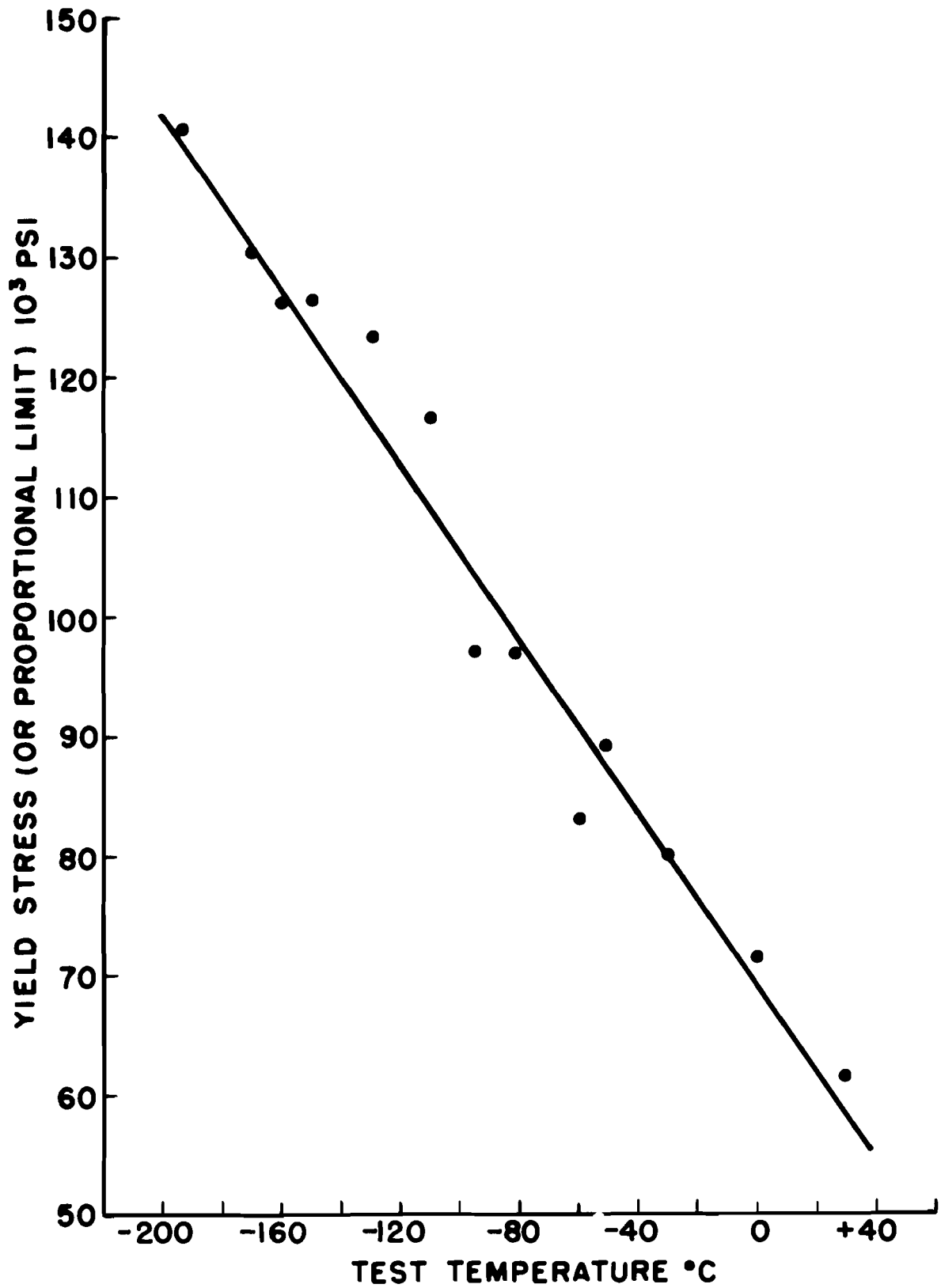
FIG. 12 YIELD VS. TEST TEMPERATURE FOR CRYSTALS
UC 60 AND UC 61
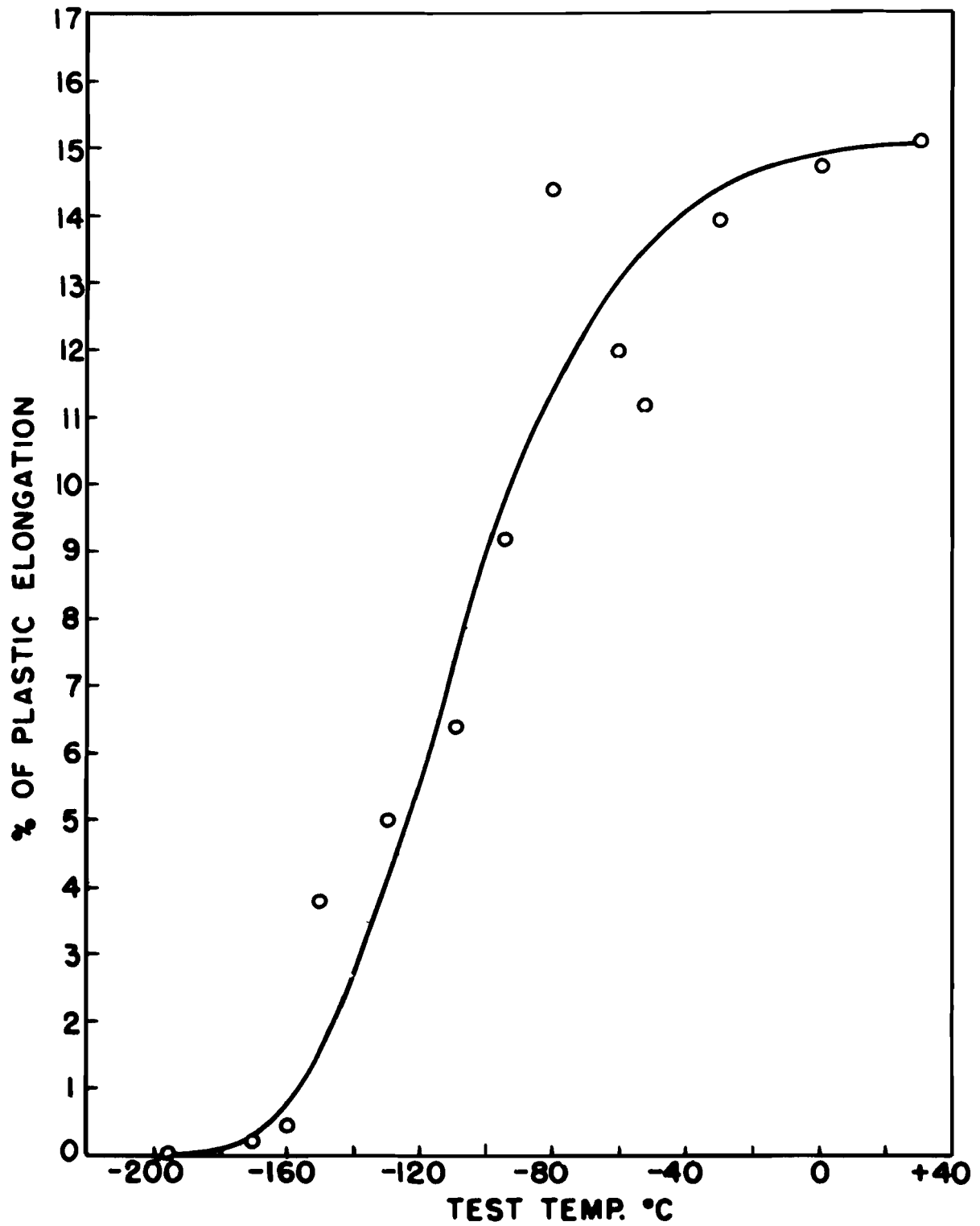
FIG. 13 % OF ELONGATION VS TEST TEMPERATURE FOR
CRYSTALS 60 AND 61 EXTENDED AT 3.3 x 10^{-3}/SEC.

polycrystalline tungsten. The ductility data of crystals 71 and 73 had very large scatter and were therefore not included in this plot.

Effect of Purity on Yield Stress and Ductility

Since the same orientation was retained in each crystal, any differences in mechanical behavior between specimens having one and five zone-melting passes cut from the same crystal can be attributed solely to the difference in purity level rather than orientation. Strong evidence that the five-pass specimens were purer than the one-pass specimens was provided by their differences in yield stress and ductility. Some typical load-elongation curves are shown in Fig. 11, in which the middle number of each specimen refers to the number of zone-melting passes. Again, in all cases no upper yield point was observed.

Values of yield stress and elongation for crystals 54 and 67 are given in Table 7. These data show that the one-pass specimens had consistently higher yield stress and lower ductility than the five-pass specimens tested at the same temperature. The yield stress of the one-pass specimens was higher than that of the five-pass specimens by an average of 57% for crystal 67 and 31% for crystal 54. Furthermore, the amount of plastic elongation prior to fracture of the five-pass specimens was higher than that of the one-pass specimens by an average of 150% for crystal 67 and 70% for crystal 54. The observed differences in yield stress and ductility between the one-pass and five-pass specimens are taken to indicate that the five-pass specimens were purer than the one-pass specimens, as might be expected.

The observed effect of the number of zone-melting passes on yield stress and ductility is in good agreement with the recent work of Lawley et al (39) on molybdenum single crystals. In the same range of test temperature, they found that the critical resolved shear stress of their one-pass crystals was about 50% higher than that of the six-pass crystals and that the amount of uniform elongation prior to fracture of the six-pass crystals was approximately 100% higher than that of the one-pass crystals.

Also included in Table 7 are values of critical resolved shear stresses. Since Schadler showed that slip in tungsten single crystals at -196°C is confined to the {110} type planes (27), the values of critical resolved shear stresses in Table 7 are shear stresses resolved along ($\bar{1}01$) [$11\bar{1}$], which corresponds to the system of maximum resolved shear stress for both crystals 67 and 54. The orientation factor, $\cos \phi \cos \Theta$, was 0.476 for crystals 67 and 0.449 for crystal 54. The critical resolved shear stresses obtained in the present experiments are comparable to the results of Rose et al (40) and Wolff (41) but are substantially higher than those determined by Schadler (42). At equivalent test temperatures the present values, even for the five-pass specimens, are almost twice as large as those obtained by Schadler (27) on crystals grown with three melting passes at a speed of 3 mm per minute.

31

Table 7

Comparison of Yield Stress and Elongation
Between the One-Pass and Five-Pass Tungsten Crystals

Specimen No.	No. of Zone Melting Passes	Test Temp.°C	Yield Stress, psi (Proportional Limit)	Critical Resolved Shear Stress, psi ($\bar{1}01$) [111]	% of Uniform Plastic Elongation
67-1-2	1	-130°	197,000	89,000	2.0
67-5-2	5	-130°	120,000	59,000	4.2
67-1-4	1	-145°	199,000	94,000	1.5
67-5-4	5	-145°	120,000	59,000	5.0
67-1-3	1	-160°	231,000	110,000	0
67-5-3	5	-160°	139,000	66,000	1.2
67-5-5	5	-160°	129,000	61,000	1.2
67-1-1	1	-196°	231,000	110,000	0.8
67-5-1	5	-196°	163,000	78,000	2.0
54-1-3	1	-130°	141,000	63,000	4.0
54-1-4	1	-130°	160,000	72,000	3.2
54-5-4	5	-130°	120,000	54,000	8.2
54-5-5	5	-130°	119,000	53,000	4.0
54-1-2	1	-196°	245,000	110,000	0
54-4-3	5	-196°	176,000	79,000	1.0

Although this difference in the values of the critical re-
solved shear stress suggests that Schadler's crystals were sub-
stantially purer than those used in the present experiments, a
comparison of the resistivity ratios between his and the crystal
used here does not appear to support this view. While Schadler
obtained a ratio of 2600-5400 (27), the five-pass crystals grown
for this experiment had a ratio of 14,000. (See Table 5.) A
possible explanation for this is that the type of residual impuri-
ties in these crystals was different because of the different
starting materials used or a difference in the efficiency of the
pumping system of the electron-beam furnace. Schadler's crystals
possibly contained more impurities of the type which contribute
strongly to resistivity, while the crystals in question probably
contained more impurities of the type which contribute more strong-
ly to mechanical strengthening.

In spite of the differences observed in yield stress and
ductility between specimens having one and five melting passes,
quantitative spectrographic and vacuum fusion analyses failed to
reveal any significant differences in impurities between crystals
which showed marked differences in mechanical behavior. Results
obtained in some of the tensile specimens tested are shown in
Table 8. Metallic elements which normally run below 1 ppm were
not analyzed.

Table 8

Impurity Analyses of Tungsten Single Crystal Tensiles
Tested at Sub-Zero Temperatures*

Specimen No.	No. of Melting Passes	Al	Fe	Si	Mg	Ni	Cu	O_2	H_2	N_2	C
54-1-2	1	2	8	5	50	4	1	20	5	1	-
54-1-4	1	5	2	12	13	4	1	3	4	.5	-
67-1-1	1	1	1	13	18	3	1	3	2	.3	-
54-5-3	5	4	8	5	28	4	1	24	3	3	-
54-5-1	5	2	2	9	16	3	1	4	6	.3	-
67-5-3	5	2	2	10	25	4	1	3	1	.7	-
67-1-3	-	-	-	-	-	-	-	-	-	-	19
67-5-5	-	-	-	-	-	-	-	-	-	-	7

* The carbon analyses were made by a conductometric method by
  National Research Corporation.

These data thus indicate that the difference in purity levels
must be very small and is below the precision of the current
analytical techniques.

33

Effect of Purity on Deformation Twinning

A marked difference in the frequency of deformation twinning between specimens of two purity levels was observed. Twinning, as indicated by load drops accompanied by audible clicking, was observed in all the five-pass specimens cut from both crystals 54 and 67 and tested at -130°C, -145°C and -160°C (Fig.14). In general, two or three small load drops occurred in each of the five-pass specimens at stress levels well below the microscopic proportional limit. The load-elongation curve of a five-pass specimen which had an exceptionally large amount of twinning is shown in Fig. 15. Among the seven tests made on the one-pass specimens, however, twinning was not observed (except specimen 67-1-4 as shown in Fig. 14), since there were no load drops or audible clicking. Since the specimens having a different number of zone-melting passes cut from each crystal had the same orientation, the possibility that the observed difference in the frequency of twinning between crystals having one and five zone-melting passes was due to an orientation effect could be ruled out. These results thus indicate that increasing the overall purity by additional zone-melting passes facilitates deformation twinning.

That the purer crystals twinned more readily than the less pure crystals was also confirmed by metallographic examination on deformed specimens. Twins were positively identified in the five-pass specimens but were not found in any of the one-pass specimens remote from the fracture surface for which load drops were absent. Typical twins in a five-pass specimen are shown in Fig. 16. (Note that the short segments indicated by arrows in Fig. 16 were actually closely-spaced dislocation etch pits. Possibly these were accommodation boundaries similar to those frequently observed in zinc crystals (43).

Since twins on or near the cleavage surfaces were often observed, it was necessary to ensure that at least some of the twins observed in the five-pass specimens after fracture were formed during deformation, and that not all the twins were nucleated by the cleavage crack. For this reason an additional five-pass specimen was strained until load drops accompanied by audible clicking occurred; and it was then unloaded prior to fracture. After sectioning, metallographic examination again revealed the presence of twins. This observation was confirmation that load drops accompanied by audible clicking observed during testing of the five-pass specimens were indeed due to the formation of twins.

Dependence of Twinning on Temperature

For all the five-pass specimens tested, an unusual dependence of twinning on test temperature was found. Twinning occurred only within an optimum temperature range and did not increase continuously with decrease in test temperature as has been commonly observed in other b.c.c. metals (44). Twinning occurred in specimens cut
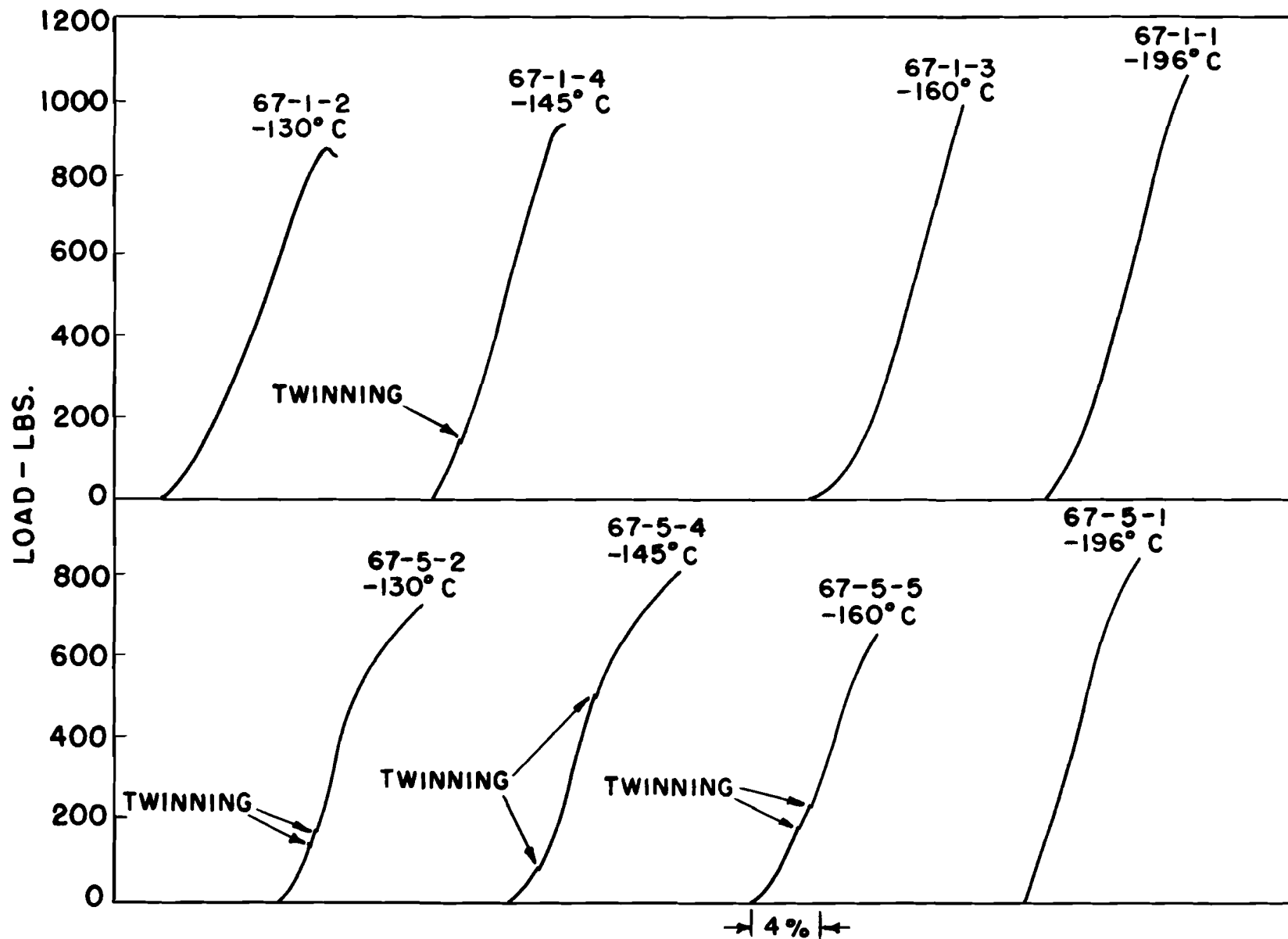
FIG. 14 LOAD VS. ELONGATION OF TUNGSTEN SINGLE CRYSTALS
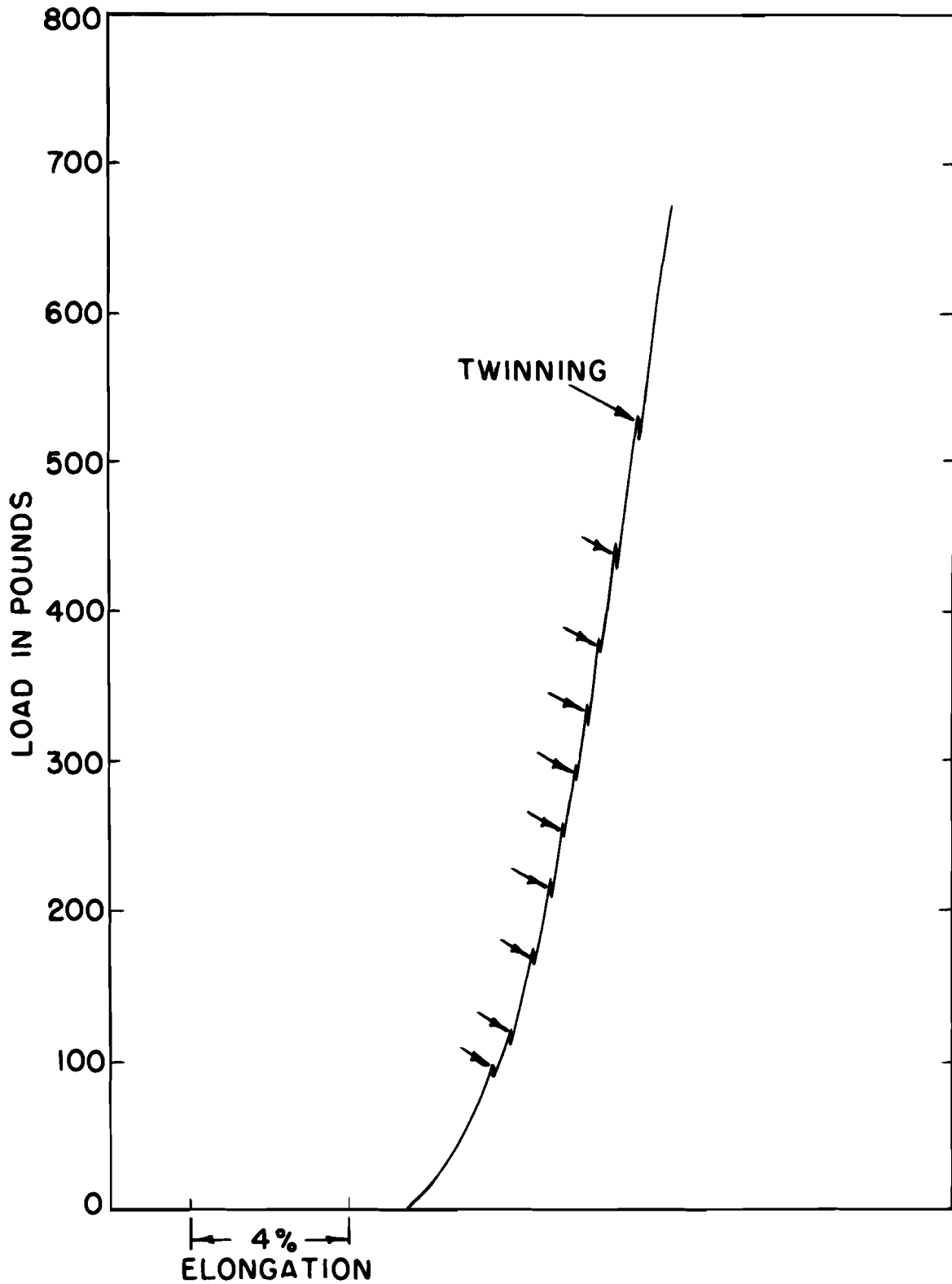
FIG. 15 SPECIMEN 71-5-8 PULLED AT -178°C; ARROWS
INDICATE TWINNING.

36

Fig. 16   Deformation Twins in Tungsten
           Single Crystals as Revealed
           by Polishing and Etching - 500X

from crystals 60 and 61 and tested at temperatures from -95°C to -160°C and in specimens cut from crystals 71 and 73 tested at temperatures from -100°C to -178°C. However, twinning did not occur during deformation of all specimens at -196°C, as indicated by the absence of load drops (see Figs. 11 and 14).

The absence of twinning in specimens which showed no load drops was also ~confirmed by sectioning a deformed specimen prior to fracture. These results thus gave confidence in the conclusion based on the load-elongation curves that twinning occurred only within an optimum range of test temperature.

Discussion

The present experiments have shown that, in spite of the small difference in purity between crystals which had one and five zone-melting passes, increasing the purity by additional zone-melting passes lowered the yield stress and facilitated deformation twinning. Furthermore, the purer crystals exhibited an unusual dependence of twinning on test temperature such that twinning occurred only within an optimum temperature range. The following discusses the various mechanisms which might possibly explain these observations.

Effect of Purity on Yielding

The question to be answered is how a small difference in purity levels could lead to as much as 57% difference in yield stress, whereas the total difference in impurities, as suggested by the impurity analyses, was probably less than 100 ppm. It is difficult to ascertain the exact mechanism of strengthening by impurities observed in the present experiments, since the controlling mechanism of yielding and plastic flow in a pure b.c.c. metal has not yet been established. Nevertheless, several possible interpretations of the present experimental results can be discussed.

The higher yield stress of the less pure crystals could be caused by: (1) the classical Cottrell atmosphere of interstitial impurity atoms, (2) pinning of dislocations by random solute atoms, particularly of the interstitial type, (3) interaction of moving dislocations with interstitial impurity atoms by the Snoek effect of ordering of the solute atoms, (4) an increase in the density of jogs along dislocations frozen-in upon cooling from the melt, (5) the creation of dislocation dipoles or trails of point defects by cross-slip of screw dislocations, or (6) other mechanisms such as the interaction of dislocations with submicroscopic precipitates.

The observed increase in yield stress in the less pure crystals cannot be attributed entirely to the pinning of dislocations by a Cottrell atmosphere. The classical model of tearing-off of dislocations from a Cottrell atmosphere requires that once the dislocations are unlocked from the solute atoms, i.e., in the plastic

38

range, the flow stress becomes relatively insensitive to impurities. However, the experimental results show that both the yield stress and flow stress were raised in the less pure crystals by approximately the same amount (see Fig.14). It is therefore concluded that Cottrell locking cannot be the controlling mechanism responsible for the differences in the yield stress and flow stress observed between crystals of different purity levels.

Since interstitial impurity atoms are known to have a high binding energy with dislocations in a b.c.c. crystal, e.g. the binding energy of a carbon atom with a screw dislocation in tungsten is estimated to be 0.87 eV (see Appendix A at the end of this section), it is conceivable that a sufficient amount of interstitial solute atoms distributed at random might cause an appreciable strengthening effect. Based on a calculation presented in Appendix B, it is believed that the interaction of random impurity atoms with dislocations alone could not account for the observed differences in strength between crystals of two purity levels. The expected difference in tensile stress between crystals having zero and 50 wt. ppm of carbon atoms in random solid solution is only 3-4 x 10^3 psi. This is one order of magnitude smaller than the observed difference in yield stress between crystals of two purity levels. Furthermore, the fraction of impurities expected to be distributed at random is very small for crystals which were furnace-cooled and then aged at 600°C.

The third possible mechanism which could account for the higher stress of the less pure crystals is the Snoek-type interaction of interstitial impurity atoms with moving dislocations, i.e., the ordering of the interstitial solute atoms by the stress field of a dislocation as proposed by Schoeck and Seeger (45). It is estimated in Appendix C that the increase in tensile stress caused by the Snoek-type of ordering of carbon atoms in tungsten is approximately 3 x 10^7 psi/wt. % of carbon. Therefore, in order to account for a difference of 120,000 psi in yield stress observed experimentally between crystals of two purity levels (see Table 7), a difference of 40 wt. ppm of carbon is necessary. Although the difference in carbon between crystals of one and five zone-melting passes was found to be 12 ppm, it is conceivable that the true difference was somewhat higher in view of the limited number of analyses made. The ordering mechanism of Schoeck and Seeger (45) has one attractive feature in explaining the present experimental results: that is, the stress due to ordering is independent of temperature. Although the range of test temperatures used was rather limited, the data in Table 7 do suggest that the difference in yield stress between crystals of two purity levels was relatively constant at all test temperatures.

The difference in yield stress and flow stress observed in crystals of two purity levels can also be explained with the assumption that the yield stress at low temperatures is primarily controlled by the stress required to generate point defects by the

non-conservative motion of jogs along screw dislocations as proposed by Schoeck (46). It is conceivable that as a result of the segregation of impurity atoms along dislocations in a less pure crystal a higher density of jogs is frozen-in from the melt. Although thermodynamically most of the impurity atoms are not expected to segregate along dislocations at high temperatures, an appreciable amount of segregation can still occur even at temperatures close to the melting point. For example, kT at the melting point of tungsten is about 0.3 eV, which is smaller than the binding energy of 0.87 eV estimated for a carbon atom with a screw dislocation in tungsten. A rough estimate can be made on the average spacing between jogs necessary to account for the observed yield stress. As shown in Appendix D, an average spacing between jogs of 25b and of 17b, where b is the Burgers vector, could account for the observed yield stress of the five-pass and one-pass crystals, respectively.

Aside from the four possible mechanisms discussed in the preceding paragraphs, the possibility that impurities may affect the cross-slip of screw dislocations must also be considered. Recent work by transmission electron microscopy has shown that in b.c.c. metals screw dislocations frequently undergo cross-slip (47). When a screw dislocation undergoes cross-slip, jogs are created and, depending on their size, a trail of point defects or dislocation dipoles of opposite sign are left behind the moving screw dislocation (48,49). It is conceivable that the higher concentration of impurities in the less pure crystals might affect the cross-slip of screw dislocations as follows: In a less pure crystal more screw dislocations are strongly locked by impurity atoms, so that a moving screw dislocation has a higher probability of meeting a locked screw dislocation. This induces cross-slip of the moving screw in order that its motion may continue. The jogs on the screw dislocation after cross-slip will create a drag on the moving screw because of the additional work which must be expended in creating trails of point defects or dislocation dipoles. Unless "pinching-off" occurs, the drag on the moving screw will greatly reduce its velocity so that a higher applied stress will be required in order to move the screw at a velocity imposed by the rate of extension of the specimen.

A rough estimate can be made of the additional density of super-jogs required to yield 120,000 psi of tensile stress, which was the difference observed between crystals of two purity levels. As shown in Appendix E, the additional density of jogs required is ~6 x 10^4 per centimeter of dislocation. Jogs of this order of magnitude have actually been found in silicon ferrite deformed 1% in compression (50). It thus appears that the cross-slip mechanism is a plausible explanation of the present experimental results, so that further work with transmission electron microscopy is highly desirable.

40

Among the various mechanisms of strengthening by solute impurity atoms discussed in the preceding paragraphs, calculations have shown that, for the difference in purity levels between the one-pass and five-pass crystals investigated in the present experiments, the following mechanisms can increase the yield stress to the same order of magnitude observed experimentally: Snoek-type of ordering of interstitial solute atoms in the stress field of a dislocation, generation of point defects by jogs in moving screw dislocations, and the creation of trails of edge dislocation dipoles by super-jogs in moving screw dislocations. It is conceivable that all these mechanisms may be operating simultaneously and it is not possible to decide which of these is the dominating mechanism.

A number of experiments can be performed to elucidate these mechanisms further. For example, for the Snoek-type of ordering of interstitial solute atoms, the yield stress is expected to be directly proportional to the concentration of the interstitial atoms in solution. Furthermore, the increase in yield stress due to ordering of additional solute atoms should be temperature independent. On the other hand, if the yield stress is controlled by the generation of point defects by jogs along dislocations frozen-in from the melt where the jogs are too small to be resolved by transmission electron microscopy, then the increase in residual resistivity for a given amount of deformation should be appreciably higher in a less pure crystal than that in a purer crystal containing less jogs frozen-in from the melt. Finally, if the creation of edge dislocation dipoles is the dominating mechanism, the dipoles should be readily visible in transmission electron microscopy.

Effect of Purity on Deformation Twinning

The present experiments have shown unambiguously that increasing the overall purity by additional zone-melting passes facilitated deformation twinning in tungsten crystals. In view of the lack of detectable differences in impurities by analyses between crystals which have one and five melting passes, the specific impurities responsible for the difference in the twinning behavior are not known. Recently Lawley et al (39) have found a similar twinning behavior in molybdenum single crystals grown by electron-beam zone-melting. Twinning, as suggested by load drops with audible clicking, occurred only in crystals with six zone-melting passes, but not in crystals with one or three melting passes. These results thus suggest that the increase in the ease of deformation twinning with increase in the overall purity is not only a general behavior for the Group Va metals, but also for the Group VIa metals as well.

In spite of the overwhelming evidence in various b.c.c. metals that purification facilitates deformation twinning, speculation on the mechanism by which this can occur is not available in the literature. In view of the fact that both yield stress and flow stress depend strongly on a small amount of residual impurities, one is

tempted to speculate as follows: At the tip of a deformation twin which is usually lenticular in shape, a large amount of localized slip is necessary in order to accommodate the high stresses set up at the tip. This localized slip may require the operation of many slip systems and extensive cross-slip of screw dislocations. In a crystal of very high purity, twinning is facilitated because of the relative ease in attaining a large amount of localized accommodation slip. On the other hand, in a less pure crystal, accommodation slip is much more difficult because of the higher stresses required to operate dislocation sources and to move dislocations, so that twinning is suppressed. On this basis, one can also explain the suppression of twinning in tantalum and columbium by the addition of oxygen. That is, when a sufficient concentration of oxygen is added, slip accommodation becomes difficult as a result of pinning of dislocations and twinning is suppressed.

Dependence of Twinning on Temperature

The present experiments have also revealed an unusual dependence of twinning on temperature such that twinning occurred only within an optimum temperature range. The only metal in which twins are formed more easily at high temperatures than at low temperatures is magnesium (51). These data thus show that twins are not always formed more easily at low temperatures than at high temperatures as has been commonly observed in other b.c.c. metals and assumed as a rule.

One may speculate on the unusual dependence of twinning on test temperature as follows: Twinning and slip may be regarded as competitive processes. The dominating process at a given test temperature is that which requires the lower stress. A schematic of the dependence of yield stress and twinning stress on temperature which could account for the observed behavior is depicted in Fig. 17, in which the linear variation of yield stress with temperature has been found experimentally (see Fig.12). At temperatures between T_1 and T_2 twinning is favored over slip, because in this range the stress required for twinning is less than that for slip. On this basis the effect of purity on twinning can be rationalized as a result of a relative shift of the two curves in Fig.17. Therefore, for a small change in purity, twins can also form in tungsten at room temperature (41) or higher (52).

The reason that the unusual dependence of twinning on temperature has not been observed in any other b.c.c. metals is considered to be the very high purity achieved in tungsten crystals as compared with other metals. Since purification by electron-beam melting is mostly the result of vacuum distillation and since tungsten has the highest melting point among metals, purification is expected to be most extensive in tungsten. Evidence in support of this conclusion is that, among all the refractory metals purified
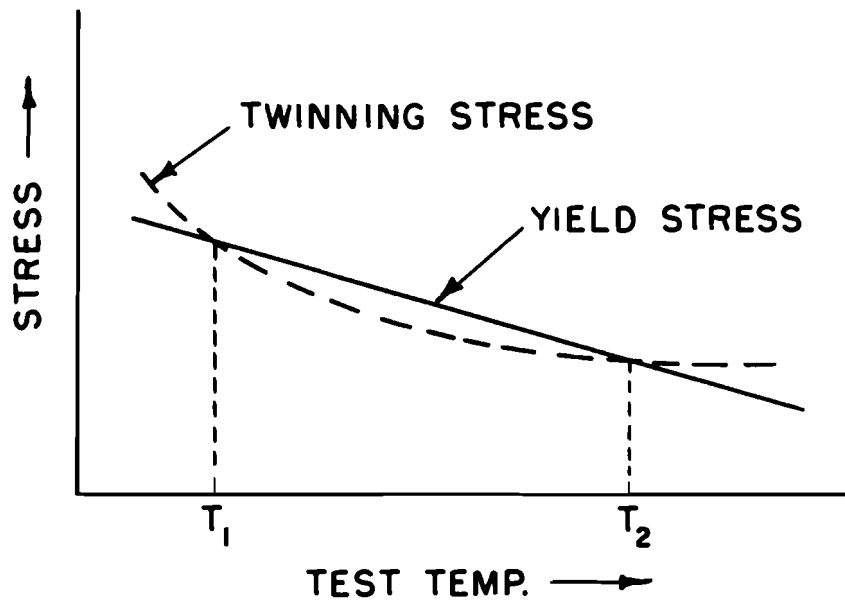
FIG. 17 SCHEMATIC DRAWINGS OF THE DEPENDENCE OF YIELD
STRESS AND TWINNING STRESS ON TEST TEMPERATURE
FOR SINGLE CRYSTALS OF HIGH PURITY.

by electron-beam zone-melting, the tungsten crystals grown for the present experiments had the highest residual resistivity ratios.

Appendix

A. The interaction energy, U, of an interstitial solute atom with a screw dislocation in a b.c.c. crystal is given by: (53)

$$U = A \frac{\cos \phi}{r}, \qquad \text{where } r > b,$$

and where

$$A = \frac{\sqrt{2}}{3\pi} b \cdot G \cdot a^3 (\epsilon_1 - \epsilon_2)$$

where ϕ = 60, 180 and 300 degrees are the three equivalent positions of lowest energy, r is the distance from the dislocation line to the solute atom, b is the Burgers vector = 1/2 $\sqrt{3}$a, a is the lattice parameter, ϵ_1 and ϵ_2 are the principal strain of the unit cell caused by the solute atom, and G is the anisotropic shear modulus 1/2 $(C_{11} - C_{12})$.

For tungsten b = 2.734 $\overset{\circ}{A}$, a = 3.158 $\overset{\circ}{A}$, and 1/2 $(C_{11} - C_{12})$ = 1.6 x 10^{12} dynes/cm^2 (54). Assuming that the distortion created by a carbon atom is inversely proportional to the lattice parameter, one can use values of ϵ_1 and ϵ_2 for carbon in iron multiplied by 0.9, since the lattice parameter of tungsten is about 10% larger than that of iron. Values for ϵ_1 and ϵ_2 for carbon in iron are 0.38 and -0.026, respectively. Using these values one finds that for carbon in tungsten:

$$A \cong 7.8 \times 10^{-20} \text{ DYNE cm}^{-2}$$

$$U \cong 0.87 \text{ eV} \qquad \text{WHEN} \quad r \approx b$$

B. Cracknell and Petch (55) have derived the following equation for the tensile stress σ_0 due to the interaction of dislocations with random interstitial solute atoms:

$$\sigma_0 = \frac{N^{11/9}}{(\alpha \mu)^{1/3} b^{5/3}} \left[\frac{16 A}{\pi} \ln \left(\frac{1}{2 r N^{1/3}} \right) \right]^{4/3}$$

where N is the number of interstitial solute atoms per cm^3,

$$\alpha = 1/2, \qquad r = b, \mu$$

the shear modules, and A is given in Appendix A.

For 50 weight ppm of carbon in tungsten, $N = 48.3 \times 10^{18}$ carbon atoms per cubic centimeter of tungsten. Using values obtained in Appendix A, one calculates that the increase in tensile stress σ_0 due to 50 weight ppm of carbon is $\sim 2.2 \times 10^8$ dynes/cm^2 or 3,200 psi.

C. Schoeck and Seeger (45) have derived the following equation for the stress required to move a dislocation around which ordering of the Snoek-type by interstitial solute atoms takes place. The shear stress τ to move a screw dislocation in a crystal containing an atomic fraction p of interstitial solute atoms is:

$$\tau = \kappa \frac{\rho A}{2a^3 b} \quad ,$$

where

$$\kappa = 2\pi \left[1.1 + \ln \left(\frac{L k T}{A} \right) \right]$$

L is the cut-off radius $\sim 10^{-4}$ cm. The authors pointed out that the temperature dependence of the elastic constants in A is to a large extent balanced by the temperature dependence in the logarithmic term, so that the stress is practically independent of temperature.

Using the value of A computed in Appendix A one calculates $\kappa \cong 25$ for carbon in tungsten and $\tau \cong 9.8 \times 10^5$ psi per atomic % of carbon or 1.5×10^7 psi per weight % of carbon in tungsten. Therefore, for an additional 50 weight ppm of carbon in tungsten, an increase in tensile stress of 1.5×10^5 psi is expected.

D. On the basis that the yield stress at low temperature is governed by the generation of point defects by jogs in moving dislocations, the stress without thermal activation is then: (46)

$$\sigma \cong \frac{E_f}{\lambda b^2}$$

where E_f is the energy of formation of a point defect and λ is the spacing between jogs. If vacancies are predominantly generated, the energy of formation E_f for a vacancy can be estimated from the relationship $E_s = E_f + E_m$ assuming that self-diffusion in tungsten occurs by the vacancy mechanism. E_s is the energy for self-diffusion and E_m is the energy for migration of a vacancy. For tungsten $E_s = 5.2$ eV (56) and $E_m = 1.7$ eV (57) so that $E_f = 3.5$ eV. If the yield stress at 4.2°K is assumed to be twice that at 78°K, as has been found to be the case for molybdenum single crystals, then at 4.2°K, the yield is expected to be $\sim$ 240,000 psi for the five-pass crystals and $\sim$ 360,000 psi for the one-pass crystals. The spacing between jogs necessary to give these stress values are then found to be $\sim$ 25b for the five-pass crystals and $\sim$ 17b for the one-pass crystals.

E. On the basis that the differences in yield stress and flow stress between crystals of different purity levels were caused by a higher density of super-jogs in the moving screw dislocations which left behind trails of edge dislocation dipoles in the less pure crystals, the difference in the density of these super-jogs between the crystals of different purity levels can be estimated from the difference in yield stress observed. Equating the work done in moving the dislocation over a distance b to the energy stored in the crystal by the generation of edge dislocation dipoles, one obtains the difference in the density of jogs Δn per centimeter of dislocation as: (48,50)

$$\Delta n \cong \frac{\Delta \tau b^2}{2E_e}$$

where $\Delta \tau$ is the difference in yield stress in shear, and E_e is the energy of an edge dislocation for a length b. The energy of an edge dislocation in tungsten has been estimated to be $\sim 9 \times 10^{-4}$ erg/cm (22) or 24.6×10^{-12} erg per length b. For the observed difference in yield stress in tension of 120,000 psi, $\Delta \tau$ in shear becomes $\sim 60,000$ psi or 41.4×10^8 dynes/cm^2, so that $\Delta n \cong 6 \times 10^4$ jogs per centimeter.

3. Deformation Behavior Between Room Temperature and 800°C.

It has been recognized for some time that impurities, especially interstitial impurities, affect the mechanical properties of b.c.c. metals. Cottrell and co-workers (58) were first to point out that the existence of a yield point in b.c.c. metals might be related to the locking of dislocations by interstitials. Nabarro (59) also concluded that not only impurity atmosphere locking of dislocations is important, but interstitial precipitates can affect the mechanical properties as well as a stress induced ordering of interstitials. With the advent of the electron beam floating zone melting process, single crystals of refractory metals including tungsten (2) became available. It was thus possible to study the effects of impurities on the mechanical properties of tungsten without having to consider the influence of grain boundaries as well. With the foregoing in mind the investigation of the deformation behavior of tungsten single crystals was extended from room temperature (R.T.) to 800°C.

Experimental Technique

Previously, the mechanical properties of high purity polycrystalline tungsten had been investigated rather extensively in this laboratory (1) and tensile tests were carried out at a strain

rate of 8.33×10^{-5} per sec. In order to be able to compare the results of the single crystal tensile tests with those of polycrystalline tungsten, the same strain rate was chosen. Single crystals having the same orientation (obtained by seeding) namely $\sim$[001] were used throughout. Tests were carried out in the temperature range from R.T. to 800°C and some special tests were made below R.T. When it turned out that tensiles of this orientation were rather brittle at the lower test temperatures, it was decided to conduct some compression tests in the temperature range from -196°C to 400°C as well. Strain rate in this case was 3.5×10^{-4} per sec. Unfortunately, the crystals available had a different orientation, $\sim$[510] . Carbon and vacuum fusion analyses were obtained throughout this investigation.

For the tensile tests, specimens having the dimensions shown in Fig. 18 were ground from 9-11 inch long single crystal rods. These rods had the standard 5 electron beam melting passes. After grinding, the specimens were electropolished in a 10% NaOH solution in order to remove the worked surface. Specimens in this state are designated as being in the "as melted" condition. Tests were carried out on a Baldwin-Emery SR-4 (Model FGT, capacity 50,000 pounds) and a Wiedmann-Baldwin SR-4 universal testing machine (capacity 20,000 pounds), respectively. Load was measured by SR-4 gaged load cells and strain by a Baldwin SRD2-1 deflectometer which measures the cross head travel, equaling the specimen extension.

Tests at and below R.T. were conducted in air. For tests below room temperature, specimens were enclosed in a cold chamber which used liquid nitrogen as a coolant. Tests higher than R.T. were made in an argon atmosphere. Two thermocouples were attached directly to the gage length of the tensile specimens. One thermocouple was used to operate a temperature controller whereas the other thermocouple served as a separate control and was therefore connected directly to a potentiometer. Elongations and reduction in area to fracture were computed from the measured dimensions of the specimens after testing. When a specimen shattered during testing, the elongation was taken from the recorded stress-strain curve.

The compression specimens were ground into cubes from a rod having 2 melting passes. (See Fig. 19.) Care was taken to grind the end faces exactly parallel and these in turn were exactly perpendicular to the specimen axis. The compression tests were performed in a tensile testing machine using a self-aligning jig designed by E.T. Wessels (60). The experimental arrangement at low temperatures has been previously described by Alers et al (61).

Tensile Test Results

Tensile test results for the temperature range from -77°C to 800°C are presented in Table 9 and the yield stress (.2% offset) as a function of test temperature is plotted in Fig. 20. A correspond-

.107" DIA.
.110" DIA.

195"
+.000"
−.002
DIA.

1/16"R.

1.000" +.005"
−.000"

.195"
+.000"
−.002"

.195"
+.000"
−.002"

1.500"
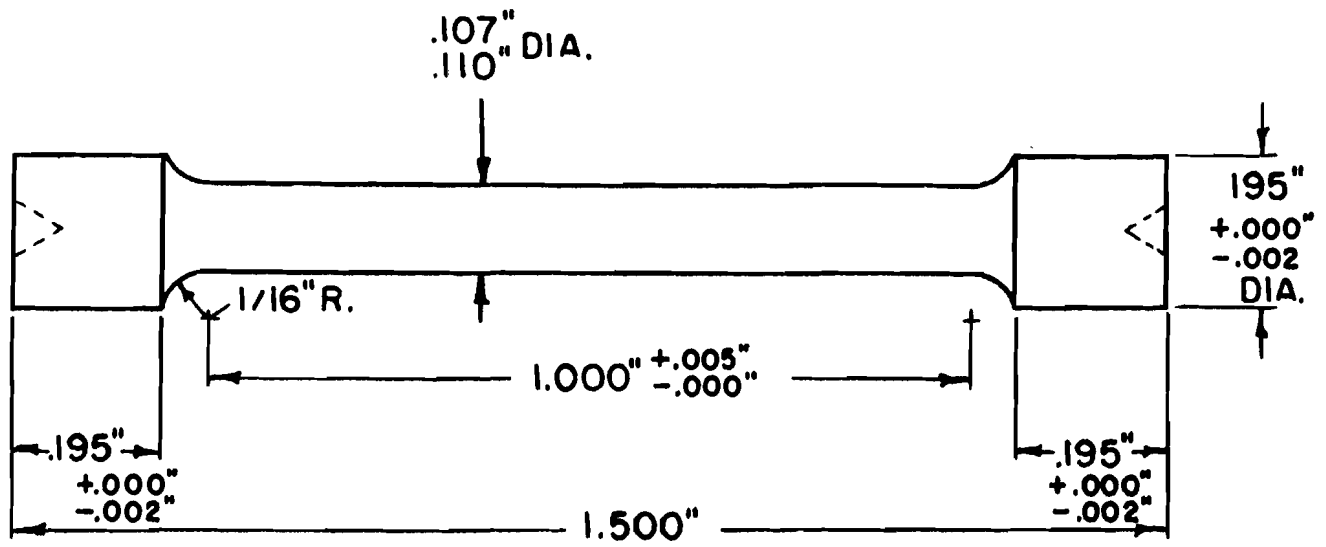
FIG. 18 SINGLE CRYSTAL TENSILE SPECIMEN

.145"

.145"

.350"
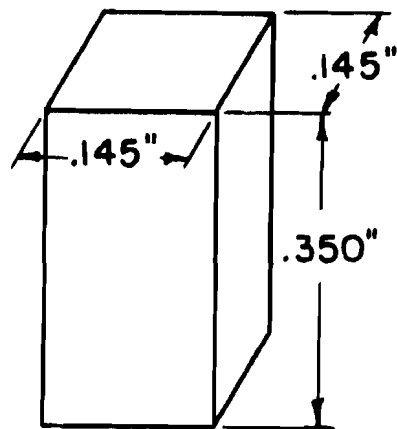
FIG. 19 SINGLE CRYSTAL COMPRESSION SPECIMEN.

48

Table 9
Results of Tensile Tests on Single Crystal
Tungsten Specimens (~[100]) Tested in the
Temperature Range from -77°C to 800°C

Speciman	Gage Diameter (Inches)	Testing Temp.	0.2% Offset Yield Stress PSI	Ultimate Stress PSI	Total Elong. in 1" (%)	Red. in Area (%)
UC72-5^{S+P}		-77°C	123,850	184,600	3.8^{S-E}	1.4^{S-E}
UC74-3$^+$	.091	-77°C	92,300	172,300	1+	4+
UC74-5$^+$	.092	-77°C	91,000	148,100	0+	0+
UC76-1^S	.091	-77°C	123,100	160,000	5.7^{S-E}	0.0^{S-E}
UC72-1^S	.091	-25°C	75,700	170,000	8.0^{S-E}	1.4^{S-E}
UC74-2$^+_*$	.090	-25°C	77,050	150,150	2+	9+
UC29-1*	.0975	RT	36,250	157,350	12	7-12
UC74-1$^+$	.093	RT	60,400	114,850	1+	4+
UC74-4	.092	RT	90,250	146,150	4	17-22
UC72-6^{S+P}	-	RT	90,750	160,750	8.7^{S-E}	1.4^{S-E}
UC29-2$^+$	.0950	50°C	75,050	115,500	6+	3+
UC29-3*	.0990	50°C	81,550	140,250	15	8-13
UC77-1	.092	50°C	90,250	143,600	2	19-24
UC29-4	.0980	100°C	70,400	124,000	25	36-41
UC29-5	.0990	150°C	61,700	99,100	26	31-36
UC29-6	.0980	150°C	63,850	101,600	27	37-42
UC63-1	.090	200°C	40,950	67,500	20	100Δ
UC63-2	.093	250°C	29,400	51,900	23	100Δ
UC63-3	.093	250°C	28,700	51,150	33	100Δ
UC63-4	.092	300°C	25,150	46,750	95	75-80
UC72-5^S	.091	300°C	-	-	-	-
UC72-6^S	.091	300°C	17,700	-	-	-
UC77-2	.0915	350°C	12,500	26,650	69	57-62
UC77-3^Y	.088	400°C	26,500^Y	29,300	100	58-63
UC77-4	.092	450°C	6,000	24,800	65	60-65
UC77-5^Y_A	.092	500°C	15,400^Y	24,500	61	57-62
UC77-6	.093	500°C	5,150$_S$	26,900	85	67-72
UC63-5^{S*}	.093	500°C	2,650^S	27,500	86	69-74

Table 9 (continued)

Speciman	Gage Diameter (Inches)	Testing Temp.	0.2% Offset Yield Stress PSI	Ultimate Stress PSI	Total Elong. in 1" (%)	Red. in Area (%)
UC76-2	.098	550°C	2,150	19,200	38	70-75
UC76-3	.098	600°C	2,400	18,400	49	71-76
UC76-4	.097	600°C	2,250	20,400	37	71-76
UC76-5	.097	650°C	2,350	16,750	62	69-74
UC72-2	.098	700°C	4,400	22,350	97	80-84
UC72-3	.098	700°C	3,950	22,750	104	80-84
UC72-4	.098	800°C	2,750	19,450	87	65-69

+) Specimen broken in fillet

Δ) Specimen necked down to knife-edge

*) Specimen broke into pieces upon fracturing

S) Reduced diameter in center of specimen to insure fracture in gage length

P) Plastically deformed about 4% at about 300°C, tested at temperature indicated

S-E)Elongation primarily in reduced section

S*) Slip resembling easy glide probably due to eccentricity of specimen

Y) Discontinuous yield point

A) Heated at 600°C for 3 hrs.

Tests were made in an Argon atmosphere at a strain rate of 8.33×10^{-5}/sec.
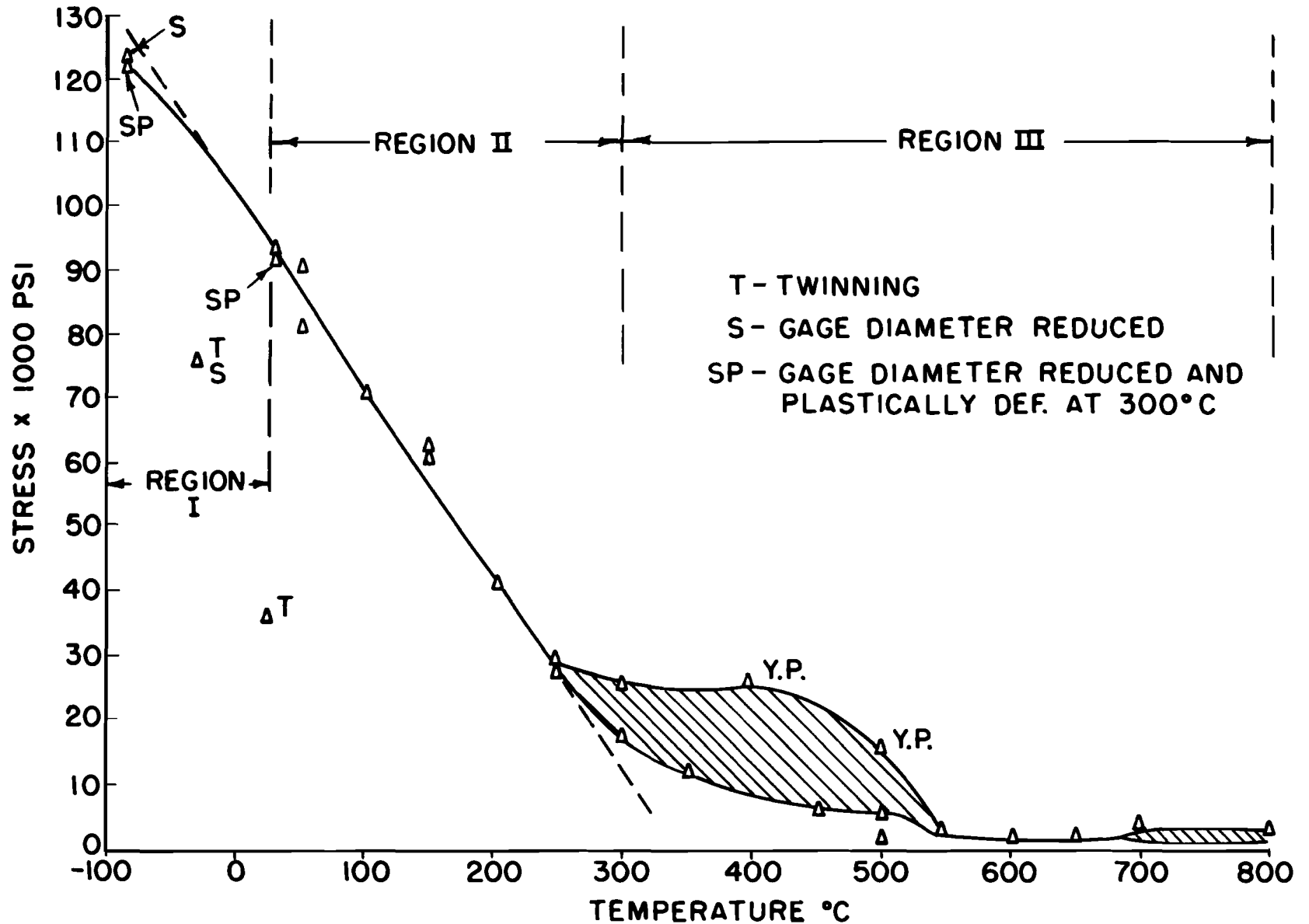
FIG. 20 .2% OFFSET YIELD STRESS OF SINGLE CRYSTAL TUNGSTEN ($\sim$[001]) AS A
FUNCTION OF TEMPERATURE. (STRAIN RATE 8.33 × 10^{-5}/SEC.)

ing plot of the proportional limit is shown in Fig. 21. All pertinent chemical, vacuum fusion, and carbon analyses are compiled in Table 10. Also listed in this table are the "as melted" hardness values of the single crystal rods from which the tensiles were ground. The data in this table are listed in such a manner that UC77-1 stands for rod UC77 and the 1 (one) designates the first tensile specimen ground from this rod at the position of the starting end of the zone.

From the data in Table 9 and the temperature dependence of the yield stress as shown in Fig. 20, it is apparent that one can conveniently separate the yield stress results into three characteristic regions: (I) a low temperature region from about -77°C to R.T. or 150°C, (II) a medium temperature region from R.T. to about 300°C, and (III) a higher temperature region from about 300°C to 800°C. This breakdown into three regions is somewhat arbitrary because several of the phenomena studied (e.g., twinning, mode of fracture and surface appearance) overlap the various regions.

Region I: Specimens tested at temperatures ranging from -77°C to R.T. had a marked tendency to twin and often failed prematurely (fillet breaks). The specimens, indicated by "T", had also serrated stress strain curves. Twinning was found to occur adjacent to the fracture area up to 150°C. Fig. 22 shows twins on a fracture surface of a specimen tested at R.T. and Fig. 23 shows a twin in a necked region of a specimen tested at 100°C.

To insure that fracture occurred within the gage length, some specimens (indicated by "S") were ground to a slightly smaller diameter before electropolishing. Some specimens (indicated by "S-P") which were ground to a smaller diameter first, were also plastically deformed about 4% (elongation) at 300°C and then tested at lower temperatures. This treatment, as has been shown by other investigators (62) for polycrystalline tungsten, suppresses twinning. Although twinning was not evident by serrations in the stress strain curves of the plastically deformed specimens, twins were noted upon metallographic examination of the surfaces after fracture. The yield stress measured was comparable to that of specimens having no prior plastic deformation at 300°C. In some instances, specimens which twinned and exhibited serrated stress-strain curves had a somewhat lower yield stress. It will be noted from Table 9 that some specimens which exhibited fillet breaks had elongations varying from 1-6%. However, since a fillet break makes a tensile test doubtful the yield stress of these specimens was not included in Fig. 20.

Slip markings in single crystal tungsten appear to be similar to those in other b.c.c. metals. This is especially true of the waviness and forkedness of slip lines when viewed in a plane perpendicular to the slip direction, and the striated appearance when viewed in a plane parallel to the slip direction. The appearance of the markings is, however, very temperature sensitive.

Table 10

Quantitative Spectrographic Analyses, Vacuum Fusion Analyses, Carbon Analyses, and Hardness Measurements of Specimens Used for Tensile Testing from -77-800°C

Quantitative Spectrographic Analyses (weight ppm)

Specimen	Al	Fe	Ni	Mg	Mn	Cu	Cr	Si
UC29-2	2	2	-*	28	-*	2	-*	36
UC63-1	2	6	2	24	-	2	-	18
UC63-2	1	5	1	10	-	2	-	4
UC63-4	4	2	2	22	-	10	-	30
UC63-5	30-44	4	1	14	-	1	-	43
UC72-4	2	3	-	15	-	-	-	36
UC74-3	3	4	-	17	-	-	-	23
UC74-4	3	2	-	31	-	11	-	20
UC76-3	1	<1	-	12	-	-	-	49
UC77-2	3	1	-	34	-	7	-	19
Poly Rod	6	51	<9	<3	2	-	-	14

Vacuum Fusion and Carbon Analyses (weight ppm) - Hardness Values

Disposition of Single Crystal Rod

	1	2	3	4	5	6

"as melted" ↑   ↑ finishing end
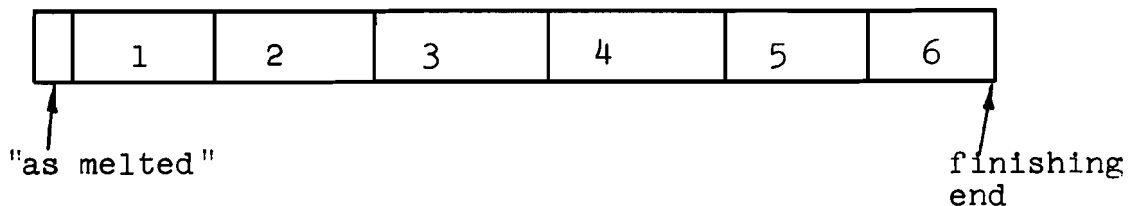
Crystal No. 29

Position	Test Temp.	C	O_2	N_2	H_2	Knoop (1 Kg scale)
As melted	-	N.D.	N.D.	N.D.	N.D.	355
1	RT	N.D.	8	1	.9	
2	50°C	16	N.D.	N.D.	N.D.	
3	50°C	N.D.	8	2	.9	
4	100°C	N.D.	8	4	.6	
5	150°C	20	N.D.	N.D.	N.D.	
6	150°C	N.D.	7	2	.6	

*-Not detected   ND - Not determined

53

Table 10 (continued)

Crystal No.63

Position	Test Temp.	C	O_2	N_2	H_2	Knoop (1 Kg scale)
As melted	–	N.D.	3	5	.6	364
1	200°C	N.D.	7	.7	2	
2	250°C	N.D.	4	1	.6	
3	250°C	31	12	4	.9	
4	300°C	34	N.D.	N.D.	N.D.	
5	400°C	44	N.D.	N.D.	N.D.	

Crystal No.77

Position	Test Temp.	C	O_2	N_2	H_2	Knoop (1 Kg scale)
As melted	–	N.D.	12	4	2	358
1	50°C	34	4	3	1	
2	350°C	41	4	.7	.9	
3	400°C	22	9	.8	.4	
4	450°C	38	3	.7	1	
5	500°C	24	5	10	.2	
6	Annealed at 600°C 3 hrs., tested at 500°C	29	10	15	2	

Crystal No.74

Position	Test Temp.	C	O_2	N_2	H_2	Knoop (1 Kg scale)
As melted	–	N.D.	21	2	4	354
1	RT	36	4	1	.9	
2	-25°C	24	3	2	1	
3	-77°C	N.D.	4	.7	1	
4	RT	N.D.	6	1	.3	
5	-77°C	26	6	3	.5	

Crystal No.72

Position	Test Temp.	C	O_2	N_2	H_2	Knoop (1 Kg scale)
As melted	–	14	6	11	4	388
1	-25°C	53				
2	700°C	35	14	6	.7	
3	700°C	39	31	6	.3	
4	800°C	40	13	5	.8	
5	-77°C	64				
6	RT	72				

Crystal No.76

Position	Test Temp.	C	O_2	N_2	H_2	Knoop (1 Kg scale)
As melted	–	N.D.	4	7	6	432
1	-77°C	72				
2	550°C	N.D.	8	2	2	
3	600°C	70	47	2	1	
4	600°C	72	9	7	.9	
5	650°C	55	51	24	.7	
Compression Specimens(Avg)-196°C - 400°C		16	7	.9	1.1	N.D.
High Purity Poly W Rod	150-500°C	10	4	7	4	N.D.

FIG. 21 PROPORTIONAL LIMIT OF SINGLE CRYSTAL (~[OOI])
AND POLYCRYSTALLINE TUNGSTEN IN TENSION AS
A FUNCTION OF TEMPERATURE, STRAIN RATE
8.33 × 10⁻⁵/SEC.

55

Fig. 22 Twins on Fracture Surface
of Single Crystal Tensile
Specimen Tested at 300°C
- 150X
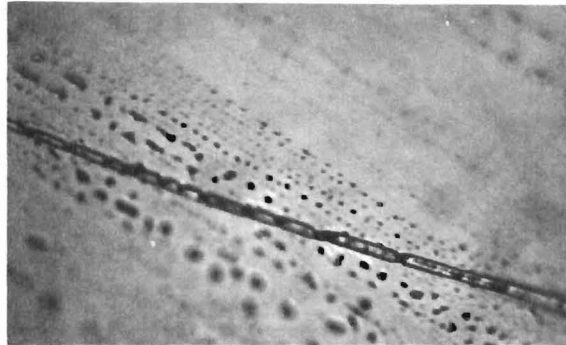
Fig. 23 Twins near the Necked Region
on the Cylindrical Surface of
a Single Crystal Tensile Specimen
Tested at 100°C - 500X

56

The waviness and forkedness of slip lines as found in other
b.c.c. metals was evident over the entire gage length for speci-
mens tested above 300°C and also in the necked region of specimens
deformed at 200°C and 250°C. However, below 200°C, twins and
markings similar to those shown in Figs. 24a and 24b were noted.

Region II: Aside from some scatter, the yield stress
decreased rapidly as the test temperature was increased from
about R.T. to 300°C, and this decrease can be approximated by a
straight line as shown in Fig. 20. A cleavage type fracture was
observed from -77°C up to 150°C. The cleavage fracture plane was
measured by X-ray diffraction and found to be [100] , the same as
in other b.c.c. metals. In some instances, tensiles tested at
-77°C, R.T., and 50°C shattered like glass.

If per cent R.A. or per cent elongation is plotted as a
function of test temperature, Fig. 25, it is noted that the ductile-
brittle transition temperature is about 150°C (taking about the
mid-point of the per cent R.A. curve). However, reduction in area
measurements are extremely difficult to perform on these small
specimens and are measured to within 5% at best. Some necking was
evident at about 100°C and specimens necked to a knife edge at
200°C and 250°C. The plastic deformation as deduced from tensile
tests in this region (200°C-250°C) is localized, whereas above
300°C and up to 800°C the plastic deformation is quite uniform.
Thus the curves for plastic strain shown in Fig. 25 give a rather
false impression with respect to ductility.

Region III: From about 300°C to 800°C, the scatter in yield
stress is high with some specimens exhibiting discontinuous yield-
ing, although most of the specimens were ground from the same single
crystal rod. Some liberties have been taken in drawing the two
curves (Fig. 20) in the temperature region from about 300°C-500°C -
one curve for those at a higher stress level generally exhibiting
discontinuous yielding, and another at the lower stress level.
Increase in yield stress is also noted from about 700°C-800°C.
These increases in yield stress have been found by other investi-
gators (63,64) in similar temperature regions.

Compression Test Results

The variation of the proportional limit and the variation of
the flow stress at 3% and 6% strain as a function of temperature
have been plotted in Fig. 26. Because of difficulties with align-
ment and end effects at high strains, only the flow stress up to
6% plastic deformation has been plotted. Proportional limits of
compression specimens, tensile specimens of single crystals and
tensile specimens of polycrystalline tungsten are compared in
Fig. 27.
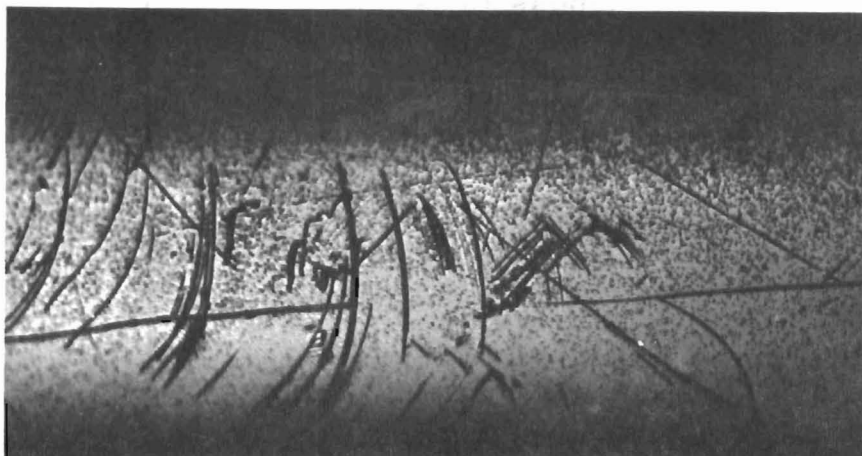
Fig. 24a. Surface Markings on a Tensile
           Specimen Tested at 150°C - Etched
           but not Polished - 150X
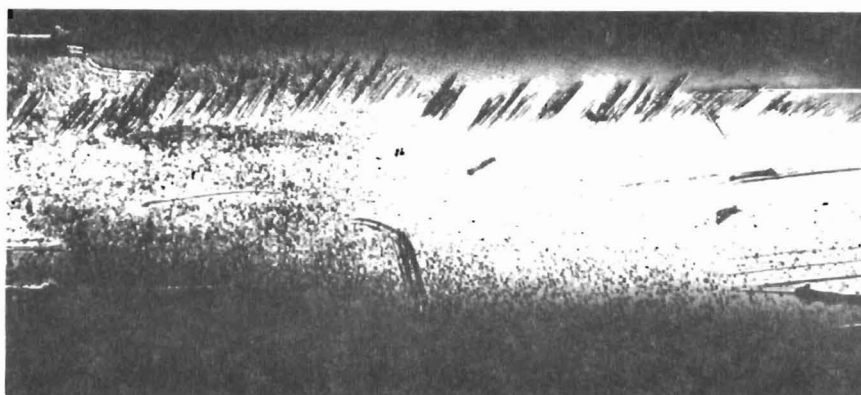
Fig. 24b. Surface Markings on a Tensile
           Specimen Tested at 100°C - Etched
           but not Polished - 100X
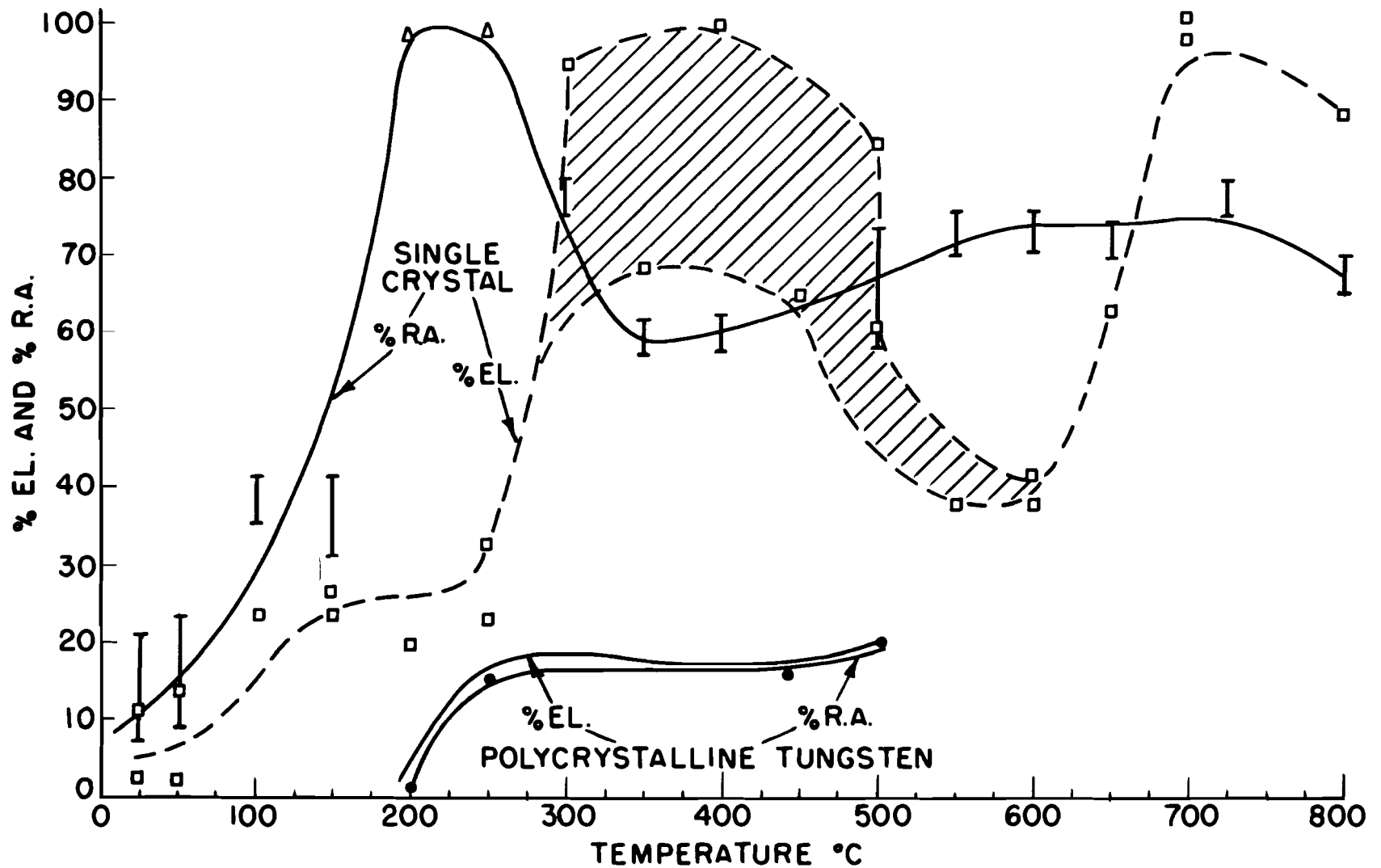
FIG. 25 PERCENT ELONGATION AND REDUCTION IN AREA OF SINGLE CRYSTAL
(~[OOI]) AND POLYCRYSTALLINE POWDER METALLURGY TUNGSTEN
AS A FUNCTION OF TEMPERATURE.
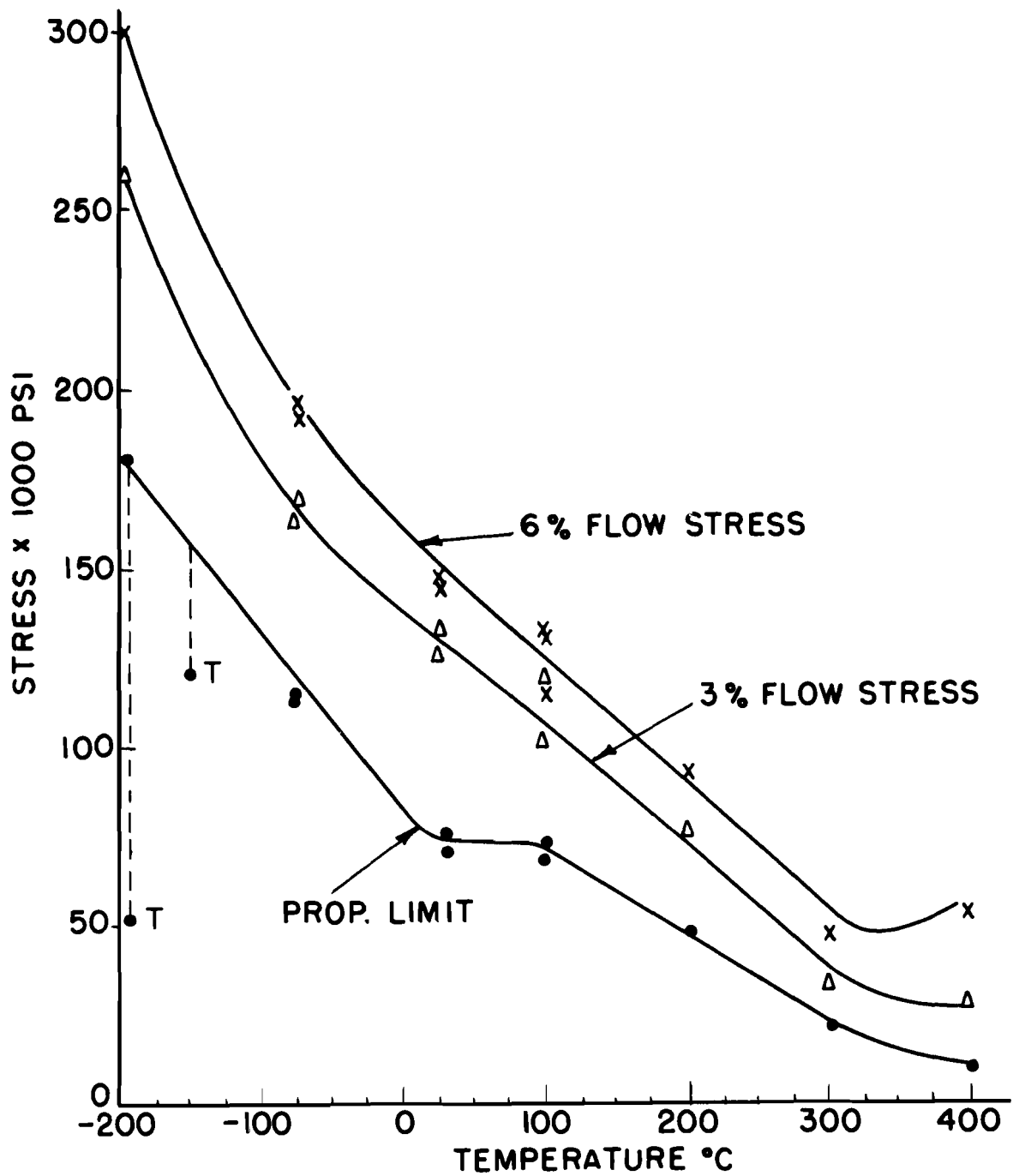
FIG. 26   PROPORTIONAL LIMIT AND FLOW STRESS OF
SINGLE CRYSTAL TUNGSTEN (~[501]) IN
COMPRESSION AS A FUNCTION OF TEMPERATURE.
(STRAIN RATE 3.5 × 10⁻⁴/SEC.)

60
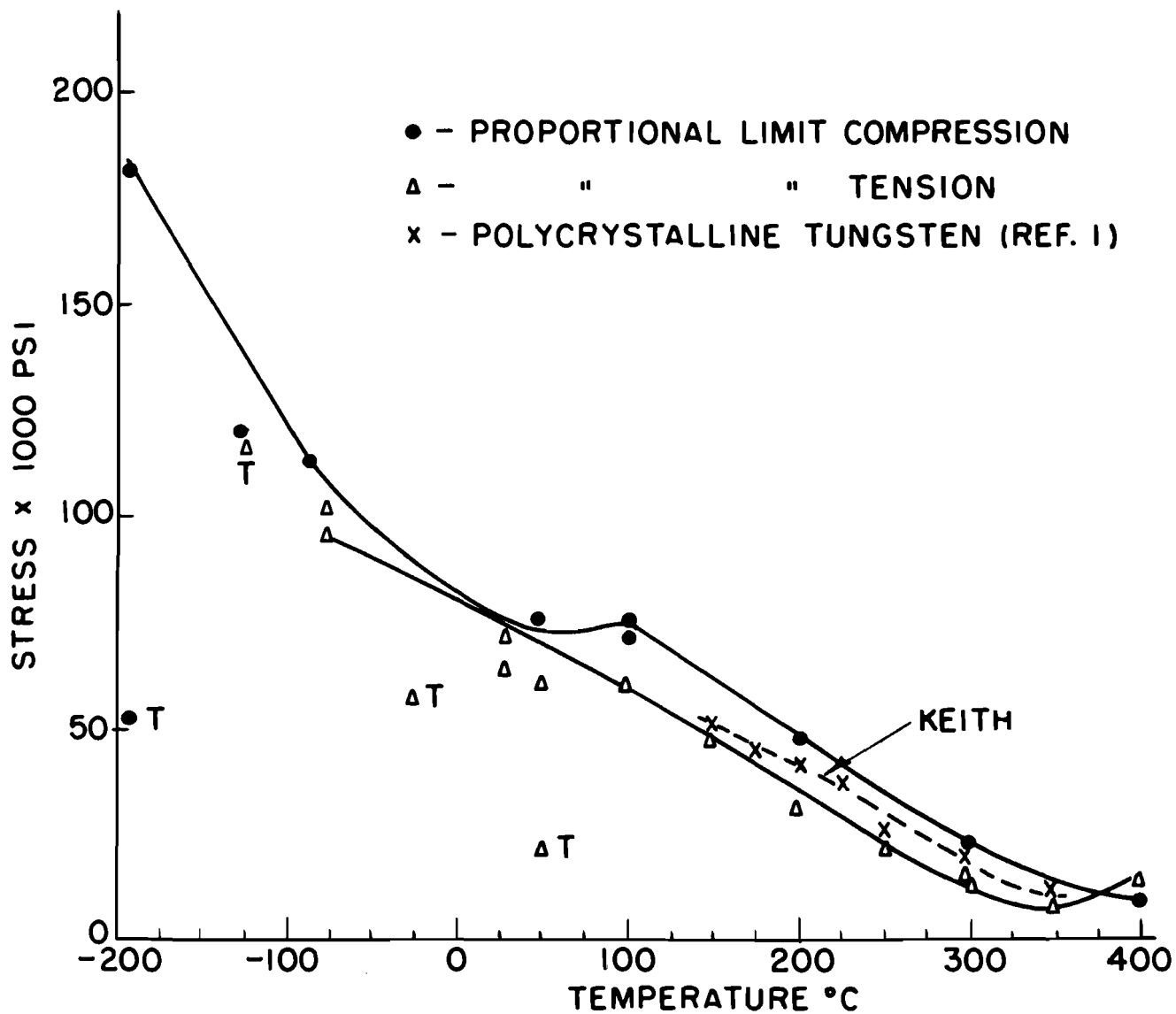
FIG. 27 PROPORTIONAL LIMIT OF SINGLE CRYSTAL (~[OOI]) IN
TENSION, SINGLE CRYSTAL (~[5IO]) IN COMPRESSION,
AND POLYCRYSTALLINE TUNGSTEN IN TENSION AS A
FUNCTION OF TEMPERATURE.

61

As can be seen in Fig. 26, a break occurs in the curve at about room temperature. The curves for 3% and 6% flow stress indicate a break in the curve also at about room temperature. At lower temperatures the proportional limit increases rather drastically. At -150°C and -196°C, serrated stress strain curves and twinning were noted (indicated by "T"). It must be mentioned, however, that a specimen which had a very high proportional limit at -196°C had no serrations in the stress strain curve, although metallographic examination of all specimens tested at -196°C, including this one, showed a profusion of twins.

Similar to the observation made in tensile testing, surface markings on the compression specimens exhibit a temperature dependence. From about 100°C to about 400°C, slip markings were evident. However, with decreasing temperatures to -77°C surface markings similar to those shown in Figs. 24a and 24b, and a few twins were noted. Below -77°C twinning occurred in profusion.

Discussion of Results

In the following, results will be discussed first in terms of the three temperature regions previously defined, and then on the basis of a comparison of single crystal tungsten versus polycrystalline tungsten. Finally, a summary of the present status of the experiment and the data will be presented.

Region I: The most outstanding characteristic of single crystal specimens tested in tension or compression in this region is the increased frequency of mechanical twinning with decreasing test temperature; this being associated with increasing brittleness and a substantial scatter of yield stress values. The yield stress or the proportional limit of b.c.c. metals at low temperatures are theoretically predicted to increase continuously with decreasing temperature (37,58). The results obtained indicate a deviation from theory in this respect (Figs. 28 and 29) and this deviation is attributed to the intervention of twinning.

Twinning as a mode of deformation has also been noted by Wolff (41) at room temperature for a single crystal having approximately the same orientation as used in this experiment. Erickson and Low (65) have suggested that for iron the low temperature region may be broken up into the three characteristic sections (a) slip, (b) slip followed by twinning, and (c) twinning. It is believed, however, that twinning and slip cannot be divorced from each other and such a distinct breakdown into separate sections was not apparent for tungsten. Twinning and slip are intimately related and, depending on the particular circumstances (as yet unknown), most probably one or the other is the predominant mode of deformation.

Aside from the stress concentration which may be necessary to nucleate a twin, it has become apparent that other twin or slip systems must operate within the matrix to accommodate a twin. As a
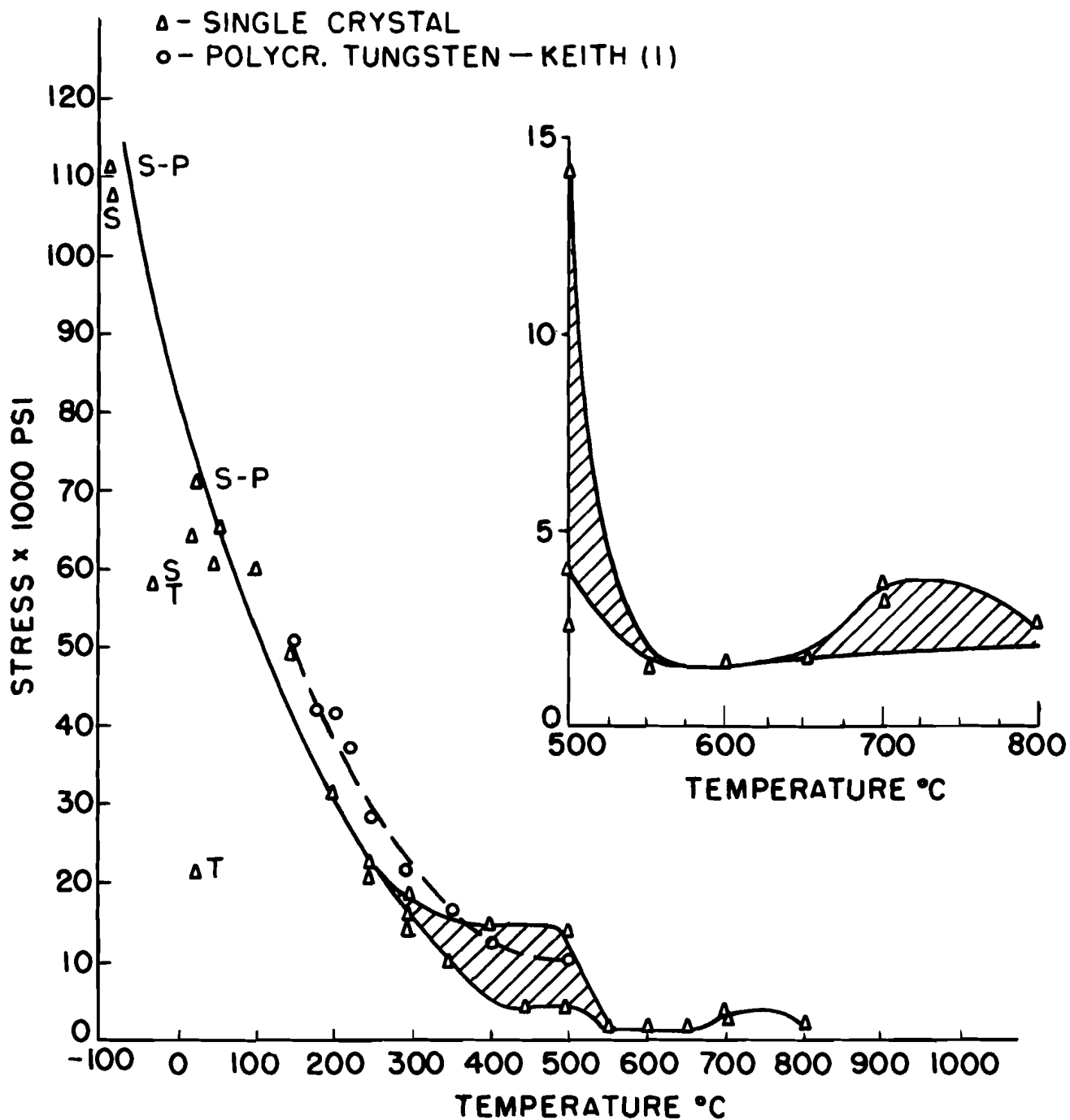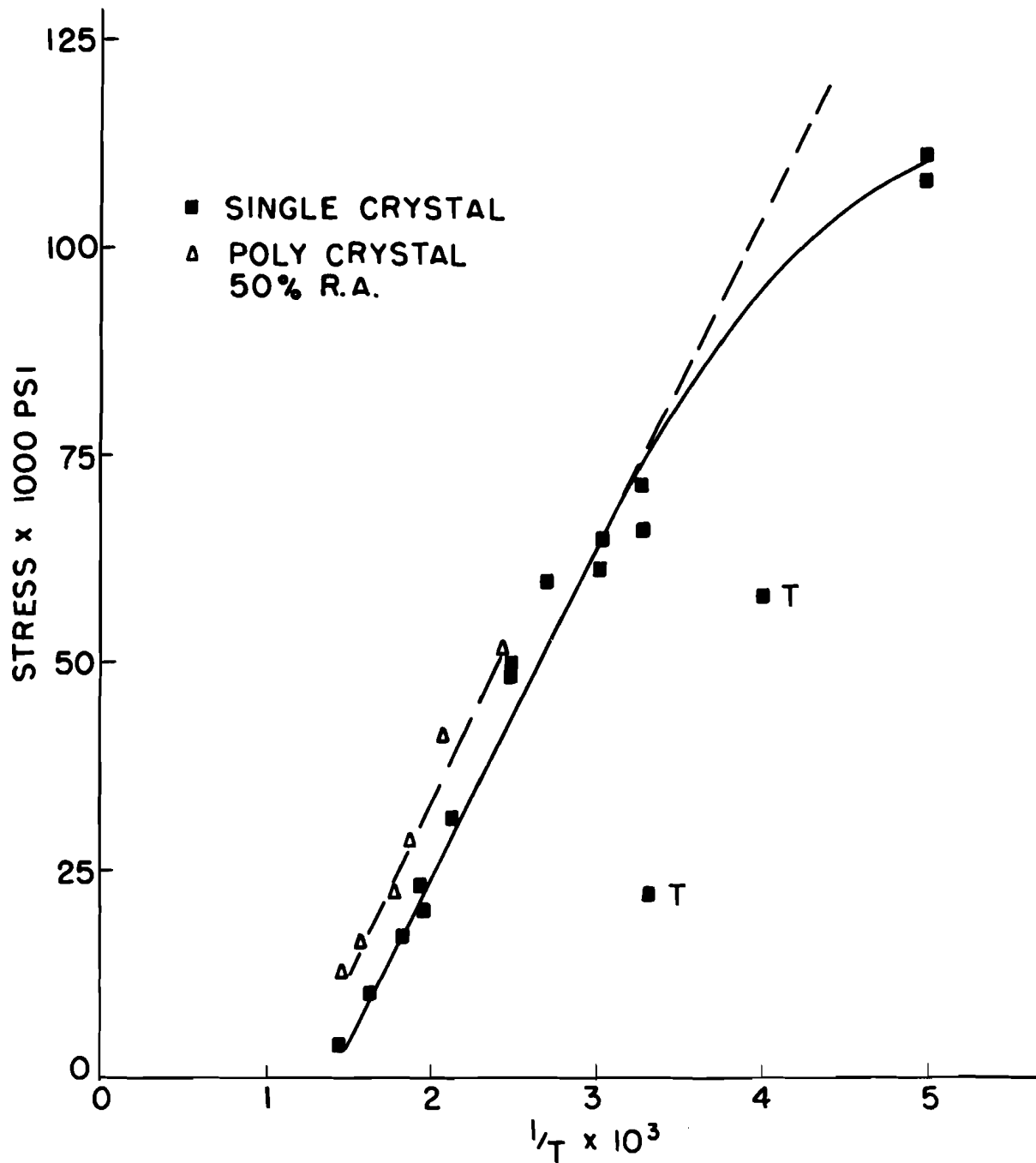
FIG. 28 PROPORTIONAL LIMIT OF SINGLE CRYSTAL AND
POLYCRYSTALLINE TUNGSTEN AS A FUNCTION OF
INVERSE TEMPERATURE. STRAIN RATE 8.33 × 10⁻⁵

63
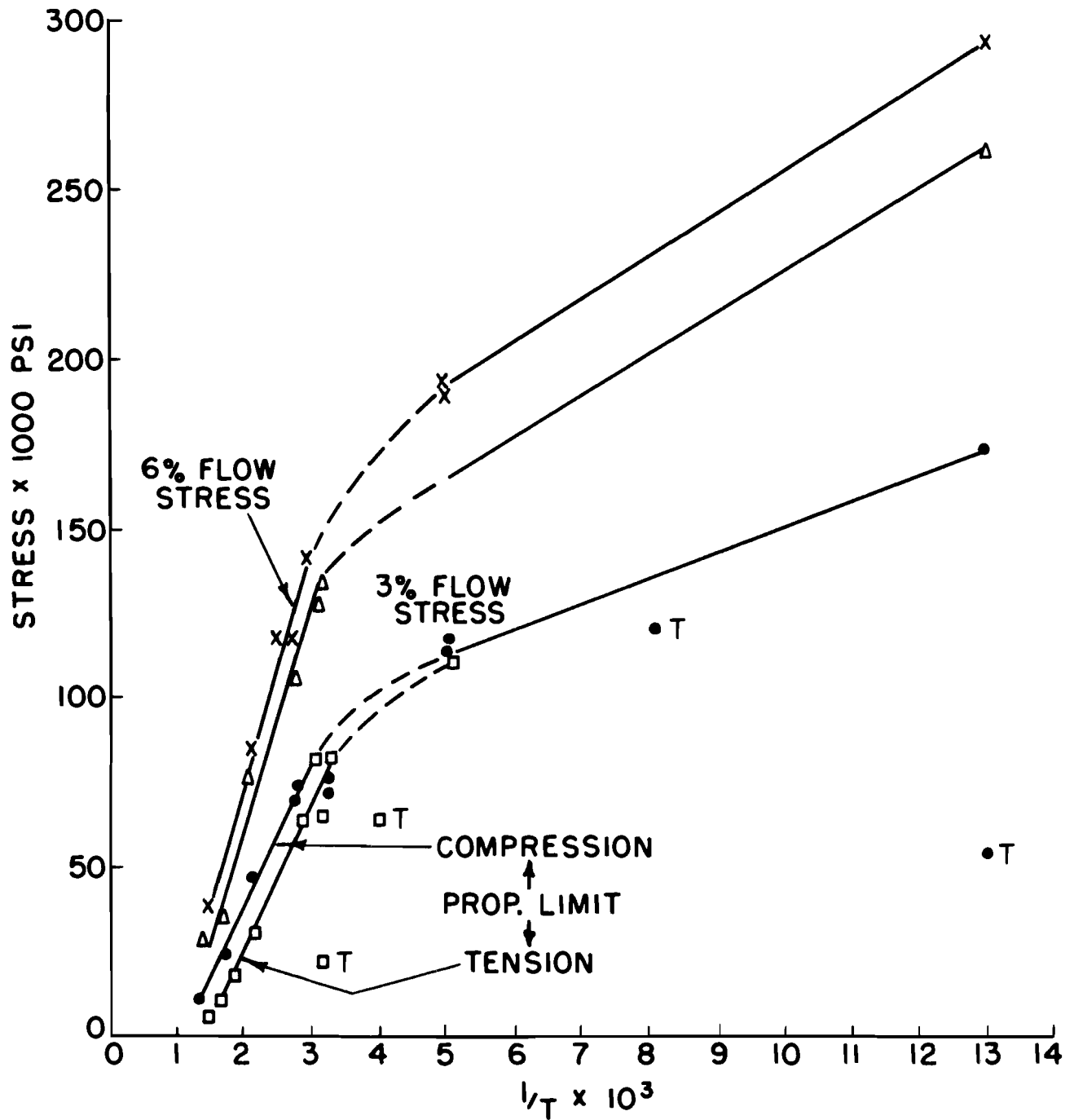
FIG. 29 PROPORTIONAL LIMIT AND FLOW STRESS OF SINGLE
CRYSTAL TUNGSTEN IN TENSION AND COMPRESSION
AS A FUNCTION OF INVERSE TEMPERATURE.

consequence of the complex deformation systems operating within tungsten during twinning, it may be rather difficult to determine the exact critical resolved shear stress for twinning. This may account for the notorious variation exhibited in the yield stress at lower test temperatures.

Although the specimens which were given a high temperature prestrain and then tested in Region I produced a high yield stress similar to the specimens which were not prestrained, twins were still evident upon metallographic examination. It is apparent that 4% prestrain at 300°C may not be enough to suppress twinning. This suggests for the higher stress levels of this region that plastic deformation may be initiated and predominated by slip followed by twinning. On the other hand, for those specimens without prestrain having somewhat lower stresses and indicating discontinuous yielding, plastic deformation may have been initiated by twinning followed by slip. It was, however, impossible to entirely distinguish one process from the other.

Since twinning and slip are intimately involved in the plastic deformation of single crystals of tungsten, it is believed that twinning in tungsten does not necessarily have to produce a discontinuous or serrated curve. This is indicated by one of the compression tests conducted at -196°C. Although twins were present in profusion throughout the gage length of this particular specimen, no drop in load or flow stress was noted on the curve. Erickson and Low (65) have made similar observations for iron at 20°K.

The inability to observe fine slip in Region I does not necessarily mean that slip does not occur. Aside from the coarse surface markings fine slip lines may be obscured. As in the case of iron, the ability to observe slip and suppress twinning may depend on the amount of plastic strain (4%) or the etching technique (66). In tungsten, as noted, 4% plastic deformation is not sufficient to suppress twinning.

Whether or not twinning can initiate brittle fracture is uncertain, but it appears that in single crystals of tungsten, brittleness is promoted by twinning. In support of this, one can cite the appearance of deformation twins adjacent to the surface of a cleavage fracture, the shattering of specimens when the temperature was lowered, the frequency of twins observed in the neighborhood of brittle fracture surfaces (also in the necked region of some specimens), and the formation of many cracks adjacent to and within twins.

Whether or not impurities have an important effect on twinning and subsequently brittleness, cannot be answered unambiguously from the test results. Numerous impurity effects, such as that on accommodation slip, etc., can be envisioned. The single crystals used for tests in this investigation are certainly not impurity free.

Carbon, in particular, varied between 20-70 ppm in 5 pass single crystals, and since Goldschmidt (23) found numerous twins in carbon dosed polycrystalline tungsten samples, it is conceivable that carbon has a pronounced effect on twinning. There is other evidence that interstitials can promote twinning in b.c.c. metals (30,67). For high purity iron it has been noted that at about 100°K-140°K the yield stress is somewhat lower than for impure iron, and that this occurs about in the same temperature region where twinning is noted. Conrad (38) has attributed this to an impurity effect rather than a twinning effect. One cannot exclude the possibility that twinning may depend on the state of the interstitial impurities. Since internal friction peaks are present in tungsten, it is apparent that some ordering exists for these solid solutions. What effect ordering has on twinning is still not known.

Region II: The behavior of the yield stress in this temperature region when plotted as a function of the inverse of temperature can be represented by a straight line and seems thus to agree with the Fisher treatment (37) of the Cottrell and Bilby theory (53), Figs. 28 and 29. As will also be noted in Fig. 29, the temperature dependence of the flow stress (at 3% and 6% plastic deformation) in compression is similar to that of the yield stress but with a somewhat steeper slope. No discontinuous yielding was observed in this temperature region.

According to Cottrell (68), at high temperatures serrations are expected to occur due to the diffusion, reforming and re-anchoring of the interstitial impurity atmospheres. Using the following relationship between strain rate $\dot{\epsilon}$, and minimum rate of interstitial diffusion D,

$$(1) \quad \dot{\epsilon} = D \times 10^9 \; SEC^{-1} \quad , \quad WHERE$$

$$D = D_0 e^{-H/RT} \; [cm^2/SEC] \; ; \; WITH \quad D_0 \cong 0.01 \; [cm^2/SEC]$$

the approximate temperatures where repeated yielding or serrations should occur (assuming the activation energies determined from internal friction peaks; see Section IIB-4) can be calculated. The results have been compiled in Table 11.

Table 11
Calculated Temperatures for Repeated Yielding

Temperature of I.F. Peak	Approximate Activation Energy	Calculated Temperature
150°C	25,000 cal/mole	200°C
300°C-350°C	40,000 cal/mole	500°C
450°C-500°C	50,000 cal/mole	800°C

Although markings which resemble serrations have been evident in the stress strain curves of polycrystalline tungsten at about 175°C-300°C and at 600°C (1), markings in the stress strain curves of single crystals cannot be positively identified to be serrations.

However, the inability to observe discontinuous yielding or serrations in this temperature region may depend on the sensitivity of the testing machine and, therefore, Cottrell locking may still occur. The somewhat stronger temperature dependence of the flow stress at 3% and 6% strain may be caused by pinning and also by an increased resistance to dislocation motion by newly created forests of dislocations or entanglements. From the Cottrell-Bilby model it would be expected that after appreciable deformation the freed dislocations would permit additional deformation at a reduced stress at low temperatures.

It has been suggested recently that the yield and flow stress are controlled by the same mechanism, namely a temperature dependent frictional stress (69). This frictional stress should act not only during the unpinning process but also can contribute to the flow stress, and therefore show up in the temperature dependence of the flow stress. Conrad and Schoeck (70) consider microstrain, yielding and flow to be associated with the movement of free dislocations. Gilman and Johnson (71) have explained the shape of the stress-strain curve on the basis of the stress dependence of the average dislocation velocity. They assumed that the number of dislocations increases linearly with strain and were thereby able to account for the presence of a yield hump without having to postulate an escape mechanism of dislocations from impurity atmospheres. In their work on LiF, they found no evidence for unlocking; grown-in dislocations remained locked, but dislocations responsible for slip are heterogeneously nucleated and multiply rapidly. Hahn (72) has applied these concepts to iron, in particular, and b.c.c. metals, in general, and his model appears to apply qualitatively to single crystals of tungsten. He suggests that the abrupt drop is a consequence of at least three factors:

1. The presence of a small number of initially mobile dislocations;

2. Rapid dislocation multiplications;

3. Stress dependence of the dislocation velocity.

However, as Hahn has indicated, the model hinges critically on the number of dislocations in motion.

Since the tensile and compression tests in this temperature region were not designed to obtain the number of dislocations in motion nor their velocity, a quantitative assessment of the theory cannot be made. While Gilman and Johnson (71) and Hahn (72) postulate that it is not necessary to unpin stationary dislocations,

the possibility of a dynamic unlocking of dislocations as proposed
by Holden (73) should not be overlooked. As pointed out by Hahn
(72), both concepts, that of Cottrell (68) and that of Gilman and
Johnson (71) can then be combined.

Region III: As shown in Fig. 20, the results obtained in this
temperature region have been plotted as two curves:one curve from
300°C-500°C for the higher yield stress data of about 25,000 psi,
and a second at the lower stress levels of 5000-6000 psi between
400°C-500°C. At 550°C the yield stress decreases and at about
700°C-800°C a second small plateau is noted.

In search of an explanation for the yield stress behavior,
two mechanisms will be considered. These are:

(1) Cottrell atmosphere locking, or (2) the Snoek (74) effect
attributed to the local ordering of interstitials as described by
Schoeck and Seeger (45). The latter mechanism gives rise to internal
friction peaks in b.c.c. metals. Since internal friction peaks are
known to exist for single crystals of tungsten (see Fig. 30, also
Section BII-4) in this temperature region, it is of interest to
interpret the results in terms of interstitial effects.

One would, therefore, expect that the various specimens having
distinctly different stress levels would have variable interstitial
content. Although some scatter does exist in the vacuum fusion
analysis, Table 10, and the carbon concentration does vary from
one single crystal rod to another, (with inhomogeneity also occur-
ring along the melted rods) there is no correlation at present
between the exact interstitial concentration and yield stress.
It appears rather that the state of the interstitial impurities
may be more important. This is evident for two specimens taken
from the same rod (UC77-5 and 6), and having about the same level
of interstitial impurities. The specimen tested in the "as melted"
condition had a yield stress about three times greater than the
second specimen which was vacuum annealed at 600°C for three hours.

Although impurity analyses are inconsistent, the Schoeck and
Seeger (45) treatment will be applied to tungsten in the following.
Since two internal friction peaks are evident and also two yield
stress plateaus, as shown in Figs. 20 and 30, it is reasonable to
assume that at least two interstitials are responsible for this
behavior. If one uses the activation energies of about 40,000
cal/mole and 50,000 cal/mole, respectively, for the internal fric-
tion peaks at 300°C and 475°C, one can make an estimate of the
temperature at which the Snoek (74) effect should cease to be
influential in accordance with the following equation:

$$(2) \quad \frac{\dot{\epsilon}}{N \cdot b} = \gamma_6 \frac{A}{kT} e^{-\Delta G/kT} \quad ,$$

68
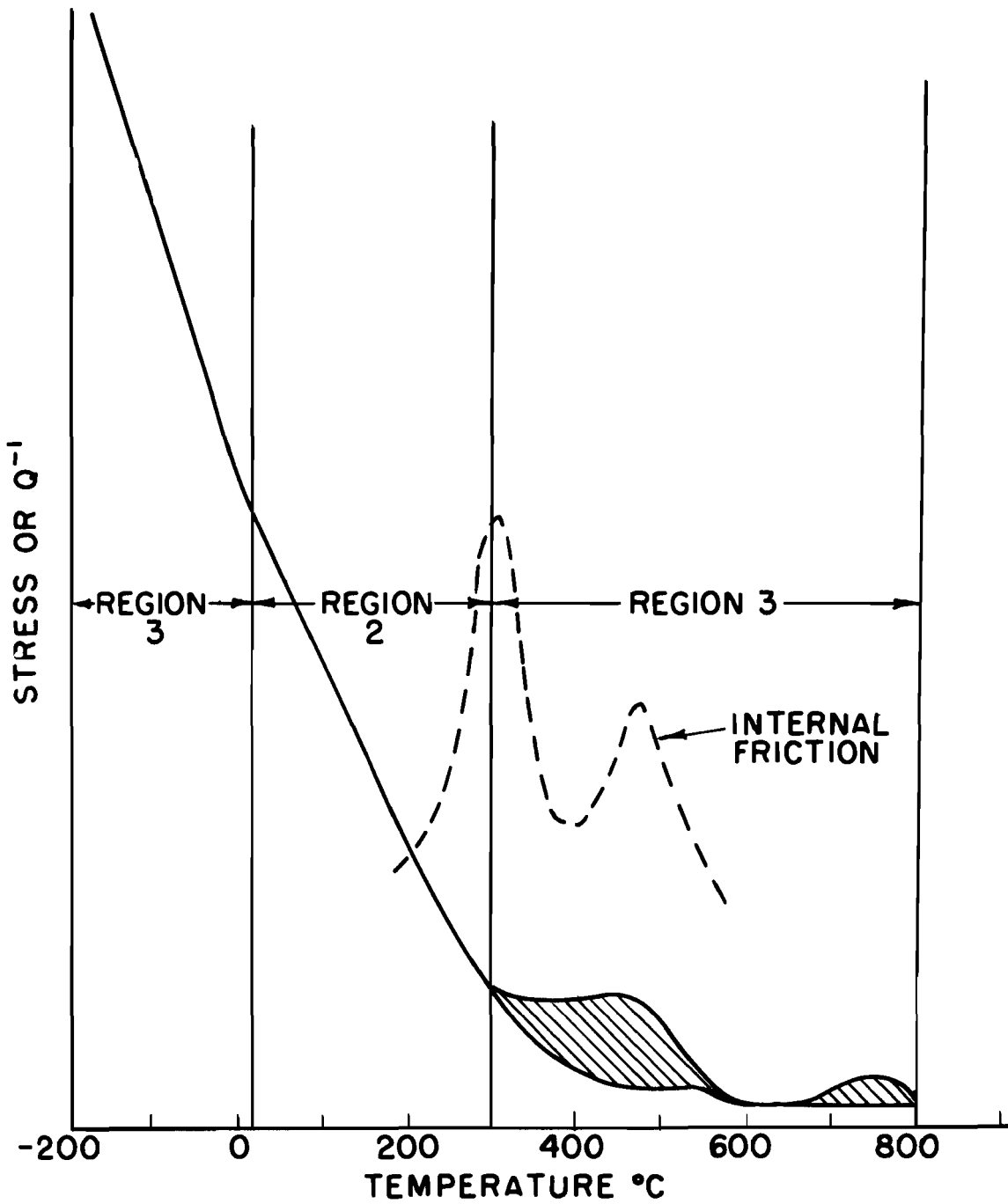
FIG. 30 SCHEMATIC DIAGRAM SHOWING YIELD STRESS AND
INTERNAL FRICTION OF SINGLE CRYSTAL TUNGSTEN
AS A FUNCTION OF TEMPERATURE.

where A is the interaction constant having a value of about 10^{-19} dynes/cm^2 (making appropriate corrections for tungsten, and assuming a similar distortion of the tungsten lattice to be due to carbon, as in the case of iron), N is the density of dislocation ($\sim 10^6$/cm^2 - 10^8/cm^2), γ_0 is the frequency of vibration ($\sim 10^{13}$ per sec.), k is Boltzman's constant (1.33×10^{-16} ergs per degree), $\dot{\epsilon}$ is the strain rate used (8.3×10^{-5}/sec.), and ΔG is the activation energy determined from internal friction peaks.

Inserting these values into equation (2) one finds that the equation holds for temperatures of about 500°C and 700°C, respectively. If the dislocation density is assumed to be 10^6 per cm^2, the equation holds for temperatures of about 650°C and 850°C, respectively. Since these values are in reasonable agreement with observations one would like to know the amount of interstitials necessary to lock the dislocations by this mechanism. Following the treatment of Schoeck and Seeger, the following equation (3) can then be evaluated for the critical resolved shear stress.

$$(3) \quad \tau_s = \frac{K}{2} \frac{A}{ba^3} \cdot P \; [\text{DYNES}/cm^2]$$

where τ_s is the critical resolved shear stress (dynes/cm^2), K (W) is approximately 30 with L about 10^{-4}cm, b is Burgers vector (2.74 Å), a is the lattice constant (3.16Å), and p is the atomic concentration which is proportional to the stress. Using these values it follows that $\tau_s = 2.5 \times 10^5 \times p$ lbs/inch^2/atomic %. (The conversion from dynes/cm^2 to lbs/inch^2 is contained in the proportionality constant.)

Knowing the critical resolved shear stress it is now quite simple to calculate the concentration of a specific impurity, as is done in equation (4).

$$(4) \quad P = \frac{\tau_s}{K} \times \left(\frac{W_i}{W_w} \right) \; [\text{WGT. PPM}]$$

where W_i represents the atomic weight of the interstitial impurity and W_w that of tungsten. A linear plot of the critical resolved shear stress versus interstitial impurity concentration, which will facilitate the enumeration of impurity concentrations corresponding to measured stresses, is given in Fig. 31. Since the factor W_i/W_w is relatively constant (the atomic weights of C, O_2, and N_2 vary only between 12 and 16) this plot will not allow one to discriminate between impurities.

Since the frictional stress due to the Snoek effect is additive to the stress opposing the dislocation movement, and considerable plastic flow can only occur if moving dislocations overcome the internal stresses, τ_G , of other dislocations, one would expect that

FIG. 31   CRITICAL RESOLVED SHEAR STRESS AS A FUNCTION OF
IMPURITY CONCENTRATION PER EQUATION:

$$\mathcal{T}_s = 2.5 \times 10^5 \times \rho \ [LBS./INCH^2/ATOM \ \%]$$

(5) $\quad \tau_Y = \tau_s + \tau_G$ = Snoek stress + internal stress, where the internal stress is given by equation (6):

(6) $\quad \tau_G = \dfrac{1}{5} \cdot G \cdot b \cdot \sqrt{N}$

Inserting the value of G for tungsten ($\sim 1.73 \times 10^{12}$ dynes/cm^2) into equation (6) and assuming N, the dislocation density, to be 10^8 per cm^2, one calculates τ_G to be approximately 1500 lbs/inch^2.

A comparison with the experimental data from 300°C-500°C, Fig. 32, shows that the critical resolved shear stress is about 7500 psi for the upper curve and about 2,000 psi or very close to for the lower curve over the range from 400°C-500°C. Therefore, subtracting τ_G or 1500 lbs/inch^2, from the measured resolved shear stress one obtains about 6000 psi. In accordance to Fig. 31, this corresponds to a concentration of about 15 ppm. For the higher temperatures, between 700°C-800°C, the interstitial concentration required would be negligibly small.

From the carbon and vacuum fusion analyses, Table 10, (excluding H$_2$), it is apparent that carbon and oxygen could be causing the observed yield plateaus. Carbon varies between 20-70 ppm and oxygen is present at about 10 ppm. Whether or not the vacuum fusion analyses are sensitive enough to eliminate nitrogen as a likely suspect cannot be determined at this time. However, it would appear reasonable to suspect all three interstitial impurities until specific dosing experiments are tried.

Whether Cottrell locking takes place in this temperature region seems rather difficult to decide. The Cottrell effect may, however, account for the evidence of discontinuous yielding, especially at 500°C, the only temperature at which a distinct upper and lower yield point was found. Assuming a Petch (9) type of relationship exists between yield stress and subgrain size in tungsten, as suggested by Ball (12) for iron an approximate calculation of the Cottrell pinning strength k_y can be obtained using Owen's extrapolation method (75). For a subgrain size of .04 cm, as determined by linear analysis on the specific (500°C) specimen, k_y is $\sim 0.4 \times 10^7$ dynes/cm$^{3/2}$ and the frictional stress σ_0 about 2.8×10^8 dynes/cm^2. The very low value of k_y suggests in this case that Cottrell atmosphere locking is not too important. Most of the increase of the yield stress can thus probably be attributed to the Snoek effect.

Single Crystal versus Polycrystalline Tungsten

In comparing the results of single crystal specimens with those of polycrystalline specimens previously reported (1, 63, 64) it is immediately evident that similarities do exist, Figs. 21, 27, 33.
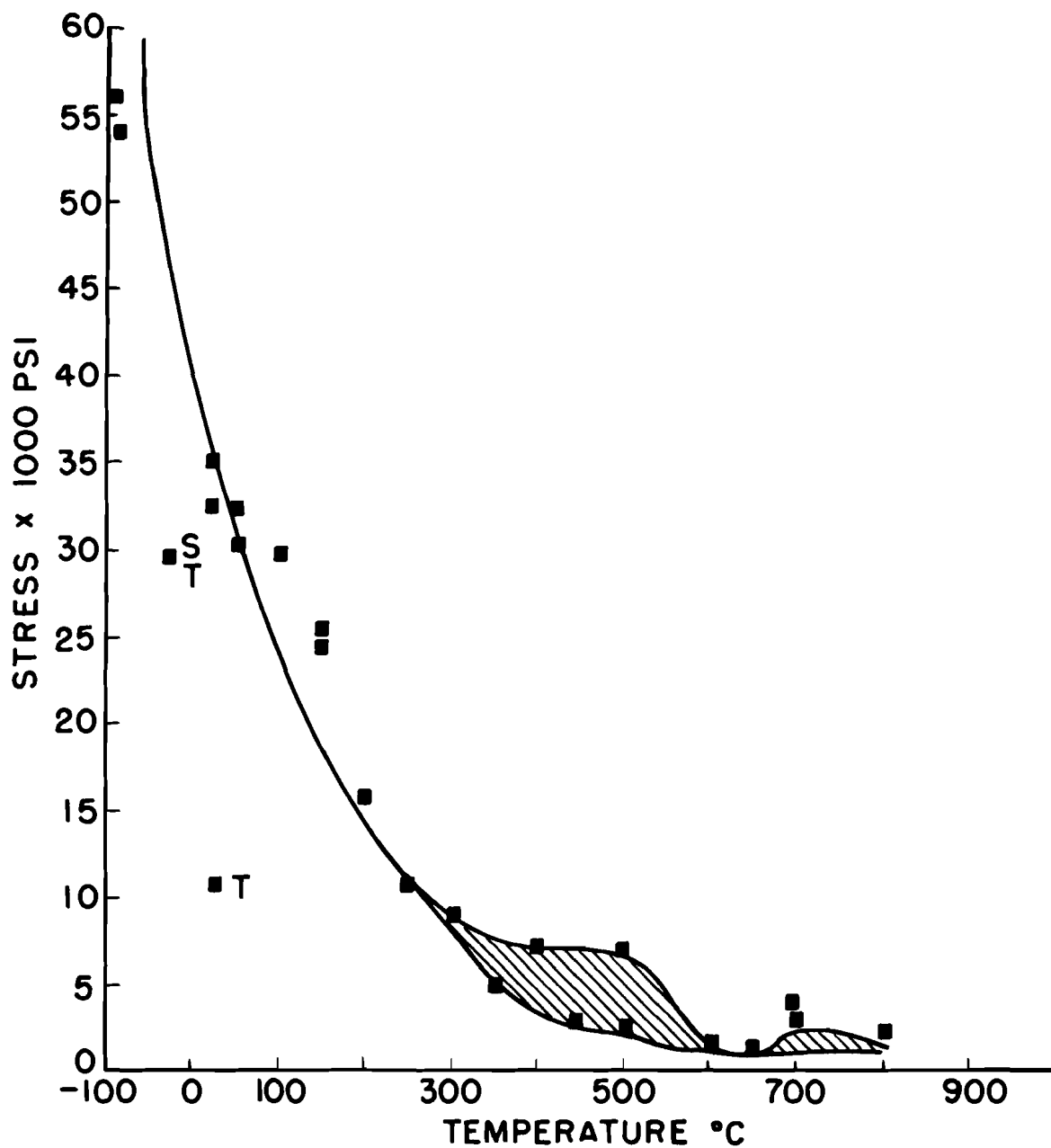
FIG. 32 CRITICAL RESOLVED SHEAR STRESS OF SINGLE
CRYSTAL TUNGSTEN (~ [100]) IN TENSION AS A
FUNCTION OF TEMPERATURE.

The rather obvious result that the yield stress (proportional limit) of high purity polycrystalline (1) and single crystal tungsten are practically the same over a comparable temperature range is not remarkable. It should be noted from Table 10 that the particular polycrystalline specimens had exceptional purity having about 10 ppm of carbon.

As shown for iron (38) the strong temperature dependence of the yield stress is associated with the combined effects of interstitial impurities and grain boundaries. If either is absent, the effect of temperature on the yield stress is somewhat reduced. In fact, for iron single crystals, the yield stress does not seem to be particularly affected by small variations in interstitial impurities. A somewhat similar observation can be made for single crystal tungsten, particularly for temperature region II. However, in general, since current analytical techniques have been unable to reveal great differences between high purity starting material (6) and zone melted rods (if the starting material is itself of high purity) one must conclude that the polycrystalline and the single crystal materials used have about the same impurity level.

For single crystal tungsten of the above mentioned orientation, twinning appears to be more frequent than in polycrystalline tungsten. Hull (76) observed in silicon iron that twins formed in large grained polycrystals at the same temperature and strain rate where only slip occurred in small grained specimens. From the observations of Armstrong (77) and in accordance with section IIB-7, it would be expected that due to the tendency of twins to buckel the matrix, greater difficulty would be experienced in trying to accommodate a twin within a small grain than a large grain or a single crystal. Consequently, one would expect that some sort of a grain size effect for twinning does exist.

A possible explanation of the grain size effect on some of the brittleness in polycrystalline tungsten may be as follows. If it is assumed that the stress required to cause twinning is lower than the stress required to initiate grain boundary cleavage (twinning in some instances does occur at low stresses in tungsten), the first twin formed must produce a sufficiently high local stress to start a crack or subsequent fracture. As shown in Section IIB-7, cracks are associated with twin accommodation. Consequently one could expect some brittleness due to twinning in large grained specimens.

A difference between the two materials exists for the ductile-brittle transition temperature in single crystal tungsten of the [100] orientation. The D.-B. transition temperature is at about 150°C (taking about the midpoint of the % R.A. curve). High purity polycrystalline tungsten tested in tension has a ductile-brittle transition temperature at about 200°C-250°C. Since the temperature difference is small and since twins have been noted at 150°C in single crystals, this suggests that twinning may account for the

74
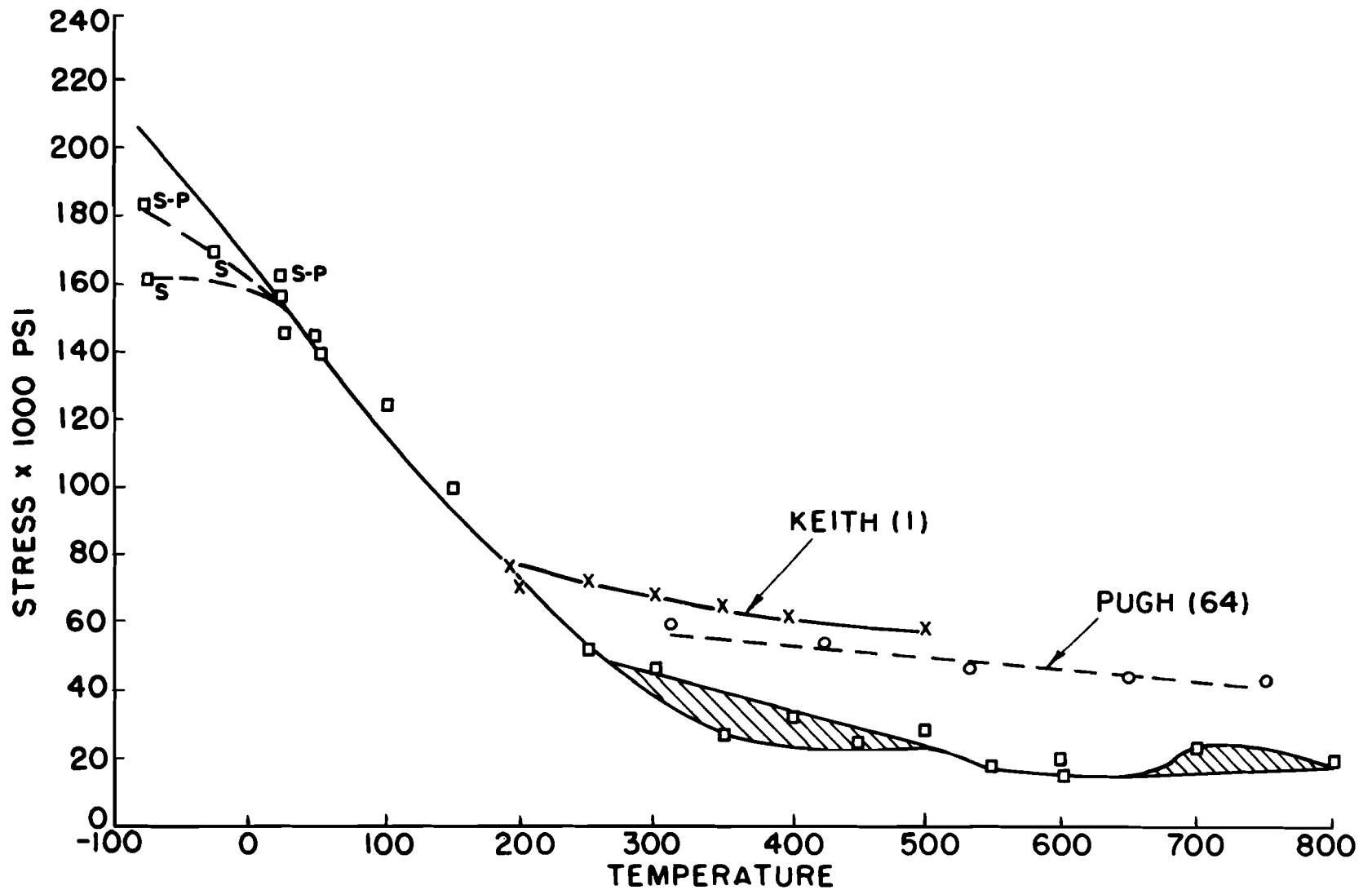
FIG. 33 ULTIMATE TENSILE STRENGTH OF SINGLE CRYSTAL (~[OOl]) AND POLYCRYSTALLINE TUNGSTEN AS A FUNCTION OF TEMPERATURE. (STRAIN RATE 8.33 x 10⁻⁵/SEC.).

observed ductile-brittle transition in large grained polycrystalline tungsten.

At higher temperatures, polycrystalline tungsten has a somewhat higher stress level than single crystal tungsten, Fig. 33. This is not unexpected since it has been generally observed in metals that polycrystals are somewhat stronger than single crystals below $1/2$ T_m.

Summary

The tensile and compression test results of single crystals of tungsten have been analyzed in terms of three rather arbitrary temperature regions: (1) $-196°C$ to R.T., (2) R.T. to $300°C$, and (3) $300°C$ to $800°C$.

(1) Region I - This region seems to be characterized by the intervention of twinning as a form of plastic deformation. It is believed that one cannot divorce slip from twinning and vice-versa. Since lattice strains necessary to accommodate a twin set up complex deformation systems, the yield stress may be variable. Under some conditions of twin accommodation within a lattice, cracks can result. Twinning, therefore, in some instances can initiate brittle fracture.

(2) Region II - The yield stress and the proportional limit appear to obey the predictions of the Cottrell-Bilby theory as modified by Fisher and so does the flow stress at 3% and 6% elongation, but with a stronger temperature dependence. It is, however, difficult to understand why the flow stress should be governed by the same mechanism. The observed stress-strain curves could also be interpreted in accordance to Hahn (72) in terms of dislocation velocities and frictional stress on moving dislocations. However, at this stage the experimental observations are not extensive enough to determine which is the most probable mechanism.

(3) Region III - It appears that the mechanical properties of tungsten can be affected by two interstitials. The Schoeck-Seeger treatment of the Snoek effect agrees rather well with the observed mechanical properties using the activation energies obtained by internal friction measurement for peaks at $300°C$ and $475°C$. Although Cottrell atmosphere locking may occur, the effect, if it exists appears to be quite small. It is also apparent from this work that not only may interstitials be important, but also their specific state may be equally important.

Vacuum fusion and carbon analyses do show that interstitial impurities are not only present in single crystals of tungsten, but are inhomogeneously distributed. Carbon is especially variable and the concentration seems to increase as the number of melting passes is increased from 2 to 5 (as was also found by Allen et al) (78).

The mechanical properties of single crystal and polycrystalline tungsten are similar. The various mechanical characteristics of tungsten have also been observed in one or the other of the b.c.c. metals.

4. Internal Friction of Single Crystal Tungsten

In recent years internal friction has become an important scientific tool because it allows the study of certain atomic processes which cannot be observed easily by other techniques. One of the most successful applications of internal friction, or anelasticity, to metallurgy is the study of interstitial effects in b.c.c. metals. V (79), Nb (80), Ta (81) and Fe (74) exhibit internal friction peaks which can be attributed to one or the other of the interstitials. Attempts to extend these measurements to other b.c.c. metals, notably tungsten, have been and are being made in several laboratories. To date, experiments with polycrystalline tungsten have not been very fruitful. Recently, tungsten of a somewhat higher purity in the form of single crystals has become available. This material has a purity of the order of about 99.99% tungsten, whereas sintered powder metallurgical tungsten has a purity of the order of 99.98% tungsten. Using this new material, experiments were carried out in the temperature range from room temperature to 600°C. In this section the internal friction studies made on single crystal tungsten will be discussed and compared with results on high purity tungsten produced by powder metallurgy techniques.

Experimental Technique

Internal friction measurements on single crystals of tungsten were conducted in an apparatus of conventional design consisting essentially of a Ke type torsion pendulum in an evacuated chamber at a pressure of better than 10^{-5} mm Hg. The apparatus and the preparation of the internal friction specimens have been described in a previous report (1). Briefly reviewed, single crystals are ground to about 0.040-0.030 inch in diameter and then electropolished to about 0.020 inch diameter. For these single crystal specimens, which varied in length from about 3-9 inches, the frequency of the pendulum varied from about 1-2 c.p.s. Single crystals which were ground, electropolished, and had no subsequent heat treatments are designated as being in the "as melted" condition. Sintered, swaged, and drawn polycrystalline specimens were in a few instances prepared in a similar manner after high temperature anneals in the electron beam furnace. The axial orientations of the various single crystals used are listed in Table 12.

Table 12
Crystallographic Orientation, Vacuum Fusion Spectrographic and Carbon Analysis of Tungsten Single Crystals Used for Internal Friction Measurements

Single Crystal	Approx. Axial Orientation
1	221
2	111
3	441
4	511
5	540
6	531
7	110
8	N.D.*
9	331
10	210
11	100

* - not determined.

Quantitative Spectrographic Analyses (in wgt ppm)

	Mo	Fe	Al	Si	Cu	Mg	Mn	Ni	K
Single Crystal (.180 rod and tensiles)	N.D.	3	3	30	N.D.	24	N.D.	0-2	N.D.**
PB-5-1 (polycrystalline wire)	27	7	14	20	5	5	5	5	13

** - not detected.

Vacuum Fusion and Carbon Analyses (in wgt ppm)

	C	O_2	N_2	H_2
Single Crystal	30 (13-70)	10 (4-30)	2 (1-20)	1 (.7-15)
Polycrystalline Wire	80-150	27-190	5-25	.8-10

Internal Friction of "As Melted" Crystals

In a previous report (1), it was indicated that it is extremely difficult to observe internal friction peaks in sintered, swaged, and drawn polycrystalline tungsten. However, when peaks were found they were generally located below 250°C and above 500°C. These peaks were rather broad, generally of low magnitude, and not reproducible.

Typical results of a series of measurements performed on various single crystals in the "as melted" condition are summarized in Fig. 34. As is evident from this figure, three characteristics of the peaks are immediately apparent: (1) a variation in the background internal friction; (2) the broad skewed appearance of the peaks on the lower temperature side; and (3) the consistent occurrence of a peak at about 300°C or at slightly lower temperatures. These results are quite different from those previously reported for polycrystalline tungsten (1).

The variation of the background internal friction is not understood. However, this variation may be the result of either impurities or orientation. Evidence in support of impurity effects on the background is apparent since upon retesting these specimens over the same temperature region, the background internal friction is decreased. An orientation effect is apparent from the observation that the specimen which had a 111 orientation also had the lowest background internal friction. (See curve No. 11, Fig. 1.) However, since these experiments have not been conducted systematically, a definite conclusion on the variation of the background cannot be given at this time.

The broad and skewed appearance of the internal friction peaks at their low temperature side raises the question as to their relaxation time. True interstitial peaks should be narrow, rather symmetrical, and represented by a single relaxation time. The magnitude of the skewness is demonstrated in Fig. 35 for the 300°C peak of specimen #9, by superimposing a symmetrical peak in the drawing. The cause for the skewness has not yet been determined, however, Powers and Doyle (82) have noted that the interactions of interstitial impurities are responsible for the broadening of a peak; in some instances, substitutional impurities can also cause a skewed peak.

Of the eleven single crystals tested to date in the "as melted" condition, ten have exhibited internal friction peaks at about 300°C. In a few instances a peak was also noted at about 475°C. The one specimen (No. 2) which did not exhibit an internal friction peak at this temperature had an orientation close to 111 , for which - on theoretical grounds - there should be no Snoek or interstitial peak. This is an especially strong indication that the observed peaks are probably of interstitial origin.

79
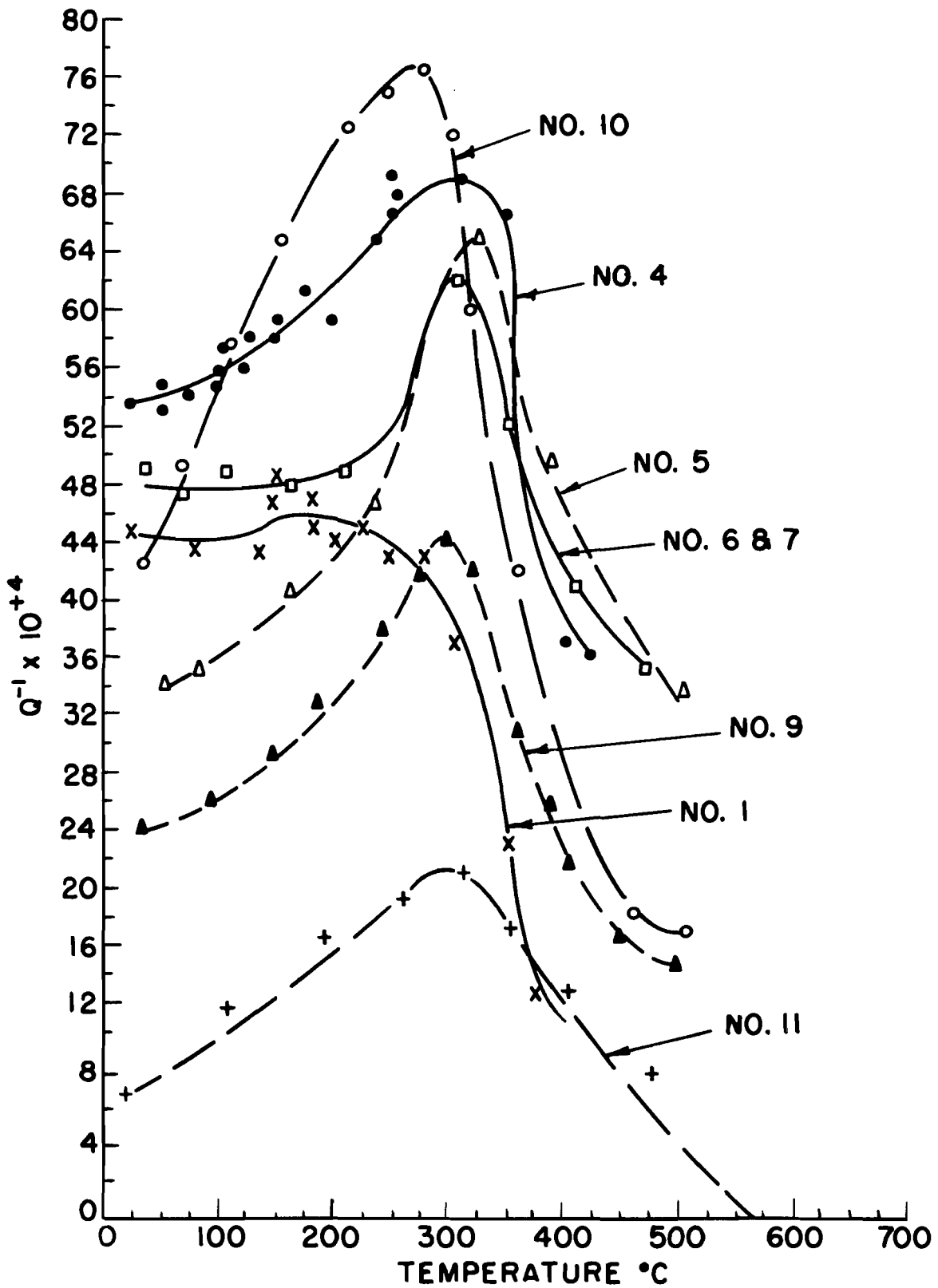
FIG. 34 SUMMARY OF INTERNAL FRICTION MEASUREMENTS ON TUNGSTEN SINGLE CRYSTALS IN THE "AS MELTED" CONDITION.
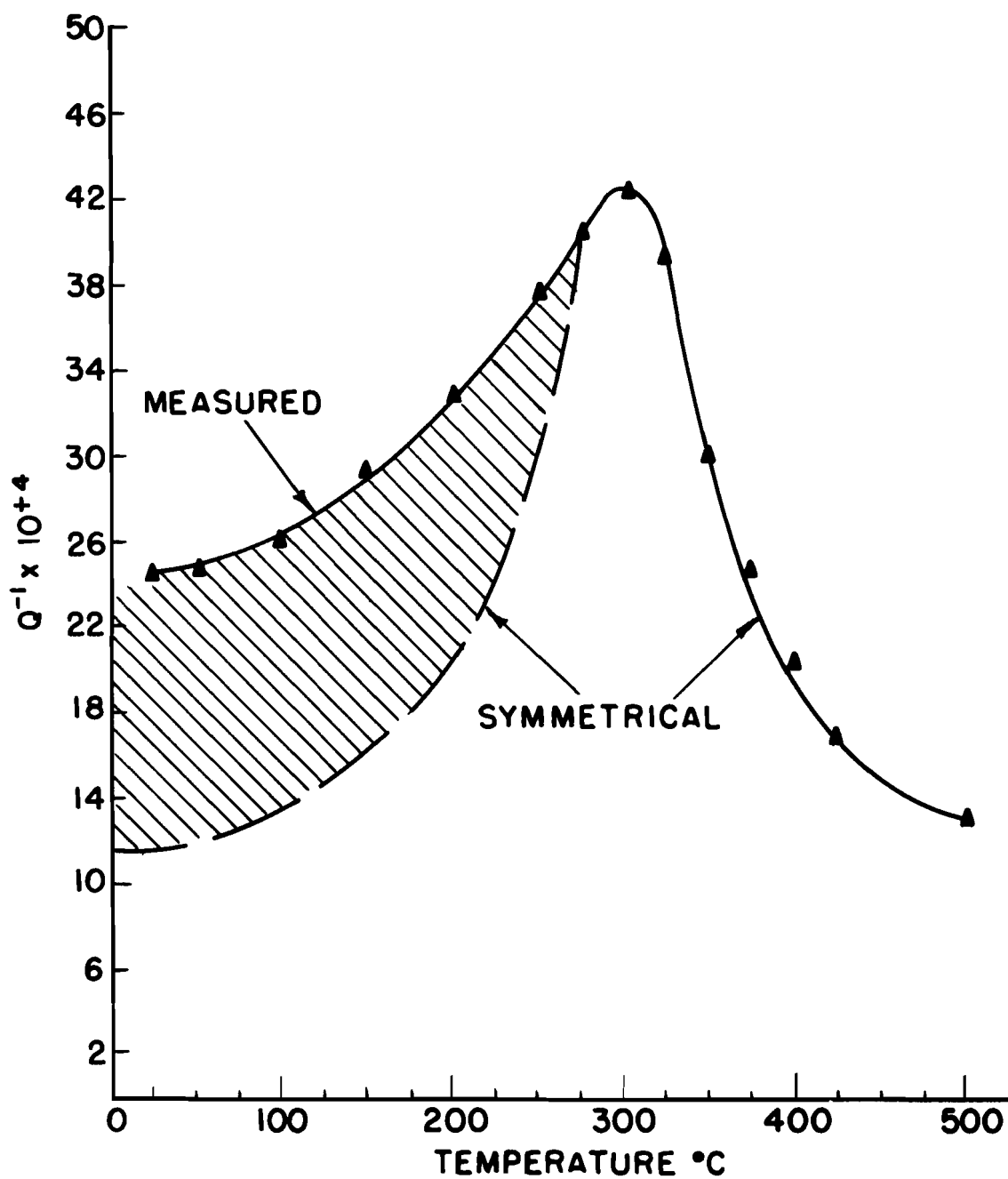
FIG. 35 APPARENT "SKEWNESS" OF PEAK AT ABOUT
300°C ; NO. 9.

81

The most puzzling result of this series of experiments is
that upon retesting after measuring to about 500°C, the peak at
about 300°C either disappears, leaving a small plateau, Fig. 36,
or a greatly reduced peak, Fig. 37.

Effect of Cold Work

The question arises from these results as to whether or not
a peak can be induced in the single crystals by the grinding (cold
work) or the electropolishing treatment. To determine whether
interstitials are introduced during electropolishing, a single
crystal specimen was ground directly to 0.020 inch diameter and
then tested. Internal friction peaks were evident at about 325°C
and 475°C in this specimen, as shown in Fig. 38. To determine the
effect of plastic deformation on the internal friction, specimen
No. 9 was plastically deformed 5% (elongation) and annealed at
2000°C for 5 minutes after the "as melted" internal friction was
obtained. As is evident in Fig. 39, the peaks which occur in
single crystal tungsten at about 300°C and 475°C cannot be cold-
work peaks. Although the plastic deformation may not have been
sufficient, it appears that a cold-work or Koster peak occurs at
about 600°C-650°C.

Effect of Heat Treatments

Since the peak which is apparent at 300°C can be made to dis-
appear by heating to 500°C, it would be important to know whether
the peak can be recovered by heating to higher temperatures.
Recovery of this peak can, indeed, be accomplished by heating to
a temperature of 2000°C for 10 minutes. The effect of this heat
treatment is illustrated in Fig. 40. In order to determine
systematically at what temperature the peak would reappear, the
same crystal (No. 7) was annealed at various temperatures and times
from about 1650°C to 2250°C. The result on the internal friction
of this specimen is summarized in Fig. 41. As will be noted, two
peaks are apparent, a strong one at about 300°C and a weaker peak
at about 475°C.

As previously noted for "as melted" crystals, the background
internal friction is affected considerably by the various anneals.
(See Fig. 42.) If the indicated backgrounds are subtracted, one
finds that the magnitude of the peak at about 300°C increases with
increasing annealing temperature to about 2000°C. The magnitude
of the peaks after annealing at 2000°C and 2250°C is about the
same, indicating that a limited solubility of the interstitial
impurity is very probable. It will also be noted that the peak at
about 300°C is narrow and symmetrical enough to allow for the
conclusion that it is caused by a single relaxation mechanism.

Random heat treatments were continued on single crystal No. 7
and this also showed peaks at about 300°C and 475°C, Fig. 43. As
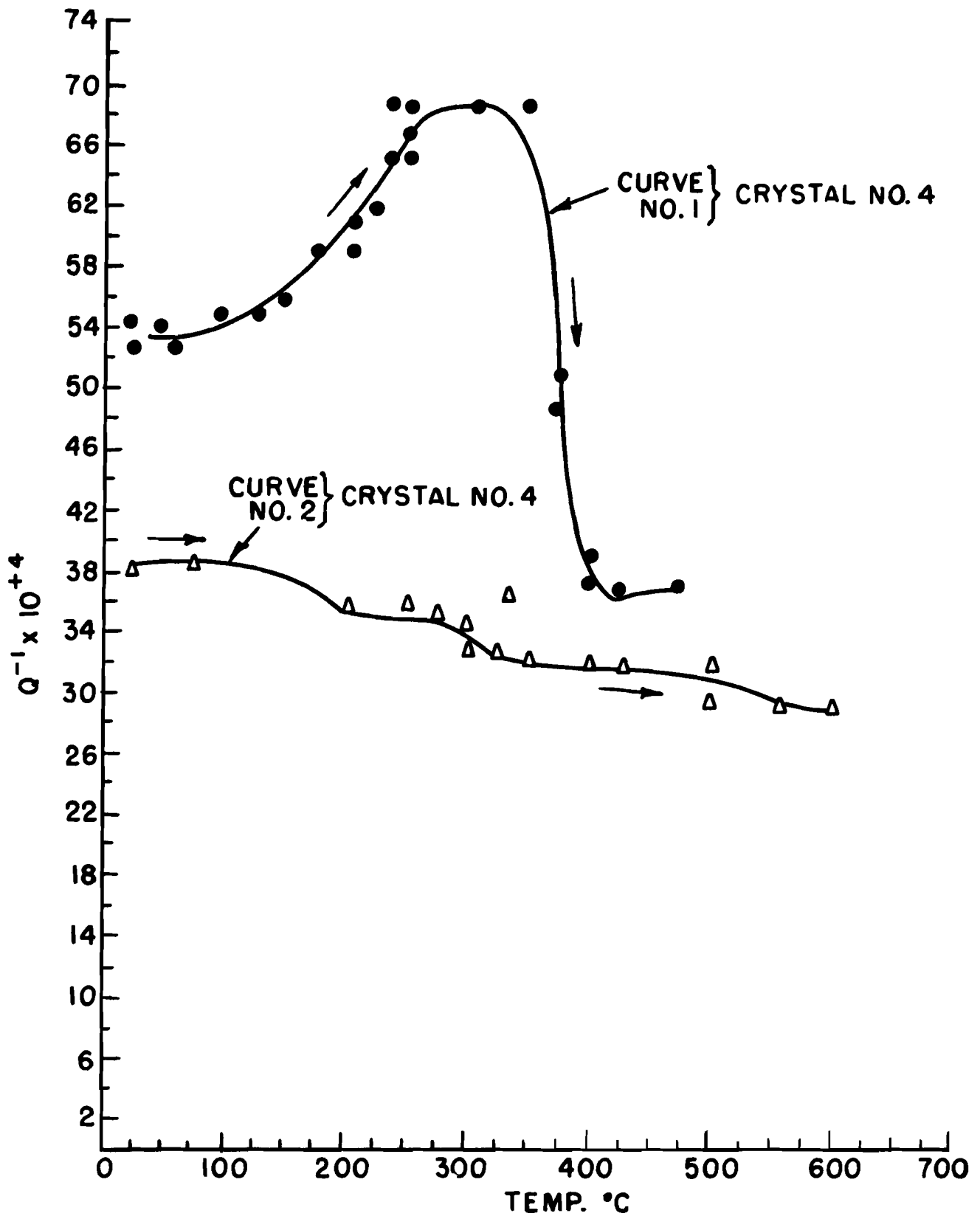
FIG. 36 BEHAVIOR OF INTERNAL FRICTION PEAK AT 300°C
UPON RETESTING.

83
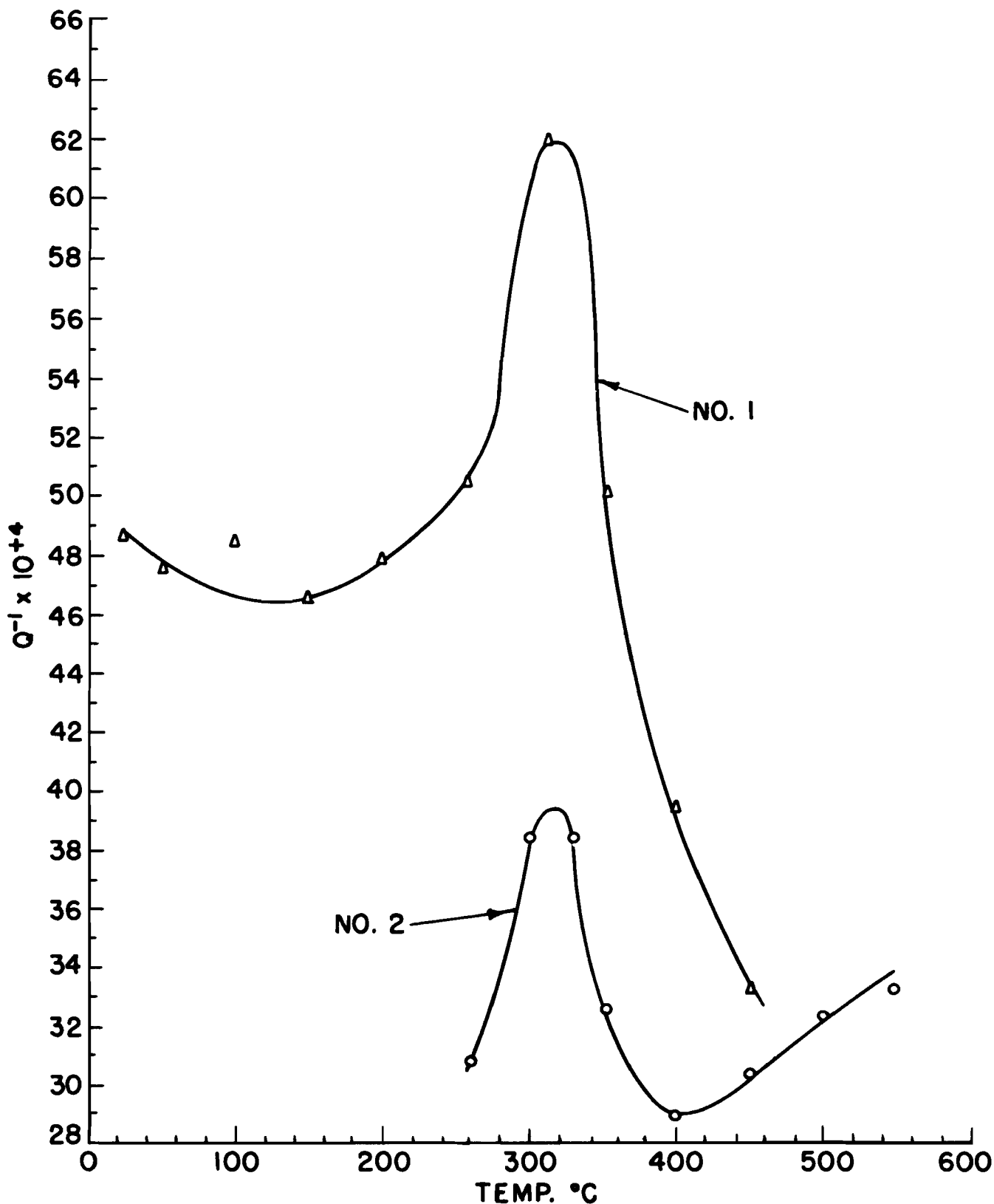
FIG. 37 PERSISTENCE OF A SMALL PEAK AFTER RETESTING; NO. 6
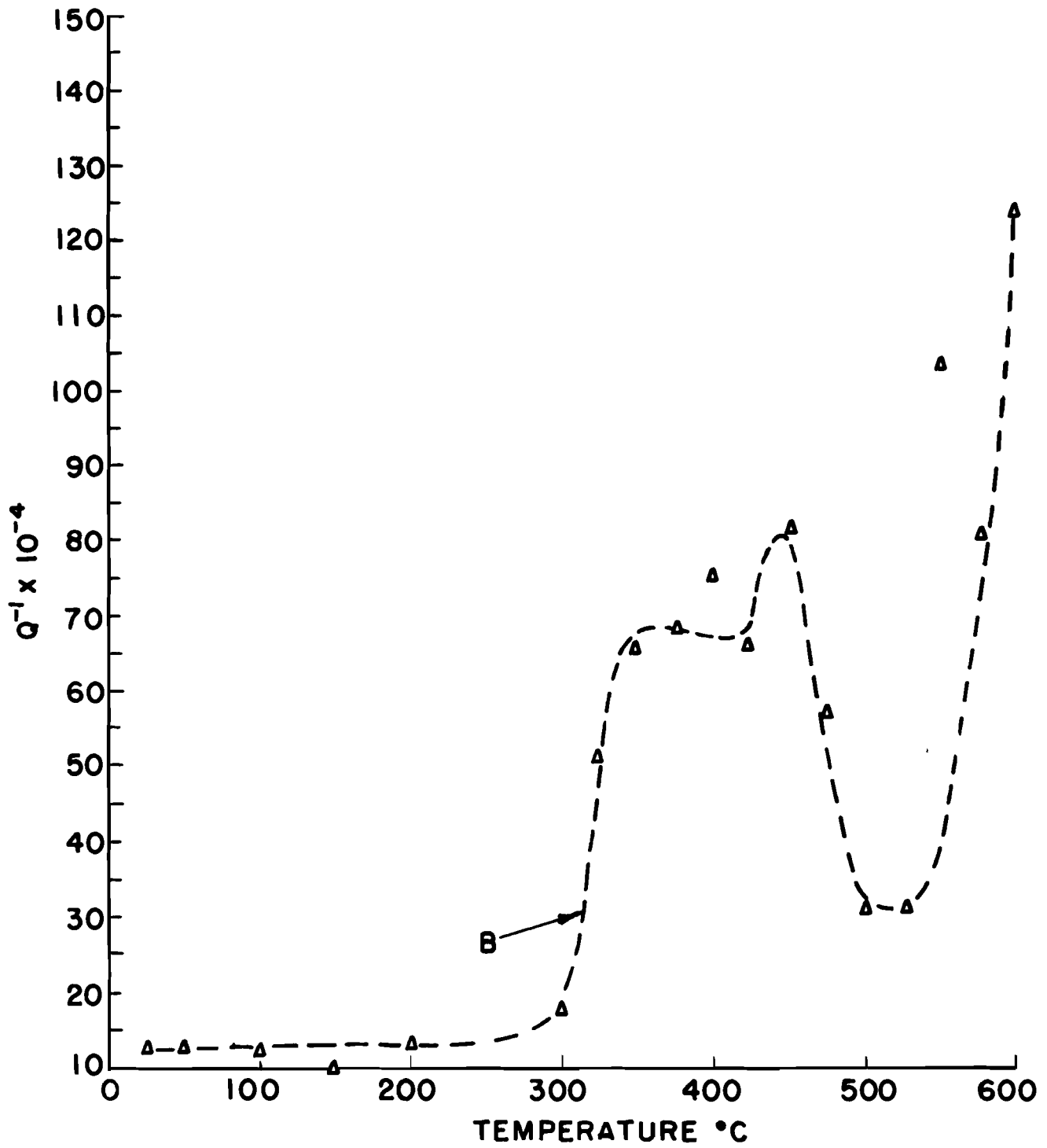
FIG. 38 INTERNAL FRICTION OF TUNGSTEN SINGLE CRYSTAL
IN THE AS GROUND CONDITION, NO. 8
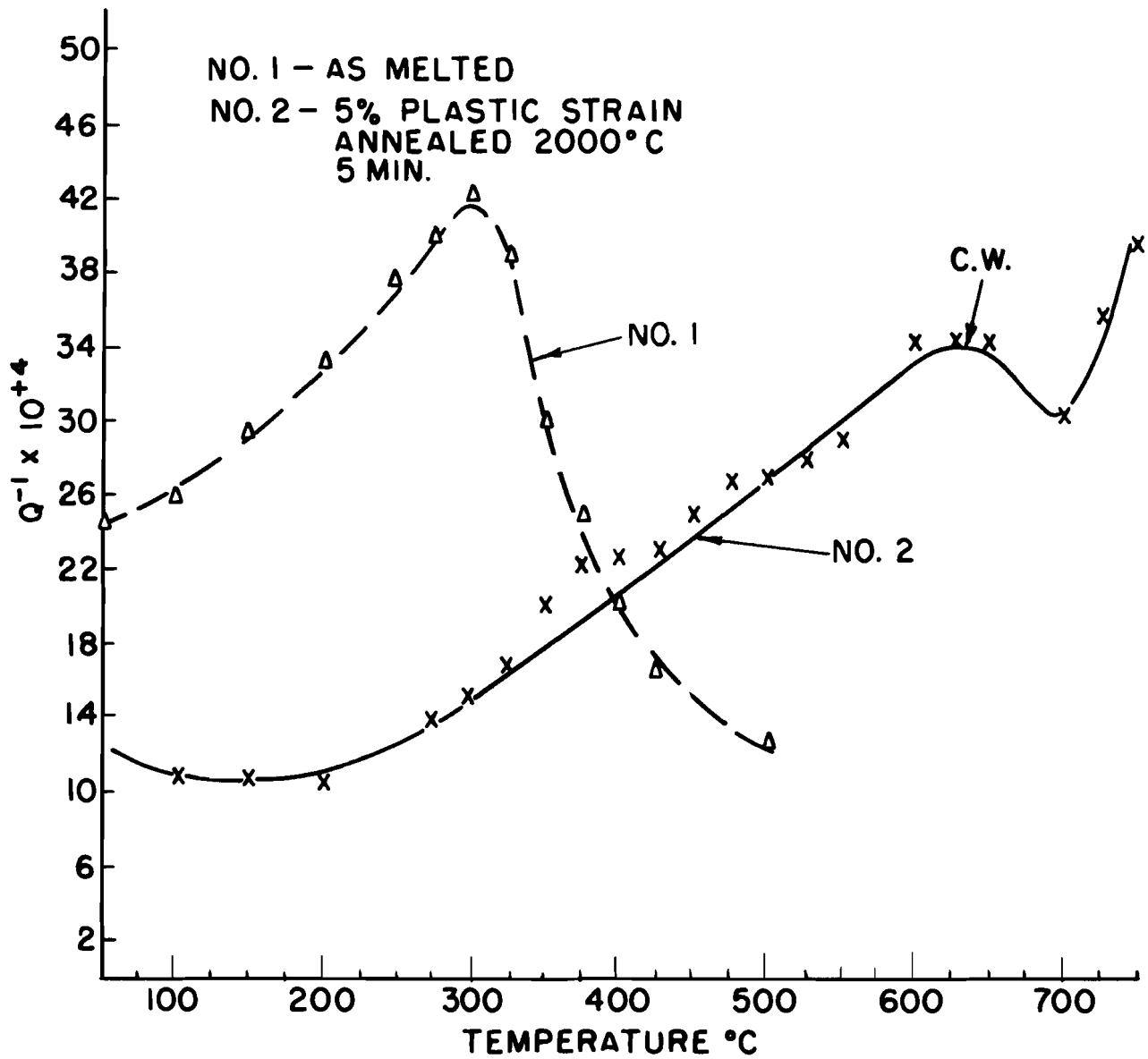
FIG. 39 EVIDENCE OF A COLD WORKED PEAK IN SINGLE
CRYSTAL TUNGSTEN; NO. 9.
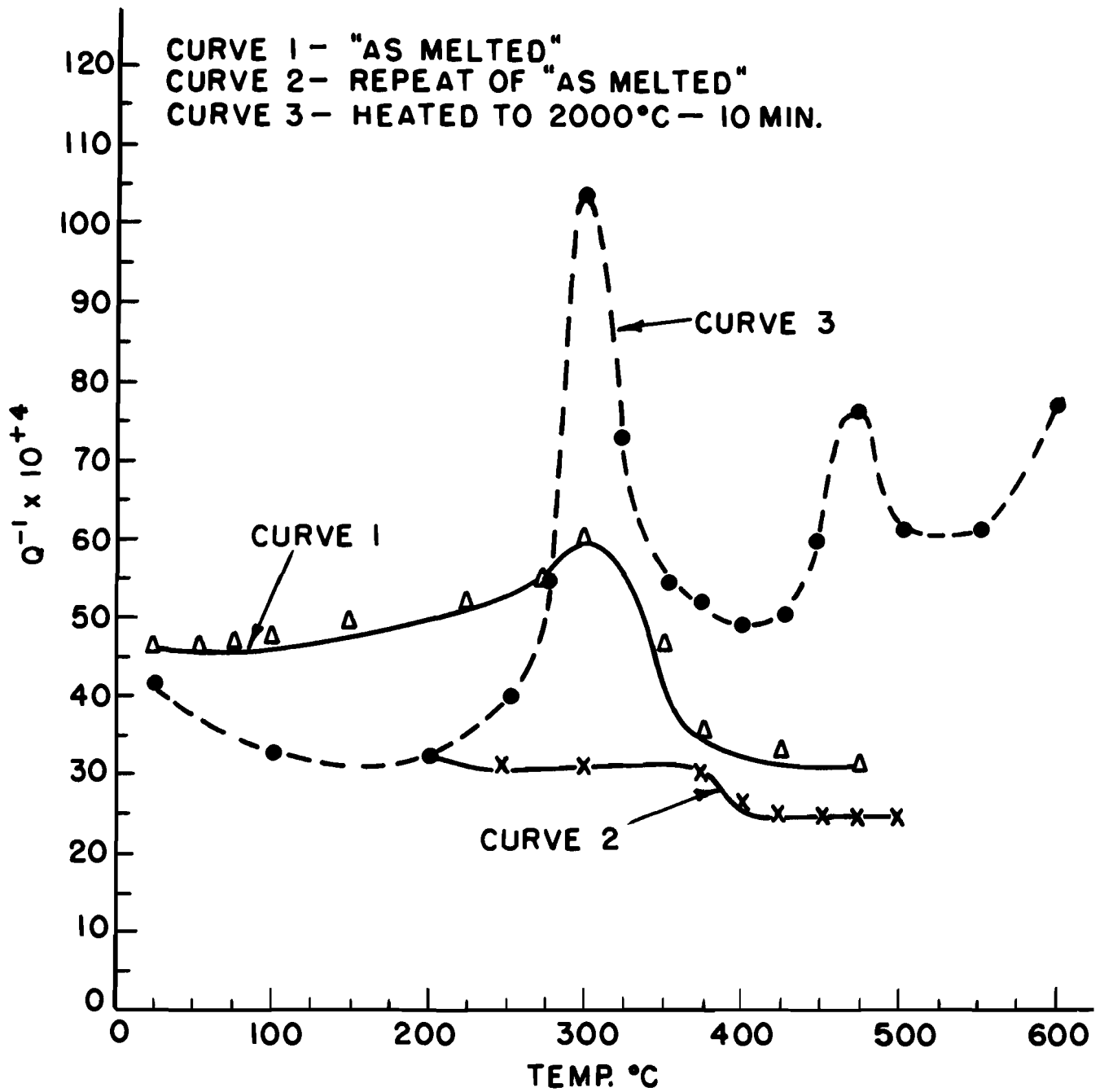
FIG. 40 EFFECT OF HIGH TEMPERATURE ANNEAL ON THE
RECOVERY OF PEAK AT 300°C, NO. 7

87
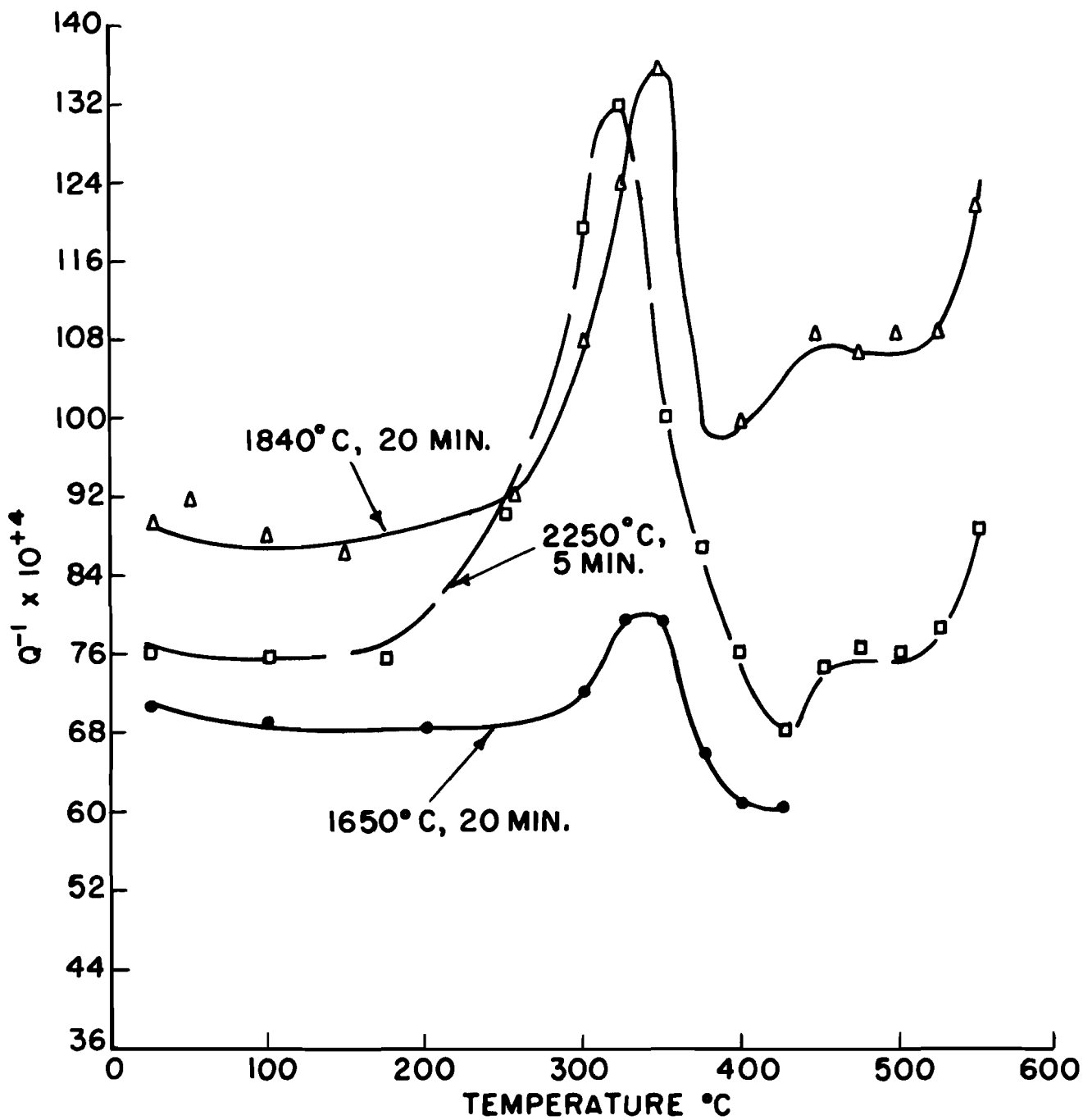
FIG. 41 INTERNAL FRICTION OF SINGLE CRYSTAL TUNGSTEN AS A
FUNCTION OF ANNEALING, NO. 7

88
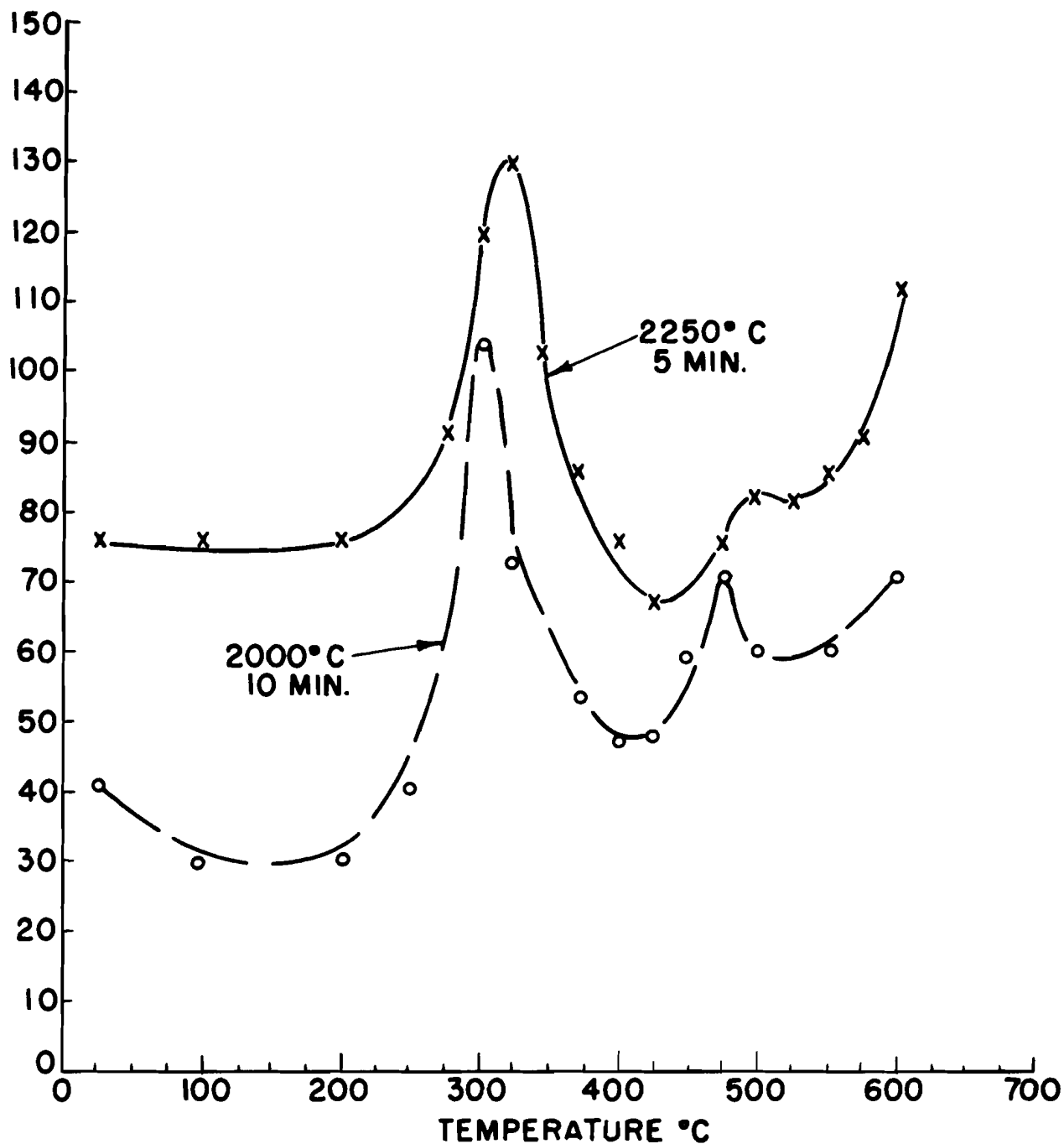
FIG. 42 INTERNAL FRICTION OF SINGLE CRYSTAL TUNGSTEN
AS A FUNCTION OF ANNEALING TEMPERATURE; NO. 7

89

will be noted, however, these treatments have the effect of shift-
ing the peak temperature. This can probably be accounted for
either by an overlapping of the two peaks or an interaction of the
interstitials causing the peaks.

Although the effect of heat treatments is not yet completely
elucidated, it appears that the peak observed at about 300°C can
be annealed out by heat treating for extended times at 2250°C.
(See Fig. 44.) Some evidence of recontamination is apparent in
curve 3 of Fig. 44, although a dynamic vacuum of 0.1 micron was
recorded. It should be mentioned that all anneals discussed
previously were conducted in the internal friction apparatus by
resistance heating of the specimens. After the contamination was
noted, the subsequent heating and dosing experiments were conducted
in a separate mercury vacuum system.

Effect of Carbon Dosing

A number of attempts were made to dose specimen No. 7 with
carbon. (See section IIB-5.) A non-equilibrium approach was
tried first. This consisted of heating the specimen at 2250°C for
5 minutes in a vapor of naphthalene. After this short time treat-
ment, a carbide case was already evident on the surface. Crystals
having a case on the surface are extremely brittle and almost
impossible to handle. However, it was possible to make an internal
friction measurement with this specimen. (See Fig. 45.) As is
evident from this figure, a peak has developed at about 475°C and
a broad plateau or peak below 200°C. A carbon analysis revealed
that the carbon had been increased from about 40 to 170 ppm. A
hardness survey was made on another specimen which had been given
a similar dosing treatment but which broke upon mounting in the
internal friction apparatus. For this specimen, an extremely high
hardness of 1580 (Knoop 200 gm load) for the carbide case and about
580 (Knoop 200 gm load) for the matrix were determined. When a
1000 gm load was used the matrix hardness increased from about
358 to 475. It was not possible to see carbide precipitates in
the matrix because of the numerous etch pits.

Internal Friction in Polycrystalline Tungsten

If a polycrystalline specimen is given a high temperature
anneal in the electron beam furnace, and the specimen is then pre-
pared in a manner similar to that of single crystal tungsten
(grinding and electropolishing), peaks are also evident. (See
Fig. 46.) It will be noted that peaks occur in the same temperature
regions as in single crystal tungsten, and in addition at about
150°C and 500°C. The peak at 150°C has never been noted in single
crystal tungsten. The absence of this peak in single crystal
tungsten may be due to the increased background caused by the
broadening of the 300°C peak at low temperatures or it may not
exist at all. The result obtained on this polycrystalline specimen

90
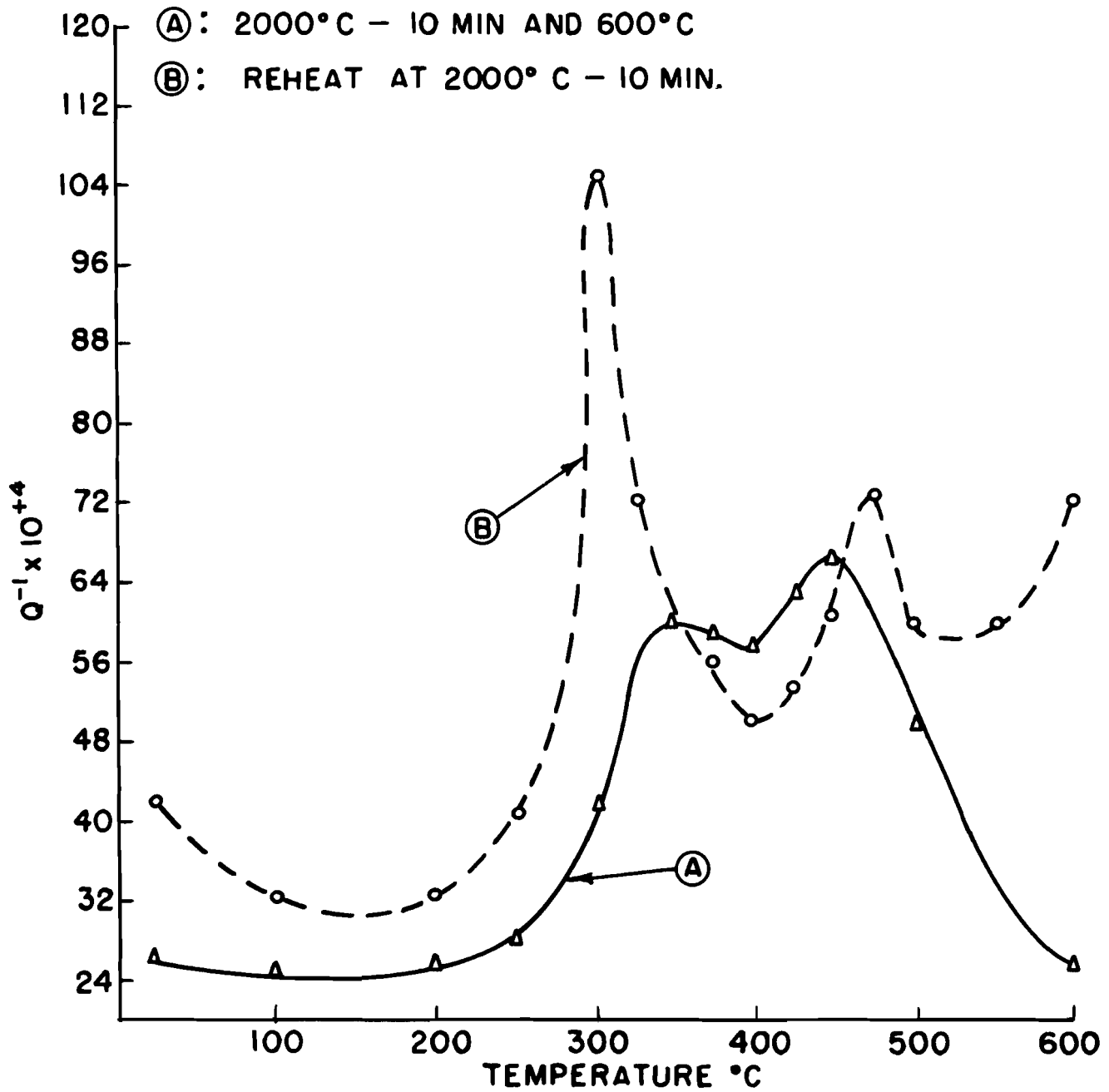
FIG. 43 INTERNAL FRICTION IN SINGLE CRYSTAL TUNGSTEN
AS A FUNCTION OF ANNEALING, NO. 7
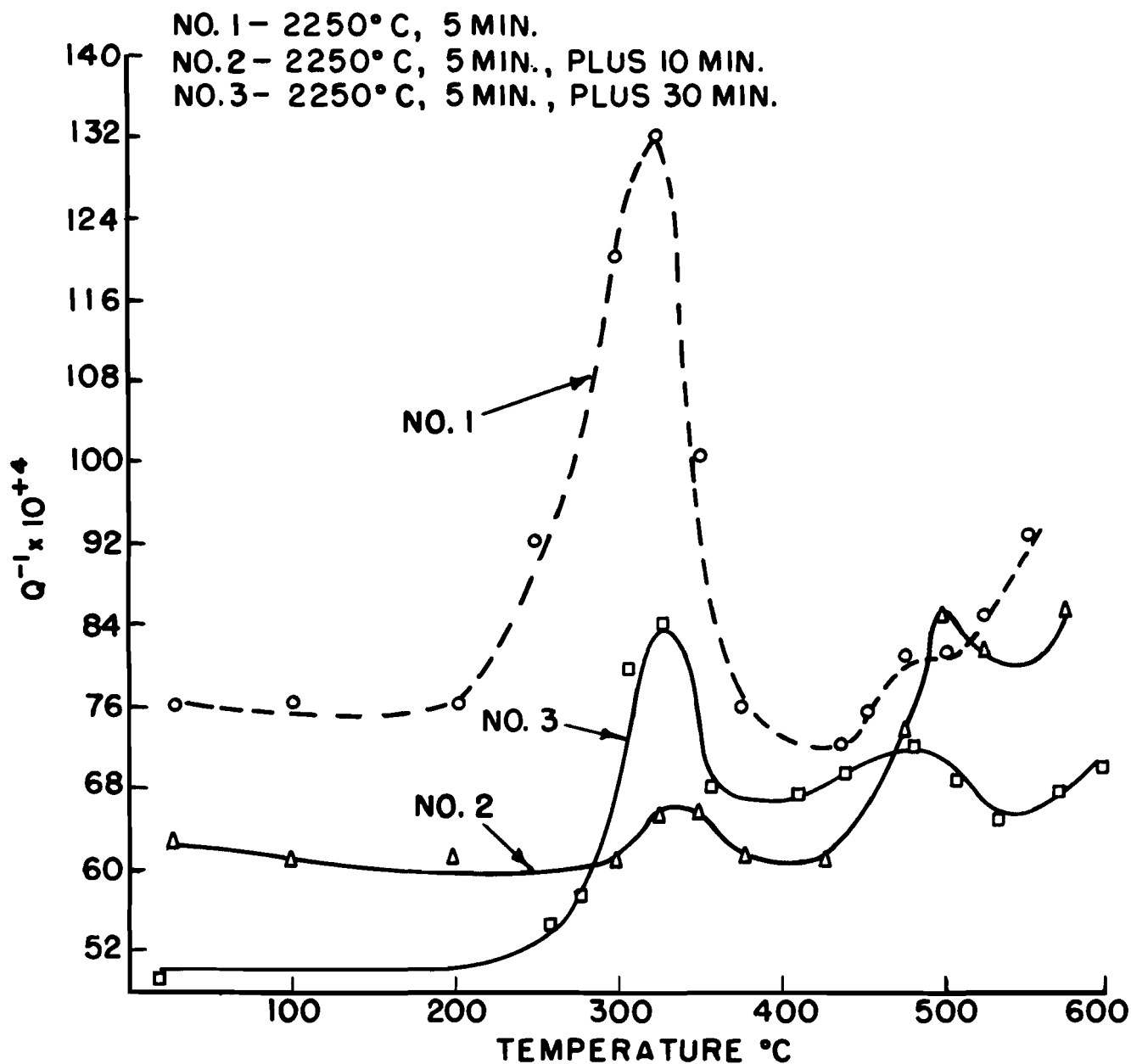
FIG. 44 INTERNAL FRICTION IN SINGLE CRYSTAL TUNGSTEN AS A FUNCTION OF ANNEALING.

NO. 1 – 2250° C, 5 MIN.
NO. 2 – 2250° C, 5 MIN., PLUS 10 MIN.
NO. 3 – 2250° C, 5 MIN., PLUS 30 MIN.

92
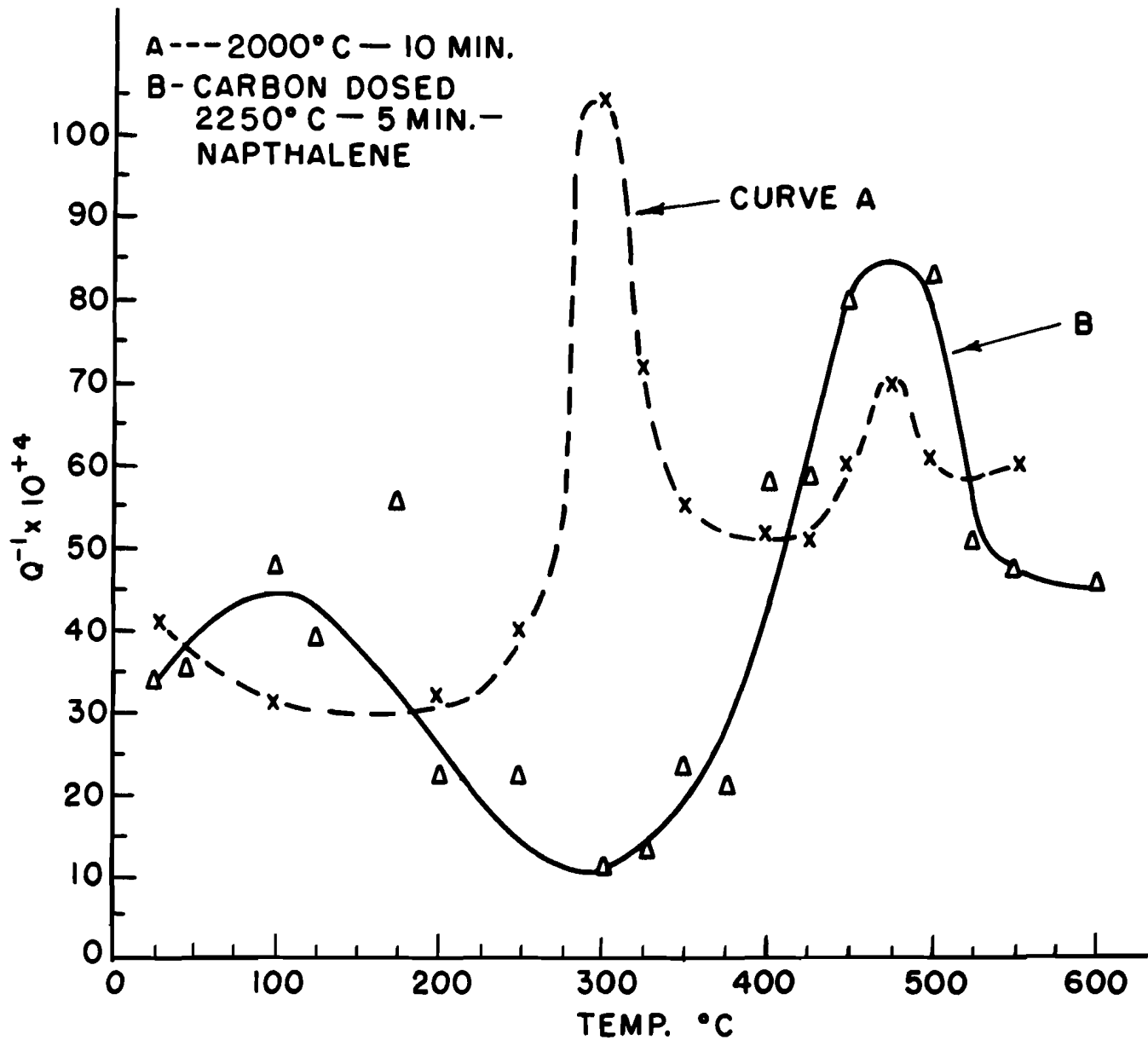
FIG. 45 EFFECT OF CARBON DOSING ON THE INTERNAL FRICTION
OF SINGLE CRYSTAL TUNGSTEN.

93
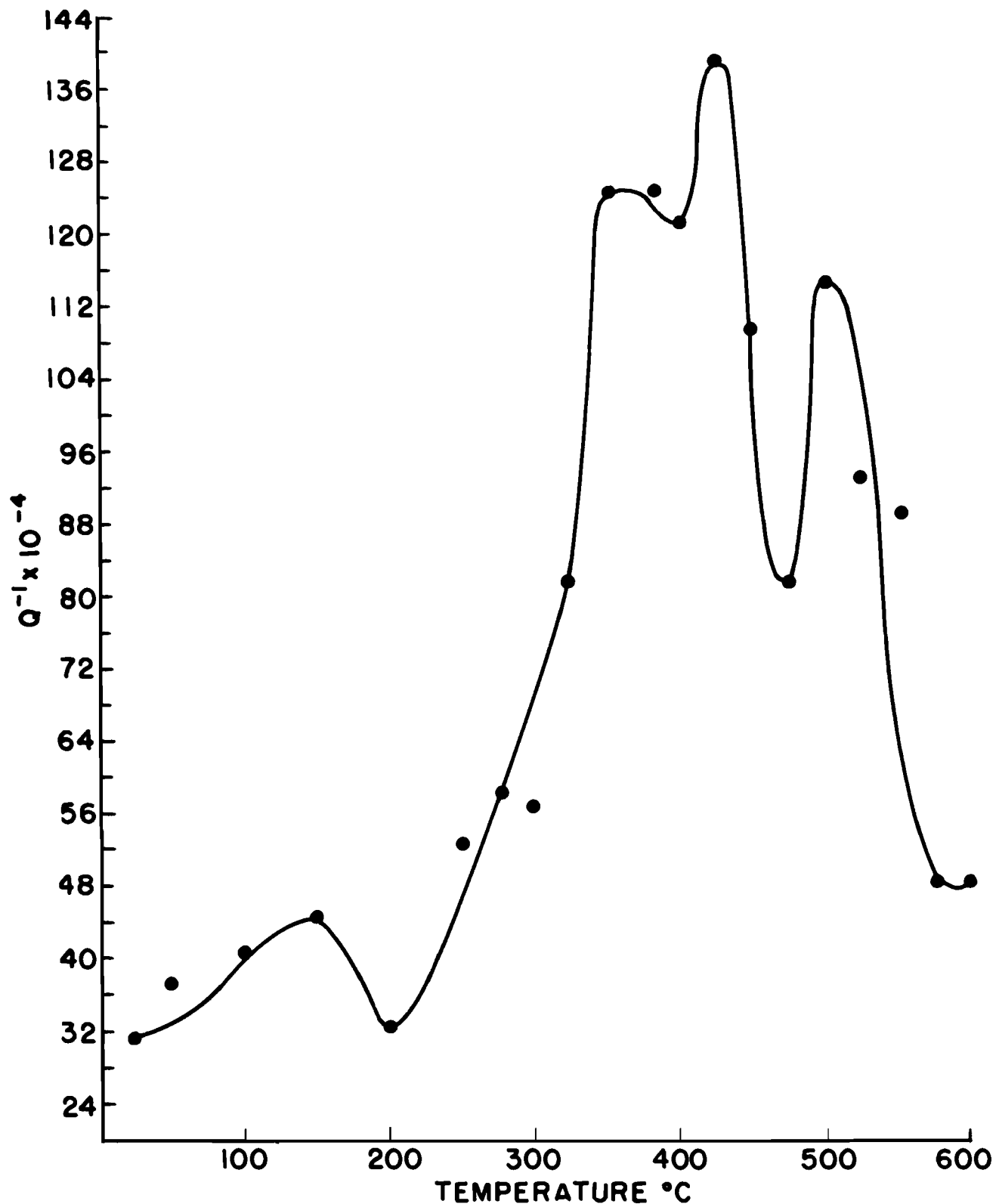
FIG. 46 INTERNAL FRICTION OF HIGH PURITY POLYCRYSTALLINE
TUNGSTEN OUTGASSED BY ELECTRON HEATING IN A
VACUUM OF < 10^{-5}MM Hg.

was surprising since all previous attempts (1) to resolve internal friction peaks in this type material were fruitless, although indications of a peak at 150°C were found.

Discussion

Typical spectrographic, vacuum fusion and carbon analyses have been compiled in Table 12. Polycrystalline tungsten has a somewhat higher interstitial content and more metallic impurities. However, single crystals do contain interstitials and metallic impurities in substantial magnitude.

From the work to date, it is concluded that probably two interstitials are apparent in single crystal tungsten. This follows from the behavior of the 300°C peak, which (a) cannot be attributed to cold working or electropolishing, (b) can be precipitated and recovered by heat treatments, (c) apparently has a single relaxation time necessary for the interstitial process, and (d) is not observed for an orientation close to [111] as predicted theoretically for the Snoek mechanism. For the second characteristic peak at 475°C it can be said that the peak, (a) is not evident for an orientation close to 111 , (b) is developed by high temperature anneals, (c) is enhanced by carbon dosing, and (d) cannot be attributed both to cold working and electropolishing. Since these peaks appear to be similar to interstitial peaks in other b.c.c. metals, a comparison can be made between the relative peak heights in tungsten and tantalum. (See Fig. 47.) From this figure it can be seen that the oxygen peak for Ta at about 150°C is by an order of magnitude stronger than the 300°C peak and the 475°C peak of single crystal tungsten. Incidentally, the internal friction measurements on tantalum were also conducted in the same apparatus used for tungsten.

Approximate activation energies can be obtained for the various peaks observed in polycrystalline and single crystal tungsten from a Marx and Wert plot (83). The peaks at about 300°C and 475°C have activation energies of approximately 40,000 cal/mole and 50,000 cal/mole, respectively. For polycrystalline tungsten the peaks at 150°C, 325°C, 475°C and about 500°C have activation energies of approximately 30,000, 40,000, 50,000 and 52,000 cal/mole respectively. Becker, et al (84) have recently obtained an activation energy of about 50,000 cal/mole for carbon diffusion in tungsten. This agrees rather well with the activation energy for the enhanced carbon peak at 475°C.

It thus appears quite certain that the peak at 475°C is most probably due to carbon. With some reservations, the peak at 300°C can be attributed to either oxygen or nitrogen. Additional work, especially that involving controlled dosing is required in order to prove these statements conclusively.

95
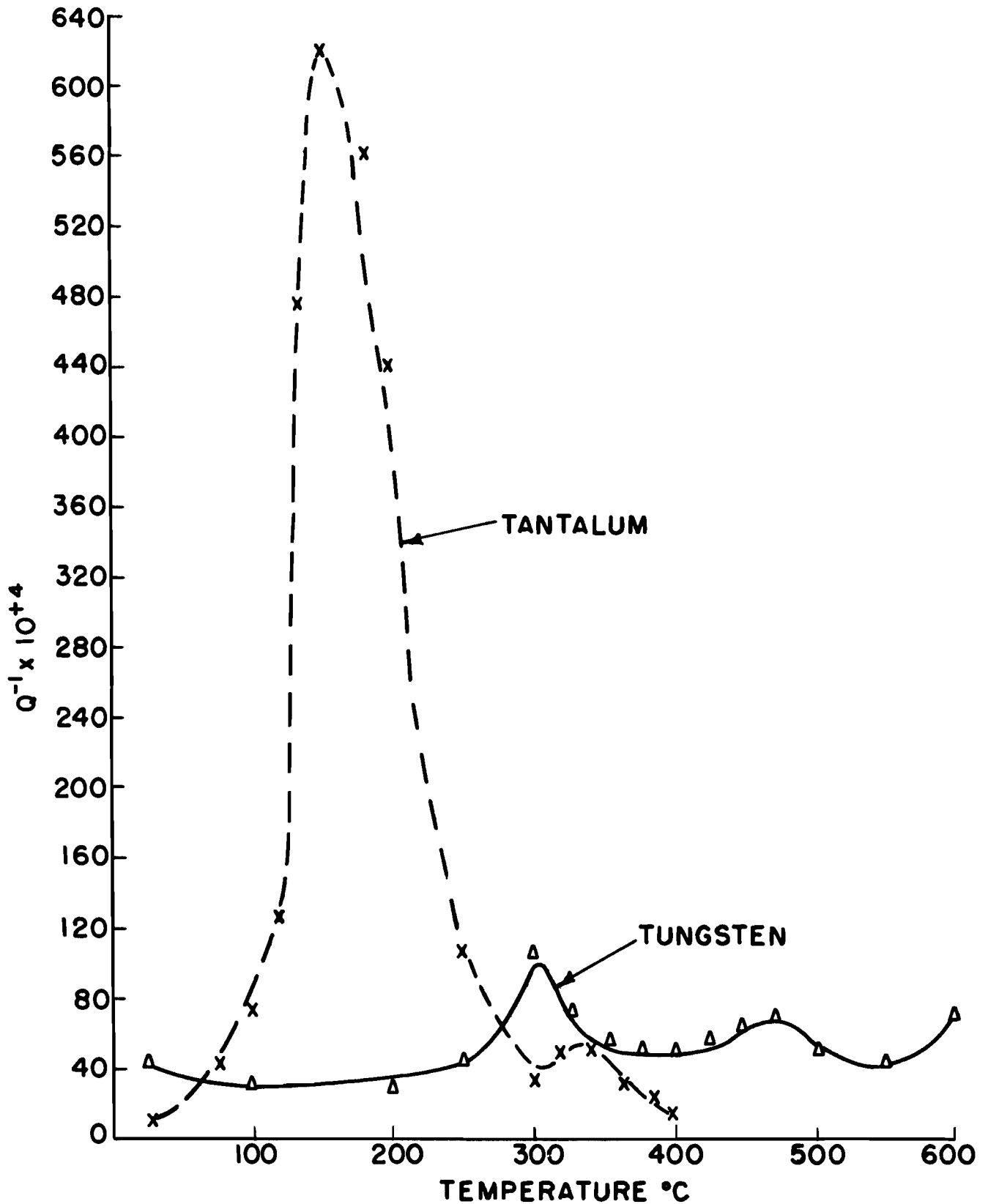
FIG. 47 COMPARISON BETWEEN THE INTERNAL FRICTION IN SINGLE CRYSTAL TUNGSTEN AND POLYCRYSTALLINE TANTALUM.

96

5. Interstitial Dosing

a) Carbon

The previous work (1,2) has served to outline in a semi-quantitative manner the phenomenology of carbon dosing. It has become quite clear that tungsten can be easily "dosed" with carbon and that carbon can conversely be removed from tungsten quite as easily. This was demonstrated in qualitative and semi-quantitative procedures using radiocarbon, both as an analytical tracer and in autoradiographic studies. A deficiency in the previous work was the lack of quantitative analytical data. In the present work, in addition to completing the qualitative picture, some quantitative data have been obtained. These data were obtained using two methods: gas volumetric analysis and quantitative radiochemical procedures.

What remained to be determined in a systematic way were the exact dosing parameters. Since two competing processes are involved - the loss of carbon versus the dosing process - it is necessary to obtain the equilibrium concentration of carbon in tungsten as a function of specimen temperature and carbon "pressure" in the dosing environment. In the present work only the latter was varied. Although the work is incomplete, the data obtained thus far have indicated quite clearly the experimental path to be followed in order to determine these dosing parameters.

Analytical Procedures

Most of the experimental and analytical procedures as well as the apparatus have been previously described (1,2). Modifications and additions are discussed in the following.

I Radiochemical - Ionization Chamber Method

As a result of a systematic study of the sources of possible error of the total system, it is now possible to realize the full potential of the ionization chamber-vibrating reed electrometer system for carbon-14 analysis. A precision of 2% is achievable on 70 milligram samples containing on the order of 0.02 microcuries of carbon-14.

II Radiochemical - Autoradiography

A further evaluation of the autoradiographic technique was undertaken in order to eliminate any possibility that the procedures used may lead to erroneous conclusions. The central question concerned the possibility that an autoradiograph of grain boundary penetration might be produced not by carbon in the boundary, but rather by carbon which may have lodged in the boundary during the polishing procedures. That such did not occur was amply demonstrated. A carbon-14 containing specimens on which a surface scratch

Fig. 48a.　Photomicrograph of Carbided Tungsten
Specimen Provided with Scratch - 200X
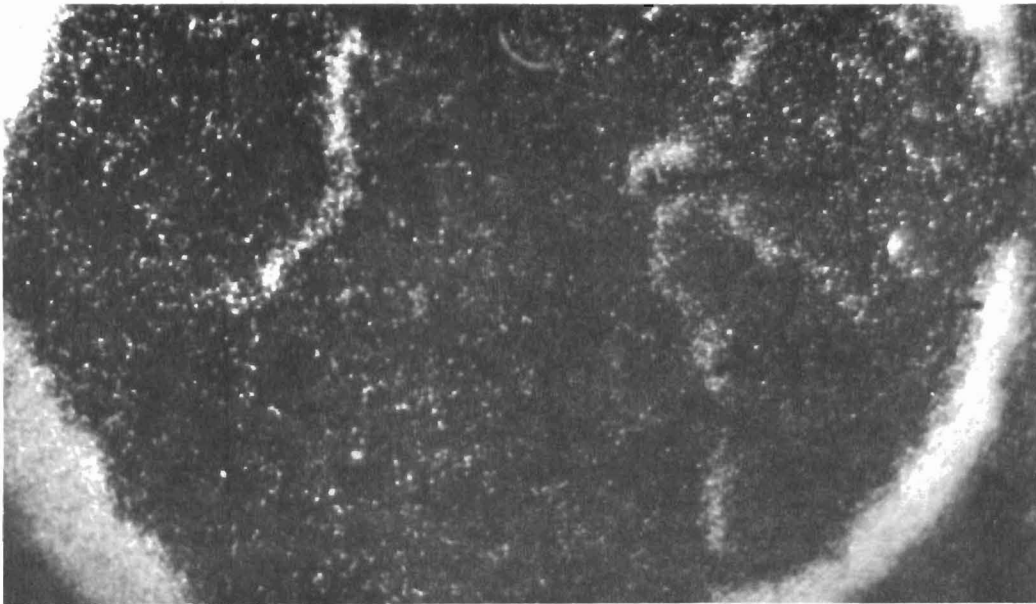
Fig. 48b.　Autoradiograph of Carbided Tungsten Specimen
Provided with Scratch - 200X

was made was polished, etched, and cleaned ultrasonically. A photomicrograph of this specimen is shown in Fig. 48a. The autoradiograph which resulted (Fig. 48b) did not reveal the presence of the scratch indicating that the etching and cleaning procedures did indeed prevent artifacts due to the polishing residues.

III. Gas Volumetric Analysis of Carbon

In this procedure, carbon is determined volumetrically as carbon dioxide liberated from the oxidized tungsten specimens.

Dosing Experiments

The results of the dosing experiments are reported in the following in a chronological order. It is felt that in this way the essential direction of the work will be better elucidated.

I. Acetylene Dosing

This work was reported previously (2), but will be briefly outlined here in order to give a complete picture. Using the radioactive hydrocarbon acetylene at pressures up to approximately 500 microns, it was qualitatively demonstrated that tungsten can be dosed with carbon. The conditions employed, however, did not allow for controlled dosing as anticipated since the specimens could not be dosed in a homogeneous manner. The work also demonstrated that tungsten readily lost carbon when subjected to high temperature vacuum anneals. This clearly confirmed the possibility of controlled uniform dosing of tungsten, since the simultaneous occurrence of the two processes (loss and gain of carbon) indicates a true thermodynamic equilibrium. Thus by the proper selection of pressure and specimen temperature the rates of the two competing processes can be adjusted independently to yield the desired equilibrium concentrations of carbon in tungsten.

II. Diffusion Pump Oil Dosing

Since the dosing in low pressures of acetylene yielded samples which contained carbide precipitates, it was evident that much lower pressures of hydrocarbons were necessary. Thus attempts were made to dose the specimens in diffusion pump oil. Worked tungsten rods, 0.040 inches in diameter, were annealed at 2700°K in the vapor of pump oil and in the presence of a small initial pressure of carbon-14 tagged acetylene. The presence of carbon in the specimen after the dosing treatment was confirmed by the ionization chamber method. Metallographic examination did not reveal any detectable differences between the dosed and undosed recrystallized structure of the specimen. This was taken to indicate that the carbon was in solution. A 30 minute anneal at approximately 600°C failed to precipitate the dissolved carbon.

A one hour anneal at approximately 2200°C in vacuum eliminated almost all of the carbon, producing the radial concentration gradient shown in Fig. 49. Figs. 50, 51, 52 and 53 show the cross sections of a tungsten single crystal specimen after various steps of a typical carbon dosing and decarbiding run. The samples were etched after dosing in boiling hydrogen peroxide. It would seem from the photomicrographs presented in Figs. 50, 51, 52 and 53 that the carbon introduced is in solution, and that during the low temperature anneal the carbon atoms have diffused to and have decorated the dislocation sites. One reservation that must be stated is the possibility that the appearance of the dislocation etch pits may be due to an orientation effect. However, as shown in Fig. 49, the radiochemical measurements do support this dosing picture, including the total loss of carbon upon high temperature vacuum anneals. Hardness data taken on the specimens did not reveal any significant differences between specimens.

III. n-Hexadecane and Naphthalene Dosing

Since the composition of the pump oil used was not known, the attainment of a precise knowledge of dosing parameters could not be expected. Therefore an oil of low vapor pressure but of known composition was sought for the continuation of the investigation. Hexadecane was chosen because the vapor pressure is known and is very closely described by the classical Clausius-Claperon equation. It was therefore expected that for controlled dosing, conditions could be exactly established using this hydrocarbon. In addition, a carbon-14 tagged hexadecane is commercially available at reasonable cost. The hydrocarbon, naphthalene, was also employed in order to evaluate the dosing procedure at higher hydrocarbon pressures.

Originally, the internal friction specimen No. 7 was dosed for six hours at 2000°C in n-hexadecane. Since the internal friction measurements made with this specimen after the treatment were inconclusive, the specimen was dosed a second time (but in naphthalene) for sixty-eight hours at 2000°C.

Internal friction measurements carried out after this treatment still did not yield any pronounced peak, and dosing was therefore repeated in naphthalene at 2000°C for one and one-half hours, again yielding no results. Following the assumption that the vapor pressure of naphthalene was too low, the sample was next dosed at 2000°C in a high (but undetermined) vapor pressure of naphthalene. The dosing anneal was allowed to progress until a drop in resistance was manifested in the self-resistant heated specimen. The specimen was then once more studied for its internal friction response. For the first time, two peaks were found as discussed in section IIB-4.

Following this success, a preliminary dosing run was made on a polycrystalline tungsten wire specimen using the C-14 tagged hexadecane. Upon analysis it was found that the sample was approximate-
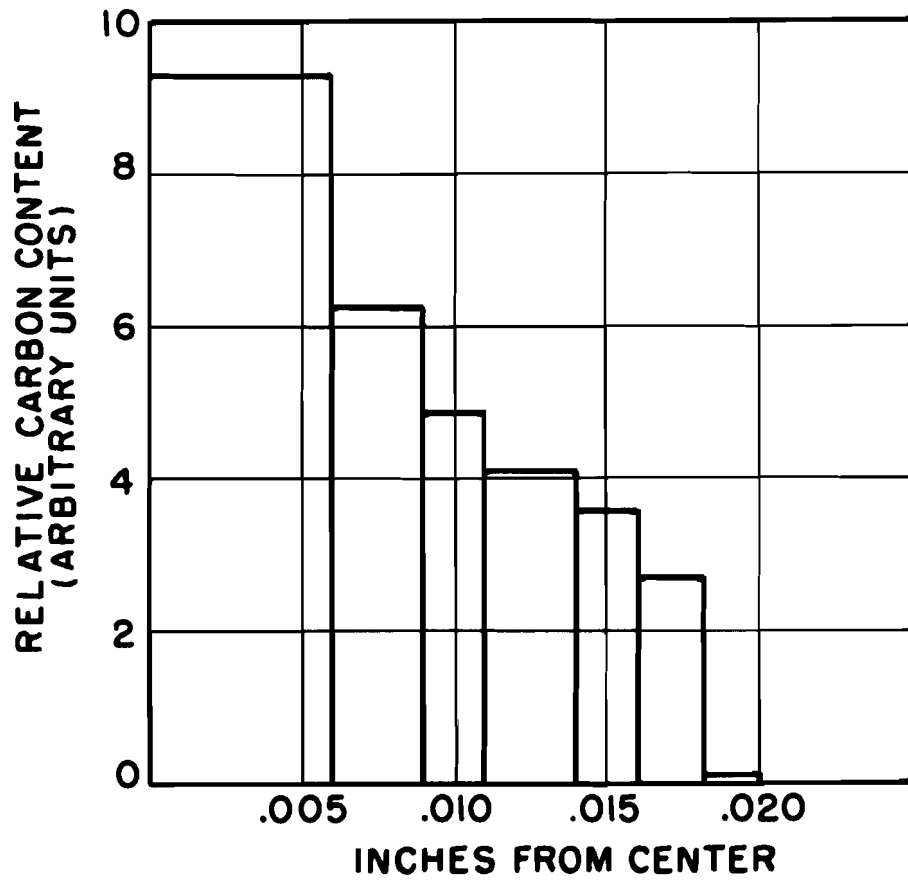
FIG. 49 RADIAL CONCENTRATION GRADIENT OF CARBON IN A DECARBURIZED TUNGSTEN ROD.

Fig. 50 Tungsten Single Crystal after Vacuum Anneal at 2200°C, 5-1/2 hrs.; 600X
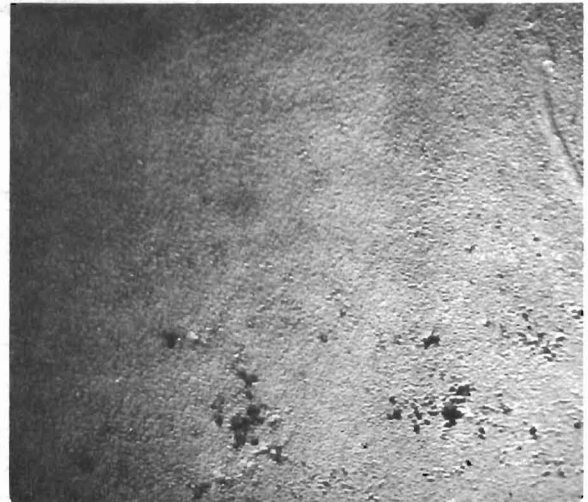
Fig. 51 Tungsten Single Crystal After Dosing Anneal per Fig. 50 following Vacuum anneal at 2200°C, 7 hrs., 600X

Fig. 52 Tungsten Single Crystal after Precipitation Anneal at 600°C, 7-1/2 hrs. following anneals per Figs. 50 and 51; 600X

Fig. 53 Tungsten Single Crystal after Vacuum Anneal at 2200°C, 6 hrs. following anneals per Figs. 50, 51 and 52; 600X

102

Table 13
Carbon Dosing of Tungsten in
C-14 Tagged Hexadecane Vapor

Material	Pre-anneal Time (min.)	Pre-anneal Temp. (°C)	Dosing Time (min.)	Dosing Temp. (°C)	Amps/gm. x 10^{-15}
S-doped	none	--	1041	2000	6.3
"	"	"	2580	2000	4.4
Undoped HF washed	"	"	3920	2000	0.0
"	161	2300	?*	2000	90.0
"	30	2300	1030	1800	1.9
"	330	2300	?*	2000	50.0
"	345	2100	1400	2000	2.1
"	345	2300	1448	2000	1.3

* Sample failed sometime after burning for approximately 100 minutes.

103

ly four times more radioactive than the background. This qualitative result indicated that the specimen was dosed when annealed approximately seven hours at 2000°C in hexadecane vapor. Seven additional dosing runs in the radioactive hexadecane vapor were then made. The results are given in Table 13. The data under the column "amps/gm" are the values of the ionization current in the electrometer chamber, and these are directly proportional to the concentration of radioactive carbon in the sample. The pre-anneal time refers to a vacuum degassing anneal given to the specimen prior to the dosing anneal. All temperatures listed are brightness temperatures uncorrected for the absorption of the sight port glass. A value of 1×10^{-15} amperes per gram represents an ionization current approximately 50% greater than the background ionization current. Although at the time an accurate correlation between the ionization current and the amount of carbon it represents could not be made, it appears that 1×10^{-15} amperes per gram may represent as little as one part per billion of carbon. It should be noted that there is a great deal of uncertainty in this estimate due to the large uncertainty in the estimated specific activity of the hexadecane.

The data thus far obtained were encouraging though rather inconclusive, although it did appear that greater hydrocarbon pressures will be required if the estimate of the specific activity is of a reasonable magnitude. It is not clear whether the two samples which showed comparatively large amounts of carbon as shown in Table 13, failed because of their carbon content. The rather large amount of carbon may be due to cracking of the hydrocarbon at the moment of burn-out, and a subsequent surface contamination by the resulting hydrocarbon fragments. It also appears from the last column of Table 13, that S-doped tungsten is dosed more readily.

At this point in the work a gas volumetric method of carbon analysis capable of determining the small quantities of carbon involved became available. Results of carbon analysis of naphthalene dosed polycrystalline pure tungsten wire (.019" diameter) are presented in Table 14. Sections were cut from the specimen at intermittent times and each were electrolytically etched before analysis to remove any surface contamination due to hydrocarbon breakdown products. Temperatures quoted are brightness temperatures. It appeared quite clear from the data of Table 14 that dosing in naphthalene vapor at the pressures used would not lead to the desired product, namely a uniformly dosed specimen containing no carbides. The vapor pressure of naphthalene is evidently too high at room temperature. Microscopic examination of the specimen and hardness values confirmed the analysis insofar as the conversion of the sample to carbide was concerned.

Table 14
Hardness and Carbon Analysis of Dosed Polycrystalline Tungsten (PB-14)

Sample No.	Condition	Weight % Carbon	Knoop Hardness
1	As received	0.0167	not taken
2	Vacuum degassed; annealed 360 min., 2200°C	0.0178	not taken
3	After above, plus anneal 1444 min. dosing 2200°C	3.1450	not taken
MQ-0	As received	0.011	not taken
MQ-1	Degassed 300 min., 2100°C	0.044	407
MQ-2	After above, plus 60 min. dosing anneal 2000°C	0.074	457
MQ-3	After above, plus additional 420 min. dosing anneal	1.662	Surface-874 Center-1324

Attempts were then made to dose in n-hexadecane vapor. Table 15 gives the results of this experiment.

Table 15
Hardness and Carbon Analysis of Hexadecane Dosed Polycrystalline Tungsten (PB-14)

Sample No.	Condition	Weight % Carbon	Knoop Hardness Surface	Center
MQ-2-0	as received	0.0098	not taken	not taken
MQ-2-1	Vacuum degassed, 180 min., 2100°C	0.0130	409	424
MQ-2-2	After treatment of MQ-2-1, Dosed, 360 min., 2000°C	0.0800	415	483
MQ-2-3	After treatment of MQ-2-1, Dosed, 2760 min., 2000°C	1.9820	1700	1638

As before, the specimens were electrolytically cleaned before analysis. These results can be made to appear reasonable if one accepts the likelihood of a contaminated system. Although the system was not specially cleaned for the MQ-2 series, the system was clean enough to hold a static vacuum overnight, the pressure increasing only 2-3 microns during that period, the normal leak rate of the system. Another possibility is that the build-up of hydrocarbon fragments in the gas phase may be sufficient to affect the conversion to the carbide. The system was then thoroughly cleaned using hydrogen fluoride on all glass surfaces and nitric acid on the copper and nickel lead supports. The dosing experiment was repeated in this clean system. The results are listed in Table 16 and will be discussed in conjunction with the data in Table 17.

Table 16
Hardness and Carbon Analysis of Hexadecane Dosed
Polycrystalline Tungsten (PB-14)

Sample	Condition	Weight % Carbon	Knoop Hardness Surface	Center
MQ-3-0	As received	0.0171	not taken	not taken
MQ-3-1	Vacuum degassed, 180 min., 2100°C	0.0113	283	249
MQ-3-2	After treatment of MQ-3-1, Dosed, 360 min., 2000°C	0.0080	445	434
MQ-3-3	After treatment of MQ-3-1, Dosed, 1495 min., 2000°C	0.0096	452	402

Before the results presented in Table 16 had become available, an experiment was performed to eliminate the possibility that the "dosing" evident in the MQ-2 series was due to an accumulation of hydrocarbon breakdown products in the dosing chamber. The system was modified by including a sidearm containing the hexadecane on the side of the dosing chamber opposite the vacuum port. During the dosing run the vacuum port was maintained open, thereby causing the decomposition products to be removed as well as causing a flow of hexadecane around the heated specimen. The results of this run are displayed in Table 17.

Table 17
Hardness and Carbon Analysis of Hexadecane Dosed Polycrystalline Tungsten (PB-14) in Flow System

Sample	Condition	Weight % Carbon	Knoop Hardness Surface	Knoop Hardness Center
MQ-4-0	As received	0.0157	not taken	not taken
MQ-4-1	Vacuum degassed, 155 min., 2100°C	0.0155	432	385
MQ-4-2	After treatment of MQ-4-1 Dosed, 350 min., 2000°C	0.0113	393	405
MQ-4-3	After treatment of MQ-4-1 Dosed, 675 min., 2000°C	0.0106	483	396

From the data of Table 16 and 17 it would appear that the concentration of carbon in tungsten at 2000°C (brightness) in equilibrium with approximately one micron pressure of n-hexadecane vapor is below 80 weight ppm, and that the apparent dosing in hexadecane vapor was due to an unknown contamination of the system. That hexadecane is decomposed in both the flow and static systems is evidenced by the presence of deposits of carbon or carbon containing compounds on the walls of the dosing chamber. The presence of carbon in the deposits was demonstrated by radiotracer methods.

Specimens which were dosed in a manner identical to the MQ-4 series except that C-14 tagged hexadecane was used did show a small pick-up of radiocarbon indicating that although there was a net loss of carbon from the tungsten, a small amount of exchange did take place. A plot of the carbon concentration versus annealing time of runs MQ-3 and MQ-4 is shown in Fig. 54. Although the data leave much to be desired, it is unmistakable that the rate of carbon loss diminishes with decreasing carbon content, i.e., that equilibrium is being approached. This strongly indicates that the conditions employed are close to those necessary for controlled dosing in the low concentration range, i.e., below and close to the 80 ppm range.

Part of the experimental difficulty is the high carbon content of the "as received" tungsten specimens. Attempts will be made in future work to more efficiently decarburize the specimens before dosing. The work will continue along quantitative lines, obtaining equilibrium carbon concentrations as a function of specimen temperature and hydrocarbon pressure.
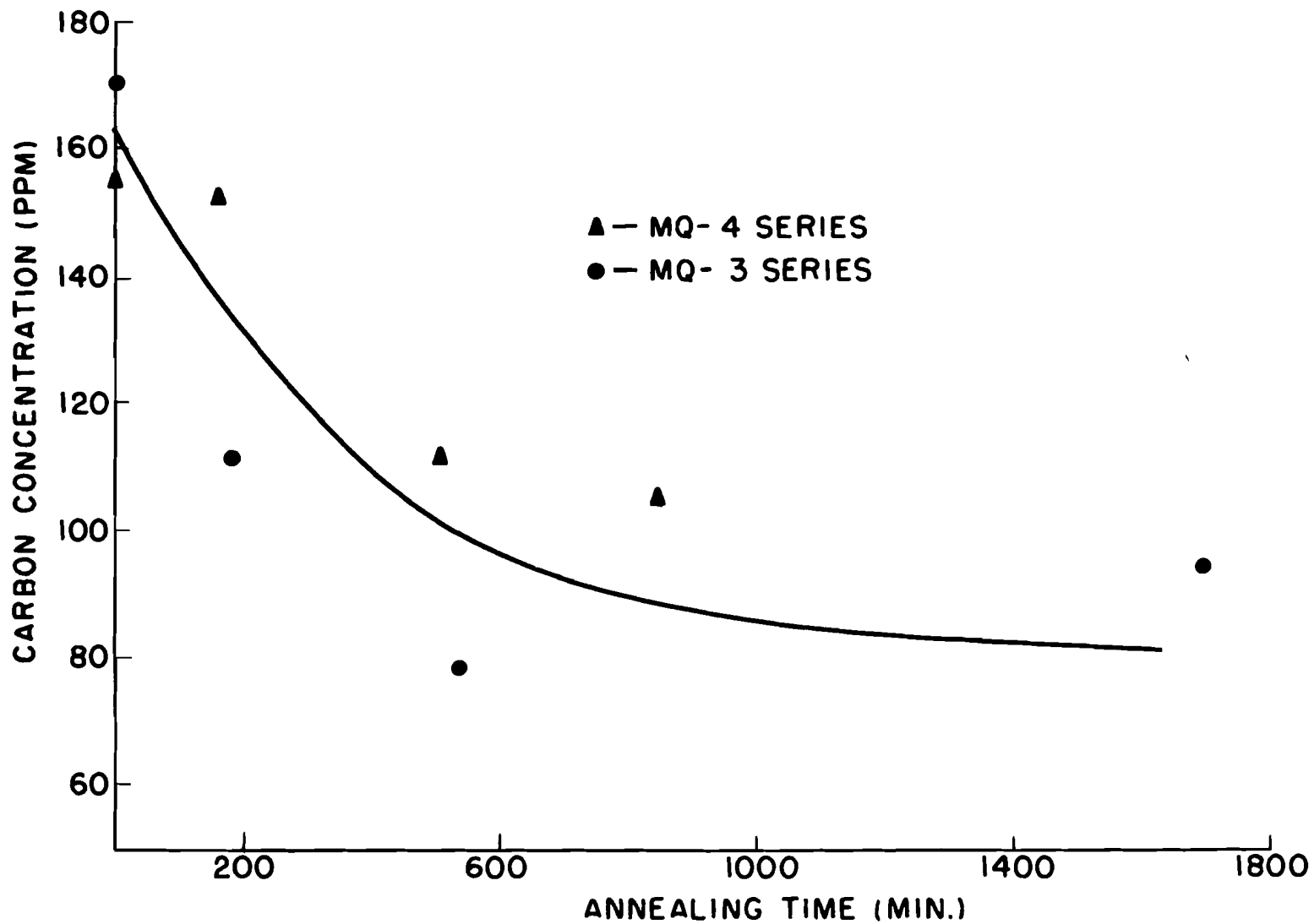
FIG. 54 LOSS OF CARBON AT 2000°C (BRIGHTNESS) IN ~ I MICRON PRESSURE OF n-HEXADECANE VS TIME.

Conclusions

The results presented allow for the conclusion that with hexadecane at room temperature, tungsten at 2000°C brightness can be dosed with carbon near (but below) the 80 ppm concentration range. The naphthalene room temperature vapor pressure apparently is too high for dosing at 2000°C (brightness), producing tungsten carbide precipitation. Naphthalene may be suitable at higher specimen temperatures. However, since in accordance with the W-C phase diagram, the maximum solubility of carbon exists at 2475°C (23) and since 2000°C brightness corresponds to approximately 2300°C true temperature (including correction for the absorption of the sight port glass), only a very small temperature increase is available for high carbon concentrations in solution to be obtained. It appears from the foregoing that with a hydrocarbon vapor pressure somewhere between that of naphthalene and of hexadecane, controlled dosing can be achieved.

b) Oxygen

Previous attempts were made to introduce oxygen into tungsten by annealing specimens in WO_3 vapor. The method of soaking in WO_3 vapor was used because at temperatures above 1000°C tungsten oxide is readily volatilized, and the inward diffusion of oxygen cannot compete with the kinetics of the volatilization process. By annealing in a WO_3 atmosphere it was expected that the oxygen concentration of the tungsten specimen would come into equilibrium with the surrounding WO_3 pressure.

After the specimens were annealed in WO_3 vapor they were electrolytically stripped in a NaOH solution to various depths and the vacuum fusion analysis performed. It was found that this technique of stripping always introduced oxygen on the surface of the specimens, and no simple method of sample preparation could be devised which would eliminate this surface oxidation which introduces spurious data. Instead, a method was developed which did allow one to differentiate between the amount of oxygen found in the samples due to actual dosing and that introduced by the preparative procedures. This method consisted of dosing with oxygen containing a known higher percentage of oxygen-18 than found naturally, then analyzing (with the mass spectrograph) the oxygen obtained from vacuum fusion for its oxygen-18 content. In this fashion it is possible to determine unambiguously the origin of the oxygen. Experiments carried out at 1000°C for 140 hours showed only a 0.002 inch penetration of oxygen-18 into the tungsten. Obviously higher temperatures were required.

Experimental

Results of a dosing run at 1400°C are shown in Table 18.

Table 18
Oxygen Penetration in Polycrystalline
0.040 Inch Diameter Tungsten Rod
Annealed for 14.5 Hours at 1400°C

Sample No.	Zone of Penetration from r_1 to r_2 (inches x 10^4)	Average Oxygen-18 Concentration (ppm)
1	3.88 - 4.00	306
	3.62 - 3.88	4.2
	3.06 - 3.62	4.3
	1.39 - 3.06	0.41
	1.00 - 1.39	15.0
	0.00 - 1.00	0.00
2	3.06 - 3.88	62.1
	1.39 - 3.06	4.3
	1.00 - 1.39	8.2

Due to certain experimental difficulties involved in the vacuum fusion analysis of oxygen-18, the data on the penetration of oxygen-18 into tungsten are quantitatively unreliable. Nevertheless, from a qualitative, or at best, semi-quantitative point of view, some useful information has been obtained. At 1400°C considerable penetration occurred with a 14.5 hour anneal.

Although the penetration was considerable, the quantities that penetrated were quite small. The conclusion thus drawn from the data in Table 18 was that dosing in WO_3 vapor at still higher temperatures was required.

In order to achieve the required higher temperatures, a new induction heated dosing furnace was constructed. A schematic of this furnace is shown in Fig. 55. A quartz vacuum bell 2 feet high by 3-1/2" diameter provided with a side port was sealed to a steel base plate using Apiezon Hard Wax W. This vacuum bell was water jacketed by means of a 6 inch diameter pyrex cylinder. Since the water in the jacket is in contact with the base plate, the Apiezon wax is kept quite cool during furnace operation. The muffle (1-1/4" diameter x 4-1/2") was supported by a tungsten platform which was in turn supported by a 3/16" tungsten rod, approximately 2-1/2" long. This assembly fits into a molybdenum rod (3/8" in diameter by approximately 7-1/2" long) which was attached to the base plate in a threaded opening holding the muffle approximately 10 inches above the base plate.

POWER

PYREX SIGHT PORT

WAX

WATER OUT

TUNGSTEN MUFFLE

INDUCTION COIL

TUNGSTEN SUPPORT

QUARTZ BELL

PYREX WATER
JACKET

MOLYBDENUM
SUPPORT

STEEL BASE
PLATE

RUBBER GASKET

WAX

TO VACUUM MANIFOLD
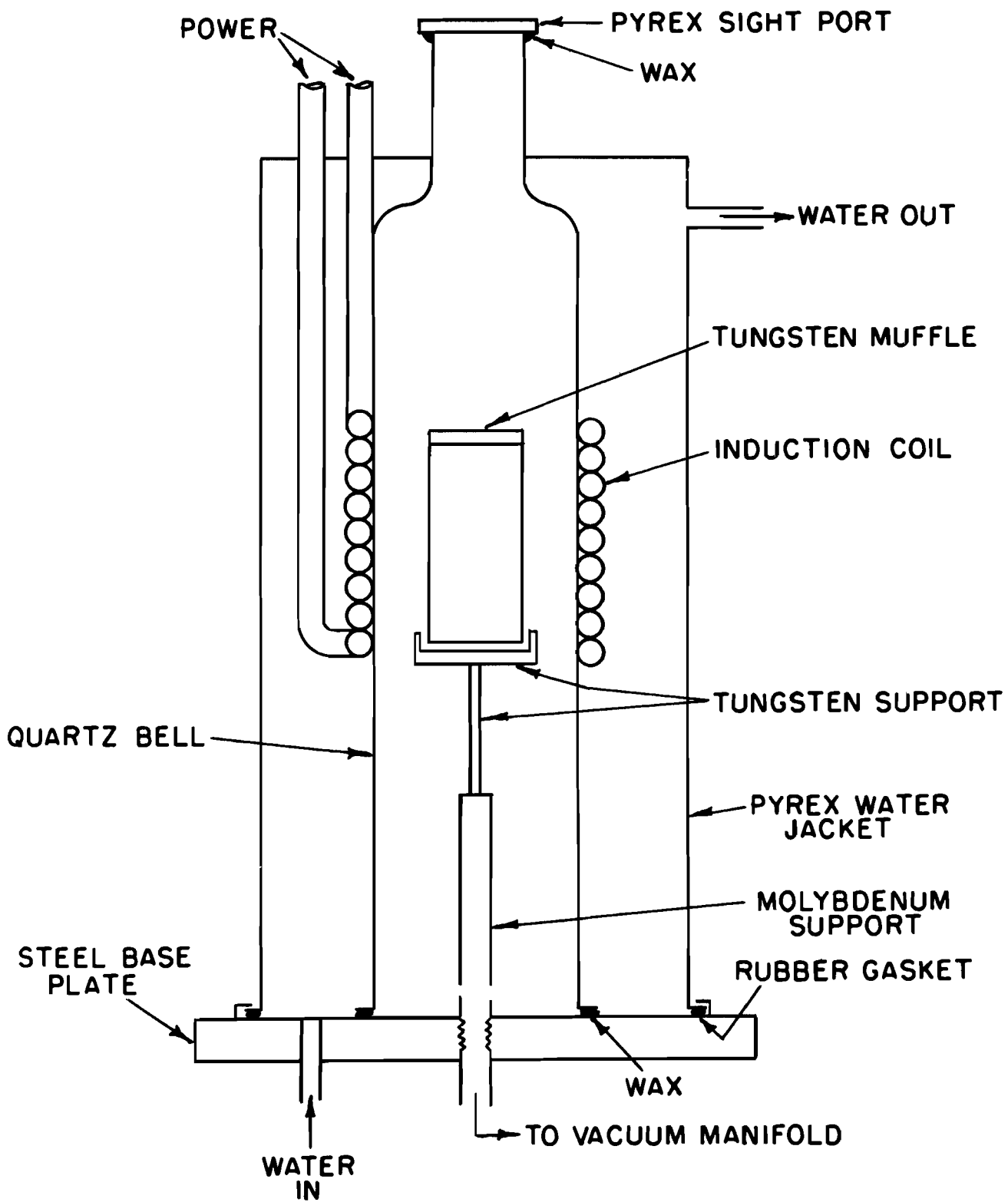
WATER
IN

FIG. 55 SCHEMATIC OF OXYGEN DOSING FURNACE

111

The sight port glass was fixed to the opening with Apiezon Hard Wax W. The water in the jacket comes to a height just 2 inches short of the sight glass.

Since the induction coil is immersed in the water, it was covered with glass fiber tape impregnated with shellac in order to prevent arcing. The power source is a 50 KW 10 kc motor generator. Preliminary runs have been made and it appears that a temperature of 2000°C can be achieved and maintained for extended periods of time. The system is at present being thoroughly tested.

It would appear from the results obtained thus far that oxygen dosing can be accomplished with the higher temperatures now available.

6. Recrystallization Behavior of Worked Single Crystal

In order to understand how alloying affects the recrystallization response of plastically deformed tungsten base alloy single crystals (0.35 and 5% Ta), the recrystallization behavior of worked pure single crystals of tungsten first had to be determined.

The experimental procedures and techniques were similar to those used in a previous preliminary investigation (85) on the recrystallization response of worked single crystals. The specimens were ground to size, encased in stainless steel tubing, rolled at a specific temperature to a predetermined reduction in area, and the stainless steel casing removed thereafter. This procedure, as was found in the previous investigation, is satisfactory in that the purity level of the starting material is essentially retained after mechanically removing the stainless steel case and then removing about 10 mils of the specimen surface by electropolishing.

The recrystallization behavior of the deformed single crystals was followed metallographically and by Knoop hardness measurements. The characteristic recrystallization response as determined by these measurements on single crystals deformed from 1100°C preheat temperature to various per cent R.A. is shown in Fig. 56. The specimens were annealed for one-half hour at each temperature. If the beginning of the drop in hardness is taken as an indication of the beginning, and an approximately constant hardness value as the end of recrystallization, the corresponding recrystallization temperature listed in Table 19 can be deduced from the curves in Fig. 56. The hardness values of the specimen used in the "as melted" condition are included in Table 20.
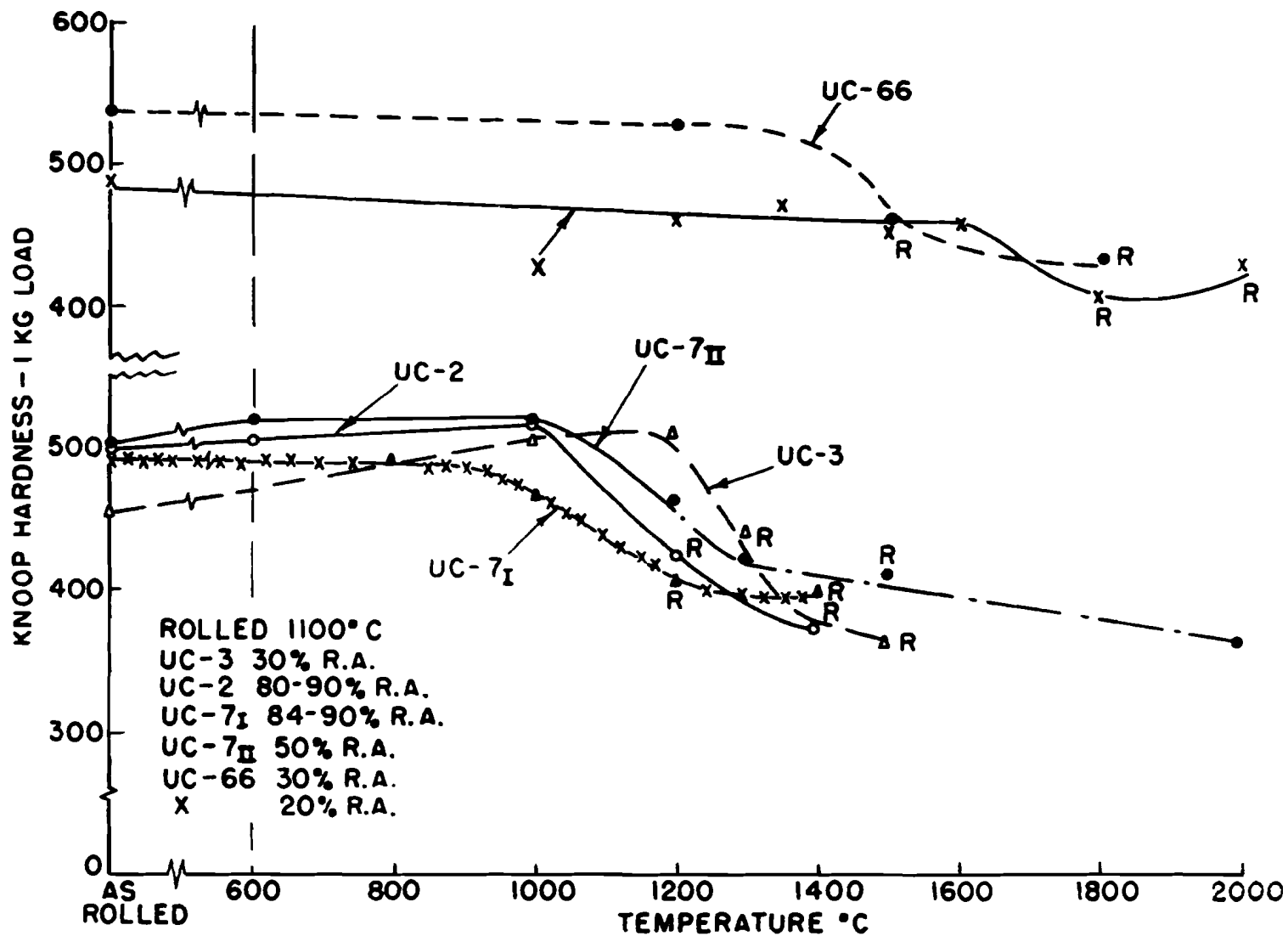
FIG. 56 KNOOP HARDNESS OF TUNGSTEN SINGLE CRYSTAL RODS ROLLED AT 1100°C
AS A FUNCTION OF ANNEALING TEMPERATURE (ANNEALED 1/2 HR. ;
R = RECRYSTALLIZED).

113

Table 19
Approximate Recrystallization Temperatures of
Worked Single Crystals as a Function of % R.A.

Specimens	Reduction in Area	Temperature for Beginning of Recrystallization	Temperature for end of Recrystallization
UC-X	20%	1600°C	1800°C
UC-66	30%	1200°C	1500°C
UC-3	30%	1200°C	1500°C
UC-7 II	50%	1000°C	1200-1300°C
UC-7 I	80-90%	1000°C	1200°C
UC-2	80-90%	1000°C	1200°C

Recrystallization temperature is defined here as it was before
(85); i.e. it is that temperature at which new grains are formed in
the entire specimen. In accordance with this definition, the hard-
ness values which correspond to the completion of recrystallization
of the specimens are indicated by the letter "R", in Fig. 56. The
recrystallization temperatures thus determined are about 1800°C for
20% R.A., 1500°C for 30% R.A., 1200-1300°C for 50% R.A. and 1200°C
for 80-90% R.A.

Vacuum fusion analyses, quantitative spectrographic analyses,
and the crystallographic axial orientations of some of the specimens
used are presented in Table 20.

An optical microscope was used to follow microstructural changes
taking place in the deformed single crystals upon annealing. Deforma-
tion bands, twins, and aligned etch pits or dislocations were observed.
If etch pits (specimens are electropolished in 10% NaOH solution and
etched in either boiling $H_2 O_2$ or in $K_2 Fe_4 Cn_6$) are identified with
dislocations, the density and configuration of dislocation change
with the amount of working. At lower degrees of working (20% R.A.)
the dislocations appear to be randomized, whereas with increasing
amounts of work the dislocations tend to be aligned in the direction
of working, see Fig. 57. In agreement with the observations of
Berlec (86), cubic and pyramidal types of etch pits characteristic
of the cubic and octahedral planes respectively, were noted.

Since deformation was heterogeneous, the structural response
upon annealing was heterogeneous. In a few instances subgrain forma-
tion was noted. However, since these specimens were worked from a
preheat temperature of 1100°C, the aligned dislocations appear to be
quite stable to annealing temperatures. At temperatures in the
recrystallization range, the aligned dislocations appear to coalesce
and form what could be termed "nuclei". (See Fig. 58.) It should

Fig. 57   Single Crystal Tungsten
           No. UC-2 as Rolled 80-90%
           R.A. - 1000X
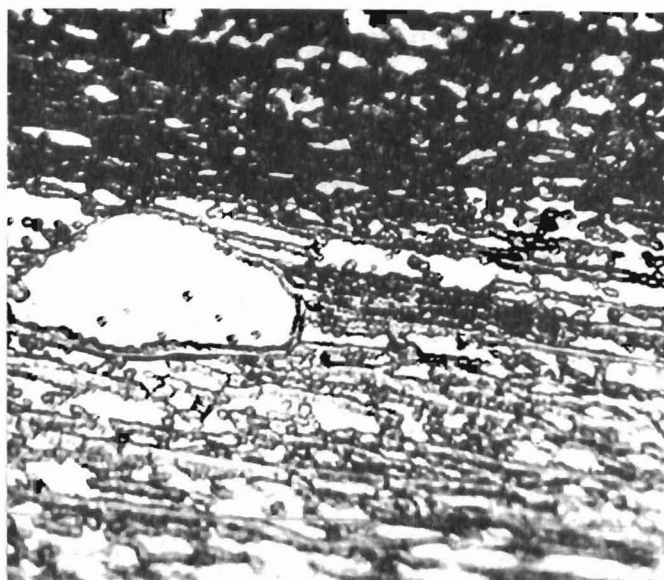
Fig. 58   Single Crystal Tungsten
           No. UC-2 Rolled 80-90% R.A.,
           Annealed for 4 Hrs. at 1000°C-
           1000X

115
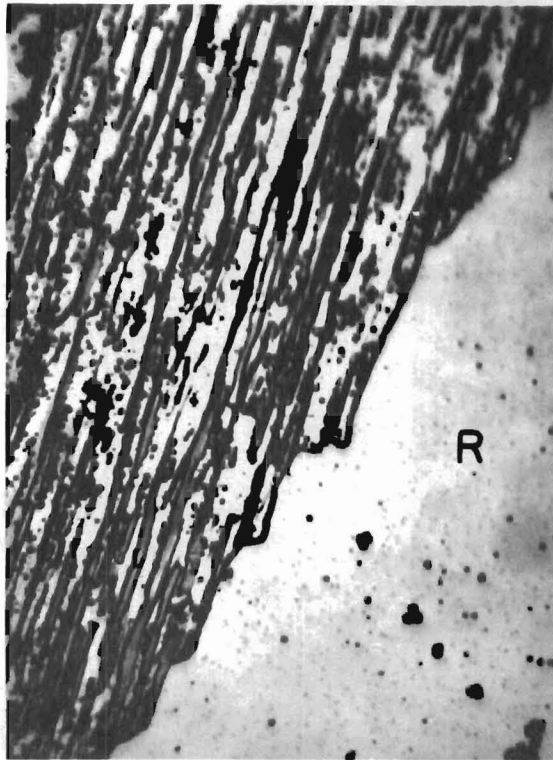
Fig. 59   Single Crystal Tung-
          sten No. UC-2 Rolled
          80-90% R.A., Annealed
          for 3 Hrs. at 1100°C-
          100X
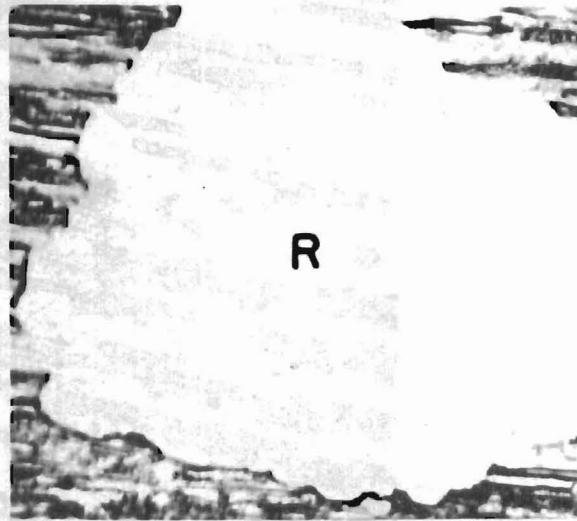
Fig. 60   Single Crystal Tungsten
          No. UC-2 Rolled 80-90%
          R.A., Annealed 1/2 Hr.,
          1100°C - 500X

Fig. 61   Evidence of Grain Boundary
          Migration in Thermally Etched
          Worked Single Crystal (1/2 Hr.
          at 1900°C) -250X

Table 20
Crystallographic Orientation and Spectrographic and Vacuum Fusion Analyses of as Melted and Worked Single Crystals of Tungsten*

Crystal	Fe	Al	Ni	Si	Mg	Cu	O_2	H_2	N_2	Axial Orient.	Knoop Hardness (1 KG load)
UC2 as melted	ND	ND	ND	ND	ND	ND	9	.6	4	110	429
UC2 worked	8	5	5	20	FT+	VF	39	4	10		-
UC3	ND	ND	ND	ND	ND	ND	ND	ND	ND	ND	386
UC7 as melted	ND	ND	ND	ND	ND	ND	3-8	ND	2-3	310	386
UC7 worked	2	4	3	1	17	2	39	6	12		-
UC66 as melted	ND	ND	ND	ND	ND	ND	15	3	7	110	384
UC66 worked	1-14	1	3	1	9	3	15	1	8		-

FT+ = .005 - .01%

VF = .0001 - .001%

ND = not determined

* = values are given in wt. ppm

be emphasized, however, that this process does not correspond to nucleation in the usual abrupt sense, but rather represents a continuous process. In some instances the coalesced dislocations or "nuclei" appear to grow with the help of the aligned dislocations. This is shown in Fig. 59. It is worth mentioning that the interface of the coalesced dislocations (or the "nucleus") exhibits inflection points at every point where the aligned dislocations intersect the interface of the "nucleus". This suggests that the driving force for growth of the "nucleus" is supplied by the interfacial energy of the aligned dislocations. Thus it appears that these aligned and quite stable dislocations in the deformed matrix possess sufficient energy to promote migration of the interface of the various "nuclei".

Assuming with Pugh (87) a simple Arrhenius relationship for the time and temperature required to obtain complete recrystallization, one can determine the activation energy of this process. Using the time to obtain complete recrystallization at 1100°C (4 hrs.) and 1200°C (25 min.) the activation energy was found to be about 90,000-95,000 cal/mole. This is comparable with the value of about 100,000 cal/mole obtained by Pugh. However, it must be mentioned that in certain instances the recrystallization response was erratic (requiring a longer time) and therefore this approach could not be applied throughout the temperature range. This erratic behavior was probably caused by impurity inhomogeneity in the single crystals during growth. As shown in Fig. 60, grain boundaries were not always seen at the interface of the deformed matrix and the "nucleus". In other instances, segments of subgrain boundaries were noted. This can be taken to indicate that the orientation of the "nucleus" and the surrounding area are nearly the same. At high annealing temperatures, the dihedral angles of the new grain appear to be unstable and the resultant grain sizes are quite variable. Also, upon annealing at high temperatures in a vacuum as previously observed (88) grain boundary migration is evident. (See Fig. 61.) As in the case of polycrystalline tungsten processed from a sintered ingot, these worked and recrystallized specimens are quite brittle, and fractured intergranularly with some twin formation.

The effect of the amount of work on the recrystallization response of single crystals deformed at 1100°C has been extensively investigated. However, the effects of other variables, such as orientation and purity, have yet to be studied. Therefore, only preliminary results like the effect of deformation temperature (which appears to be quite important) can be discussed. As part of this investigation, specimens cut from the same single crystal (UC-No. 7_I and 7_{II}) were similarly deformed at about 400°C and 1100°C to 50% R.A. The specimen which was deformed at the lower temperature had a different recrystallization and hardness response, as shown in Fig. 62. Twins were observed within the matrix and the specimen did not recrystallize. On the other hand, the specimen deformed at 1100°C did recrystallize. Since this specimen was void of twins, the inability to recrystallize may be due to twinning or some unknown precipitation phenomena.
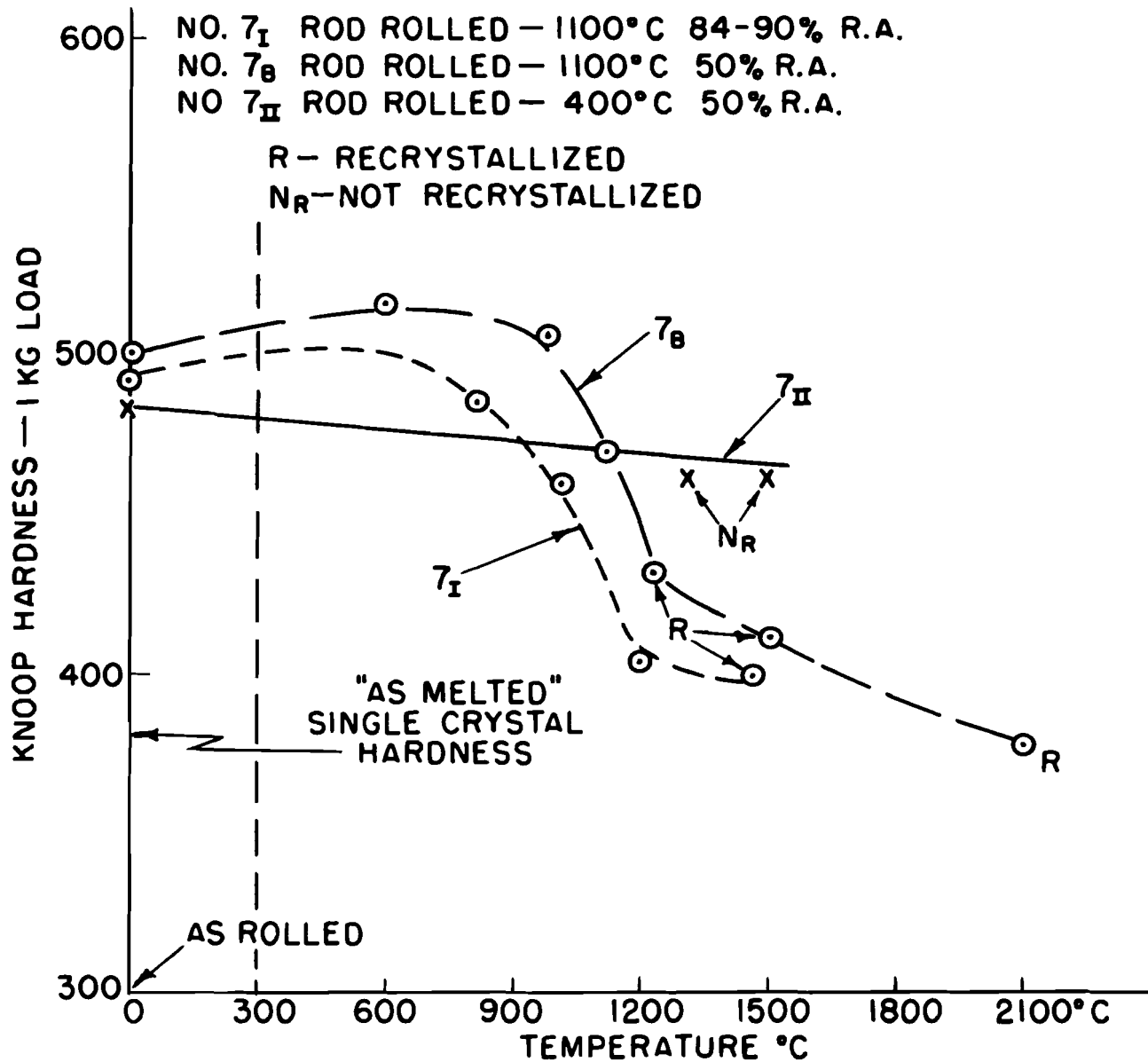
FIG. 62 EFFECT OF WORKING TEMPERATURE ON RECRYSTALLIZATION
AS DETERMINED BY HARDNESS MEASUREMENTS.

Some single crystal specimens cut from crystal #UC-66 which had an orientation close to 110 were rolled at 1100°C to a reduction in area of about 30%. The purpose of this part of the investigation was to obtain tensile specimens of the size shown in Fig. 63. Since insufficient single crystals were available, the investigation could not be pursued to conclusion. All pertinent data are listed in Table 21 and 22. Examination of the microstructure showed that these deformed crystals contained many deformation bands.

Table 21
Tensile Test Results of Worked Single Crystals

Tensile Specimen	Test Temperature	2% Offset Yield Stress PSI	Ultimate Stress PSI	Elong. in 1" %	Red. in Area %
UC-66-1	200°C	90,900	96,200	8.2	67
UC-66-2	300°C	71,600	71,800	9.1	72

Table 22
Spectrographic, Vacuum Fusion, and Carbon Analyses of Single Crystal #UC-66 in the As-Melted and Worked Condition

	Mg	Al	Fe	Si	Cu	Ni	O_2	N_2	H_2	C
As melted	-	-	-	-	-	-	15	7	3	-
Fabricated	19	1	2	21	-	4	15	3	3	30

It should be noted that little contamination occurred when the specimens were ground to size. Although the data are fragmentary, it is already apparent that the yield stress and ultimate tensile stress are greater at the test temperatures than that of single crystals in the "as melted" condition.

1/32"R. TANGENT TO GAGE LENGTH

0.093" ±.005" DIA.

0.153"
0.154"
DIA.

1/32"

1/32"

3/16"

1.250" ±.005"

3/16"

1 11/16"
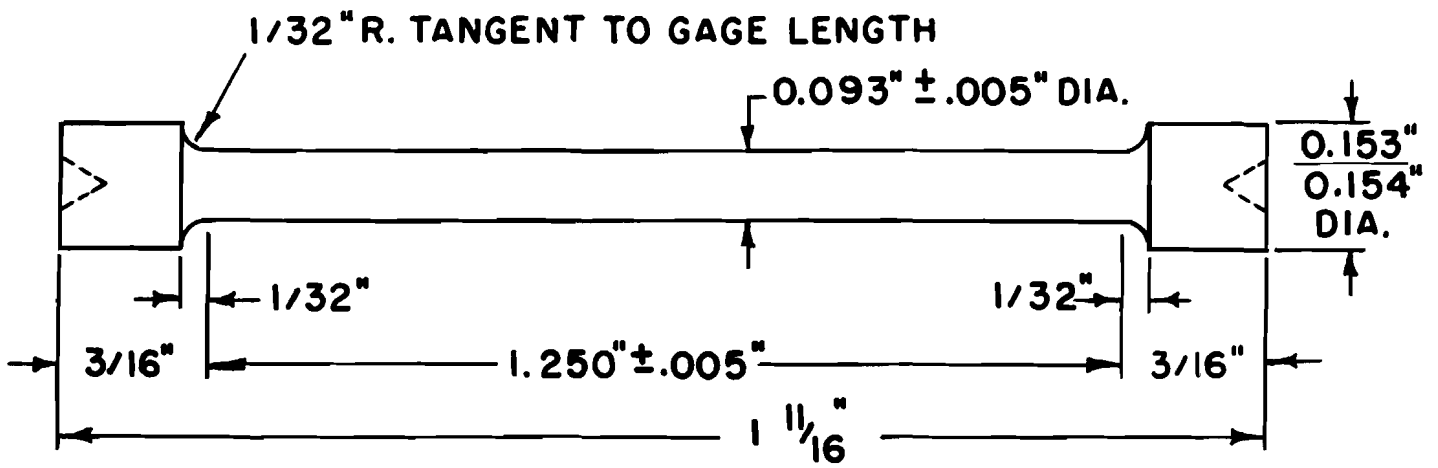
FIG. 63 MINIATURE TUNGSTEN TENSILE SPECIMEN FOR
WORKED SINGLE CRYSTALS

121

7. Mechanical Twinning of Single Crystal and Fracture

There has been much work in recent years concerning plastic deformation by glide, and the dislocation theory relating to glide has been well developed. There have been fewer studies of deformation by mechanical twinning, and the understanding of this process is far from satisfactory. This mode of deformation is interesting in b.c.c. metals since it provides an additional deformation mechanism which may result in considerable plastic flow and may cause fracture. Investigations on mechanical twinning in b.c.c. metals have been devoted primarily to iron; but since the refractory b.c.c. metals are becoming increasingly important, more attention is being paid to deformation by twinning in these metals - including tungsten. Single crystals of tungsten in some instances exhibit a profusion of mechanical twins. Schadler (27) has recently observed the occurrence of twinning in single crystals of tungsten at 20°K and 70°K, where the single crystals used had been grown by the electron beam floating zone melting process. He also noted the existence of twins on the fracture surface of a single crystal which had been drawn at room temperature.

Twins formed by compressing, rolling, and swaging single crystals have been studied in this laboratory. Specimens rolled as rods were encased in stainless steel after having been ground and electropolished to size. These specimens were then preheated for rolling in a nitrogen atmosphere furnace at 400°C and 1100°C. Specimens deformed in compression at room temperature were cubes which have been ground and electropolished. Some "as-grown crystals were swaged in air from preheat temperatures of 700°C - 1500°C. Indeed, twins were even observed in specimens mechanically deformed at temperatures up to 1500°C. Some of the characteristics and observations made on single crystal tungsten are described in this section.

The single crystals used in these experiments were also grown by the electron beam melting process. A representative impurity analysis is given in Table 23.

Table 23
Typical Quantitative Spectrographic and Vacuum Fusion Analyses of Single Crystal in ppm

Fe	Mg	Ni	Al	Si	Ca	Cu	H_2	N_2	O_2	C
3-8	20-50	0-4	2-5	5-40	1	1	1	2	3-25	20-50

These crystals were about 99.99% tungsten and thus had the same purity level as had been previously reported by other investigators (1,27) who grew crystals by this technique.
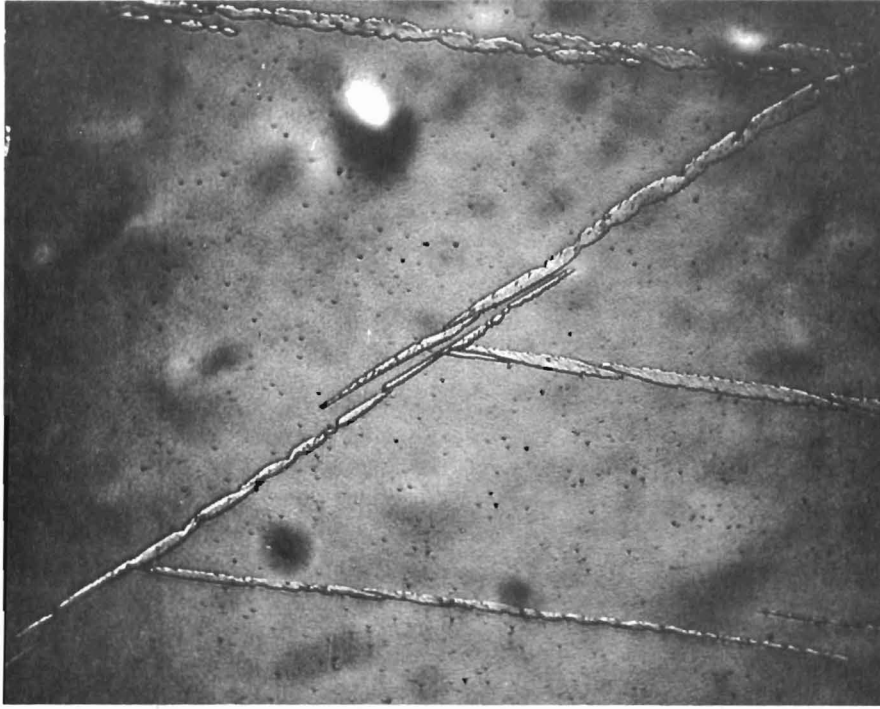
Fig. 64   Twins in Tungsten - 500X

123

Twinning Plane and Tilt Angle

After deformation, structures which were identified as twins by X-ray analysis using the two-surface technique (89) were found to be present in profusion. (See Fig. 64.) The analysis showed that twinning occurred on {112} planes, the same as in other b.c.c. metals, as had also been reported previously for tungsten (27). The twinning direction is presumed to be <111> . The micro relief of twinning traces on the polished surfaces of compression specimens was studied by interference microscopy. As is well known, with this optical method interference fringes are produced which indicate irregularities on the surface. Observations made on tungsten by this method correlate quite well with metallographic observations discussed later in this section.

An interference photomicrograph* of two twin patterns on a (112) single crystal surface is shown in Fig. 65. These mechanical twins occurred on the (21$\bar{1}$) and (211) planes. The (21$\bar{1}$) twin trace has been positively identified and corresponds in this photomicrograph to the direction of the large twin band separating the (112) crystal surface (which is in focus) from that which is almost completely out of focus. The second (211) twin trace observed in the part of the (112) crystal surface in focus forms a part of an interestingly kinked narrow twin band. Twins veering off the twin plane - or kinking - were noted on several occasions during this investigation.

The surface tilt produced in the (112) specimen surface by a twinning shear on the (21$\bar{1}$) plane has been computed from Fig. 65 by using the formula

$$\text{TAN } \mathcal{f} = \frac{\lambda}{2 S_T} \text{ TAN } \theta \; .$$

where λ is the thallium wave length (.55 x 10^{-4} cm), S_T is the true fringe spacing $S/561$ (where S is the fringe spacing on the photograph (cm) and 561 x is the magnification): θ is the measured angle between fringes on the flat surface and fringes on the tilted surface (one family of the fringes is approximately perpendicular to the line of intersection of the two surfaces), and $\mathcal{f}$ is the true angle of tilt on the two surfaces. The measured angles of the (112) surface tilt produced by twinning on the (21$\bar{1}$) plane agree well with the calculated value of 19° 30'.

Twin Morphology

Twins can be seen as relief effects on the electropolished surfaces of compressed specimens, but greater detail is revealed by first electropolishing the specimens, in a solution of 10% NaOH, and then etching in a boiling solution of 3% H_2O_2. In some

---

* The authors are indebted to Dr. R. Armstrong who kindly made these interference photographs (Figs. 65, 70 and 71) available, and provided the analyses.
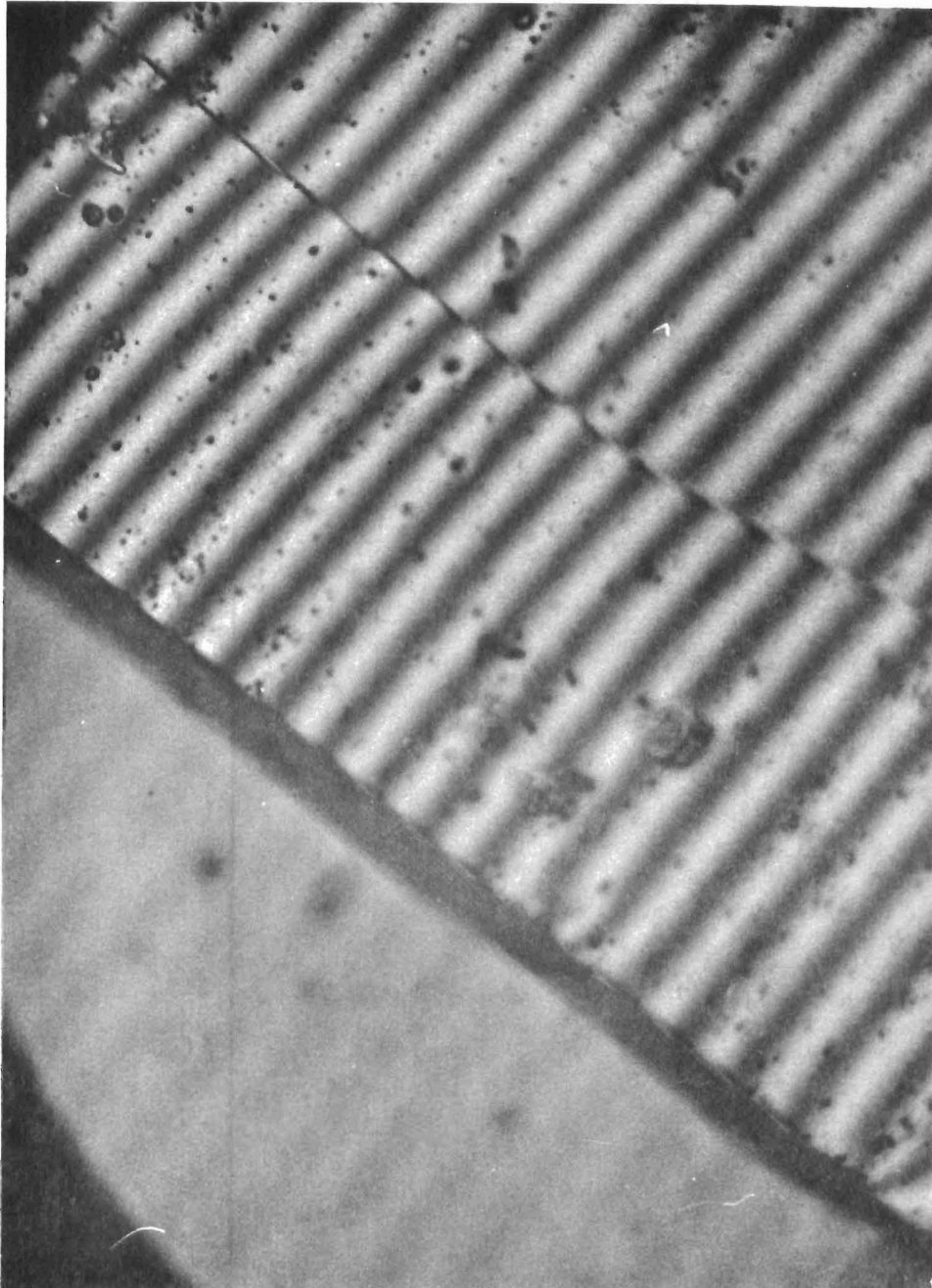
Fig. 65   Interference Photomicrograph of Twins on a
           [112] surface of a Tungsten Single Crystal
           Specimen Deformed in Compression

instances, aligned etch pits characteristic of deformation twins were noted. Twins were also found in the body of the specimens on the fracture surfaces, and in regions adjacent to cracks. Short thin twins adjacent to cracks were evidently produced by stress concentrations at the head of the propagating cracks.(See Fig. 66.) Some twins appear to be formed prior to fracture since these show off-setting at the crack intersection.

Several general types of twins were evident. Some were long lamellar twins with irregular sides, as shown in Fig. 64. Such lamellar twins have been previously reported for tantalum (90) and niobium (91). Another type of twin had one serrated side. Twins of this type are shown in Figs. 67 and 68. Twins having the same appearance have also been reported for tantalum (90). Occasionally in this investigation a third type of twin was seen with a step-like structure, and with a tendency to veer off the $\{112\}$ planes. (See Fig. 67.)

Aside from their general morphology, twins in tungsten single crystals can be classified in accordance with their size and appearance in the specimens as follows: (1) large twins trans-versing the entire specimen, (2) narrow twins, and (3) short twins which are generally associated with fracture. A closer inspection of the larger twins with an optical microscope gives the impression that these twins were composed of several smaller twins or twinning elements. Striations, grooves, and serrated grooves within such a twin are shown in Fig. 69.

The complicated nature of the make-up of a "twin-band" on a $(\bar{3}11)$ crystal surface is shown in Figs. 70 and 71. The twin band trace is produced by twinning on the $(21\bar{1})$ twin composition plane previously identified on the orthogonal crystal surface in Fig. 65. As can be seen, the twin band is made up of relatively short broad lamellae of the surface and tilts out of the $(\bar{3}11)$ crystal surface with thin distorted regions connecting these lamellae. Fig. 71, which is an enlargement of the surface in Fig. 70, shows the surface tilt in detail.

As can be observed in Figs. 65, 70 and 71, the development of the twins in tungsten occurs by the displacement of one of the twin boundaries, as indicated by a break in the interference fringes at a boundary of the wedge or trough shaped twins. It will also be noted that a region of plastic accommodation is generated with the formation of a twin. This certainly can account for the forma-tion of intersecting twins and slip lines adjacent to twins.

Thus plastic accommodation is intimately associated with twinning in tungsten. The three dimensional character of lenti-cular twin envelopes and the complex surface constraints have been previously discussed by Armstrong (77). Experimental evidence of plastic deformation occurring on several matrix systems with a cross grid of deformation systems impinging on the twin interface has been shown in Fig. 72a and 72b.
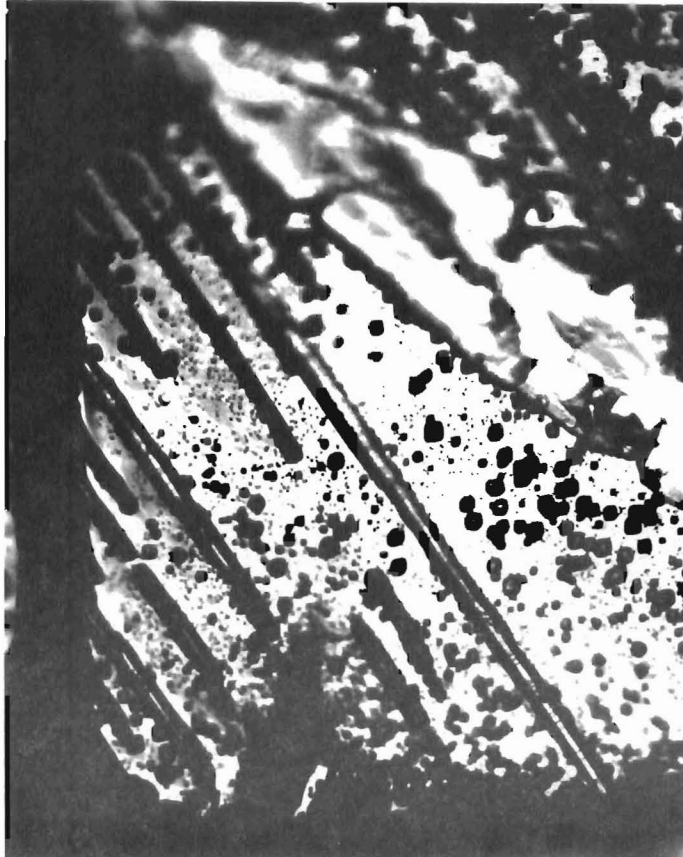
Fig. 66   Short Twins Adjacent to
           Crack - 600X
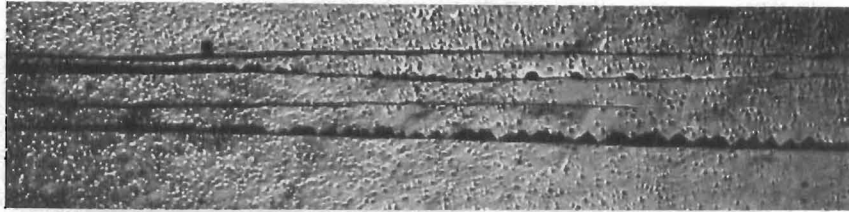
Fig. 67   Serrated Twins and Twins Tending to
Veer off Twinning Plane - 100X
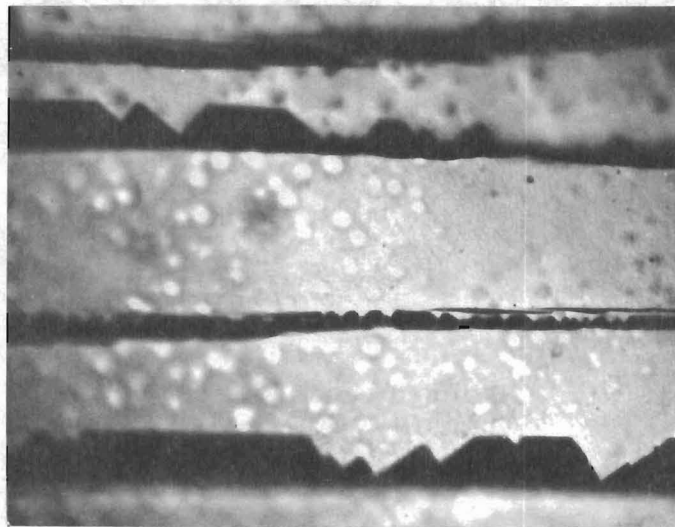
Fig. 68   Serrated Twins at Higher
Magnification - 500X

128
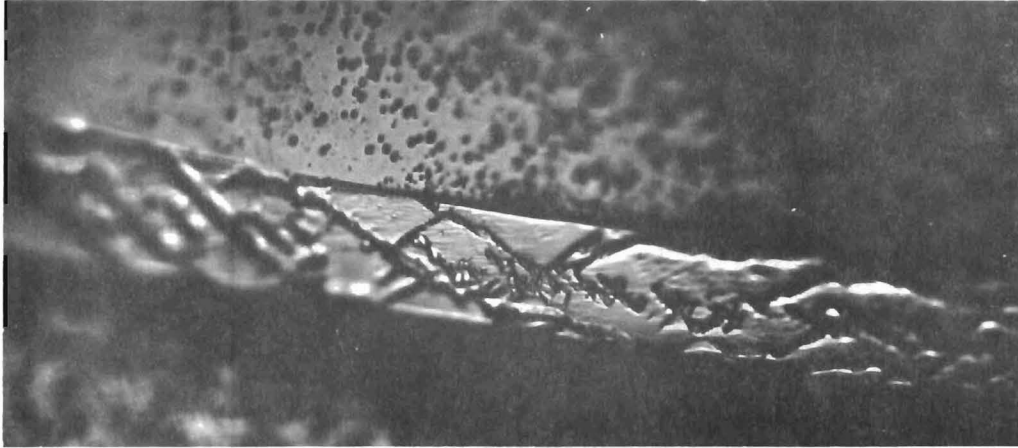
Fig. 69   Serrations within a Large Twin Formed in
           Compression - 500X
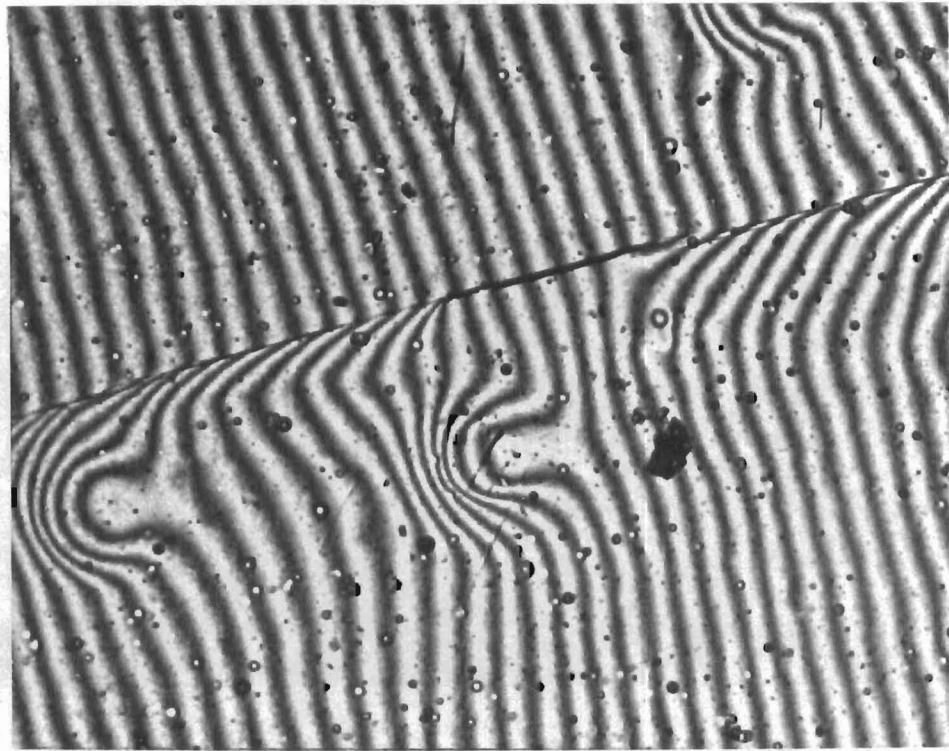
Fig. 70   Interference Photomicrograph of Twins in
           Compression Specimen Showing Distortion
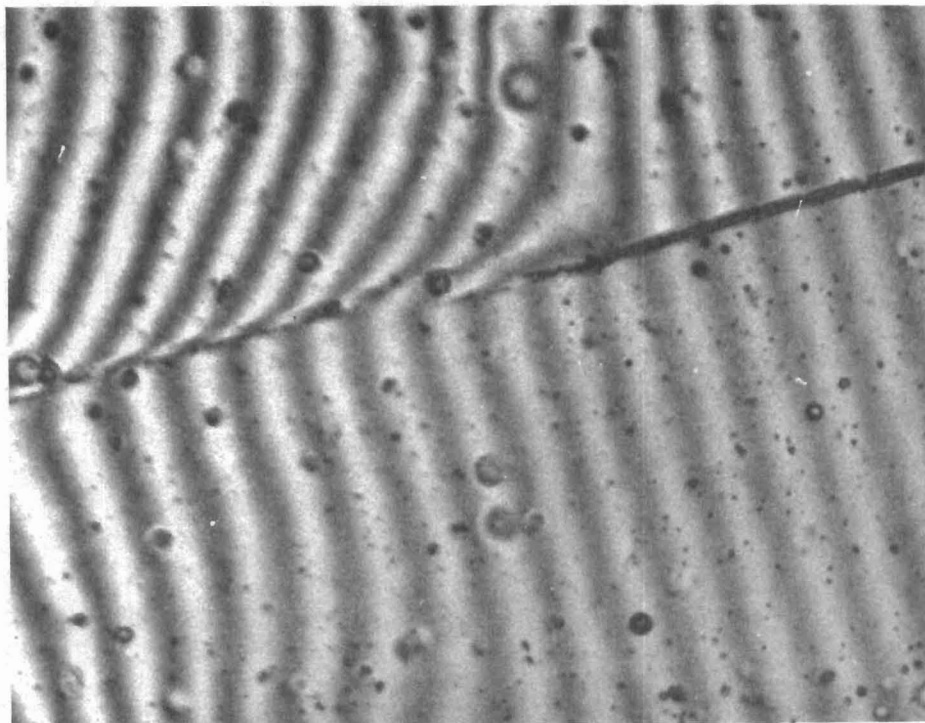
Fig. 71   Interference Photomicrograph of Twins in
           Compression Specimen Showing Distortion
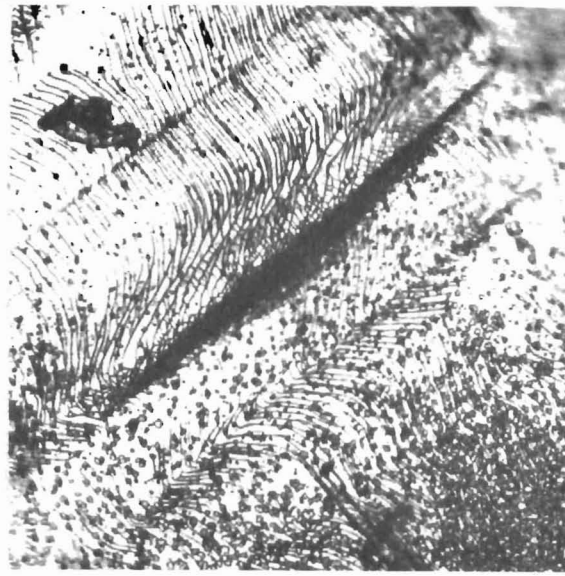
Fig. 72a.   Twin Intersecting or
Nucleating at the
Surface with Accompany-
ing Slip - 250X
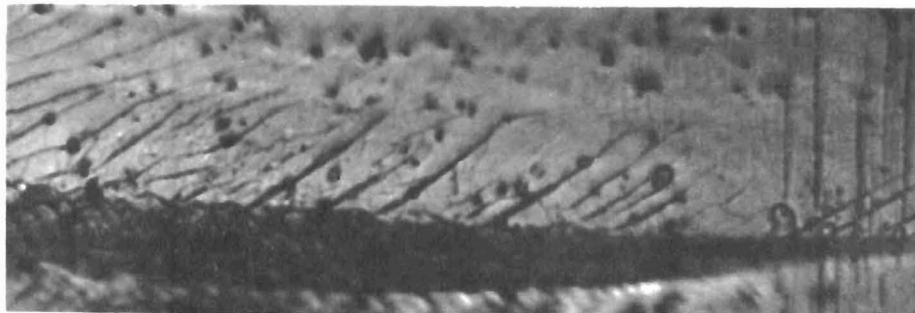
Fig. 72b.   Same as 72a, higher magnification
- 750X

Twinning and Fracture

One of the primary questions which arises in conjunction with twinning observations is whether or not brittle fracture can be initiated by twinning. No unambiguous answer can be given for tungsten at this time. However, brittleness and twinning became more and more pronounced with decreasing test temperatures or increasing yield stress. Most of the evidence seems to support the idea that twinning precedes and causes crack nucleation. For example, crack nuclei in single crystals can be formed within twins, between twins and on one particular side of a twin, but rarely, if at all, at the end of a twin. This is well demonstrated in Figs. 73, 74, 75 and 76.

In other investigations of twinning in silicon iron (92) and in molybdenum (93), it was also noted that crack nucleation does occur at twin intersections. This has seldom been observed in single crystals of tungsten. On the contrary, many intersections of twins have been observed without crack nuclei, as shown in Fig. 77. However, as Hull (92) has postulated, the condition necessary for fracture to be initiated by intersecting twins is that the line of intersection must lie in the fracture plane, [100] , and be perpendicular to the applied stress. But even with these favorable conditions, crack nuclei were not always formed in silicon iron at the intersection of the twins.

If the prerequisite for crack nucleation is a stress concentration on the [100] plane which is relieved by forming a crack, the question remains as to why crack nuclei exist elsewhere. Since in many instances twins appear to nucleate cracks within themselves and these cracks even follow the twinning plane [112] , one must draw the conclusion that brittle fracture in single crystals of tungsten is probably initiated by more than one mechanism.

One of the many possible relationships between twinning and brittle fracture in single crystal tungsten has been recently observed. Examination of the fracture surface reveals twins and the initiation of fracture close to the surface of the specimen. For these twins, which intersect or nucleate at the surface, it has been noted that a twin tapers and offsets the surface, but in a few instances crack nuclei are evident. With decreasing temperatures, twinning occurs in profusion with many twins intersecting and nucleating at the surface, causing a shattering of the specimen into many pieces (resembling fracture in glass).

When a twin originates at the surface, either of three subsequent events can take place: (1) another twin is nucleated (it is believed that most twins are nucleated at a surface), (2) a crack nuclei is formed, or (3) slip will occur. Evidence in support for the first event, namely the nucleation of a twin at the surface in an adjacent region, is shown in Fig. 78. Evidence for the second

132
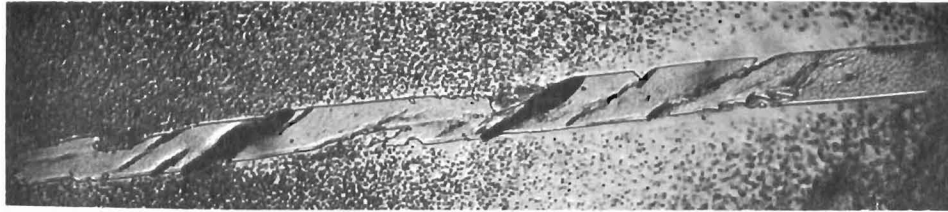
Fig. 73   Cracks within a Twin - 500X

Fig. 74   Cracks between Twins - 500X
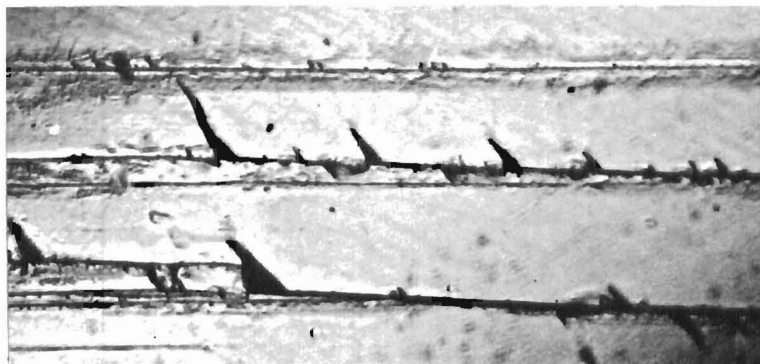
Fig. 75   Cracks on the Edge of Twins
          Formed in Compression at -196°C
          - 500X

133
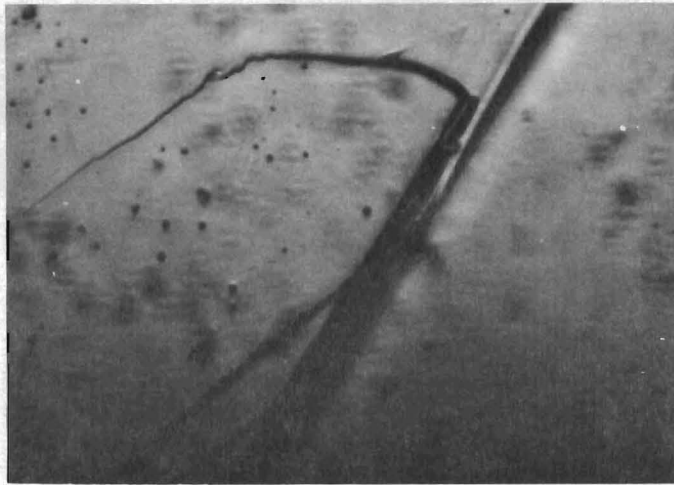
Fig. 76   A Crack at the End of a
           Twin (unetched) Compression
           at -196°C - 250X
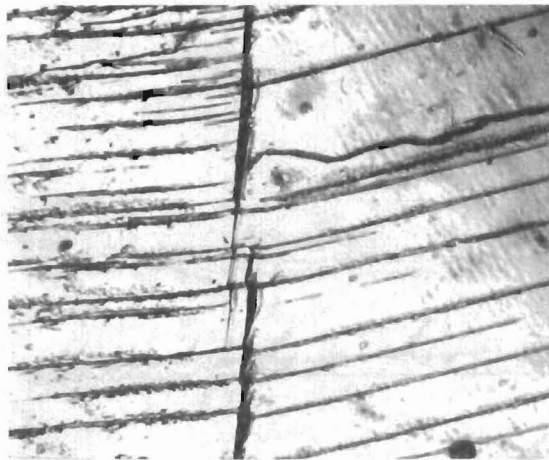
Fig. 77   Many Twin Intersections
           (unetched) - 250X
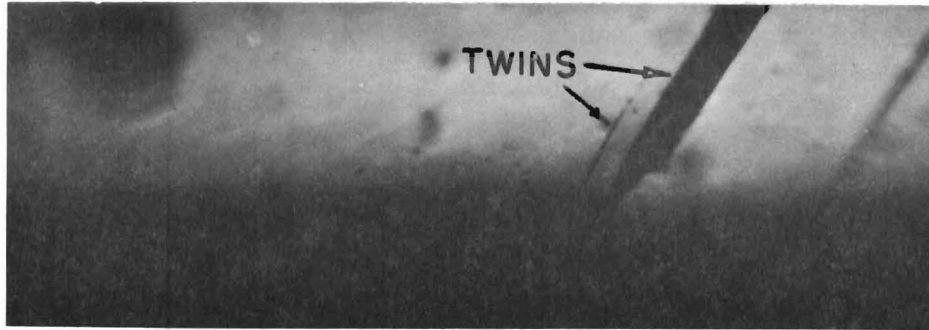
Fig. 78   Twins Intersecting the Surface,
           Nucleating Another Twin - Compression
           at R.T. - 500X
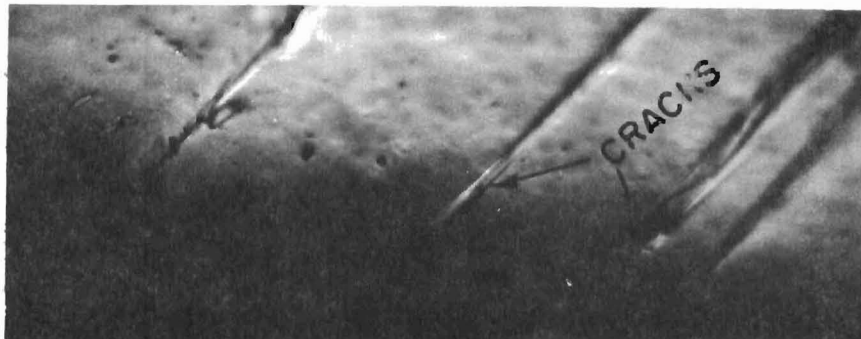
Fig. 79   Twins and Cracks formed Adjacent
           and Within Twins - 500X

event, namely, the nucleation of cracks within a twin and adjacent to a twin, is shown in Fig. 79. For the second twin from the right in the photomicrograph of Fig. 79, a crack appears to have formed at the surface and has then propagated along a groove within the twin. Evidence for slip resulting from a twin intersecting or nucleating at the surface has already been shown in Fig. 72a and 72b. As can be seen, many dislocation sources have been activated to accommodate the stress field of the twin.

Hull (92), and Muller and Parker (94) have cited slip as the cause of serrations in silicon iron and molybdenum. An example of serrated twins on a fracture surface of a tungsten single crystal is shown in Fig. 80. Barrett and Bakish (90) have observed slip as being associated with serrations in tantalum. The photomicrographs of tungsten presented in Fig. 72a and 72b also give a similar impression - that slip may be responsible for serrations. Slip in this case is believed to be caused by the accommodation of a twin within the lattice and probably occurs concurrently with twinning. It is apparent that the various deformation mechanisms can be quite complex, and it is probably impossible to divorce twinning from slip. An example of slip lines occurring on one side of a straight edge twin is shown in Fig. 81.

With numerous serrations, striations, and grooves within twins, it is believed that slip does not only occur concurrently with the formation of twins but that it can also precede twinning in localized regions. The photomicrograph in Fig. 82 supports this conclusion. In this photomicrograph, a forming twin has been held up by an obstacle with the serrations believed to be slip preceding the twin. If one imagines the twin to be extended, one finds that the serrations will be evident only on one edge of the imagined twin but extending within the body of that twin. It should also be noted for the middle twin in Fig. 82 that the last serrations change sides when approaching the surface. Hull (92) also noted that serrations changed sides when viewing a particular twin on opposite sides of a silicon iron foil.

The effects of fracture tear lines when intersecting a twin are shown in Figs. 83 and 84. Serrations give the appearance of a layer growth and seem to be associated with the particular contour area between tear lines. From these observations, one has the impression that - probably due to some slip - twins can expand on one side, forming serrations, and contract on the other.

Summary

The observations on twins in tungsten single crystals can be summarized as follows:

a. Evidence has been found that some twinning occurs prior to fracture. Twins thus formed can act as a source for crack nuclei.

136
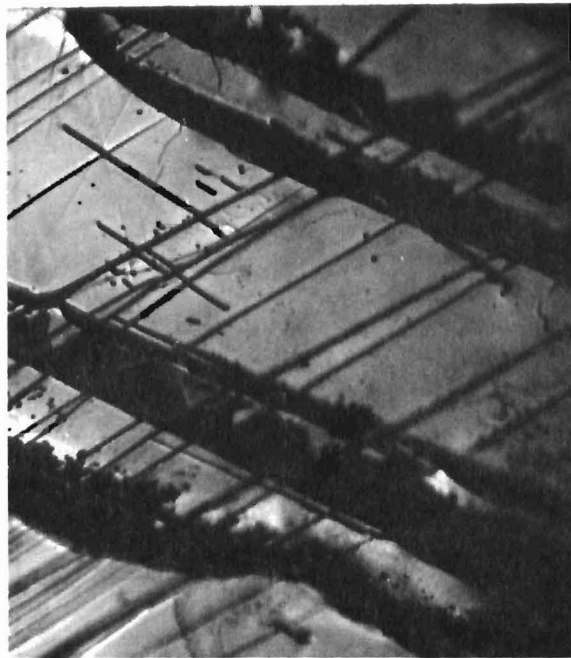
Fig. 80 Serrated Twins and
Intersections on a
Fracture Surface formed
in Compression at -196°C-
250X
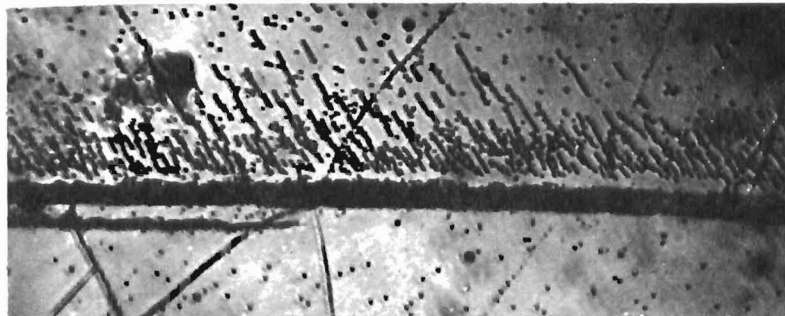
Fig. 81 Slip on One Side of a Twin Formed
in Compression at -150°C, Etched
-250X
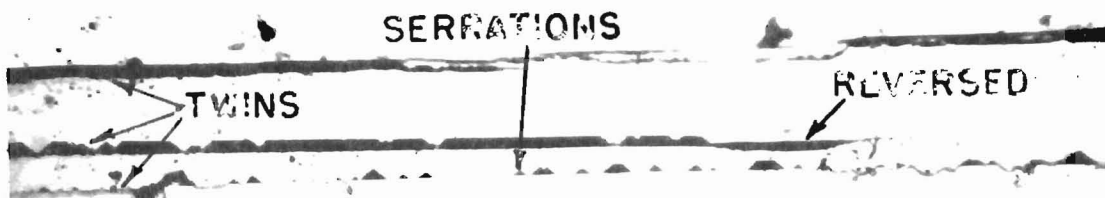
Fig. 82 Twins, Stoppage of a Twin, Continuation of
Serrations Formed in Impact Compression at
-196°C - 500X

137

Fig. 83   Twin Intersected by
          Tear Lines - 500X
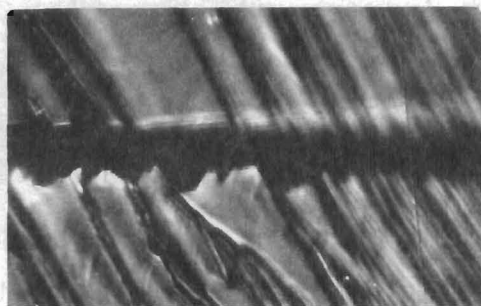
Fig. 84   Twin Intersected by
          Tear Lines - 500X

138

Other twins which are found over a wider temperature range and after some plastic deformation are probably formed as a consequence of fracture. Many mechanisms appear to be responsible for brittle fracture in single crystals of tungsten.

b. Twins originating at a surface can nucleate more twins, cause slip, or form cracks. With a number of twins originating at the surface, stress concentrations exist which cause glass-like shattering of the specimen. In specimens containing twins, fracture appears to be initiated at the surface. Since a fracture can propagate along the edges of twins, along grooves within twins, and along twin serrations, the plane along which fracture propagates does not necessarily have to be the 100 plane normally determined as the fracture plane in b.c.c. metals.

c. Large twins appear to be composed of one or more twins or twinning elements.

d. Slip may precede or occur concurrently with twinning, probably causing the formation of serrations.

III. TUNGSTEN SINGLE CRYSTAL ALLOYS OF BINARY SOLID SOLUTION

The poor reproducibility of high temperature strength values of the sintered and swaged W-.38% TaC, as well as the fact that a dispersed second phase was not observed, and that the stoichiometric composition of TaC was not retained during the fabrication process raised the question as to whether or not the alloy at hand was of the true dispersion strengthened type. It was quite possible that the matrix was a solid-solution and that the observed strengthening was due to solid-solution strengthening. In order to delineate the effects of alloying, of grain boundaries, and chemical parameters, and to determine the relative contribution of each variable to strengthening, it was thought necessary to also study the alloy in its most ideal form - a single crystal - and to systematically modify this form by introducing one variable at a time. It was felt that in this manner it should be feasible to evaluate this alloy and to understand the various strengthening processes involved.

The prerequisite for a successful conclusion of this project was, however, that W-Ta single crystals of homogeneous composition be produced by electron beam floating zone melting, the only known method by which metals and alloys of the desired high purity could be prepared. As described in detail in the following, such crystals were produced (including one W-Nb crystal), and a number of W-Ta crystals were investigated. The project is far from complete but the results obtained to date are most encouraging.

1. Growth and Characterization of Alloy Single Crystals

Originally it was attempted to produce the alloy by remelting a zone melted tungsten single crystal rod onto which a tantalum wire was wound. Since this method proved to be very tedious and unreliable, a different approach was tried. A 600 gram ingot of W-2% TaC was compacted and sintered in H_2 at 1700°C to approximately 70% of ideal density. (The assumption was made that the carbon would be evolved during sintering.) This ingot could not be melted, however, since it was found that the power required exceeded the rating of the power supply.

Thereafter, starting electrodes were prepared by the following procedure:

1) The elemental powders were dry blended in the desired proportions;

2) 350 gram ingots (1/4 inch square x 24 inches long) were die pressed at 20 TSI;

3) the pressed ingots were vacuum presintered for one to two hours at 1100°C.

One variation of this procedure was required for the preparation of the Nb alloy material. In this case, the high purity Nb pellets were too large (1/32" diameter) to allow uniform blending. These pellets were therefore first embrittled by firing in H_2 at 900°C. They were next ground in a WC ball mill to -325 mesh, and then used in accordance with the above procedure. As can be seen in Table 28, the hydrogen was successfully removed during the subsequent treatments, but there was a significant carbon contamination from the grinding operation.

The electrodes which were made, and their compositions are listed in Table 24.

Table 24
Composition, Quantity, and Weight of W-Ta and W-Nb Ingots Prepared for Starting Electrodes*

Nominal Composition	Quantity	Weight
2%TaC	4	600 gm ingots
.35%Ta	4	350 gm ingots
1%Ta	2	350 gm ingots
5%Ta	5	350 gm ingots
5%Nb	2	350 gm ingots

* All values are given in wt.%

Tungsten-Tantalum

The 350 gram compacted and presintered ingot-electrodes were
the most successful. These ingots had a smaller cross section
(0.06 inch^2), and therefore conducted less heat away from the
area of the molten zone than the 600 gram ingots. In Fig. 85 are
shown two of the electrodes, marked A and B, which were only sintered
in the electron beam furnace (one was surface melted) and two
electrodes marked C and D, which were zone melted and grown into
single crystals. The rod marked C contained nominally 5% Ta and
was melted on the first pass, and the rod marked D contained
nominally .35% Ta and had 3 melting passes.

Six W-Ta single crystals, three nominally 5% and three nominal-
ly 0.35% tantalum, were produced by this technique. The first four
were studied, while the last two were held for disposition. The
four crystals studied had a diameter of approximately 0.200 inch,
and a useable length of approximately eight inches. The crystals
were sectioned to provide specimens for chemical, physical and
metallurgical characterization as follows:

    a. Two tensile specimens, each 1-1/2 inches long;

    b. one section for fabrication study, 1-1/2 to 2 inches long;

    c. one piece retained for seeding of the same orientation into
        crystals to be grown in the future, 1 to 1-1/2 inches long;

    d. four sections for vacuum fusion and carbon analysis, 1/4
        inch long;

    e. four sections for chemical analyses, hardness measurements,
        X-ray determination of lattice parameter and orientation,
        and microscopic examination.

Samples were labeled consecutively starting with the end from
which the zone was initiated, with a prefix designating the crystal.
Thus sample 1-2 indicates the second section of crystal No. 1.
Table 25 summarizes the impurity analyses, Knoop hardness values, and
the crystallographic orientation of those crystal sections evaluated
to date. The orientations of the alloy single crystals were deter-
mined by the Laue X-ray back reflection method.

For chemical analysis, the sections were crushed and a 10 mg
piece was removed for tantalum determination by activation analysis.
The remaining material was oxidized and submitted for quantitative
spectrographic analysis. Prior to the destruction of the specimen
for chemical analysis, the samples were mounted in standard metal-
lurgical mounts, polished, etched and examined microscopically.
Hardness measurements were taken, and one specimen was also
selected from each crystal for X-ray characterization.
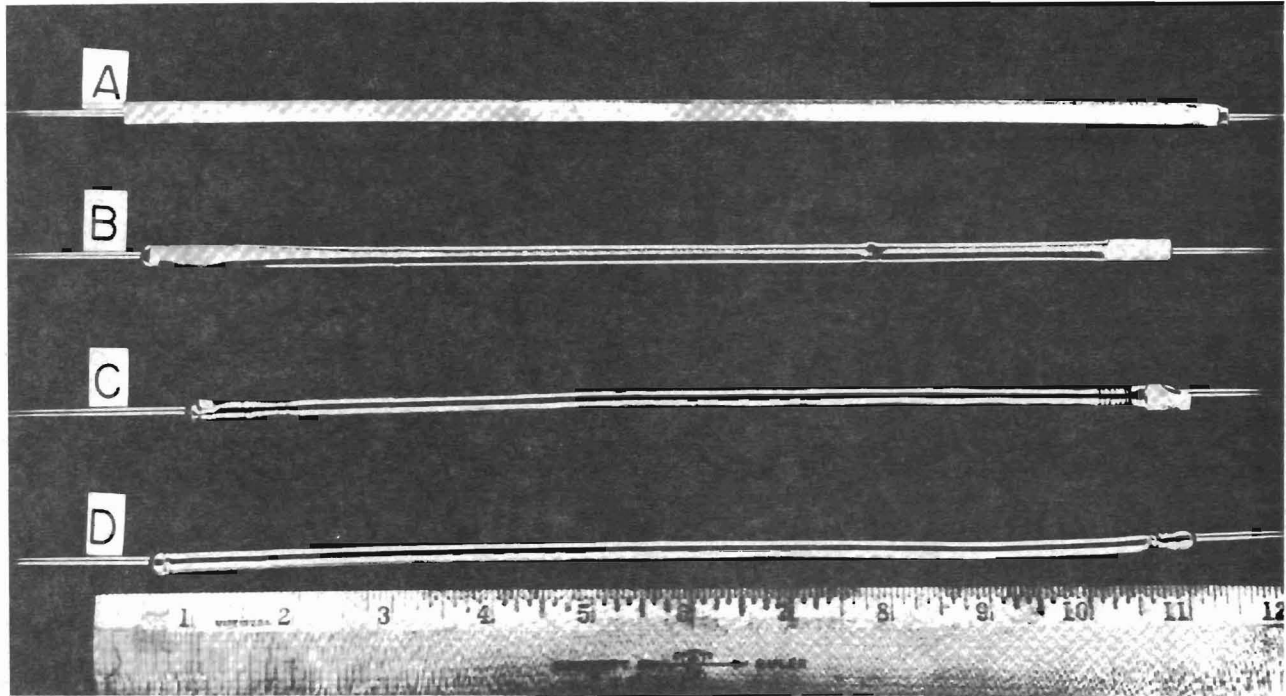
Fig. 85   W-Ta Starting Electrodes (A and B) and W-Ta Alloy Single
Crystals (C and D) Produced by Electron Beam Floating
Zone Melting

Table 25
Impurity Analyses, Knoop Hardness and Crystallographic
Orientation of W-Ta Alloy Single Crystals

Crystal Characterization	Distance from Starting End	Ta %	H_2 ppm	N_2 ppm	O_2 ppm	Al ppm	Mg ppm	Ni ppm	Cu ppm	Si ppm	Knoop Hardness
Crystal 1 - 5% Ta [521]											
3 sintering passes at 12 mm/min. First four	1/2"	3.66	1.0	6	3	3	9	2	12	19	397
inches zoned with 5 passes at 6 mm/min.	3/4"	3.50	ND	ND	ND	ND	ND	ND	ND	ND	ND
Remainder zoned with 3 passes at 6 mm/min.	2-1/2"	3.90	0.5	5	5	2	7	2	10	24	391
	4-1/2"	ND*	1.0	5	5	ND	ND	ND	ND	ND	405
	6-1/2"	4.21	0.7	3	4	1	13	2	--°	9	467
Crystal 2 -.35% Ta 310											
2 sintering passes at 12 mm/min. One pass	1-1/4"	0.271	0.6	2	4	2	35	3	4	38	363
partially molten. One pass fully molten at	2"	0.254	ND	ND	ND	ND	ND	ND	ND	ND	ND
6 mm/min.	3-1/2"	0.289	0.6	2	8	5	18	4	4	46	338
	5-1/2"	ND	1.0	6	8	ND	ND	ND	ND	ND	367
	7-1/4"	0.291	0.8	2	8	2	28	2	7	21	380

Table 25 Cont'd

Crystal Characterization	Distance from Starting End	Ta %	H$_2$ ppm	N$_2$ ppm	O$_2$ ppm	Al ppm	Mg ppm	Ni ppm	Cu ppm	Si ppm	Knoop Hardness
Crystal 3 - 5% Ta [311]											
1 sintering pass at	1-1/2"	ND	0.6	11	3	2	28	2	7	1	ND
12 mm/min. 1 pass partially molten, 2	3-1/4"	4.04	0.4	3	7	2	22	3	24	65	415
passes fully molten at 6 mm/min.	5-1/4"	3.95	0.2	3	5	2	700	2	4	133	442
	5-1/2"	3.77	ND	ND	ND	ND	ND	ND	ND	ND	ND
	7-1/4"	3.90	0.4	3	10	ND	ND	ND	ND	ND	403
Crystal 4 - .35% Ta 542											
3 sintering passes at	1-1/4"	ND	ND	ND	ND	ND	ND	ND	ND	ND	408
12 min/min. 3 full zoning passes, 2 at	3-1/4"	0.258	0.2	2	9	3	27	2	15	40	366
12 mm/min, 1 at	5-1/4"	0.265	0.5	5	6	5	17	3	--°	8	ND
4 mm/min.	5-1/2"	0.217	ND	ND	ND	ND	ND	ND	ND	ND	ND
	7-1/4"	ND	0.9	6	17	52	12	2	3	23	409

*ND - not determined

--° - not detected

144

Three specimens were selected from three of the four crystals in order to determine the transverse distribution of the tantalum concentration. The results of this analysis are given in Table 26.

Table 26
Tantalum Concentration Profiles
in W-Ta Single Crystals
(Diameter = .200 inch)

Crystal No.	Distance Along Diameter	% Ta
1	Surface to .050"	3.71
	.050" to center	3.95
	Center to .050" (opposite side)	3.80
2	Surface to .050"	0.258
	.050" to center	0.287
	Center to .050" (opposite side)	0.317
	.050" to surface	0.280
4	Surface to .050"	0.237
	Core Section extending .025 from center	0.262
	.050" to surface (opposite side)	0.337

There seems to be an indication that the core of the crystals is richer in tantalum than the surface regions, although the data are far from conclusive on this point. Further work will have to be done on the question of homogeneity. Since no attempt was made to select the same transverse section in the preparation of the samples listed in Table 25, not too much significance can be attached to the variation in tantalum concentration from one end of the crystal to the other. Therefore no comment can be made on the existence of a zone refining effect along the rod. Certainly there is no marked difference in the longitudinal concentration distribution.

The reason for the loss of tantalum by evaporation cannot be explained at this time. Although there is a difference between the tantalum concentration in the starting material and the final alloy, this in itself may not be of significance since the loss may have

145

occurred during sintering by evaporation of tantalum oxide or another volatile compound. That a loss by this mechanism can occur has been demonstrated in the case of the W-TaC alloys discussed in Section V.

However, if one speculates with the data at hand, it does appear that a loss of tantalum from the alloy does occur at the melting temperature. The trend observed in the transverse concentration profiles of Table 26 supports such a conclusion. Also supporting this conclusion is the fact that the first half of crystal No. 1 which had two more zoning passes than the second half of the same crystal shows a lower tantalum concentration than the second half.

The Knoop hardness values reported in Table 25 reveal that at least for alloys No. 1 and No. 2, the hardness increases toward the finishing end. Comparing the average hardness values of the third and fourth position for crystals 1, 2 and 3, it can be seen that alloys of higher tantalum concentration have higher hardness. From the survey of hardness across the cross section, it was generally noted that the interior or the center of the ingot was harder. These hardness values cannot be unambiguously correlated with chemical composition as evident from Tables 25 and 26, although they do tend to support the possibility of a concentration gradient from the center to the surface. This is further evidence of the loss of tantalum from the alloy during zoning.

Carbon analyses of the first four tungsten-tantalum single crystal alloys are reported in Table 28. In comparison with carbon concentrations determined in pure tungsten single crystals, the alloys have, on the average, a lower carbon content. There appears to be no correlation of carbon concentration with the number of zoning passes used in producing the crystal, nor is there any evidence of zone refining for carbon.

Tungsten-Niobium

Only one W-Nb crystal was grown. This crystal (#7) had nominally 5% Nb and was zone leveled with four passes. A portion was made available for analysis and preliminary study. Quantitative spectrographic, vacuum fusion and carbon analyses as a function of position are presented in Table 27. Originally, a zone refining effect was seen but subsequent analyses tended to disprove this. In Fig. 86 are shown the data for C, O_2, and Al, as a function of position. Within the limits of the data, no zone refining is seen. It should be noted also that the qualitative spectrographic analyses do not indicate a zone refining of Nb.

The spread in iron and silicon values found in specimens 2, 6, 10 and 14 is believed to be sample contamination caused during preparation since these samples were used previously in compression tests.

Table 27
Quantitative Analyses of W-Nb Alloy (wt. ppm)

Position	Si	Al	Cu	Fe	Mg	C	O	N	H
1	17	2-25	-	4	6	ND	ND	ND	ND
2	92-140	14-37	3	6-98	3	64			
3	7-17	7-25	3	100	9	ND	ND	ND	ND
4	ND	ND	ND	ND	ND	200	4	3	.2
5	43-86	2	3	2	4	ND	ND	ND	ND
6	42-75	2	3	1	8	48	19	2	2
7	18-40	2	-	3	5	ND	ND	ND	ND
8	ND	ND	ND	ND	ND	110	28	4	2
9	5-23	2	-	6	7	ND	ND	ND	ND
10	66-140	3-11	6	18-145	12	31	8	2	2
11	7-15	2	-	1-11	5	ND	ND	ND	ND
12	ND	ND	ND	ND	ND	93	55	9	1
13	3-12	1	-	2	4	ND	ND	ND	ND
14	33-80	4	-	1-15	12	72	9	1	.8
15	3-15	2	4	20	2	ND	ND	ND	ND
16	ND	ND	ND	ND	ND	75	5	2	.6
Powder	ND	ND	ND	ND	ND	170	ND	ND	ND

- = not detected

ND = not determined

147
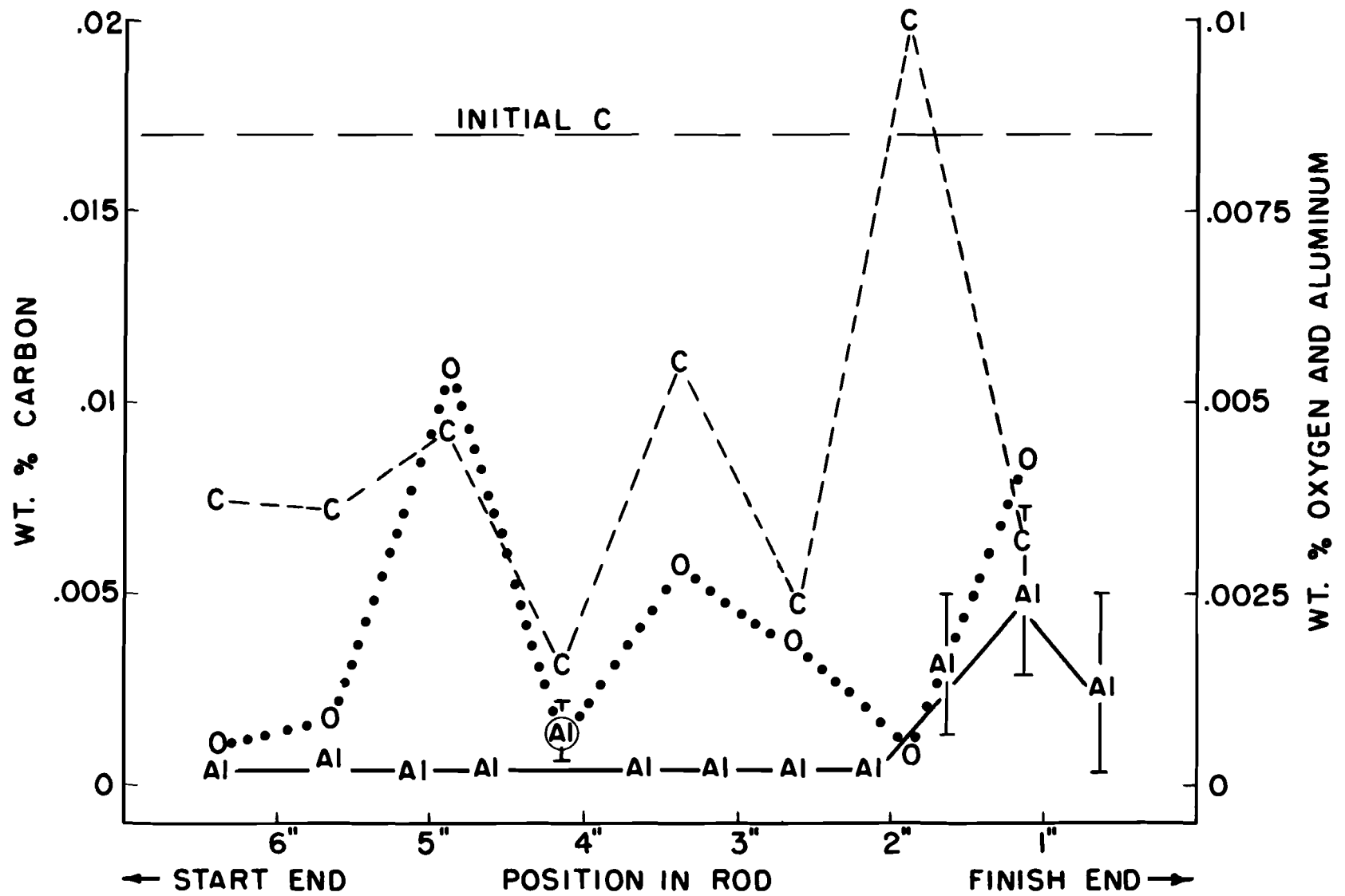
FIG. 86 CARBON, OXYGEN AND ALUMINUM CONTENT AS A FUNCTION
OF POSITION IN THE W-5% Nb ZONE LEVELED CRYSTAL #7.

Table 28
Carbon Analysis of Tungsten-Tantalum Alloy
Single Crystals

Crystal No. and % Tantalum	Appr. Distance from Starting End (Inches)	Carbon Concentration (ppm)
1 (5%)	.25	18
	2.50	31
	4.00	13
	6.25	26
2 (.35%)	1.25	30
	3.25	20
	5.25	22
	7.25	38
3 (5%)	1.50	26
	3.50	20
	5.25	21
	7.50	18
4 (.35%)	3.25	14
	5.25	24
	7.50	23

Metallographic Examination

Metallographic examinations were performed on most of the W-Ta alloys. A NaOH electropolishing solution of about 10% or less was found satisfactory. Etching was accomplished using a modified tungsten etch (7-10% potassium ferricyanide). Various cubic or triangular etch pits were seen in these specimens. Specimens from Crystal No. 2 (.35% Ta) electropolished and etched readily. A photomicrograph from section 5 of crystal No. 2 showing etch pits and subboundaries is reproduced in Fig. 87. In the metallographic examination an inclusion was also noted in this specimen, as shown in Fig. 88.

It should be added that this was the only inclusion seen in the various alloy specimens examined. Occasionally, some blowholes or porosity was revealed.

Not all the specimens from the various alloy rods etched readily. For Crystal No. 4 (.35% Ta), specimens could only be etched when they were cut at an angle to the crystal axis, indicating an orientation effect. Specimens from Crystal No. 3 (5% Ta) were finally successfully etched by using the procedures outlined. Specimens from Crystal No. 1 were never successfully etched.
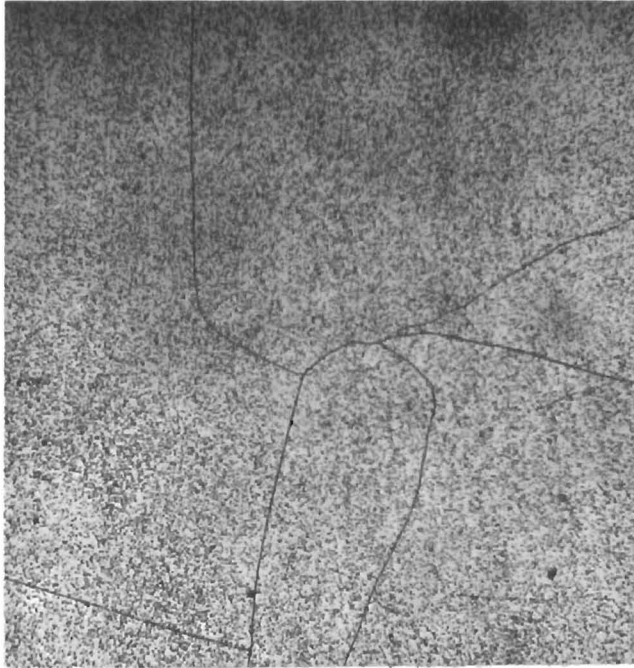
Fig. 87   Subgrain Boundaries in
           W-0.35% Ta Single Crystals
           (Specimen No. 2-5) - 150X
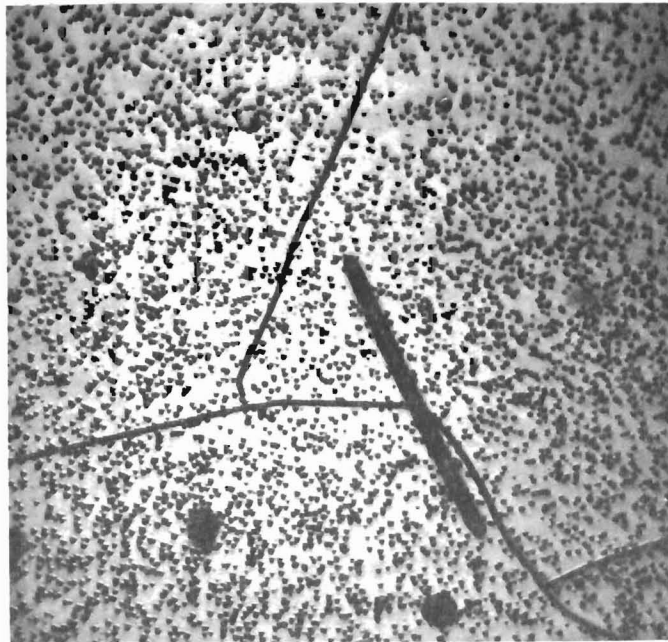
Fig. 88   Inclusions in W-0.35% Ta Single
           Crystals (Specimen No. 2-5) - 500X

There does not appear to be a preferred growth orientation since the various crystals grew with different orientations.

2. Tensile Properties

Enough material was made available from each crystal for two tensile specimens of the dimensions shown in Fig. 18. One test on each crystal was run at room temperature and also at 100°C. The strain rate was kept the same as for the tungsten single crystals, 8.33×10^{-5}/sec. The tensile test results are presented in Table 29, and interstitial analyses of the broken specimens are given in Table 29.

Table 29
Vacuum Fusion and Carbon Analyses
of Broken W-Ta Alloy Tensiles

Specimen No.	%C	%H	%N	%O
1-6	ND	.00005	.0011	.0017
2-6	ND	.00004	.0005	.0006
2-9	.0030	.0001	.0009	.0021
3-4	ND	.0001	.0002	.0004
3-7	.0030	.00002	.0002	.0004
4-4	.0044	.00005	.0001	.0006
4-7	.0041	.00005	.00003	.0006

Due to the low number of tests, it is difficult to draw any conclusions based on the different mechanical behaviors between the tungsten single crystal tensiles and the W-Ta alloy single crystals. Unfortunately, a number of fillet breaks did occur. Furthermore, the orientations of the various alloy single crystals are quite different from the [100] orientation of the single crystal tungsten tensiles used. The variation in interstitial content does not appear significant in these tests.

However, it does appear from the data in Table 30 that the ductile-brittle transition temperature of the single crystal alloys lies between room temperature and 100°C. This is about in the same temperature range as determined for single crystal tungsten having a [100] orientation. It is also interesting to note that a discontinuous yield point existed for crystal No. 4 (.35% Ta). This alloy has the closest orientation to [110] and Rose, Ferriss, and Wulff (40) obtained discontinuous yield points in single crystal tungsten tensiles of this orientation.

Table 30

Tensile Test Results of W-Ta
Alloy Single Crystal Specimens*

Specimen No.	Testing Temp.	Alloy and Composition	Yield Strength .2% Offset psi	Ultimate Strength psi	Elongation 1" (%)	Red. in Area %
1-6	R.T.	W-5% Ta	98,150	120,950	6.5	4.0
3-4[+]	R.T.	W-5% Ta	86,750	111,150	3.4	8.0
1-9[+]	100°C	W-5% Ta	48,000	72,150	38.0	43.0
3-7[+]	100°C	W-5% Ta	75,450	112,150	22.0	21.0
2-6[+]	R.T.	W-.35% Ta	50,400	116,650	15.0	17.0
4-4Δ	R.T.	W-.35% Ta	98,000	98,000	2.0	0.3
2-9	100°C	W-.35% Ta	42,000	96,300	18.4	85.0
4-7Δ	100°C	W-.35% Ta	56,900	89,600	24.0	76.0

+ Broke at fillet

Δ Yield point

* Tests were made in an Argon atmosphere at a strain rate of 1/2% per minute.

152

3. Fabrication

The portion of each of the four Ta alloy crystals which was made available for preliminary fabrication and recrystallization studies was ground to 0.195 inch diameter, electropolished to 0.185 inch diameter (to remove the heavily worked surface caused by grinding) and encased in stainless steel tubing for fabrication. A rolling temperature of 1100°C was selected, and the alloys were rod rolled for nominal reductions of 10-80%. The rolling schedule used was 30 minutes preheat, 10 minutes reheat, with a double pass (with reheat) on the final pass. Those alloys rolled in excess of 50% were given a stress relief of one-half hour at 1100°C after 55% reduction in area. Nominal reduction per pass was 10%. The steel tubing was dissolved in aqua regia and the samples electropolished to remove any surface contamination. The results of these experiments are summarized in Table 31 (fabrication) and Table 32 (impurity analyses).

Before any comments on the above results can be made, it must be emphasized that:

1) Chemical inhomogeneity is evident.

2) Orientations are vastly different.

3) Fabrication results are based on one test specimen only.

With these points in mind, it can be stated that with the exception of the low alloy at a high reduction, fabrication was reasonably successful by rolling at 1100°C. Solution hardening is evident even in the low tantalum alloy since pure tungsten single crystals can be worked more than 80% at temperatures below 1100°C without difficulty. Some interstitial contamination is found which is of the same order as that occurring during similar fabrication of pure tungsten. Metallic contamination effects can not be separated from initial heterogeneity in the as grown crystals.

4. Recrystallization Behavior

As mentioned before, the working procedures were kept comparable to those used on pure single crystals so that a direct comparison of measurements could be made. The recrystallization studies were carried out using 30 minute vacuum anneals at the various temperatures. Recrystallization was followed by optical microscopy and hardness measurements. The nominal 5% Ta alloys were studied after rolling 50% and 80% at 1100°C. Enough additional material was made available so that the low alloy (nominal .35% Ta) could be studied after reductions of 20% and 35% in addition to 50% and 80%.

The characteristic hardness-recrystallization response of the worked alloy single crystals W-5% Ta and that of the W-.35% Ta is presented in Fig. 89. The hardness values corresponding to complete

153

Table 31

Alloy Single Crystal Fabrication Data**

Specimen No.	% Reduction in Area		As Rolled Hardness (1 Kg Knoop)		Remarks
	Nominal	Actual	Trans.	Long.	
4-10	10	17-20	485	465	Small end crack
2-3	30	35-37	490	510	O.K.
4-10	50	51	505	525	O.K.
2-3	80	78	570	525	Split full length
1-3	50	49	615	540	45° cross cracks - 1-1/2 inch broke off
3-10	80	78	550/610*	550	Three 45° cross cracks- small end crack

** NOTE: Alloys 1,3 nominal 5% Ta
           "   2,4   "   .35% Ta

* Two distinct areas having these values were found; avg. of 5-10 readings

154

Table 32

Quantitative Spectrographic and Vacuum Fusion
Analyses of W-Ta Alloy Single Crystal Specimens
As Received and After Fabrication*

Specimen No.	Ta**	Fe	Ni	Al	Mg	Si	Cu	H$_2$	N$_2$	O$_2$
4-10 as rec'd.	.217	1	2	2	5	7	2	.5	5	6
4-10 10%	.217	1	2	2	6	1-16	--	2	13	14
4-10 50%	.217	8-65	3	3	7	10	--	1	7	10
2-3 as rec'd	.254	1	2	2	6	11	2	.6	2	8
2-3 30%	.254	1	2	2	6	8	--	3	14	14
2-3 80%	.254	2	2	3	2-16	10-41	--	2	5	7
1-3 as rec'd	3.5	1	13	5	5	12	2	.5	5	5
1-3 50%	3.5	74	2	30	6	28	--	3	6	16
3-10 as rec'd	3.77	40	2	80	6	40	5	.2	3	5
3-10 80%	3.77	1	2	2	7	8->140	2	2	11	5

-- = not detected   * = ppm by weight   ** = Average, see table 26

NOTE: A range is shown where the scatter in triplicate determinations is too
great to average.

155
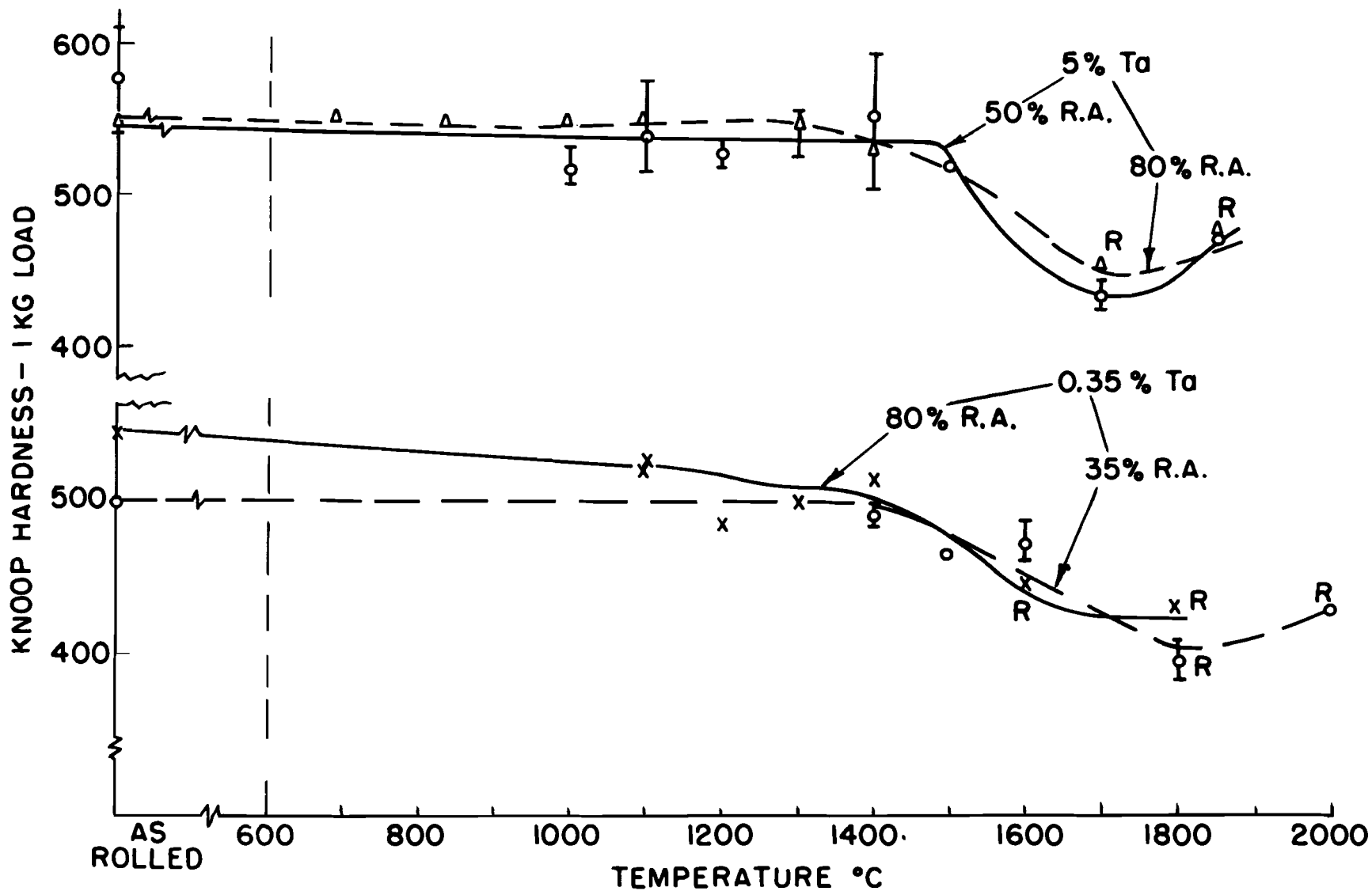
FIG. 89 KNOOP HARDNESS OF WORKED W−.35% Ta (ROLLED AT 1100°C) AND W−5% Ta ALLOY SINGLE CRYSTALS AS A FUNCTION OF ANNEALING (1/2 HR.) TEMPER- ATURE. (R = COMPLETE RECRYSTALLIZATION)

recrystallization (as defined in section IIB-6) are indicated by the letter "R" in this Figure. It is apparent that the recrystallization temperature of the 5% Ta alloy is higher by about 500°C - 600°C. The respective recrystallization data are compiled and compared with pure worked single crystals in Table 33 below.

Table 33
Comparison of Recrystallization Temperatures of
Worked Tungsten and W-5% Ta Alloy Single Crystals

Specimen	Approx. % R.A.	Approx. Re-xl Temp.
Alloy 1-3 (5% Ta)	50	1800°C
" 3-10 (5% Ta)	80	1800°C
Tungsten UC-7$_I$	80-90	1200°C
" UC-7$_{II}$	50	1200-1300°C

The recrystallization temperatures of the worked .35% Ta alloy single crystals is about 300°C - 400°C higher than that of pure tungsten single crystals. The data of this alloy are summarized and compared with those of pure tungsten single crystals in Table 34.

Table 34
Comparison of Recrystallization Temperatures of
Worked Tungsten and W-.35% Ta Alloy Single Crystals

Specimen	Approx. % R.A.	Approx. Re-xl Temp.
Alloy 2-3 (.35% Ta)	35	1800°C
" 2-3 (.35% Ta)	80	1600°C
Tungsten UC-3	30	1500°C
" UC-7$_I$	80-90	1200°C

It must be emphasized that the above results are tentative and will have to be reproduced for verification. The general course of recrystallization followed by the alloys is, however, quite similar to that of pure tungsten but with a shift to considerably higher temperatures. The classic increase in recrystallization temperature with decrease in cold work is observed in the alloys as well as the increase in recrystallization temperature with increasing alloy content.

157

Fig. 90   W-.35% Ta, 80% R.A.
           after 1/2 hour at
           1500°C - 500X

Fig. 91   W-5% Ta, 80% R.A.
           after 1/2 hour at
           1500°C - 500X

Fig. 92   W-.35% Ta, 30% R.A.
           after 1/2 hour at
           1500°C - 500X

158

These results may be better understood by examining the photo-micrographs reproduced in Figs. 90, 91 and 92, all taken at a magnification of 500X after annealing at 1500°C. The recrystallized grain in Fig. 90 (.35% Ta - 80% R.A.) is seen to be growing into the deformed matrix. The aligned etch pits (arrows) seem to be providing a driving force such that the grain has grown significantly faster in those regions than the bulk of the material. In Fig. 91 (5% Ta - 80% R.A.) it can be seen that recrystallization has not as yet started. The structure is that of a heavily worked crystal and contains a deformation band such as is found extensively in deformed single crystals of tungsten. Fig. 92 (.35% Ta - 30% R.A.) demonstrates the effect of work on recrystallization when compared with Fig. 90. Here again, recrystallization has not started but the structure has become completely polygonized.

In general it may be stated that dilute additions of Ta to W appear to show a much greater effect than would be expected from a casual study of the phase diagram and relative size of the atoms. This effect does not appear in the limited tensile tests conducted on "as melted" crystals in the vicinity of room temperature, but apparently results in a substantial increase in recrystallization temperature (400°C - 600°C), and reduces the workability at lower temperatures. The effect of orientation (if any) is yet to be established.

Discussion

Thermodynamic considerations are of considerable importance to the analytic interpretation of alloys with respect to both achievable compositions, and homogeneity. Solid solution alloys and dispersed second phase alloys are non-equilibrium systems, i.e., a chemical potential provides a driving force which as a function of temperature and environment tends to make these systems change with time. Since the change of these systems is time dependent, the usefulness of an alloy with respect to the mechanical properties depends on the rate at which these changes occur.

The microscopically observed time dependence is, however, not characteristic of a single process. This time dependence is a function - in the case of a two phase system - of the rate of decomposition of the second phase, the rate of diffusion of the components and the rate of loss of material from the surface, i.e., the vapor pressure. Any of these processes may be rate determining. Stable alloys are obtained when the rate of loss of all components have become equal. It should also be recognized that a stable alloy at one temperature may not be stable at another.

In the case of solid solution alloys of tantalum and tungsten, if ideal solution is assumed, published vapor pressure data (95) allow for a calculation of the steady state concentration by using the following relationship:

159

$$P(W) = P_0(W) \cdot N(W) \quad \text{AND} \quad P(Ta) = P_0(Ta) \cdot N(Ta)$$

where $P(W)$ and $P(Ta)$ are the vapor pressures of the components in the alloy, $P_0(W)$ and $P_0(Ta)$ are the vapor pressures of the components in the pure state, and $N(W)$ and $N(Ta)$ are the mole fractions of the components. The steady state is described by the condition.

$$P(W) = P(Ta) \quad \text{OR} \quad P_0(W)N(W) = P_0(Ta)N(Ta)$$

Since $N(W) + N(Ta)$ must equal unity, and further, since the ratio of vapor pressures of the pure components is essentially constant at all temperatures (96), namely

$$\frac{P_0(Ta)}{P_0(W)} = 6.5$$

one obtains by solving for $N(Ta)$:

$$N(Ta) = 0.18$$

One might expect that the value of 0.18 for the tantalum concentration is quite reasonable since a complete range of solid solutions exist for these metals, implying ideal behavior.

Since the analytical data are certainly suggestive of a loss of tantalum during zoning, this would mean that tantalum tungsten solutions deviate considerably from ideality. The vapor pressure of the tantalum according to the present data is at least forty times greater than that expected from ideal solution considerations.

It should be noted at this point that it is possible that the tantalum is evaporating in the form of some volatile compound. However, it is difficult from the analytical data to substantiate any such possibility. The only real difference in impurity analysis between the 5% and .35% tantalum crystals is in the oxygen contents, Table 25. On the average the 5% tantalum alloy contains 5 ± 1 ppm, whereas the .35% tantalum alloy contains 9 ± 2 ppm oxygen. Although the difference may be significant it is hard to relate these values quantitatively to the tantalum loss. If the vapor pressure of tantalum is significantly higher than ideal behavior would predict, it should be expected that a correlation with metallurgical properties would be found.

Deviation from ideality strongly suggests that the atomic arrangements will differ from a random distribution since the bond energy between W and W, W and Ta, and between Ta and Ta, are significantly different. These differences may manifest themselves through such phenomena as short range ordering, clustering, or as

160

atmospheres of solute atoms around lattice defects when a positive deviation from ideality is observed, as in the present case. This occurs because the tungsten lattice tends to "expel" the tantalum as evidenced by the high vapor pressure of tantalum, and one might therefore expect the lattice to be less than random. Also, the tantalum atoms would have greater stability at lattice defects.

Such deviations from an ideal crystal arrangement and the possibility of dislocation pinning should affect the metallurgical properties of the alloy, especially strengthening via the solid solution mechanism. Although admittedly not conclusive, the data indicate that the alloys do exhibit greater strengthening than expected. Hardness data also support the possibility of solution hardening in these alloys. The effect of alloying by tantalum on the recrystallization temperature and on the hardness thus seems to confirm the conclusion that the W-.35% TaC alloys produced to date were, indeed, solid solution alloys and not alloys of the dispersed second phase type.

IV. ACTIVATION ANALYSIS OF TANTALUM IN TUNGSTEN

In the process of the alloy development program, it became necessary to determine tantalum in tungsten in a percentage range of approximately 0.1 to 10%. Since the chemical separation of tantalum from tungsten is rather difficult and since analysis was required on a large number of samples, an analytical method was sought which would be both rapid and simple. Neutron activation analysis appeared to be quite favorable for the determination of tantalum because of the relatively long half life and high thermal neutron cross section of this element. Ta-182, the product of the n, γ reaction of TA-181, is a gamma emitter with photopeaks in the region of 1.2 Mev. The isotope has a half life of 111 days. The cross section for the activation process is 20.6 barns. Tungsten on the other hand gives rise to the gamma emitting isotope, tungsten-187 with a half life of 24 hours. The cross section for this reaction is approximately 35 barns. Tungsten-187 has a photopeak at .675 Mev. Two other radioactive isotopes of tungsten are formed: Tungsten-185, a pure beta emitter which will not interfere, and tungsten-181, a gamma emitter. The gamma energies of the latter isotope fall well below that of the tantalum photopeak, and therefore will not interfere with the analyses. However, if the analysis of tantalum in trace levels is required, some thought must be given to the possibility of a secondary reaction of tungsten-181 which can form tantalum-182 during irradiation. No calculations were made for this case since it was of no importance for the present work.

In order to determine the activity of the tantalum in the tungsten matrix, it is necessary either to discriminate against the .675 Mev gammas of the tungsten or to delay the determination until a sufficient number of tungsten-187 half lives have elapsed so as to

161

reduce this contribution to negligible levels. In practice a combination of both techniques was used; i.e., the analysis was carried out after five to ten half lives of tungsten-187 had elapsed; and since the tungsten radiation still exists, although greatly reduced, pulse height discrimination was used. In order to encompass as much of the photopeak of the tantalum as possible, the base line of the spectrometer was placed at 1 Mev and the window set to accept all events above that energy. Since the tail end of the tungsten-187 photopeak extends above the 1 Mev value, tungsten standards were used in order to determine the contribution of the tungsten-187 events which must be deducted from the Ta-182 photopeak.

Experimental

Samples of approximately 10 mgs each were accurately weighed on a microbalance. These samples can be metal chips or oxidized powder. At least three standards of both pure tungsten and pure tantalum were included. The samples were then sealed in clean polyethylene bags, the dimensions of which are of the order of $1/2$ inch^2 with a wall thickness of .004 inch. Labeling is accomplished by use of a ball point pen on a tab on the bag. Before counting, the tabs may be removed if any significant activity is developed in the ink, although with the particular ink used (origin unknown) this was not necessary. The aggregate of some fifty labels showed only negligible activity. The samples were irradiated in the Brookhaven National Laboratory graphite reactor using the pneumatic tube facility. An irradiation of approximately 1×10^{15} nvt gave rise to a tantalum specific activity (with the counting conditions described above) of 28,000 counts per minute per milligram.

A cooling off period of 1-2 weeks, depending on the activity level of the tungsten matrix, is required. Activity determinations were made using a single channel gamma ray spectrometer utilizing a 2 inch x 2 inch NaI-thallium activated well crystal.

The concentration of tantalum was determined from the specific activity of each sample as shown below. The activity, T, of a sample can be expressed as follows:

$$(1) \quad T = A(Ta) \cdot Ta + A(W) \cdot W$$

where $A(Ta)$ and $A(W)$ are the specific activities above 1 Mev of tantalum and tungsten, respectively. Since Ta is the weight of tantalum, and W the weight of tungsten present in the sample, the total weight, G, of the sample is

$$(2) \quad G = Ta + W$$

It follows by combining equations (1) and (2) that

$$T = A(Ta)Ta + A(W)(G-Ta)$$

Upon rearranging and solving for the ratio Ta/G one obtains

$$(3) \quad \frac{Ta}{G} = \frac{\frac{T}{G} - A(W)}{A(Ta) - A(W)}$$

Ta/G is the fractional weight of tantalum in the sample, the desired quantity, and T/G on the right hand side of equation (3) is the specific activity of the sample including contributions from both radioactive species. In those cases where sufficient decay of the tungsten-187 has been allowed to occur, the contribution of the specific activity of the tungsten, A(W) becomes negligible relative to A(Ta) and may be neglected in the denominator. Equation (3) is easily modified in the case of oxides to give

$$\frac{Ta}{G} = \frac{\frac{T}{G} - .739 A(W)}{A(Ta) - .969 A(W)}$$

Results

Table 35 lists the results of an analysis of samples consisting of blends of tungsten and tantalum oxides containing varying known quantities of tantalum. These blends were irradiated at a flux of approximately 3×10^{14} neutrons per cm^2 per sec^2.

Table 35
Activation Analysis of Tantalum in Tungsten
(Irradiation = 1 x 10   nvt)

Sample Wt. (Mgs.)	Tantalum Present (Micrograms)	Tantalum Found (Micrograms)	% Error
1.37	2.38	2.37	-0.4
1.77	3.08	3.19	+3.6
2.99	5.20	5.02	-3.6
8.30	14.4	14.5	+0.7
10.5	18.2	18.5	+1.6
13.2	22.9	22.8	-0.4
19.9	34.5	34.3	-0.6
1.15	43.7	42.1	-3.7
2.55	96.8	100.3	+3.6
3.32	125.8	125.8	0.0
3.66	138.7	139.9	+0.8

Discussion

The slope of the regression line of a plot of tantalum present versus tantalum found is within 1% of 1.00 for the data presented in Table 35. The correlation coefficient is .9998 giving the value of the slope a confidence limit of better than 99%. The average per cent error is somewhat less than 2% for the eleven samples.

The greatest source of error appears to arise from the weighing of powder samples. Specimens were packed for irradiation in polyethylene vials of such volume as to give a bulk density of approximately 0.02 grams per cm^3. This effectively prevents the occurrence of shadowing. Since no correlation between the error and sample size is evident, it is quite clear that self-shadowing did not occur with the small samples used.

Although the entire photopeak of the tantalum activity was not counted, apparently a sufficient area was included to give a good proportionality between activity and concentration. The subtraction of the contribution from the tungsten-187 tail is open to an objection in that one would not expect a direct proportionality between this activity and concentration. However, since the samples were of quite similar weight and since this correction was in all cases quite small compared to the activity of the tantalum, it apparently offered no difficulties. Care should be exercised on this point if samples are analyzed in which the tantalum activity is close to that of the tungsten (i.e., above 1 Mev), and if large variations in sample size are encountered. This deviation from proportionality can be easily taken into account by appropriate calibration, as necessary.

If time is not an important factor, one can allow the tungsten-187 to decay to negligible levels and determine the activity of the sample over its total spectrum, thereby gaining a factor of somewhat more than ten in sensitivity. Of course, greater sensitivity can also be achieved by subjecting the sample to longer periods of irradiation. Increasing sample size would also increase the concentration sensitivity, but care must be exercised to prevent self-shadowing. Finally, some thought must be given to the possibility that other contaminating nucleides can contribute activity to the sample in the energy bands being counted. Thus it is important that not only a gamma ray spectrum be run on the specimens, but a half life determination should also be made in order to insure radioactive purity.

Using the technique described, upwards of seventy-five samples have been irradiated as a unit. Counting and calculation time for those seventy-five samples amounted to less than three days. Depending on the tantalum concentrations, somewhat more or less time may be involved. Samples can be analyzed by this method in a nondestructive manner provided the dimension of the samples do not introduce shadowing effects.

164

V. FABRICATION AND MECHANICAL PROPERTIES OF DSP ALLOY SYSTEMS

This part of the contract program as originally conceived contained two major phases. The first and more immediate was the scale up of the alloy W-.38% TaC, including a study of an attempt to optimize processing conditions. The second phase was the application of the screening process to other alloy systems with the aim of producing an alloy with greater strength at higher temperatures than could be expected to be imparted by TaC as a dispersed second phase. In addition, two studies initiated during the previous two contracts (1,2) were completed. These studies involved a survey of the effect of the concentration of TaC on fabricability, as well as high temperature tensile strength of W-TaC alloys and a determination of the strength properties of the W-2% ThO_2 and W-.5% HfO_2 systems at 2700°F-3500°F.

1. Effect of Concentration of TaC on the Tensile Strength of W-TaC Alloys at 3000°F and 3500°F.

Short time tensile tests were completed at 3000°F and 3500°F on the series of alloys containing 0.1, 0.65 and 1.0% TaC. Alloys of these three compositions had been worked by swaging approximately 60% at 1700°C. Tensiles were ground and annealed for 30 minutes at 1600°C in H_2. A redesigned grip system was employed for tensile testing (3) but no change was made in specimen gage diameter or length (Fig. 93). The strain rate was kept constant at 30% per hour.

The results are summarized in Table 36 and the ultimate tensile and 0.2% yield strengths at 3000°F are plotted as a function of composition in Fig. 94 for all conditions. Included in Table 36 also are the results on the W-.38% TaC alloy obtained during the previous investigation (2). Since several processing conditions were used (2) in obtaining the results shown in Fig. 94, it cannot be stated conclusively that the alloy of optimum strength will contain 0.4% TaC. However, the indication is definite that higher additions do not impart substantial gains in strength.

There are wide variations of properties as a function of prior history. If the TaC is present as a discrete particle, this alloy may be heat treatable. If this is indeed the case, an explanation for the variability of properties may be found. The preliminary heat treating studies conducted on an extruded and swaged alloy (discussed below) were inconclusive regarding this point.

Annealing behavior of the three systems was determined by the techniques used throughout this program. The results are presented in Fig. 95, including those of the 0.38% TaC extrusion billet for comparison. The results are in agreement with the strength properties given above. Note that recrystallization temperature and hardness increase with increasing alloy content. It should also be noted that the recrystallization temperature of the 0.1% alloy is
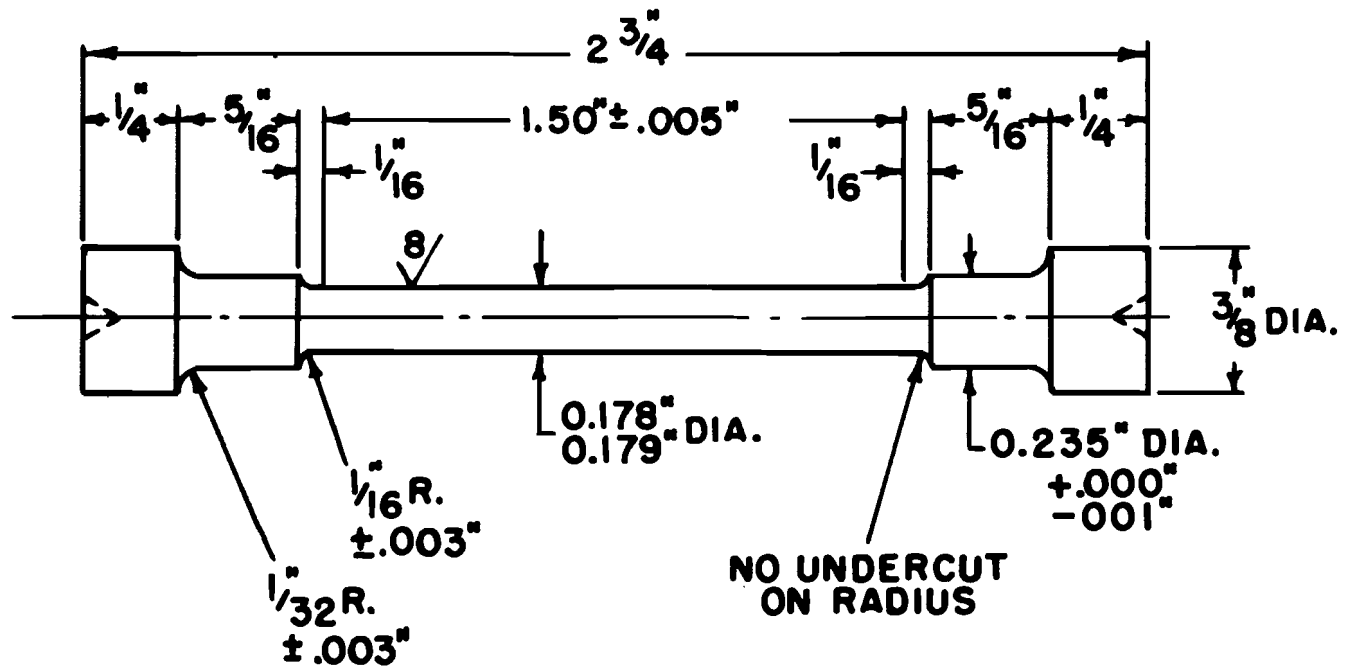
NOTE: ECCENTRICITY ON END CENTERS MUST NOT EXCEED 0.0005. END CENTERS OPTIONAL.

FIG. 93 MODIFIED REFRACTORY ALLOY TENSILE FOR VACUUM CREEP-RUPTURE TESTING.
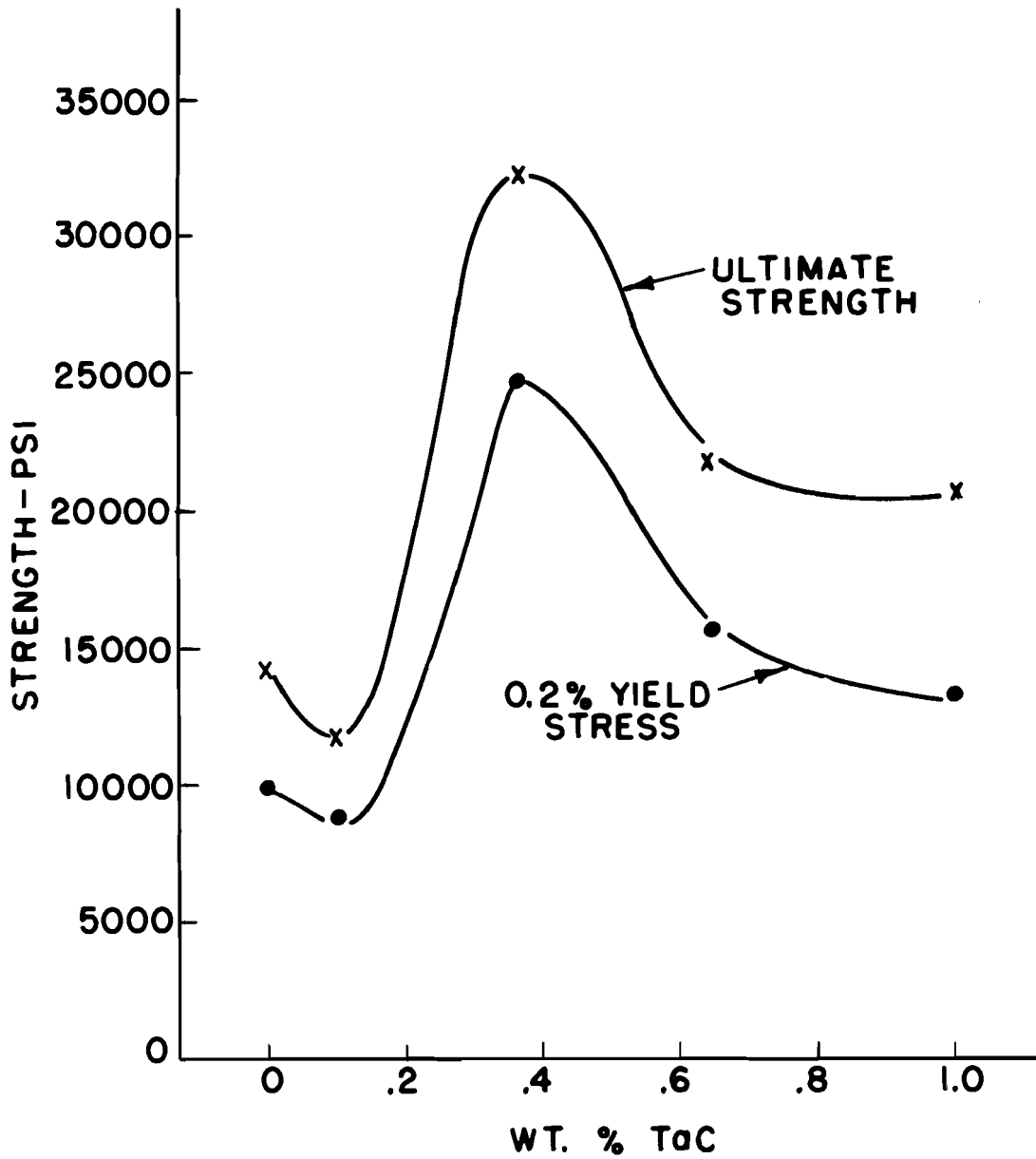
FIG. 94 EFFECT OF COMPOSITION ON TENSILE
STRENGTH OF W-TaC ALLOYS AT
3000° F

167
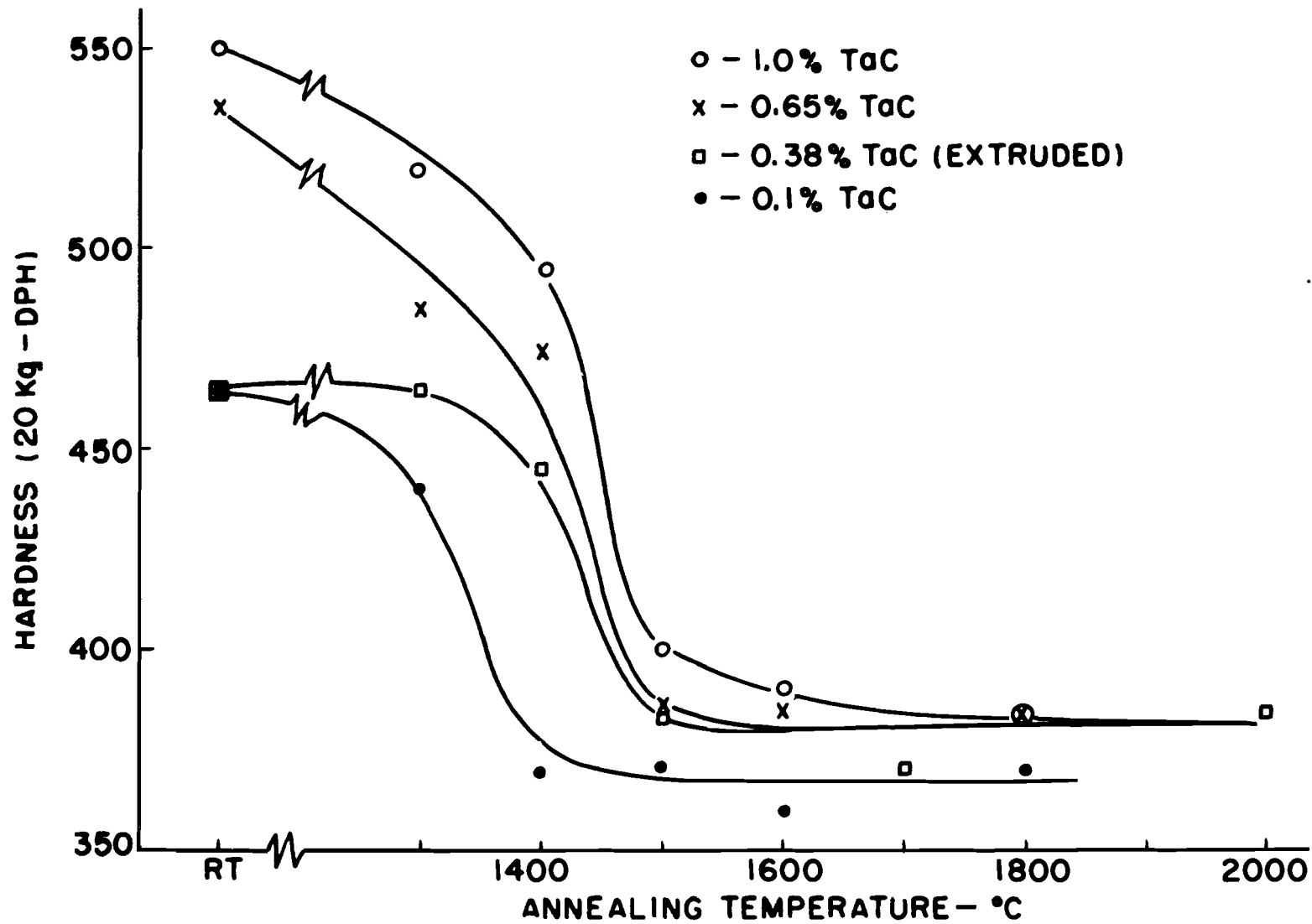
FIG. 95   HARDNESS AS A FUNCTION OF ANNEALING TEMPERATURE OF
W-TaC ALLOYS.

lower than that of pure tungsten, and this is also in agreement with the measured strength values.

Table 36
High Temperature Tensile Properties of W-TaC Alloys

Alloy	.2% Yield Strength 1000 psi	Ult. Tensile Strength 1000 psi	Elong. %	Red. in Area (%)
.1% TaC (3000°F)	8.80	12	23	25
.1% TaC (3000°F)	9.0	11.5	26	24
.38% TaC (3000°F)	16-26	22-32	7-33	16-42
.65% TaC (3000°F)	18	24	21	17
.65% TaC (3000°F)	15.5	20.5	17	16
1% TaC (3000°F)	17.5	29.0	21	1
1% TaC (3000°F)	10.0	12.5	16	18
.1% TaC (3500°F)	3.8	6.8	16	15
.1% TaC (3500°F)	4.5	6.4	15	15
.65% TaC (3500°F)	6.5	7.5	11	11
.65% TaC (3500°F)	7.2	8.1	14	13

These alloys were analyzed for Ta by the neutron activation technique and the data are presented in Table 37.

Table 37
Tantalum Analyses of the W-TaC Alloys

Alloy	%Ta Found	% Ta Nominal	Number of Samples
.01% TaC powder	.084, .092	.094	2
.065% TaC powder	.529, .540	.61	2
1.0% TaC powder	.828, .867	.94	2
0.1% TaC Ingot	.037	.094	1
0.65% TaC Ingot	.304	.61	1
1.0% TaC Ingot	.507, .655	.94	2

The results show:

a. A definite loss of Ta of the order of 30%-40% during sinter-ing.

b. A marked heterogeneity in the samples.

The loss of Ta may be caused by the formation of a volatile compound after the decomposition of the carbide. From the hardness values reported above, and the analyses obtained to date, one may speculate that a portion of the Ta has gone in solution ($\sim 1/2$). There is then enough carbon retained to account for the remaining Ta as a carbide. The heterogeneity may be accounted for by the

preparation method of direct blending of the powders, and the extreme smallness of the analytical samples (of the order of one milligram).

Although the data are sparse and there is considerable scatter in what are presumably duplicate tests, this system shows promise. Since enough material will be available from the extruded alloy to conduct rather extensive studies (primarily heat treatments) it is hoped that the variables already mentioned, i.e., fabrication history and alloy and impurity concentrations, can be minimized enough to develop a clearer picture of the properties of this alloy.

2. Advanced Development of the W-.38% TaC Alloy

The approach taken for this portion of the work was to produce a large (3" diameter) billet of the alloy to be extruded to rod and then swaged under various conditions to final size. In order to prepare this billet, 30 kg of pure tungsten were obtained, powder blended to a 0.38% TaC alloy, hydrostatically pressed, and presintered in hydrogen to a 3-1/2" diameter by 7" long ingot. (two ingots were pressed but one broke during pressing.) The round ingot after pre-sintering at 1700°C was 3-3/8" diameter with a density of 14.5 g/cm^3 (75% density).

It had originally been planned to have the ingot sintered to 93% of theoretical density at the pressing location, but furnace failure necessitated the design and construction of a laboratory sintering furnace. The construction of this furnace is shown schematically in Fig. 96. A first attempt to sinter the ingot in hydrogen failed because the maximum temperature which could be obtained did not exceed approximately 1800°C true temperature. The ingot was then packed into pellets of stabilized zirconia and was sintered for four hours at a minimum true temperature of 2200°C. The density after sintering was 17.0 grams/cm^3, i.e., only 88% of theoretical density rather than the desired 93%. In addition, an extensive reaction had taken place resulting in a 15% loss in weight of the ingot. Furthermore, the ZrO$_2$ used as an insulator contaminated the surface of the ingot. Qualitative spectrographic analyses (Table 38) taken on surface chips from the top and bottom of the ingot show the level of contamination which occurred.

The nature of the reaction which occurred was the subject of a separate study. Iridescent tetragonal crystals which had covered the surface of the sintered ingot were removed and examined. As revealed by an X-ray analysis, the crystals were composed of pure tungsten and had a cubic structure. Since this result indicated a removal of tungsten, probably via an oxidation-reduction cycle rather than by chemical reaction with the ZrO$_2$, it was suspected that wet hydrogen had been responsible for the mass transport. During the experiment some cooling water had seeped into the hydrogen line and thus moistened the hydrogen used for protection.

170
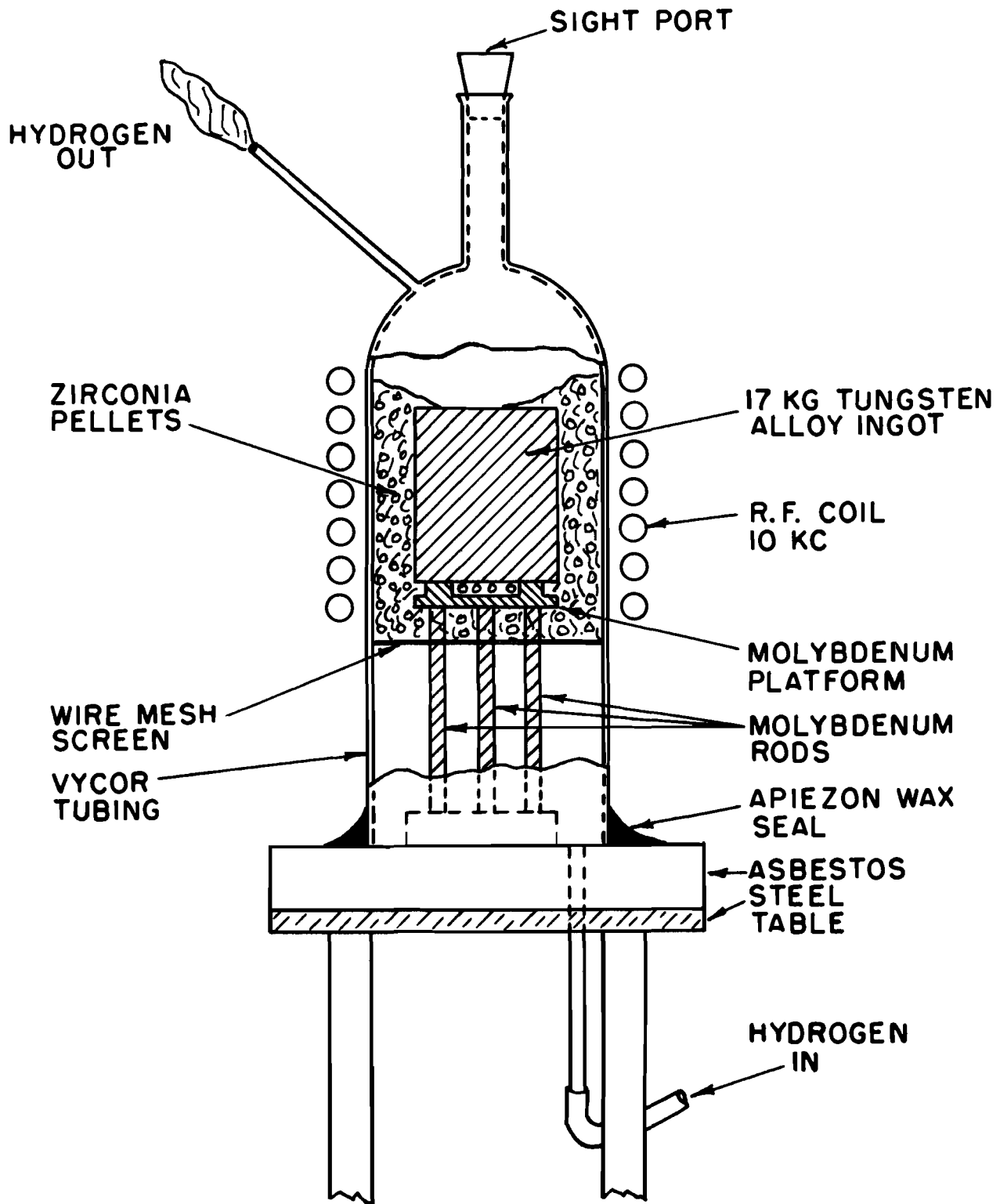
FIG. 96 INDUCTION FURNACE USED FOR SINTERING
W-.38% TaC INGOT.

171

Small compacts of pure tungsten were, therefore, pressed and heated in wet H_2. Iridescent crystals were found to grow on the compacts when the hydrogen was thoroughly wet. Crystals also grew on the sides of the crucible containing the compacts and also on a tungsten wire freely suspended near the compacts. These findings indicated that the stabilized zirconia had not caused the 15% loss of tungsten from the ingot by means of chemical reaction. The observed surface contamination with Zr must have been the result of some vaporization of zirconia subsequently reduced by hydrogen at the metal surface.

Table 38

Qualitative Spectrographic Analyses of W-.38% TaC Ingot Sintered in H_2 and Insulated by Zirconia Pellets

Specimen		Al	Ta	W	Mo	Ti	Zr	Ca
Top	1	T	ST	VS	FT	T	S	VS
"	2	T	ST	VS	FT	T	S	VS
"	3	T	S	VS	FT	T	VS	VS
"	4	T	S	VS	FT	T	VS	VS
Bottom	1	T-	ST	VS	VS	T-	VS	ST
"	2	T-	S	VS	FT	T-	VS	ST
"	3	T-	S	VS	FT	T-	S	ST
"	4	T-	S	VS	FT	T-	S	ST

$$VS = 10-100\%$$
$$S = 1-10\%$$
$$ST = .1-1\%$$
$$T = .01-.1\%$$
$$FT = .001 -.01\%$$

A one-half inch thick section was also removed from the bottom of the billet and the depth of contamination was determined. The analysis of the bulk of the ingot, as reported in Table 39, showed that the contamination was confined to a thin surface layer ($\sim 1/16$ inch) and that the ingot was otherwise sound. Quantitative analyses from the center of the billet confirmed this. However, due to the loss of material which was encountered, the ingot was undersized and could not be conditioned to a billet specified to have a diameter of 2.97 inches. The final size of the conditioned billet was only 2.72 (diameter) x 5-1/2 inches.

Table 39

Spectrographic Analysis of Bulk of the Sintered W-.38% TaC Billet

	Al	Fe	Si	Mg	Ca	W	Mo	Ta	Ni
Qual.	VF	FT-	FT-	VF	VF	VS	FT	ST	FT-
Quant.	11	62	89	10-66	ND	ND	ND	ND	10

Not detected - Mn, V, Ag, Ti, Zr, Ye, Yb, Cu, Hf

This billet was then canned in mild steel to a diameter of 2.97 inches and extruded by ASD at 4000°F and 6:1 reduction ratio. The extruded billet (1-1/4 x 15 inches) was not straight and had to be straightened prior to conditioning. The melted steel and lubricant used during extrusion was therefore first removed by leaching in a 1:1 solution of HF-HNO₃. The surface quality of the first three inches of the nose end was good but was less satisfactory toward the butt end, presumably as more and more of the steel can melted (see Fig. 97). The billet was, however, successfully straightened at 1700°C and conditioned to 0.908 inch diameter.

Since an extruded length of only 15 inches was obtained, no attempt was made to vary the working schedule during swaging. The ingot was routinely swaged to 0.435 inch diameter at 1650°C-1700°C. The material yields of 8% and 28%, based on starting powder weights and starting billet weights, respectively, were extremely low. The yield of 73% on swaging is extremely good for an experimental alloy. All pertinent fabrication data are summarized in Table 40.

<div align="center">

Table 40

Fabrication of W-0.38% TaC Extrusion Billet

</div>

Material	Operation	Weight	Yield %
Powder	Blending alloy	30 kg	-
Ingot	Pressing	17 kg	-
Ingot	Sintered at 2200°C	15 kg	-
Billet	Conditioned for extrusion	8.6 kg	29
Billet	Extruded 6:1 at 4000°F	-	
Billet	Conditioned	3.3 kg	11 (a) 38 (b)
Rod	Swaged to 0.435 at 1700°C, 77% R.A.	2.4 kg	8 (a) 28 (b) 73 (c)

(a) Based on starting powder.
(b) Based on conditional billet prior to extrusion.
(c) Based on conditioned billet after extrusion.

Chemical analyses of the material at several stages of fabrication were obtained and are given in Table 41.

As can be seen, a significant contamination by nickel occurred, the source of which is not known. More important, however, a study of the microstructure during the various stages of working definitely revealed the presence of precipitates aligned in the direction of working. (See Figs. 98-103.) This precipitate has not been seen previously in this alloy even at a level of 1% TaC, and thus may well be a result of contamination rather than TaC.
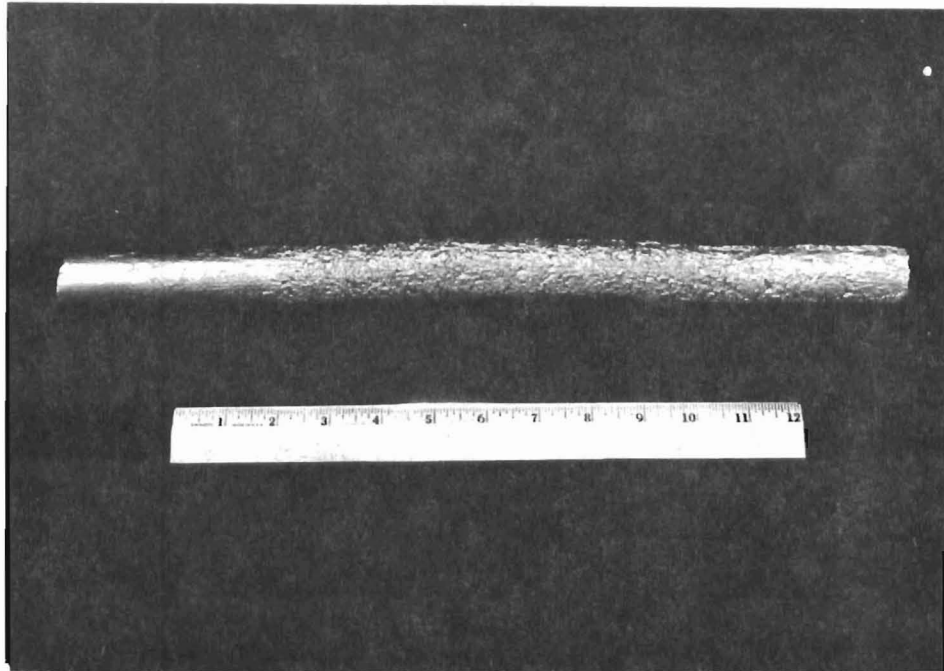
Fig. 97   Surface Quality of Extruded W-.38% TaC
          Billet after Leaching in HF-HNo$_3$ (1:1)
          Solution

174

Table 41
Chemical Analyses of Sintered, Extruded and Swaged W-.38% TaC Alloy
(ppm by wt.)

Condition	Al	Fe	Si	Mg	Ni	Ta(%)
Sintered	11	62	89	10-66	10	ND
Extruded	37	76	33	3	51	.32-.37
Straightened	5	94	19	6	74	ND
Swaged-nose	6	45	36	4	60	.31-.34
Swaged-tail	8	85	20	8	44	.32-.35

Examination of the "as extruded" microstructure (Fig. 98) shows that the alloy was completely recrystallized to a fine grain equi-axed structure. No grain growth occurred during the straightening operation at 1700°C (Fig. 99). After swaging 77% at 1650°C-1700°C, the structure was heavily cold worked (Fig. 100).

The recrystallization response of the "as swaged" material was studied using the same procedures as used previously; i.e., 30 minute vacuum anneals with subsequent study of hardness and microstructural changes. The hardness values of the alloy as a function of annealing temperature are plotted in Fig. 104. An extremely sharp drop in hardness is seen at about 1450°C corresponding to complete recrystalli-zation, as can also be seen in the change of the microstructure (Fig. 101). The recrystallization temperature of 1450°C is approxi-mately the same or perhaps somewhat lower than that reported pre-viously (2). This may be accounted for by the greater amount of cold work during swaging (77% R.A. vs.~60% R.A.) than that used previously or it may possibly be due to the contamination which occurred during extrusion.

A comparison of Figs. 98, 99, 102 and 103 with respect to grain size is of interest. No significant grain growth occurred during straightening of the extruded billet, an operation conducted at 1700°C with a preliminary soak of 30 minutes and several 10-15 minute reheats. However, recrystallization at 1700°C from the heavily worked swaged rod resulted in a substantial increase in grain size. Presumably this condition of exaggerated grain growth can be controlled by the proper choice of initial recrystallization condi-tions. The main point to be learned is that this alloy is very sensitive to prior conditions.

Some preliminary heat treating studies were made on the swaged rod. This survey took the form of solution heat treating in vacuum for one hour at 2100°C or 2400°C followed by ageing for one hour at various temperatures from 1650°C to 2025°C. The changes were again studied by hardness measurement and metallographic observation. Only one slight indication of hardening was found for material solu-tion heat treated at 2100°C and aged at 1950°C (hardness increase of ~15 VHN-20 kg load). No detectable changes in microstructures were noted. The work, is, however, preliminary and therefore must be
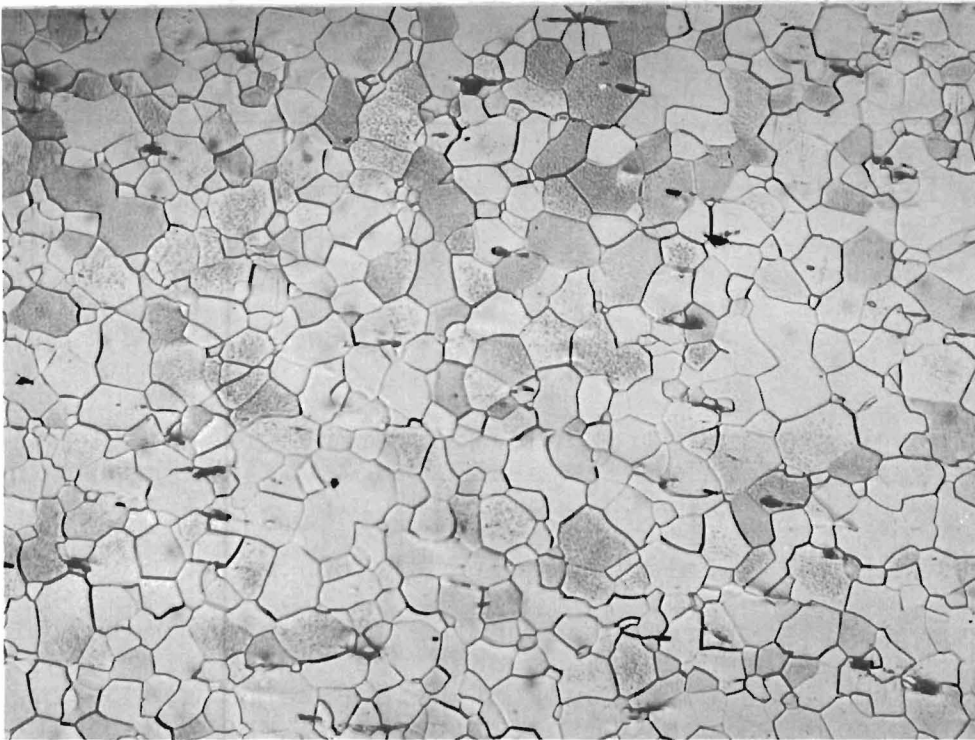
Fig. 98   W-0.38% TaC Alloy - as extruded 6:1 at 4000°F
           (2200°C).   Direction of working is horizontal
           - 250X
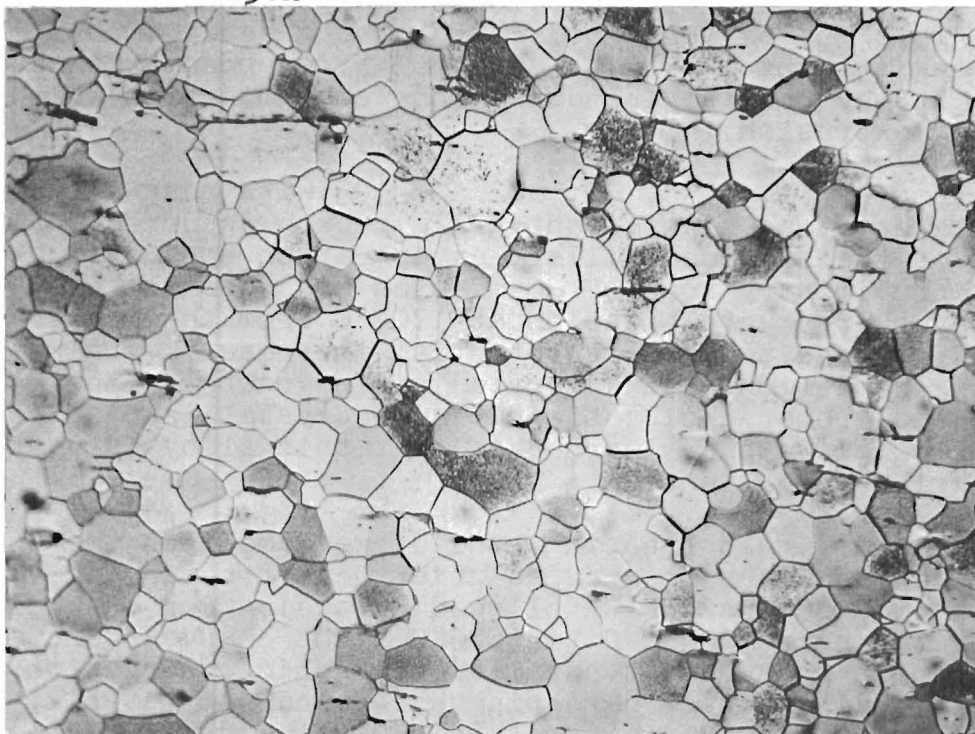
Fig. 99   As above after straightening
           1/2 hr. at 3100°F (1700°C) - 250X

Fig. 100   W + 0.38% TaC - as swaged % R.A. at 1650°C-
1700°C.   Direction of working - horizontal
- 250X

Fig. 101   As above but annealed 1/2 Hr. at 1400°C
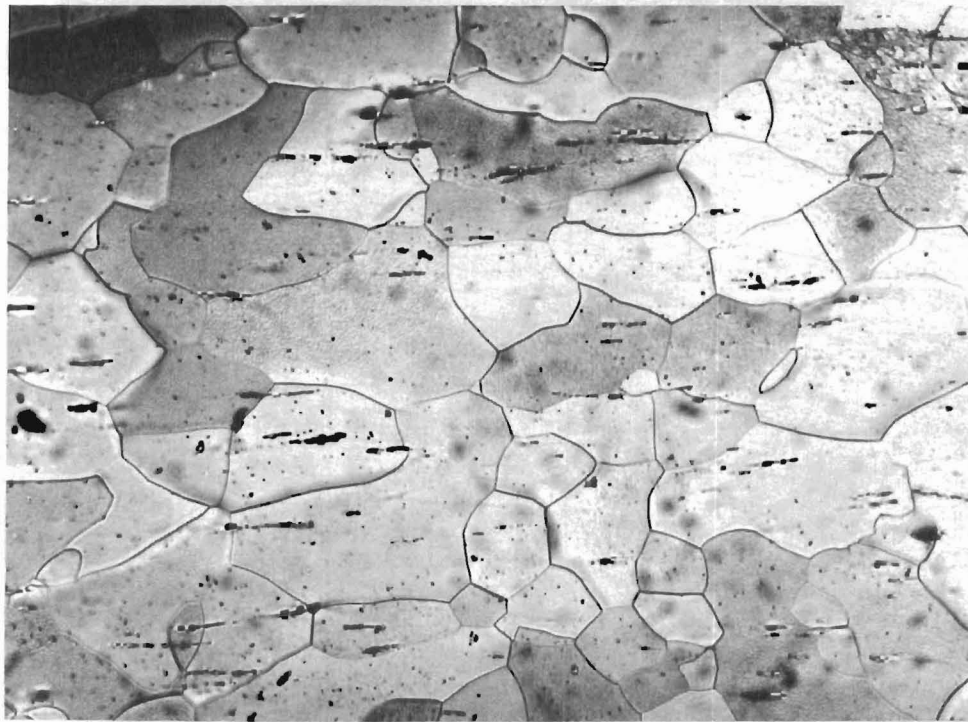- 250X

177

Fig. 102   As Fig. 100 but Annealed 1/2 Hr.
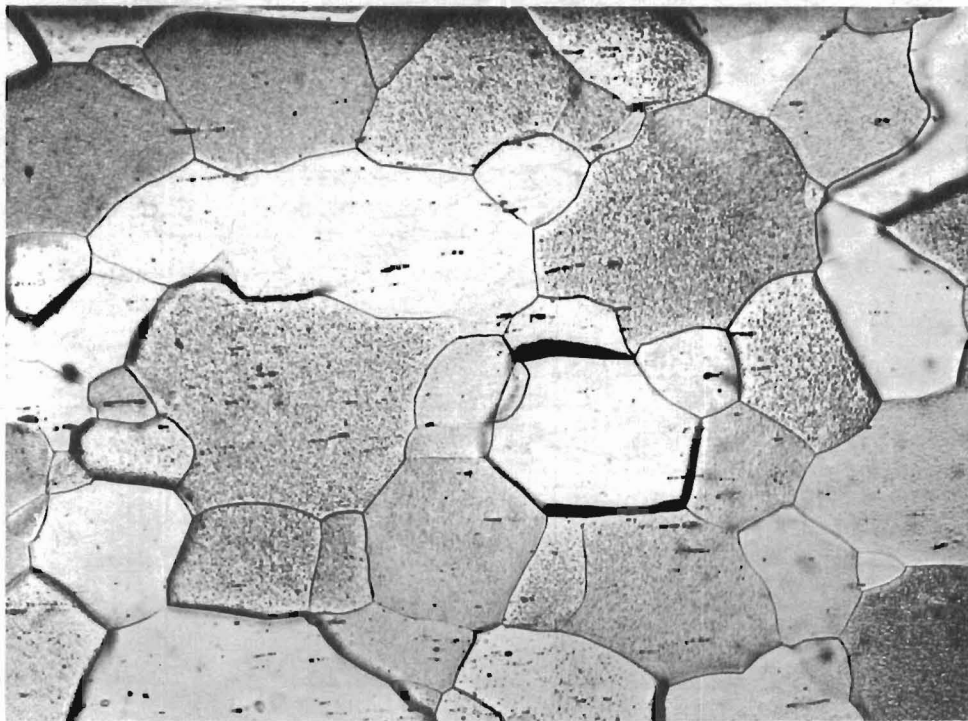   at 1500°C - 250X

Fig. 103   As Fig. 100 but Annealed 1/2 Hr.
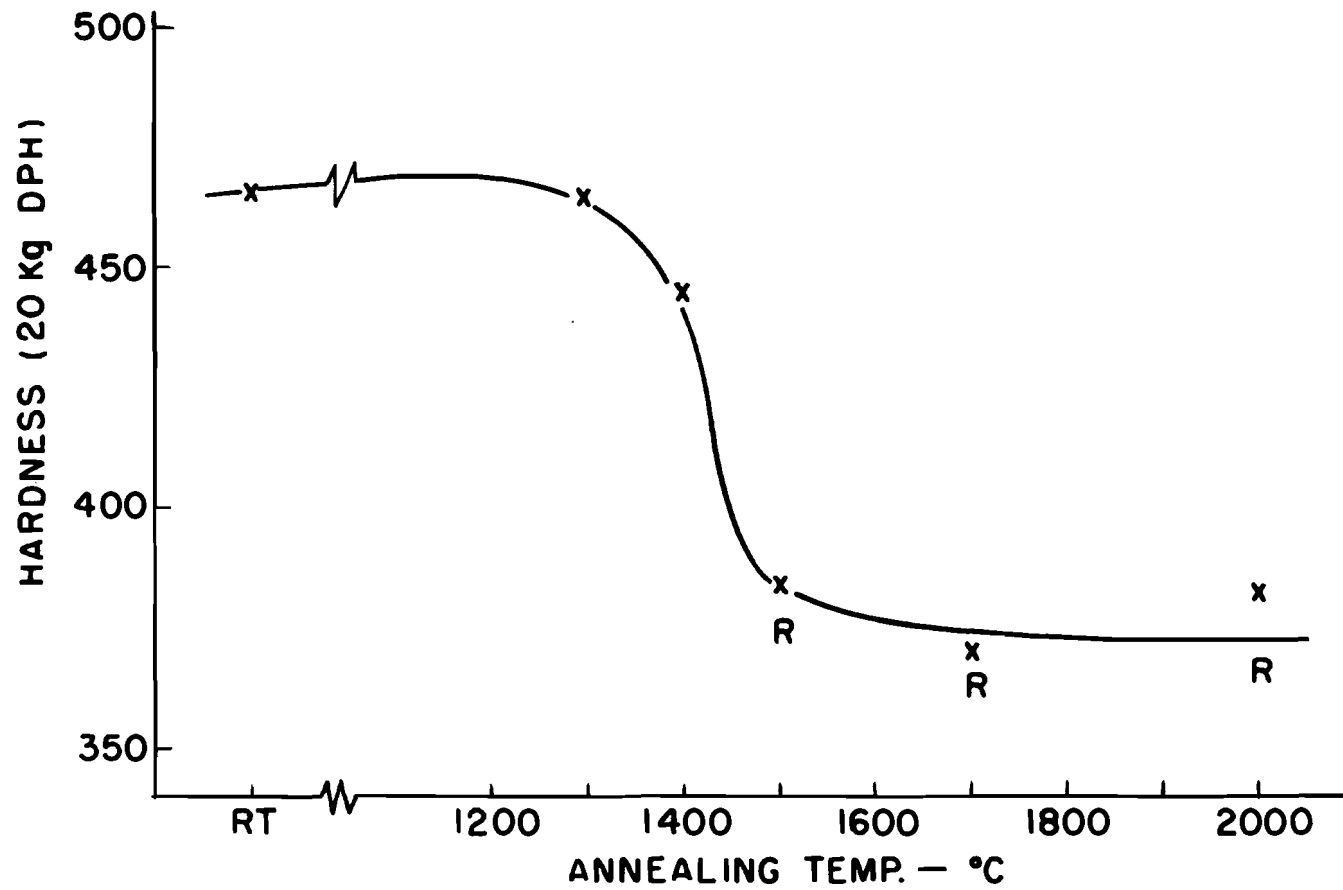   at 1700°C - 250X

178

FIG. 104 ANNEALING BEHAVIOR OF EXTRUDED AND SWAGED
W-TaC ALLOY.

179

considered inconclusive.

Although enough material was obtained from this billet to allow
a thorough evaluation of the mechanical properties, the problems
encountered during sintering delayed the project to the extent that
only the above preliminary data could be obtained. Tensiles have
been ground and will be tested after the proper annealing procedures
have been determined.

Since any information obtained from the above billet will be
subject to some question with regard to the sintering and extrusion
conditions (particularly contamination), it was deemed necessary to
produce a second billet under better controlled conditions. It was
felt desirable to determine the effect, if any, of vacuum sintering
on the properties of this alloy. Powder for another ingot was
therefore blended, pressed and presintered in hydrogen at 1050°C.
This ingot was then induction vacuum sintered to a density of
17.7 g/cc (92%)*. A photograph of the induction furnace with the
billet in position is shown in Fig. 105. This billet, which was
full size, was ground to 2.935 inches diameter and successfully
extruded by ASD at 4000°F and 6:1 ratio. The actual reduction
was 83% corresponding to a ratio of 6:1, indicating that there was
no significant die wear during extrusion. It is estimated that the
yield on extrusion will be 85% after cropping. This material will
be used for further study of fabrication variables.

3. Strength Properties of W-HfO$_2$ and W-ThO$_2$ between 2700°F and 3500°F.

W-HfO$_2$: The high temperature tensile data of the alloy
W-.5% HfO$_2$ were obtained for two conditions of working - swaging at
1600°C and 1700°C, respectively. The test results over the tempera-
ture range from 2700°F-3500°F are presented in Table 42.

Table 42
High Temperature Tensile Data of the W-.5% HfO$_2$ Alloys

Working Temp.	.2% Yield Strength (psi)	Ult. Tensile Strength (psi)	Elong.(%)	Red. in Area	Test Temp.
1700°C	12600	18000	21	27	2700°F
1700°C	19200	26000	21	19	3000°F
1700°C	5400	6500	9	8	3500°F
1600°C	11400	19000	29	27	2700°F
1600°C	7900	13000	17	20	3000°F
1600°C	5900	7000	11	10	3500°F

---

* The authors are indebted to Dr. G. Comenetz of the Westinghouse
  Research Laboratories who designed the induction coil, the billet
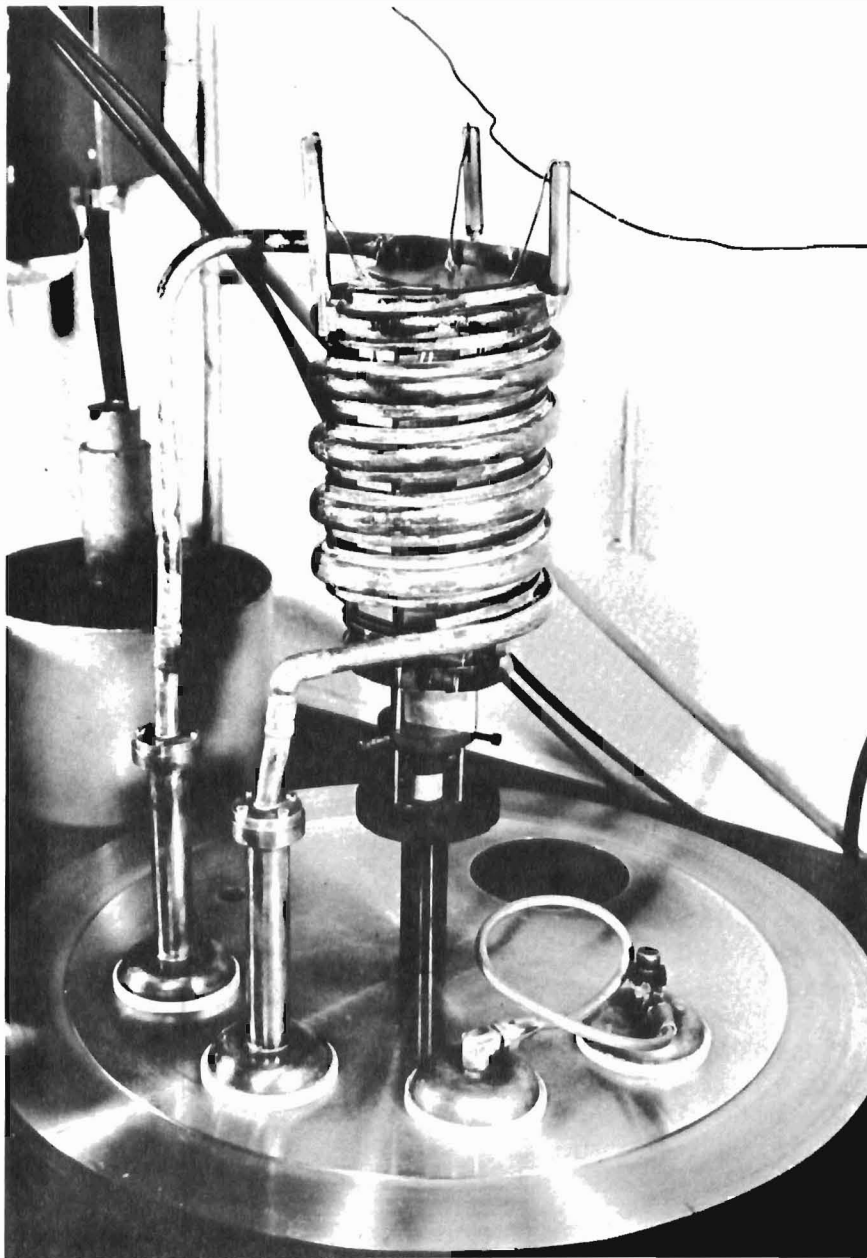 support and supervised the sintering of the billet.

Fig. 105   Photograph of Stainless Steel Bell Jar
            Vacuum Induction Furnace (open) with
            W-.38% TaC Billet placed on Support

181

Within the limits of the data, no effect of working temperature can be seen. The one specimen which is out of line (1700°C work, test at 3000°F) had an annealed Vickors hardness value some 30 points higher than the other specimens (400 vs. 370) and this value dropped to 370 after testing. It is felt that this specimen was probably not fully recrystallized prior to testing.

The HfO_2 system has thus shown only minimal strength gains, if any, and does not appear promising as a high temperature dispersion strengthened alloy.

W-2% ThO_2: Additional stress-rupture data were obtained for the commercial and the coprecipitated W-2% ThO_2 alloy at 3000°F. The results are compiled in Table 43.

Table 43
3000°F Creep Data of W-2% ThO_2 Alloys

Material	Stress (psi)	Life (hrs.)	M.C.R. (%/hr.)	Rupture Strain (%)
Comm.**	15000	4.4	.383	3.5
	12500*	5.7	.22	3.3
	7500	10.5	.076	1.3
Copp't.***	15000	2.0	.79	3.3
	12500	3.3	.34	2.6
	10000	4.9	.33	2.7

* This test was interrupted several times.
** Commercial
*** Coprecipitated

The stress-rupture time appears to be normal for this material (2). The slope of the stress versus rupture life·curve for these alloys at this temperature appears to be much steeper than was expected. By decreasing the stress considerably only a relatively small increase in life is found. (This may not be true at a stress below about 7500 psi.)

Of interest is the fact that the commercial ThO_2 alloy possessed very little ductility in the third stage of creep. This might indicate a tendency toward notch sensitivity. The coprecipitated material did not exhibit this behavior.

4. Screening Alloys

Several alloy systems were selected for further study on a screening basis. The approach adopted was to prepare 1-1/4" diameter x 2" long compacts of the alloys to be forged at ASD, and then evaluate these alloys for their high temperature strength (using miniature tensile specimens) and recrystallization behavior. Toward

182

this end a 2-1/2 x 3 inch long induction coil for preheating was made up and shipped to ASD , as well as a pure tungsten compact to be used for study of the heating characteristics of the coil.

The following alloy systems were prepared: W + TaC + HfC, W + TiB$_2$ and W-Ce. These alloys (1% by volume) were blended, pressed and sintered. However, by the time the compacts had been sintered, the alloy screening program was discontinued.

VI. ELECTRONIC STRUCTURE STUDIES

With the constantly expanding volume of information becoming available on the mechanical behavior of tungsten as affected by the defect state of the metal and by impurity composition and concentration, it is most desirable to interpret this information not only in terms of elasto-mechanical defect theory, but also in terms of the electronic structure properties of the metal. This requires, however, that one knows the electronic band structure of tungsten and preferably that of the other b.c c. metals of groups Va and VIa of the Periodic Table also. A number of experimental techniques have been devised by means of which one is able to deduce the electronic band configuration in metals, and in particular, the shape of the all-important Fermi surface (96). With the exception of magneto-resistance (97) and magneto-acoustic (98) measurements, none of these methods have been applied to the evaluation of the electronic structure properties of tungsten. One observable property which has been well characterized for tungsten as well as for other metals having a high melting point may be useful for a partial elucidation of the electronic structure of this metal. This property is the spectral emissivity as a function of temperature, generally referred to as an optical property of a metal.

In most instances the spectral emissivity as a function of temperature at 6500 Å is measured simply because a knowledge of the emissivity at this wavelength is required for accurate temperature determinations by optical pyrometry. Tungsten, because of its extensive use as a lamp filament, has been more thoroughly investigated. The reflection factors of tungsten were measured by Weniger and Pfund (99) as early as 1919 and more recently by Roberts (100). The first spectral emissivity measurement as a function of temperature based on a direct method was carried out by Krefft (101); (See Fig. 106). Later, DeVos (102) repeated these measurements and completely confirmed Krefft's results.

The most important feature of the set of spectral emissivity curves shown in Fig. 106 is the sign reversal of the temperature coefficient β , which results in a cross-over point at 1.27   . This was called the X-point by Price (103). Marple (104) who μ measured the spectral emissivity of rhenium as a function of temperature, found a set of curves very similar to that of tungsten with an X-point at approximately 0.95μ . Recently, Riethof (105), using the
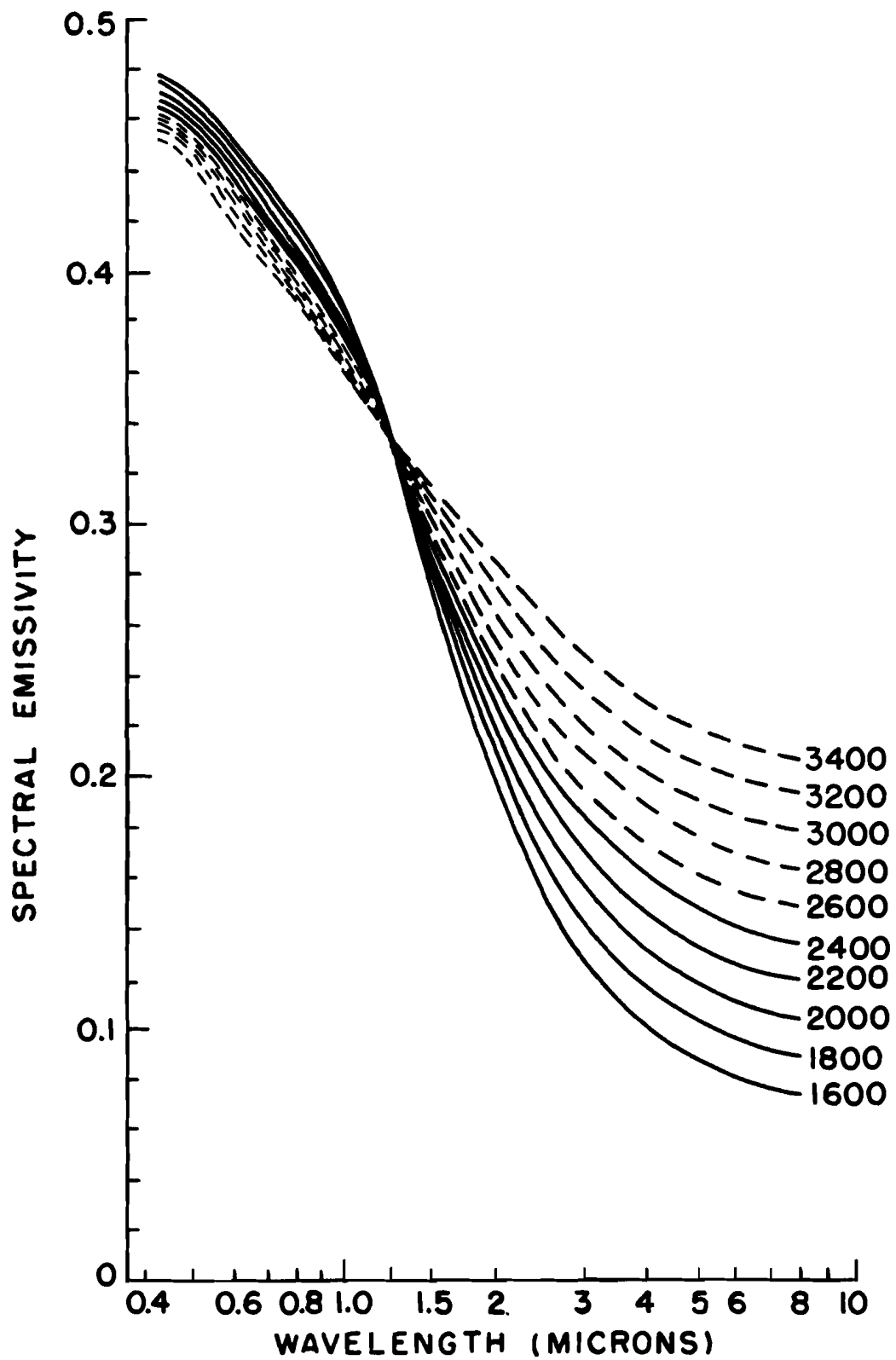
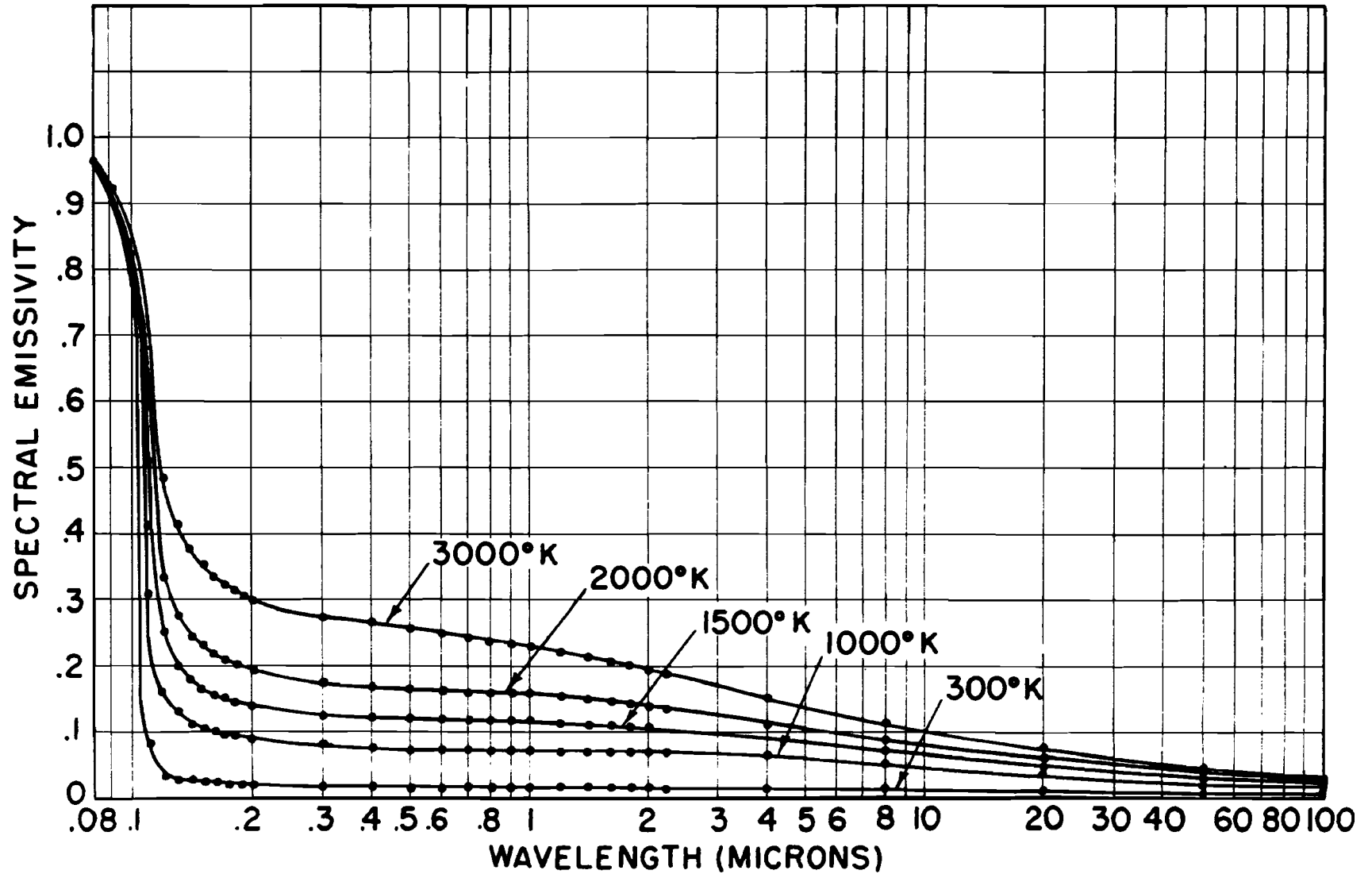FIG. 106 EMISSIVITY OF TUNGSTEN AS A FUNCTION
OF WAVELENGTH (AFTER KREFFT).

FIG. 107 SPECTRAL EMISSIVITY OF TUNGSTEN AS A FUNCTION OF WAVELENGTH
AND TEMPERATURE AS CALCULATED FROM FREE ELECTRON THEORY.
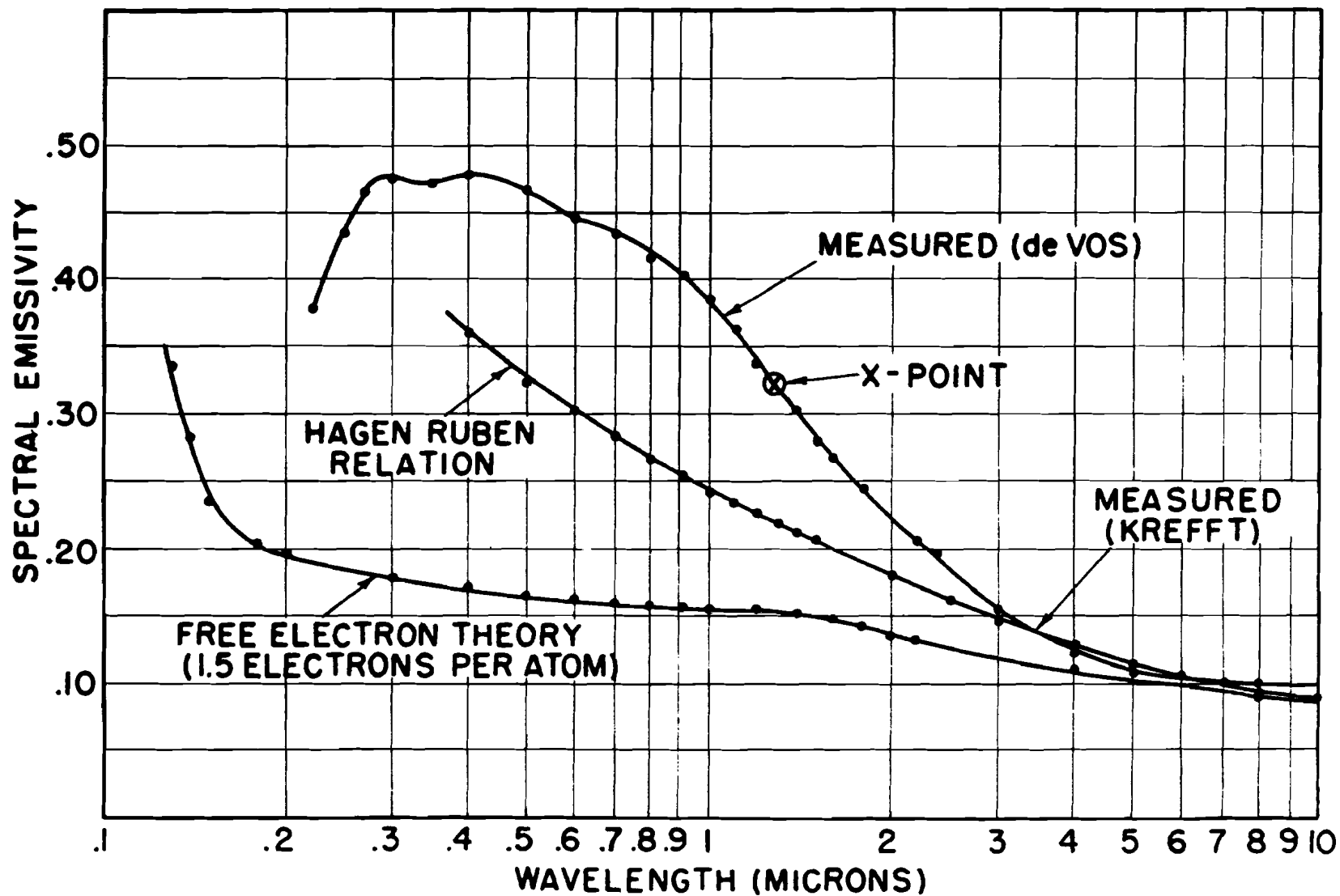(NUMBER OF FREE ELECTRONS 1.5)

FIG. 108 COMPARISON OF MEASURED AND CALCULATED SPECTRAL
EMISSIVITIES OF TUNGSTEN AT 2000° K

newly developed "induction furnace emissometer" determined the spectral emissivity of tantalum and found an X-point of approximately 0.7μ . Some carbides were also found to exhibit X-points (105), TaC at approximately 0.6μ and ZrC at approximately 2.2μ , for example. The emissivity curves all have a common property - at wavelengths shorter than the X-point wavelength the emissivity decreases with increasing temperature while at longer wavelengths the emissivity increases with increasing temperature.

Several investigators have attempted to explain the X-point theoretically. Weil (106) seemed to be able to derive the X-point from free electron theory, and Weale (107) applying Weil's calculation, deduced an X-point for tungsten at 4.32μ . Price (103), on the other hand, came to the conclusion that the free elctron theory cannot account for the X-point. The result of a machine calculation of the spectral emissivity for tungsten based on free electron theory equations by Mott and Jones (108) are shown in Fig. 107. A comparison of the magnitudes of the calculated and measured emissivities is presented in Fig. 108. Results obtained from the Hagen-Ruben approximation which is applicable at longer wave lengths (dielectric constant ϵ =1) have been included. The curves in Figs. 107 and 108 demonstrate that the free electron theory yields a wrong wavelength dependence of the emissivity in the wavelength interval from 0.2 to approximately 5 microns, and intrinsically cannot generate an X-point.

The observance of an X-point is, however, not restricted to spectral emissivity measurements on high melting point metals where such measurements are possible. Joos and Klopfer (109) have obtained clearly defined X-points for copper, aluminum, and the noble metals from measurements of absorption constants over the temperature range from 20°K to approximately 450°K. It is interesting to note in this case that the X-points fall onto an absorption edge. Since, in accordance to Kirchhoff's law, the absorption and the emission of metals are equal, the X-point must have the same origin and must be an intrinsic property of metals (or even solids) in general.

How then can one understand the X-point, the wavelength at which the point occurs, and the general shape of the spectral emissivity curves? Furthermore, how can one interpret the wavelength and temperature dependence of the emissivity in terms of electronic band structures? Spectral emissivity ϵ_λ is defined as the ratio of the energy I_λ radiated by a unit free surface of an opaque body in the wavelength interval from λ to $\lambda + d\lambda$ to that of a black body at the same temperature:

$$(1) \quad \epsilon_{\lambda,T} = \frac{I_{\lambda,T} \text{ (OPAQUE BODY)}}{I_{\lambda,T} \text{ (BLACK BODY)}}$$

In order to calculate the spectral emissivity, one must first derive an analytical expression for the spectral radiation intensity

$I_{\lambda,T}$ (opaque body). The denominator of equation 1, the spectral radiation intensity of the black body, is given by Planck's law. For the following, Kirchhoff's law is applied and it is assumed that the emission of radiation in the visible and near infrared spectrum is due to a mechanism which has been called "internal photoeffect" for the case of radiation absorption. The internal photoeffect has been used successfully to interpret the absorption measurements on copper and the noble metals. According to this effect, the absorption of energy from an incident monochromatic radiation is caused by interband-transitions of electrons whereby the reduced wave vector k remains constant; i.e., electrons are excited into states of higher energy which lie in a different band but have the same k value. As shown in Fig. 109, the same concept can be applied to emission of radiation. Electrons excited into states of higher energy by thermal vibrations of the lattice (or some other mechanism) recombine with ground states in a lower energy band with the emission of radiation (photons) having an energy characteristic of the transition.

An expression for the spectral radiation intensity can then be derived as follows: Assume the energy of the photons emitted by a transition with constant k to be $(E-E_0) = h\gamma$, and the number of transitions in unit time is given by the transition probability P_{12}. Then one must multiply these two terms by the number of states in the energy interval from E to E + dE in the upper band which is occupied by electrons, namely Z(E) .f (E) .dE, where f(E) is the Fermi probability. These two terms must also be multiplied by the probability $[1 - f(E_0)]$ for empty states in the lower band, E_0. Finally, the self-absorption of the metal must be taken into account since only radiation emitted from a certain depth can penetrate to and escape from the surface. This self-absorption is represented by the factor δ_s, which is related to the mean depth of penetration. The general expression for the spectral radiation intensity in terms of energy and as a function of temperature is then given in the following equation.

(2) $\quad I_{(E,T)} \, dE = Z(E) \cdot (E-E_0) \cdot P_{12} \cdot \delta_s \cdot f(E) \cdot [1-f(E_0)] \cdot dE$

The next problem is to evaluate the term representing the density of states $Z(E)$, the transition probability P_{12}, and the self-absorption δ_s. With respect to P_{12}, containing the matrix elements or the oscillator strength, one may make use of experimental data such as absorption coefficients, and this will be done later. The three quantities are, however, practically temperature independent and will be collected in the general function $\mathcal{Y}(E)$. With C as a normalization factor - equation 2 assumes the form of equation 3:

(3) $\quad I_{(\lambda,T)} dE = C \cdot \mathcal{Y}(E) \cdot (E-E_0) \cdot f(E) \cdot [1-f(E_0)] \cdot dE$
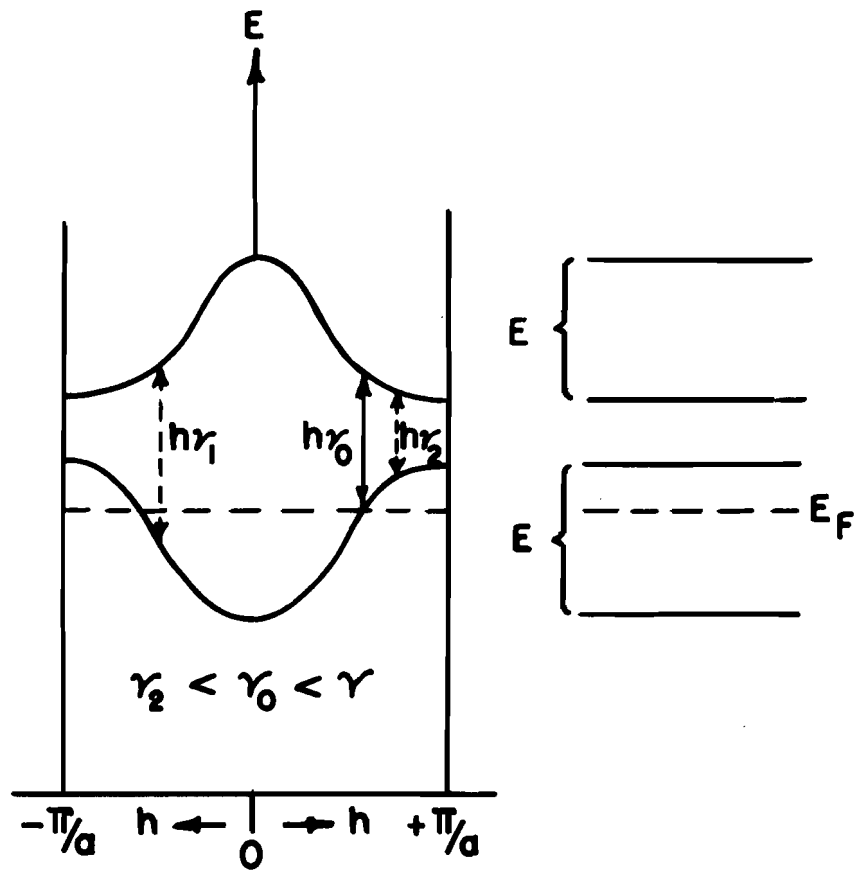
FIG. 109 ENERGY VERSUS REDUCED WAVE VECTOR

189

The temperature dependence of the spectral radiation intensity is now solely contained in the two Fermi-factors, which when evaluated yield equation 4:

$$(4) \quad f(E)\,[1-f(E_0)] = e^{-\left[\frac{E-E_F}{kT}\right]} \left[\frac{e^{\left[\frac{E_0-E_F}{kT}\right]}}{1 + e^{\left[\frac{E_0-E_F}{kT}\right]}}\right]$$

$$= e^{-\left[\frac{E-E_0}{kT}\right]} \left[\frac{1}{1 + e^{\left[\frac{E_0-E_F}{kT}\right]}}\right]$$

Combining equation 3, 4 and 1, and also expressing the denominator of equation 1 in terms of energy, one obtains equation 5:

$$(5) \quad \varepsilon_{(E,T)} = \frac{C \cdot \mathcal{T}(E) \cdot (E-E_0) \cdot e^{-\left[\frac{E-E_0}{kT}\right]}}{\dfrac{D \cdot (E-E_0)^3}{e^{\left[\frac{E-E_0}{kT}\right]} - 1}} \cdot \left[\frac{1}{1 + e^{\left[\frac{E_0-E_F}{kT}\right]}}\right]$$

Since the transitions are equivalent to or greater than an energy of 1 eV, one can neglect the 1 in the denominator, whereby the exponential functions in the first term and right hand side of equation 5 are cancelled. The spectral emissivity is thus finally given by equation 6:

$$(6) \quad \varepsilon_{(E,T)} = \frac{C \cdot \mathcal{T}(E)}{D \cdot (E-E_0)^2} \cdot \left[\frac{1}{1 + e^{\left[\frac{E_0-E_F}{kT}\right]}}\right]$$

Disregarding the first term on the right hand side of equation 6 and considering only the temperature dependent term in the square brackets, one can schematically represent the wavelengths and temperature dependence of the spectral emissivity. This is shown in Fig. 110.

The spectral emissivity in the neighborhood of the X-point is determined by E_0 ; i.e., by energy levels in the lower band. At $E_0 =$ E_F (presumably the Fermi energy) the term in the bracket is 1/2. In the direction of shorter wavelengths (higher frequency), where E_0 is smaller than E_F, the exponent becomes negative and the term in the
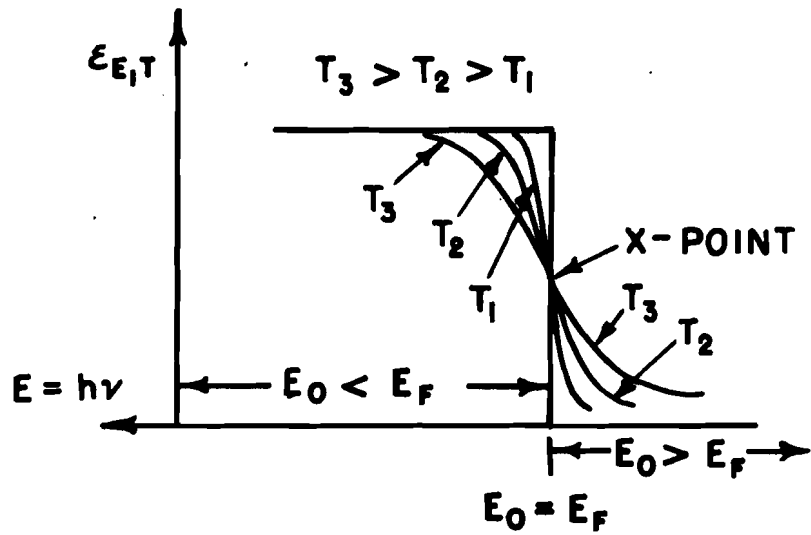
190

FIG. 110 SPECTRAL EMISSIVITY AS A FUNCTION OF
FREQUENCY AND TEMPERATURE
(SCHEMATIC)

bracket converges toward 1. In the direction of longer wavelengths (lower frequencies) where E_O is greater than E_F, the exponent becomes positive and the term in the bracket tends to zero. This is qualitatively in accordance with the experimentally observed wavelengths dependence of the emissivity.

Furthermore, the temperature dependence is also in line with experimental results. An emission edge exists at $E_O = E_F$. Thus at the absolute zero of temperature or slightly above, and when E_O is but little different from E_F, the term in the bracket will either be 1 or 0. As the temperature is increased in accordance with equation 6, the corners of the step-like function become rounded (see Fig. 110). This results in an increased emissivity at longer wavelengths and a decreased emissivity at shorter wavelengths.

It is now not difficult to calculate the temperature coefficient of the spectral emissivity β, as shown in equation 7:

$$(7) \quad \beta = \frac{1}{\epsilon_{(E,T)}} \cdot \frac{\partial \epsilon_{(E,T)}}{\partial T} = \frac{E_O - E_F}{kT^2} \cdot \left[1 - \frac{1}{1 + e^{\left[\frac{E_O - E_F}{kT}\right]}} \right]$$

The coefficient β is zero when $E_O = E_F$, negative for $E_O < E_F$, and positive for $E_O > E_F$. The experimental results on tungsten and rhenium shown in Fig. 111 agree qualitatively with the predicted wavelength dependence of β. The data on tungsten are earlier measurements by Ornstein (110) who found the X-point at 1.6 . Naturally, the temperature coefficient β must tend to zero with decreasing wavelengths. This is a consequence of the fact that lower-lying energy levels in the band E_O are not affected by temperature. Only states in the neighborhood of E_F are subjected to occupational changes when the temperature is increased. The measurements of DeVos (102) confirm this. The spectral emissivity curves for various temperatures converge into one single curve at shorter wavelengths.

Based on these considerations, one might conclude that - on the basis of energy considerations - the X-point corresponds to the last filled level in either the unfilled $5d^4$ or the $6s^2$ band of tungsten, and the X-point wavelength of 1.27μ represents an energy gap of approximately 1 eV. Spectral emissivity curves can be compared with curves of soft X-ray emission spectra. The extension of the curve at absolute zero from the X-point wavelength to the shorter wavelength where the emissivity is again zero, corresponds to the band width. The general shape of the curves (little affected by temperature, incidentally) is then a measure of the density of states.

The spectral emissivity of tungsten in the UV-spectrum has not been measured. One can, however, by extrapolating the emissivity curves to shorter wavelengths, deduce an approximate band width of 12 eV - which is too large a band width for a d-band. At present,
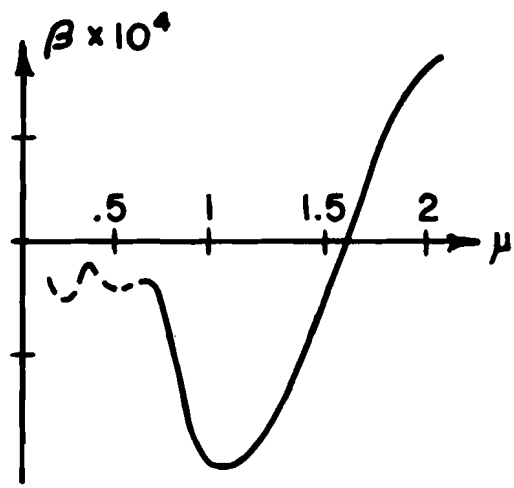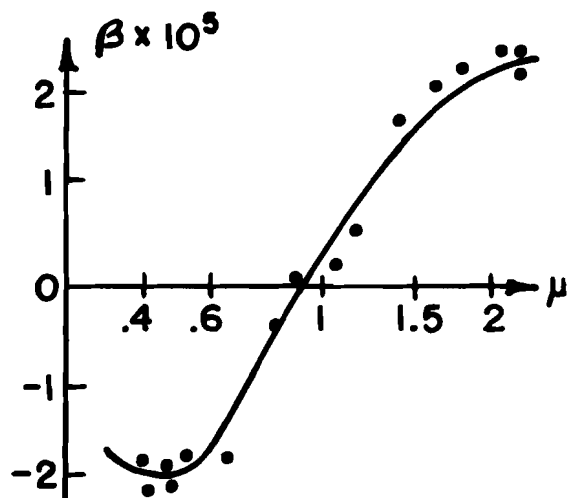
FIG. III TEMPERATURE COEFFICIENT OF THE SPECTRAL EMISSIVITY
OF TUNGSTEN AND RHENIUM.

no other information exists which would allow one to clearly identify the band. Assuming DeLaunay's (111) relationship between the electronic contribution to the bulk modulus (as given by the difference of the two elastic constants C_{12} and C_{44}) and the number of electrons and the band width to hold in this case, one may calculate the number of electrons per atom as 0.073 for this band. The electronic bulk modulus for tungsten, $K_e = C_{12} - C_{44}$, was calculated from room temperature elastic constants and amounted to 0.466×10^{12} erg cm-3. This very low number of electrons can be taken to indicate that the band in question is not the $5d^4$ band but the 6s2 band, and that the transitions are of the 6s2 - 6p type. Additional information is required to confirm this.

VII. GENERAL DISCUSSION

The programs discussed in this report have been a logical continuation of research and development efforts pursued during the past two contract periods (1,2). Since little was known concerning the mechanical properties of massive tungsten when the programs of the first contract period were conceived, a broader approach - resembling a survey in some respects - was in order. In reflecting on the status of the various programs, especially their systematic development during the three contract periods, one cannot help but recognize that this broad approach had merit and was certainly justified. A high degree of cross fertilization was achieved by carrying out simultaneously a number of related projects, and this had a beneficial effect on the development of each of the individual programs. At all times, of course, the efforts were conditioned by the principal objective - that of developing a high temperature dispersion strengthened alloy of tungsten.

In order to meet this objective two major properties of the alloys had to be studied: fabricability and strength. Neither property can be understood without first knowing the properties of the matrix - pure tungsten. This led to four principal lines of investigation which are interrelated and form a kind of closed loop of information which could be used to explain the two major properties as well as to allow for the design of an alloy.

The first principal line of investigation was the fabrication and evaluation of the high temperature strength of the dispersed second phase tungsten base alloys, specifically W-TaC alloys. The study of the strength properties of pure tungsten and the factors affecting ductility at low and medium temperatures represented the second principal line of investigation. When considering the interpretation of data, the information which can be obtained from these two investigations is limited. Therefore, a third principal program was undertaken which was concerned with parameters affecting the properties of both pure tungsten and alloys; grain boundaries, grain size and impurities. The main study under this third program was on the mechanical properties of tungsten single crystals. In order to

close the loop, a fourth principal line of investigation was needed. This line of study was devoted to tungsten base alloy single crystals produced by electron beam floating zone melting. This program, in particular, was expected to provide that information required to characterize completely an alloy with respect to its strength properties.

The main benefit derived from the work to date is the perspective which was gained in respect to the problems that still are to be solved. The conclusion can also be drawn that the broad approach has served its purpose, and greater effort is now needed in specific areas. This will become evident from the scope of the information made available and analyzed separately in each section of this report. These separate analyses have in common a certain deficiency since there are no analytical techniques suitable for accurately determining the concentration of trace impurities and clearly identifying the state of impurities in the lattice. This may appear as an obvious truth, but it is quite apparent that future progress in the understanding of the behavior of tungsten and the alloys will require a substantially greater effort in the area of impurity analysis.

This is immediately obvious if one tries to explain the two outstanding observations of the programs concerning the properties of high purity tungsten produced by powder metallurgy techniques: the loss of tensile ductility above 2500°F, and the effect of annealing temperature on the ductile-brittle transition temperature. Part of the answer to this problem lies in an understanding of the mechanisms of yielding. Another part of the answer, however, will certainly be found in exploring the state of impurities in grain boundaries. It is therefore necessary to attempt a determination of the state of impurities in the grain boundaries (wetting, clustering, or precipitation) and correlate this state with macroscopic mechanical properties.

A question frequently raised and directly related to impurity effects is whether or not the ductile-brittle transition can be lowered by increasing the purity of the metal. By all standards, the tungsten used in these investigations was quite pure. Recrystallization of worked ultra high purity zone melted single crystals produced a brittle material at room temperature. On the other hand, polycrystalline and single crystal tungsten have yield strengths of the same magnitude testifying to the fact that both materials are quite pure and that grain boundaries have little effect on the strength of tungsten at lower temperatures. With respect to brittleness one may expect to solve this problem by removing the unknown deleterious impurities or by precipitation. A greater purification of tungsten by a refinement of the electron beam melting technique holds the greatest promise at this time. Such exceptionally pure material, worked and recrystallized, should, in principle, provide an answer to the question as to whether or not greater purification will eliminate the brittleness in tungsten.

Studies of the deformation behavior of tungsten single crystals not only elucidate the possible effects of grain boundaries, but also reveal the effects of impurities. Two programs were conducted separately: one program covered the temperature range from -196°C to room temperature (R.T.) and the other the temperature range from R.T. to 800°C. This separation into two programs seemed desirable since it was felt that above R.T., internal friction measurements could be correlated with yielding phenomena. Furthermore, information on fabricability and the properties of worked and recrystallized single crystals were expected to be useful for the interpretation of data. Although strain rates and the gage length to diameter ratios of tensiles used for the two studies were not the same, the proportional limit as derived from these tests is continuous. The region at about R.T. where the curves obtained from the two programs connect - and the scatter of the data is greatest - must be considered a transition region characterized by twinning, a mode of deformation which upsets the continuity. The main difference between the two sets of results is twinning, which was restricted to a temperature interval in the one case, and found to increase continuously from 150°C to -77°C, the lowest temperature investigated under the second program. Although it would be of great interest to clear up this unexplained discrepancy, studies of deformation by twinning have not yet resulted in a quantitative relationship, and general twinning observations do not provide the answer.

The question as to whether or not tungsten single crystals have a ductile-brittle transition and, if so, the temperature at which it occurs, has also been explored. Apparently, single crystals are ductile to -196°C. As noted from plots of per cent elongation versus temperature, a small transition exists between -160°C and -40°C coinciding with the temperature range to which twinning is restricted. The ductility increases very gradually from -40°C to about 250°C above which temperature a pronounced transition takes place. A plot of per cent reduction in area versus temperature shows a ductile-brittle transition at +150°C. Since the ductile-brittle transition is not very well defined in single crystalline tungsten, but rather spread out, it appears as if grain boundaries control the narrowing of the temperature range over which the transition takes place.

Again the ductile-brittle transition of tungsten of yet higher purity than used to date, both in the form of single crystals and in the form of worked and recrystallized single crystals, must be studied before a complete understanding of the factors controlling embrittlement can be achieved. This requires, in particular, that the ductile-brittle transition temperature in dilute binary solid solution single crystals first and in dispersed second phase tungsten base alloys next be determined.

Much progress was made in reference to these much needed studies as well as a solution to the problem of high temperature

strengthening. This has come about by the development of a method
to produce W-Ta single crystal alloys of homogeneous composition
from compacted ingot-electrodes and by the successful extrusion
of two large W-.38% TaC billets. Concerning high temperature
strength measurements, a sufficient amount of information is
expected to become available with the material on hand completely
characterizing the alloy from the viewpoint of fabrication and the
strength imparted by alloying. The mechanistic interpretation of
strengthening will then follow from the comparative evaluation of
high temperature tensile properties of both fabricated pure tung-
sten single crystals and fabricated alloy single crystals.

VIII. REFERENCES

1. Atkinson, R.H. and Staff, WADD TR 60-37, Part I, (March 1960).

2. Sell, H.G., Keith, G.H., Koo, R.C., Schnitzel, R.H. and Corth, R., WADD TR 60-37, Part II,(May 1961).

3. Vandergrift, E.F., Metal Testing at High Temperatures, ASME Paper No. 62 - Met.-6.

4. Hall, R.W. and Sikora, P.F., Tensile Properties of Molybdenum and Tungsten from 2500°F-3700°F, NASA Memo 3-9-59E, (1959).

5. Sikora, P.F. and Hall, R.W., High Temperature Tensile Properties of Wrought Sintered Tungsten, NASA TN D-79 (1959).

6. Witzke, W.R., The Purification of Tungsten by Electron Bombardment Floating Zone Melting, Symposium on Electron Beam Melting, Alloyed Electronic Corp., Boston, Mass., (1959).

7. Grant, N.J., Fracture, ed. by Averbach et al, Technology Press and Wiley, 562, (1959).

8. Gifkins, R.C., Ibid. 579.

9. Petch, N.J., J. Iron St. Inst., 174, 25 (1953).

10. Petch, N.J., Phil. Mag., 3, 1089 (1958).

11. Cottrell, A.H., Trans. AIME, 212, 192 (1958).

12. Ball, C.J., J. Iron St. Inst., 191, 232 (1959).

13. Tjerkstra, H.H., Acta Met., 9, 259 (1961).

14. Hall, E.O., Proc. Phys. Soc., B64, 747 (1951).

15. Cracknell, A.and Petch, N.J., Acta Met., 3, 186 (1955).

16. Johnson, A.A., Phil. Mag., 4, 194 (1959).

17. Adams, M.A., Roberts, A.C. and Smallman, R.E., Acta Met., 8, 328 (1960).

18. Johnson, A.A., Acta Met., 8, 737 (1960).

19. Koo, R.C., J. Less-Common Metals, 4, 138 (1962).

20. Marcinkowski, M.J. and Lipsitt, H.A., Acta Met., 10, 95 (1962).

21. Heslop, J. and Petch, N.J., Phil. Mag., 3, 1128 (1958).

22.   Koo, R.C., J. Less-Common Metals, 3, 412 (1961).

23.   Goldschmidt, H.J., AF61(052)-306, Air Research and Development Command, Wright Air Development Center (1961).

24.   Hornbogen, E., private communication.

25.   Suits, J.C. and Chalmers, B., Acta Met., 9, 854 (1961).

26.   Schulz, H. and Bruns, H., Osram Studiengesellschaft Augsburg, Germany, private communication.

27.   Schadler, H.W., Trans. AIME, 218, 649 (1960).

28.   Tipper, C.F. and Hall, E.O., J. Iron St. Inst., 175, 9 (1953).

29.   Low, J.R. Jr., and Fenstel, R.G., Acta Met., 1, 185 (1953).

30.   Biggs, W.D. and Pratt, P.L., Acta Met., 6, 694 (1958).

31.   Smith, R.L. and Rutherford, J.L., J. Metals, 9, 857 (1957).

32.   Anderson, R.W. and Bronisz, S.E., Acta Met., 7, 645 (1959).

33.   Simonsen, E.B., Acta Met., 8, 809 (1960).

34.   McHargue, C.J., Acta Met., 8, 900 (1960).

35.   Leadbetter, M.J. and Argent, B.B., J. Less-Common Metals, 3, 19 (1961).

36.   Calverley, A., Davis, M. and Lever., R.F., J. Sci. Instr., 34, 142 (1957).

37.   Fisher, J.C., Trans. ASM, 47, 451 (1955).

38.   Conrad, H., Phil. Mag., 5, 145 (1960).

39.   Lawley, A., Van den Sype, J. and Maddin, R., to be published.

40.   Rose, R.M., Ferriss, D.P. and Wulff, J., to be published.

41.   Wolff, U.E., Trans. AIME, 224, 327 (1962).

42.   Schadler, H.W. and Low, J.R. Jr., Office of Naval Research Contract No. Nonr-2614(00) April 1962.

43.   Rosenbaum, H.S., Acta Met., 8, 742 (1961).

44.   Clark, R. and Craig, G.B., Progr. in Met. Phys., 3, 115 (1952).

45.   Schoeck, G. and Seeger, A., Acta Met., 7, 469 (1959).

46. Schoeck, G., Acta Met., $\underline{9}$, 382 (1961).

47. Keh, A.S. and Weissmann, S., Proc. of the Int. Conf. on the Impact of the Elect. Trans. Micros. on the Theory of the Strength of Solids, Berkeley, California (July 1961).

48. Johnston, W.G. and Gilman, J.J., J. Appl. Phys., $\underline{31}$, 632 (1960).

49. Low, J.R. Jr., and Guard, R.W., Acta Met., $\underline{7}$, 171 (1959).

50. Low, J.R. Jr., and Turkalo, A.M., Acta Met., $\underline{10}$, 215 (1962).

51. Reed-Hill, R.E. and Robertson, W.D., Acta Met., $\underline{5}$, 177 (1957).

52. Schnitzel, R.H. and Keith, G.H., J. Less-Common Metals, $\underline{4}$, 98 (1962).

53. Cochardt, A.W., Schoeck, G. and Wiedersich, H., Acta Met., $\underline{3}$, 533 (1955).

54. DeKlerk, J. and Bolef, D.I., unpublished work.

55. Cracknell, A. and Petch, N.J., Acta Met., $\underline{3}$, 186 (1955).

56. Danneberg, W., Metall, $\underline{15}$, 977 (1961).

57. Koo, R.C., in Reactive Metals, ed. by R.W. Clough, Interscience, New York, p. 265 (1958).

58. Cottrell, A.H. and Bilby, B.A., Proc. Phys. Soc. (London), A62, 49 (1949).

59. Nabarro, F.R.N., Report on Strength of Solids, 38, Physical Society, London (1948).

60. Wessels, E.T., Proceedings of the 1954 Cryogenic Engineering Conference, Boulder, Colorado, N.B.S. Report, p.170 (February 1955).

61. Alers, G.A., Armstrong, R.W., Bechtold, J.H., Trans. AIME, 212, 523 (1958).

62. McKinsey, G.R., Mencher, L., Sheely, W.F. and Wilson, J.F., ASD-Technical Report 61-3 (1961).

63. Bechtold, J.H. and Shewmon, P., Trans. ASM, $\underline{46}$, 397 (1954).

64. Pugh, J., ASTM Preprint 71 (1957).

65. Erickson, J.S. and Low, J.R. Jr., Acta Met., $\underline{7}$, 58 (1959).

66. Cox, J.J., Horne, G.T. and Mehl, R.F., Trans. ASM, $\underline{49}$, 118 (1957).

67. Churchman, A.T., J. Inst. Metals, 88, 221 (1959).

68. Cottrell, A.H., Phil. Mag., 44, 829 (1953).

69. Stein, D.F. and Low, J.R. Jr., J. Appl. Phys., 31, 362 (1960).

70. Conrad, H., Schoeck, G., Acta Met., 8, 791 (1960).

71. Gilman, J.J. and Johnston, W.G., Dislocations and Mech. Prop. of Crystals, 116, John Wiley and Sons, Inc., New York (1957) and J. Appl. Phys., 30, 2 (1959).

72. Hahn, G.T., to be published, Acta Met., 10 (1962).

73. Holden, F.N., Trans. AIME, 194, 182 (1952).

74. Snoek, J., Physica, 8, 711 (1941).

75. Owen, W.S., Gilbert, A., Reid, C.N., Hull, D. and McIvor, I., WADD Technical Report 61-181 (1961).

76. Hull, D., Acta Met., 8, 11 (1960).

77. Armstrong, R.W., Deformation Twinning in B.C.C. Metals, Westinghouse Research Labs., Sc.P.62-925-116-P2 (to be published).

78. Allen, B.C., Maykuth, M.S. and Jaffee, R.I., Inst. of Metals 90, 120 (1961-62).

79. Powers, R.W., Acta Met., 2, 604 (1954).

80. Powers, R.W. and Doyle, M.V., J. Appl. Phys., 28, 255 (1957)

81. Powers, R.W. and Doyle, M.V., Acta Met., 4, 233 (1956).

82. Powers, R.W. and Doyle, M.V., J. Appl. Phys., 30, 514 (1959).

83. Marx, T. and Wert, C., Acta Met., 1, 113 (1953).

84. Becker, J.A., Becker, E.J. and Brandes, R.A., J. Appl. Phys., 32, 411 (1961).

85. Sell, H.G., Koo, R.C., Keith, G.H. and Schnitzel, R.H., Westinghouse Lamp Div., Research Report BL-R-6-7119, 4A4-2, (March 1961).

86. Berlec, I., J. Appl. Phys., 33, 197 (1962).

87. Pugh, J.W., Third Plansee Seminar, Plansee Proceeding (1958), ed. by F. Benesovsky, Pergamon Press, N.Y., (1959).

88. Harmon, E.L. and Forgerg, W.D., ABSTRACT in J. Metals, 12, 746 (1960), AIME Session on Refractory Metals.

89. Barrett, C.S., Structure of Metals, McGraw-Hill, New York (1952).

90. Barrett, C.S. and Bakish, R., Trans. AIME, 212, 122 (1958).

91. Wessel, E.T., France, L.L. and Begley, R.T., Westinghouse Research Labs., Report No. 11-1003-1-P1 (1960).

92. Hull, D., Acta Met., 8, 11 (1960).

93. Cahn, R.W., J. Inst. Met., 83, 493 (1955).

94. Muller, F. and Parker, E., O.N.R. Report N.V. 222-52-27 (1960).

95. Honig, R.E., Vapor Pressure Curves of the More Common Metals, RCA, (1957).

96. Harrison, W.A., Webb, M.B., The Fermi Surface, John Wiley and Sons, Inc., N.Y. (1961).

97. Fawcett, E., Phys. Rev. Letters, 7, 370 (1961).

98. Rayne, J.A., Sell, H.G., Phys. Rev. Letters, 8, 199 (1962).

99. Weniger, W., Pfund, A.H., Phys. Rev., 14, 427 (1919).

100. Roberts, S., Phys. Rev., 114, 104 (1959).

101. Krefft, H., Handbuch der Lichttechnick, p.84, Springer, (1938).

102. DeVos, J.C., Physica XX, 690 (1954).

103. Price, D.J., Proc. Phys. Soc. (London) 62A, 278 (1949).

104. Marple, T.D.F., J. Opt. Soc. Am. 46, 490 (1956).

105. Riethof, T.R., General Electric Space Science Lab., Tech. Inf. R61SD004 (1961).

106. Weil, R., Proc. Phys. Soc. (London) 60, No.337, 8 (1948).

107. Weale, R., Proc. Phys. Soc. (London) 62A, No.358A, 661 (1949).

108. Mott, N.F., Jones, H., The Theory of the Properties of Metals and Alloys, 112, Dover Publishers, Inc., N.Y. (1958).

109. Joos, G. and Klopfer, A., Physik, 138, 251 (1954).

110. Ornstein, L.S., Physica 3, 561 (1936).

111. DeLaunay, J., Solid State Physics, 2, ed. by Seitz, F. and Turnbull, D., Academic Press, Inc., N.Y. (1956).